THE UNIVERSITY OF ADELAIDE

DEPARTMENT OF MECHANICAL ENGINEERING

THE ENHANCED MIXING BURNER

submitted by

Graham Jerrold Nathan, B.E.(hons)

for the Degree of Doctor of Philosophy

March 1988

Summary

A new type of enhanced mixing nozzle has been developed, which generates extremely strong mixing and a very rapidly spreading jet. The mechanism is investigated using high speed schlieren photography, surface flow visualisation within the nozzle, dye injection in water, acoustic frequency spectra measurements, smoke visualisation and hot wire anemometry.

It is postulated that the enhanced mixing is generated by a precessing asymmetric jet which is instantaneously directed at a large angle from the nozzle axis at the exit plane, but on average produces a rapidly spreading, symmetric jet. This instantaneous jet does not occupy the whole of the exit plane of the nozzle, and highly three dimensional secondary flow patterns are established as ambient fluid is drawn into the nozzle through the remainder of the exit plane.

The precessing motion is generated within the nozzle without any mechanical parts or acoustic coupling. The fluid is passed through an abrupt expansion, with a large expansion ratio, and reattaches asymmetrically to the nozzle wall downstream from the expansion. The pressure imbalances within the nozzle cause the resulting precession, and a small lip at the exit plane of the nozzle causes the jet to leave the nozzle at a large angle to the nozzle axis.

The postulate is supported by the experimental evidence, and is compared with the findings of other researchers who have investigated flow through abrupt expansions, and with acoustic, mechanical and fluidic means of jet excitation. The precession is found to occur at constant Strouhal Number based on the velocity at the throat, the step height at the upstream expansion and the precession frequency. The Strouhal Number is approximately 5×10^{-3} which is much lower than that typical of acoustic excitations, but is similar to those for two-dimensional mechanically and fluidically excited jets.

Half jet spreading angles of the order of 70 deg have been observed which indicates that very strong mixing is occuring. To provide quantitative measurement of the characteristics of the jet, an "entrainment shroud" was used to directly determine the rate of entrainment in cold flow, and flame stability was assessed in a combustion rig.

In order to sensibly compare the characteristics of the present nozzle with a simple nozzle it was necessary to introduce "equivalent" exit diameter and velocity scales, defined as the mean velocity and diameter of the instantaneous jet at the exit plane. Using these scales, the present nozzle has an entrainment appetite of approximately five times that of a simple nozzle and produces a flame with one fifth of the standoff distance and four times the blow-off velocity. This indicates a definite improvement in flame stability, which is consistent with the increased rates of mixing and spread angles observed in the cold flow experiments.

Contents

List of Figures

List of Tables

Statement of Originality

The material contained in this thesis is original and has not been submitted or accepted for the award of a degree or diploma at any other university. To the best of the author's knowledge and belief, no material which has previously been published or written by another person is included, except when due reference is made in the text of the thesis.

Permission to Copy

The author consents to the thesis being made available for loan and photocopying provided that it is accepted for the award of the degree.

Acknowledgements

I am very aware that without the help of many different people at various stages in the project, much of what is presented here would not have been accomplished. I am particularly grateful to my supervisor, Professor R.E. Luxton, for the enthusiasm for the project which he displayed, both prior to its inception, and throughout our involvement in it. His expertise and friendly advice made it a pleasure to work with him.

This project has involved a large amount of experimentation, and the manufacture of much equipment. Consequently I have been assisted by most of the technical staff in the Department from time to time, and have appreciated their cooperative spirit, technical skill and experience. I would particularly like to thank Mr. R. Jager, Senior Technical officer in charge of the workshop, for his valuable suggestions prior to the manufacture of equipment, and his supervision of construction. The assistance in the instrumentation of the experiments from Mr. H. Bode and Mr. G. Osborne is gratefully acknowledged, as is the help from the staff in the Holden Laboratory, Mr. S. De Ieso and Mr. M. Bethune.

Some experiments required facilities beyond the capacity of the Department, and I am grateful for the willingness of external organisations to allow me to utilise their equipment. All of the flow visualisation experiments in water were conducted in a water flume in the Department of Civil Engineering. A large number of the combustion experiments were conducted in a laboratory on the premises of the South Australian Institute of Technology's Adelaide campus. The remainder were conducted at the South Australian Gas Company, whose chief engineer, Mr. W. Iwanaki was most helpful in supplying relevant information on fuel properties. The mirrors used in the schlieren photography were loaned by the Defence Research Centre of Salsbury. All are acknowledged with thanks.

Many ideas were generated in discussion with members of staff and fellow post-graduate students. I would particularly like to thank Dr. D.M. Jenkins for some timely discussions.

Finally I wish to acknowledge the award by the South Australian Energy Council of the S. A. Energy Research Scholarship which provided financial support during the research.

Notation

A_{j-m} : Cross sectional area in exit plane of the entrainment shroud which is unoccupied by the jet.

B-M-C-E : Bell-Mouth-Contraction-Expansion

CCW : Counter-Clock-Wise

CW : Clock-Wise

d_0 : diameter of the supply pipe, upstream of the primary orifice

d_1 : diameter of primary, upstream orifice in the EMB nozzle

d_2 : diameter of secondary, downstream orifice in the EMB nozzle

d_{2eq} : the exit diameter of the MLC nozzle which is "equivalent" to that of a simple jet. It is defined as the diameter of the instantaneous jet at the exit plane.

d_e : exit diameter of a simple or EMB nozzle

D : diameter of cavity in EMB nozzle

D_i : outside diameter of insert

EMB : Enhanced Mixing Burner

f : frequency

f_p : frequency of precession

h_1 : step height of upstream, primary orifice

h_2 : step height of downstream, secondary orifice

Kt : an entrainment constant

l : length of cavity in EMB

L_e : Entrainment Length, ie. the distance between the exit plane of the nozzle. and the exit plane of the entrainment shroud

L_s : Shroud Length, ie. the length of the porous wall of the entrainment shroud.

LC : Long Cavity (nozzle)

$\dot{m}$: mass flow rate

MLC : Mid Length Cavity (nozzle)

O-C-O : Orifice-Cavity-Orifice (nozzle configuration)

P : Pressure (kPa)

P_d : Driving Pressure, ie. the pressure upstream of the nozzle

r_{half} : the radial distance from the nozzle axis to the "edge" of the jet, defined as the point where the mean axial velocity is one half of the centreline value

Re : Reynolds Number - defined as the characteristic velocity multiplied by the characteristic dimension and the density, and divided by the dynamic viscosity

S : angle (deg) of upstream Swirl vanes

St : Strouhal Number - a dimensionless frequency defined as the characteristic frequency multiplied by the characteristic length and divided by the characteristic velocity.

$\overline{u_{1a}}$: Measure of the mean axial velocity through the upstream orifice, based on ambient density, ie. $u_{1a} = \dot{m}/\rho_a A_1$

$\overline{u_{1c}}$: The mean axial velocity through the upstream orifice, based on compressible flow calculation.

$\overline{u_{1d}}$: The mean axial velocity through the upstream orifice, based on driving pressure, ie. $u_{1a} = \dot{m}/\rho_d A_1$

$\overline{u_{2eq}}$: The mean velocity through the equivalent exit diameter, d_{2eq}, ie. $u_{2eq} = \dot{m}/\rho_d A_{2eq}$

v_{bo} : Blow Off Velocity, ie. the mean exit velocity through the nozzle which is just sufficient to cause the flame to be extinguished

x_i : axial distance from the upstream orifice to the downstream face of the insert

x_{n1} : axial distance from the upstream orifice to the Upstream, Negative bifurcation line.

x_{n2} : axial distance from the downstream orifice to the Downstream, Negative bifurcation li

x_p : axial distance from the upstream orifice to the positive bifurcation line.

X_{so} : Stand-Off distance - axial distance from nozzle exit to flame front

Greek Letters

θ : the angle of the velocity vector with respect to the nozzle axis

μ : dynamic viscosity (kg/m.s)

ρ : density (kg/m^3)

ϕ : the expansion angle from the upstream orifice plate with respect to the nozzle axis

Subscripts

A : at upstream plane of entrainment shroud

a : based on atmospheric pressure

B : at downstream plane of entrainment shroud

d : based on driving pressure

i : of insert

m : at mouth of entrainment shroud

p : of primary flow

r : reattachment

s : of secondary flow, or separation

w : measured on wall

0 : of pipe upstream of nozzle

1 : at upstream orifice

2 : at downstream orifice

Chapter 1

Introduction

The quest for simple and efficient means of increasing the mixing and entrainment rates of a jet stems from the vital role which mixing plays in nearly all practical applications of jets. Vast amounts of time and money have been spent in the development of more compact thrust augmenting ejectors for use in V/STOL[1] aircraft [79,2][2], and in improving flame stability and combustion efficiency in furnaces and turbine combustors [90,80]. Whilst these are probably the best known applications of jets in which mixing is crucial, numerous others exist. These include unit mixing operations in chemical processing plants,eductors in steam plants and fluidic control systems.

The present thesis describes a nozzle, dubbed the Enhanced Mixing Burner (EMB), which produces a jet with mixing rates typically five times that of a simple jet. When used as a burner, it generates a very short, bulbous flame with stand-off distances an order of magnitude less than is typical of a simple lifted flame. The flow patterns which product the enhanced mixing are generated directly by the primary jet (ie. they are produced independently of any gross changes of flow patterns such as those produced by swirl) and operate throughout the entire flow range available in our laboratory; in terms of driving pressure this is 0–700 kpa. Thus, in classical combustion terminology, the EMB has continuous turn-down capability. Further, because of the intense mixing generated, the EMB virtually eliminates any need for pre-mixing the primary fuel with an oxidant, thus increasing safety and reducing costs.

[1] Vertical/Short Take Off and Landing

[2] In this thesis, the first reference to an article which is directly quoted is cited by the authors names and the date of the publication. Articles which are of passing interest are cited by a number in square brackets, [*Reference Number*].

The immediate application for which this nozzle has been developed is to improve flame stability when burning low grade fuels. This is particularly relevant to South Australia, which is currently preparing to utilise one of its sources of very low grade lignites [99,88,17] for electricity generation. The nozzle has not yet been tested or optimised for use with particulate fuels, but its geometric simplicity and insensitivity to dimensional changes of the order of ± 10 % suggests that the wear characteristics should be good. Burners based on the designs described in this thesis already possess the potential to further increase the viability of coal gasification by enabling a lower calorific value gas to be burned stably. This could enable a reduction or elimination of the expensive gas synthesis stages in the gasification process.

South Australia's coals are not only of low rank and high moisture content but when burned as a pulverised fuel they exhibit bad slagging, fouling and corrosion characteristics, due mainly to the high quantities of sodium, sulphur and chlorine. The reduction of the associated pollutants to an environmentally acceptable level, and the extra wear and maintenance to an economically viable level, are difficult and costly tasks [99]. Gasification offers significant advantages over pulverisation because it bypasses the expensive clean-up operations, such as flue gas scrubbing, which would otherwise be required. Flue gas scrubbing can increase the cost of a power station by one third.

Another important potential application of the nozzle occurs when a furnace is converted to burn, say, natural gas instead of oil. Because natural gas is both less dense and of lower calorific value than oil, such a change-over frequently requires the furnace to be de-rated in order to accommodate the new flame in the existing combustion space. The EMB produces a very short, intense flame, which remains stable with very high throughputs and consequently offers a potential solution to this problem.

1.1 Existing Methods of Producing Strong Mixing

Nozzles which are used to increase mixing and entrainment rates can be divided into two broad categories. The first use either an aerodynamic or a physical blockage (swirl[3] and bluff body flame holders respectively). The second has arisen since Brown and Roshko (1974) demonstrated that entrainment, mixing and combustion processes in a turbulent, plane mixing

[3]Claypole and Syred (1982) and others have shown that the dominant mechanism whereby swirl burners stabilize flames is by producing regions which approximate well stirred reactors and plug flow reactors by means of an aerodynamic blockage.

layer are dominanted by the dynamics of and entrainment by large-scale vortical structures, a fact that has been verified and extended by many others, eg. [22,50,62,63,64]. Nozzles in this category use some means to force, excite or control these naturally occurring structures. The more common examples include acoustic excitation [31,3], mechanical excitation [52] and fluidic excitation [95]. The EMB fits loosely into the second category, although no external excitation is involved.

The above types of nozzles, their respective advantages and disadvantages, and their relevance to the EMB, are discussed below.

1.1.1 Nozzles Which Generate Recirculation Zones

Swirl Burners and Bluff Body Flame Holders both stabilize the flame by producing a recirculation zone (RZ), which is a strong recirculating vortex just downstream from the nozzle exit plane. This is caused by imposing a strong adverse pressure gradient on the flow. Stagnation on a bluff body in the flow produces such a pressure gradient, and the subsequent separation causes the recirculation. Swirl burners produce the recirculating vortex and strong mixing by imparting a strong swirling motion to the secondary flow. The centrifugal motion of the air produces a radial pressure gradient across the jet, with a low pressure core. If the swirl is strong enough, the RZ is established [14]. Multiple swirl burners, employing both primary and secondary flow swirl, are more expensive but have application where a further increase mixing rates is required [41].

The RZ generated by a nozzle is greatly influenced by the geometry of the burner quarl [78] and the characteristics of the furnace [39,34,91]. Recirculation within a furnace may also be established by abrupt changes in furnace shape (eg. a sudden expansion [68]) or by using the secondary air to create an aerodynamic blockage, such as by injecting it annularly at a large angle to the axis [16]. Injecting the primary jet at large angles to the axis [49] also generates recirculation.

The nozzles discussed above all reflect that the establishment of a RZ has been a common aim in burner design for many years. However the mechanism which causes the improved flame stability has only recently been clarified. The influence of the RZ on a flame is complex and multi-faceted and it has been difficult to isolate the contributing factors. Furthermore, the relative importance of these factors depends somewhat on the type of nozzle, operating conditions, and fuel properties.

One of the earliest theories of the mechanism by which a RZ stabilizes a flame was proposed by Spalding (1953). He suggested that stable combustion occurs within the highly mixed RZ, and that the hot combustion products are then carried upstream and act as an ignition source for the rest of the flame. This mechanism is certainly important is some cases, as demonstrated by Ito and Sasaki (1984), who investigated a flame stabilized by the RZ formed behind the thick annular wall separating a fuel jet from the surrounding secondary air. They found that the RZ closely approximated a Well Stirred Reactor (W S R) and acted as a stabilizing pilot flame. In fact, the flame stability was dominated by the equivalence ratio[4] in the RZ rather than that of the overall mixture. Spalding also noted the importance of residence times within the RZ.

However, the establishment of a RZ is also accompanied by very high rates of mixing, and it appears that this is the most important factor in flame stabilization. Leuckel and Fricker (1976) and Fricker and Leuckel (1976), who investigated the characteristics of swirl stabilized flames, found that the improvement in flame stability gained by increasing the amount of swirl was due more to the increased mixing than to the increased reverse flow. Indeed flame stability was virtually independent of the size of the RZ, provided that some reverse flow was established. Several others [13,60,91] also note that there is no advantage to be gained by increasing swirl numbers, and hence RZ size, beyond a critical value which is mainly a function of burner geometry and fuel type. Kremer et. al. (1973) observed that it is possible to increase the size of the RZ to a point at which it becomes detrimental to flame stability by becoming longer than the flame, thereby causing cold air to be recirculated.

Claypole and Syred (1981,1982) have further strengthened the view that mixing enhancement is a more important factor in flame stability than is the amount of flow reversal. They measured the mass flow rates in the RZ of a swirling flame, and found that typically 5% of the total mass flow rate is recirculated, although it can be as high as 12%. As such, there is little true recirculation of gases, and they conclude therefore that the effect of the RZ as an ignition source is negligible. They propose instead that the result of producing a RZ, is to set up a series of Well Stirred Reactors and Plug Flow Reactors (WSRs and PFRs), which stabilize the flame through the increased mixing. This also implies that the increased residence time which occurs within the RZ alone will have little influence on the overall combustion efficiency. However, the increased residence times which occur within the WSRs and PFRs will affect a

[4] actual fuel:air ratio normalised by stoicheometric fuel:air ratio

much larger percentage of the total fuel. Residence times are only of real significance with particulate or liquid fuels where devolatilization and evaporation respectively influence burnout [14,27,55,98].

Bluff bodies are also known as "flame holders", because they generate a low velocity wake on which a flame is able to be supported [14]. The component of velocity normal to the flame front must be equal to the flame speed, and so it can be seen that low mean velocities are also important in flame stability.

The role of the solid body or aerodynamic blockage in causing mixing can also be explained in terms of interactions between streamwise and helical vorticity in swirling flow, a process which causes the "vortex bursting" phenomenon [56,23].

The present investigation indicates that the EMB generates very intense mixing and regions of instantaneous flow reversal, but without the establishment of a mean RZ. In the light of the previous investigations however, this does not appear to be a disadvantage. It is possible to conclude from them that high rates of mixing and low mean velocities are the essential characteristics produced by a high-stability nozzle. Whilst the establishment of a RZ will be accompanied by these phenomenon, it is not an essential feature itself.

Although swirl burners are capable of producing increased rates of mixing, they have significant disadvantages. Swirl burners require swirl vane arrangements which have become very complex in many commercial burners, and they are subject to serious instabilities. Fricker and Leuckel found that they could produce two types of stable flame depending on whether the fuel jet penetrated the RZ or not. Powerful oscillations between these two quasi-stable flame types can occur due to interaction between the furnace and burner. It is also possible to have an unstable flame if the swirl is insufficient to ensure that a RZ always occurs. Furthermore a Precessing Vortex Core (PVC) is generated by swirl burners, between the Reverse Flow Zone (RFZ) and the surrounding swirling flow. Claypole and Syred (1982) note that whilst the PVC improves mixing within the flame, it can also cause major problems if it couples with oscillations (eg. acoustic modes) within the furnace. They observe that the minimum swirl number required to generate a RZ increases as Reynolds Number decreases. As a consequence, when using smaller nozzles or fuels with low flame speed, it becomes necessary to use higher swirl numbers, with an accompanying increase in pressure loss through the burner.

1.1.2 Nozzles Which Amplify Existing Flow Structures

All the nozzles discussed in this section use some means of amplifying large, naturally occurring flow structures. However, they amplify different types of structures. Acoustic nozzles excite structures formed in a wake, shear layer or separation region. Fluidically and mechanically excited jets amplify much larger scale "flapping motions" of the jet. The EMB is similar to this class of nozzles in that it stimulates a large scale "precession" of a three dimensional jet, which is the axi-symmetric analogue of a two-dimensional (2-D) flapping jet.

Acoustic Resonance Nozzles

The nozzles discussed in this section use the well known phenomenon of acoustic feedback [83,84] to excite naturally occurring, large-scale vortex structures. Crow and Champagne (1971) examined the axi-symmetric structures which occur in a circular jet under the influence of acoustic forcing. They found that maximum response occurred at a Strouhal No. ($St = fd/u$) of 0.3.

Hill and Greene (1977) developed a self exciting acoustic nozzle, using a concentric annular pipe, which resonates in an 'organ pipe' mode, to act as the acoustic source. The resonance is driven by the vortices shed in the region of flow separation which occurs at the upstream end of the annular pipe. In this way, significant increases in entrainment rates are obtained. This, and similar configurations, was investigated in more detail by Hussian and Hasan (1983).

Abell (1977) used a hot-wire anemometer (measuring the frequency of the large scale structures through their disturbance of the irrotational flow close to the jet exit) in conjunction with a phase-lock-loop, feeding back to a loud-speaker in the settling chamber upstream of the nozzle, to produce greatly enhanced mixing. He and Luxton (1979,1980,1981) then developed another form of self exciting acoustic nozzle, hereafter referred to as the 'Abell nozzle'. This nozzle is discussed more fully in Chapter 3.

Although acoustic excitation can be used to generate very strong mixing, it has one major disadvantage. The vortex shedding occurs at constant Strouhal Number, and consequently its frequency is proportional to the flow velocity. However the resonant chamber or cavity will resonate only at a few discrete frequencies [45], and so the enhanced mixing can only occur at a few critical velocities. Thus, even though a resonance is strong enough to cause the Strouhal frequency to "lock on" to the resonant frequency for a range of velocities either side of the critical velocity [96,97], these nozzles have a limited operating range. This small 'turn-down

ratio' renders acoustic nozzles unsuitable for most practical applications [58].

Fluidically and Mechanically Excited Jets

The nozzles in this section aim to destroy flow symmetry by the excitation of large scale motions of the whole jet. Bradbury and Khadem (1975) have showed that a circular jet would spread more rapidly if small obstacles were introduced into the nozzle to destroy the axi-symmetry of the flow.

Cervantes de Gortari and Goldschmidt (1981) identified an apparent flapping motion of a two dimensional, plane,unexcited jet. The motion, which can be attributed either to a lateral oscillatory motion or to an asymmetric coherent structure within the jet, is concealed within the random fluctuations of the turbulent field and can be found only by long time statistical averages. The Strouhal Number[5] of the oscillation based on nozzle height and mean exit velocity, was found to varied with distance downstream, and was of the order of 0.01–0.08. This is much less than the Strouhal No. associated with acoustic excitations which is typically 0.2 to 0.3.

Both the mechanically and fluidically excited jets appear to amplify these naturally occurring instabilities. The most effective flapping motion is found to be driven at a Strouhal Number which closely approximates that of the unexcited case. Lai and Simmons (1985) used a laterally oscillating vane to excite a 2-D jet over the range $0.0016 < St < 0.0048$. Phase-averaged velocity profiles were obtained using a rake of five hot wires. Binder and Favre-Marinet (1981) also used mechanical means to excite a 2-D jet for $0 < St < 0.062$. Piatt and Viets (1979) measured a fluidically excited jet using conditional sampling at $0.0081 < St < 0.0363$. Favre-Marinet et. al. (1981) used the coanda effect to excite a flapping jet for $0 < St < 0.03$.

The EMB, which is axi-symmetric, produces a low frequency precession (the axi-symmetric equivalent to the flapping of a 2-D plane jet) at a Srouhal number[6] $St = fh_1/u_1$ of the order of 0.005. Thus the EMB appears to excite a large scale motion of the same character as that of the two-dimensional flapping jet discussed above.

The EMB has several advantages when compared with fluidically and mechanically excited jets, largely because it is three dimensional. There are many more practical applications for circular jets than for plane jets. Furthermore, because a circular jet has a larger surface area

[5] $St_h = fd/U_0$

[6] h_1 is the height of the primary orifice "step"ie. $(D - d_1)/2$

per unit volume than a plane jet, it can achieve much greater mixing rates. However, it is very difficult to use mechanical or fluidic means to excite a circular jet radially or asymmetrically. In fact no such examples have been found in the literature. In the EMB the excitation occurs naturally and so avoids the maintenance and wear problems which are associated with mechanically and fluidically excited jets.

Chapter 2

Apparatus

In this chapter is described the equipment which is general to most experiments. The details of apparatus which is specific to a particular experiment or application are given in the relevant section.

2.1 The Cold Flow Rig

The cold flow rig is illustrated in Figure 2.1. The air is supplied from the laboratory compressor. Two orifice plate flow-raters and control valves enable the primary flow through the nozzle, and the secondary flow through the "entrainment shroud", to be independently metered and controlled. The pipe work is arranged so that air through the "calibration nozzle" can be supplied through either of the orifice flow-raters. In this way they can be independently calibrated.

The cold flow nozzle, details of which may be found in Appendix B, was made from perspex to aid in flow visualisation experiments. The nominal cavity diameter selected was 90mm, corresponding to 100mm (outside diameter) tubing, which was readily available, and of a scale large enough to enable accurate positioning of probes etc. The cavity length, l, was easily adjusted by sliding the perspex "cavity pipe" over the "O" ring at the upstream orifice, the upstream and downstream orifice plates were removable and hence, any step-wise combination of orifice plate dimensions and cavity length were available.

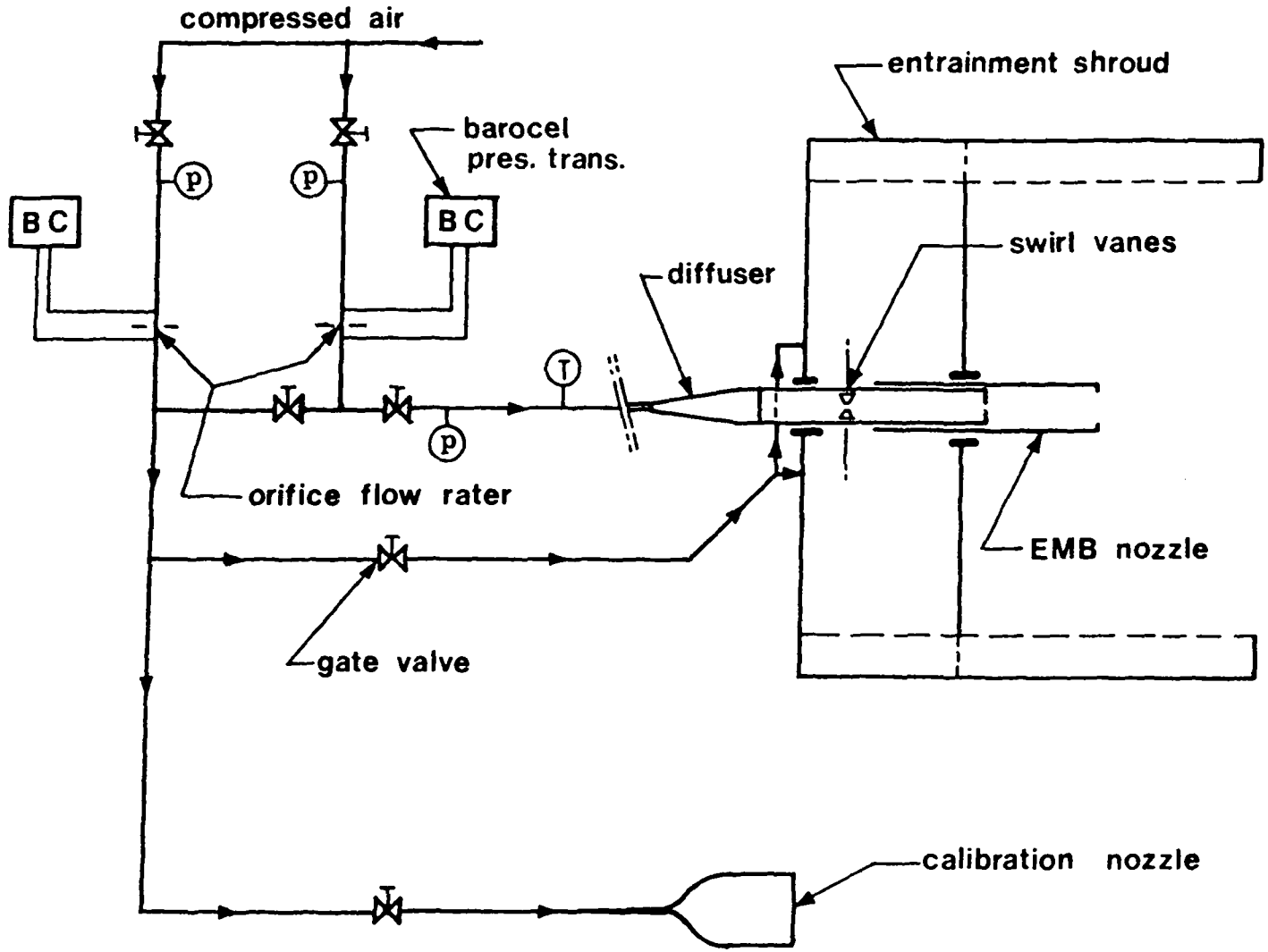

Figure 2.1: The Cold Flow Rig

2.1.1 The Diffuser

A diffuser was required to connect the 90mm nozzle to the 3/4 inch supply pipe. As shown in Figure 2.1, a conical diffuser with a diffusion half-angle of approximately 8 deg was used. It was necessary to ensure that the velocity profile at the exit of the diffuser was not triggering the asymmetric flow patterns within the nozzle.

It is not possible to achieve a fully developed pipe velocity profile at the exit of a conical diffuser with such large expansion ratios [37], nevertheless it is possible to achieve no *separation* within the diffuser. To ensure that fully attached flow was indeed occurring, total and static pressure profiles were measured at the diffuser exit plane. The results of these measurements are shown in Figure 2.2. It can be seen that the length of the pipe upstream of the diffuser has a significant influence on the profile at the exit plane and that there is good collapse of the data obtained for two different flow rates. The profiles do not indicate zero velocity at the edge of the diffuser because the pitot tube is too large an instrument to measure the velocity sufficiently close to the wall. Furthermore, because the static tube has the static pressure holes some 30mm (ten diameters) from the tip of the instrument, to measure the static pressure at the exit plane of the diffuser required the insertion of the probe into the diffuser. Consequently, because the probe was parallel to the diffuser axis, it was not possible to measure P_s at the edge of the diffuser, and extrapolated values were used[1].

It can be seen from Figure 2.2 that a larger percentage of the momentum is concentrated near the axis of the diffuser than is the case for fully developed pipe flow. Nevertheless, there is no evidence of reverse flow, or flow separation near the diffuser wall. To allow partial recovery towards a fully developed velocity profile at the entrance plane of the nozzle, a six diameter length of large diameter pipe was inserted between the diffuser and the nozzle.

In all of the experiments, the longer upstream pipe ($l/d = 80$) was used. However, the nozzle still operated with the shorter pipe and, in the smaller scale nozzles, without a diffuser, indicating that the dependence of the mechanism upon conditions upstream of the nozzle is not significant.

[1]This extrapolation was felt to be justified because the static pressure was very close to atmospheric near the wall at the exit plane, and was also significantly smaller in magnitude than the total pressure.

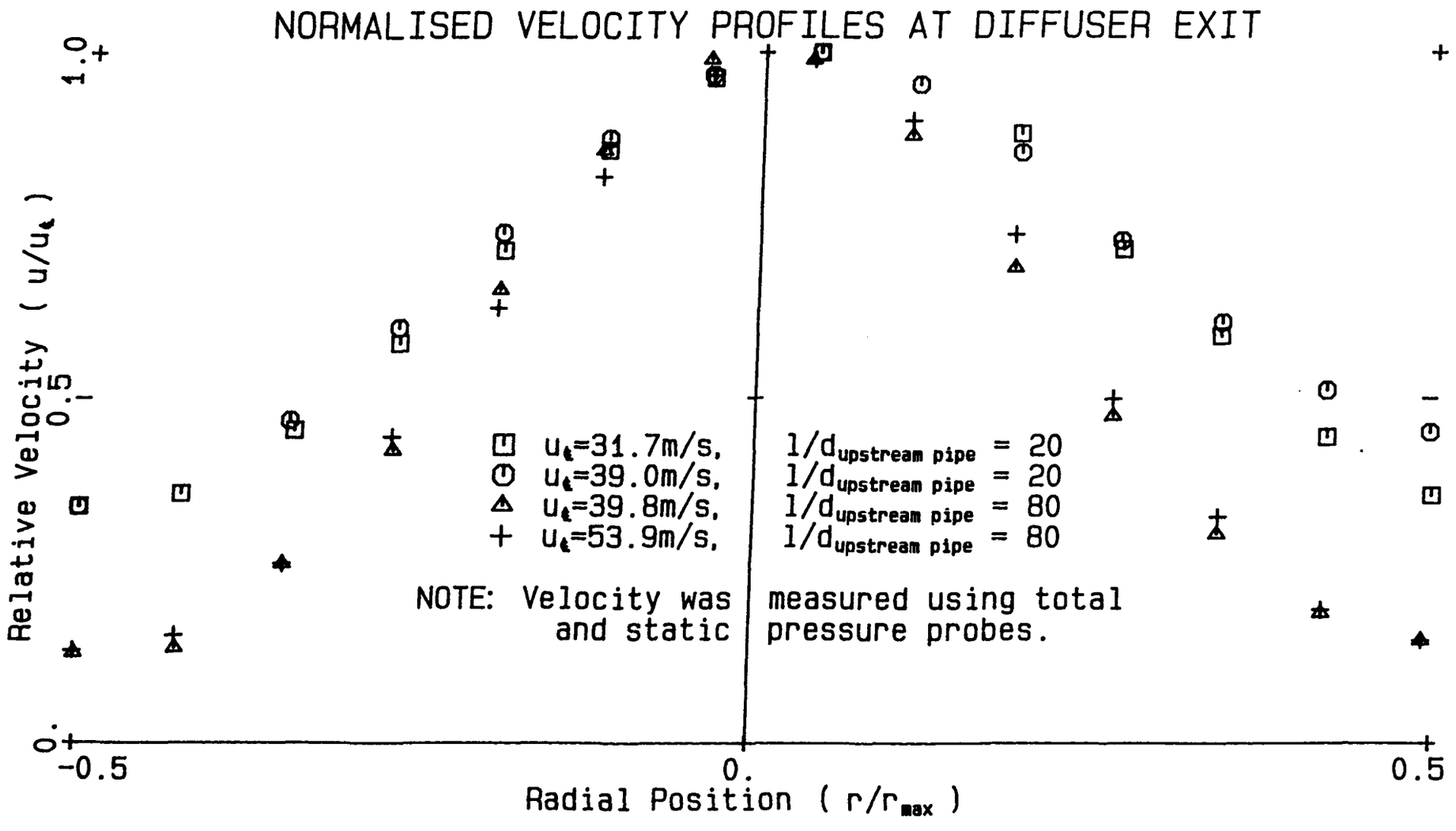

Figure 2.2: The Velocity profiles at the exit of the diffuser used in the cold flow rig, obtained from Total and Static Pressure profiles

2.1.2 The Calibration Nozzle

The "calibration nozzle" is a 2-D nozzle of rectangular cross section which produces an extremely uniform velocity profile. Its characteristics are described in detail by Lee (1984). If the velocity profile at the exit plane is uniform, it is possible to measure the mass flow rate by taking only a single point measurement at the nozzle exit plane, knowing the exit area. In this way the orifice flow raters can be independently calibrated. It is also possible to calibrate hot wire probes against a pitot static probe in the flow.

To test the uniformity of the velocity profile at the exit plane, a series of total and static pressure measurements were made. Static pressure profiles in the streamwise (x) and cross-stream (y, z) directions indicated that deviations of static pressure from atmospheric were negligible which implies that a pitot-static probe will yield accurate measurements of velocity, despite the fact that total and static pressure are measured at slightly different streamwise stations.

The profiles taken with the pitot-static probe, Figure 2.3(a), clearly show that the velocity profile at the exit plane of the calibration nozzle is indeed highly uniform. Note that these profiles also show the effect of placing a "three-wire-probe" in the nozzle. This probe was also used by Agarwal (1986), and is a means of determining instantaneous positive or negative flow direction. It was considered for use in this investigation as a means of determining the precession frequency, but was proved not to be suitable.

2.1.3 Calibrating the Orifice Flow Raters

The orifice flow raters were designed according to British Standard 1042. However, to ensure accuracy of results, they were calibrated against the flow through the two-dimensional "calibration nozzle" discussed in Section 2.1.2. The mass flow rate through the calibration nozzle was calculated from the relation $\dot{m} = \rho \bar{u} A$. Because the velocity profile at the exit plane is so uniform, $\bar{u}$ is closely approximated by a single point measurement using a pitot-static probe.

The mass flow rate through the orifice flow raters, calculated according to BS 1042 using the relationship $\dot{m} = C\sqrt{Ph/T}$, where P and T are the absolute pressure and temperature upstream of the gauge respectively, h is the pressure drop across the orifice plate and C is a constant, deviated from the measured value by 0 — 20 % over the operating range. Hence a correction factor was applied to the calculated value. The calibration curve is shown in

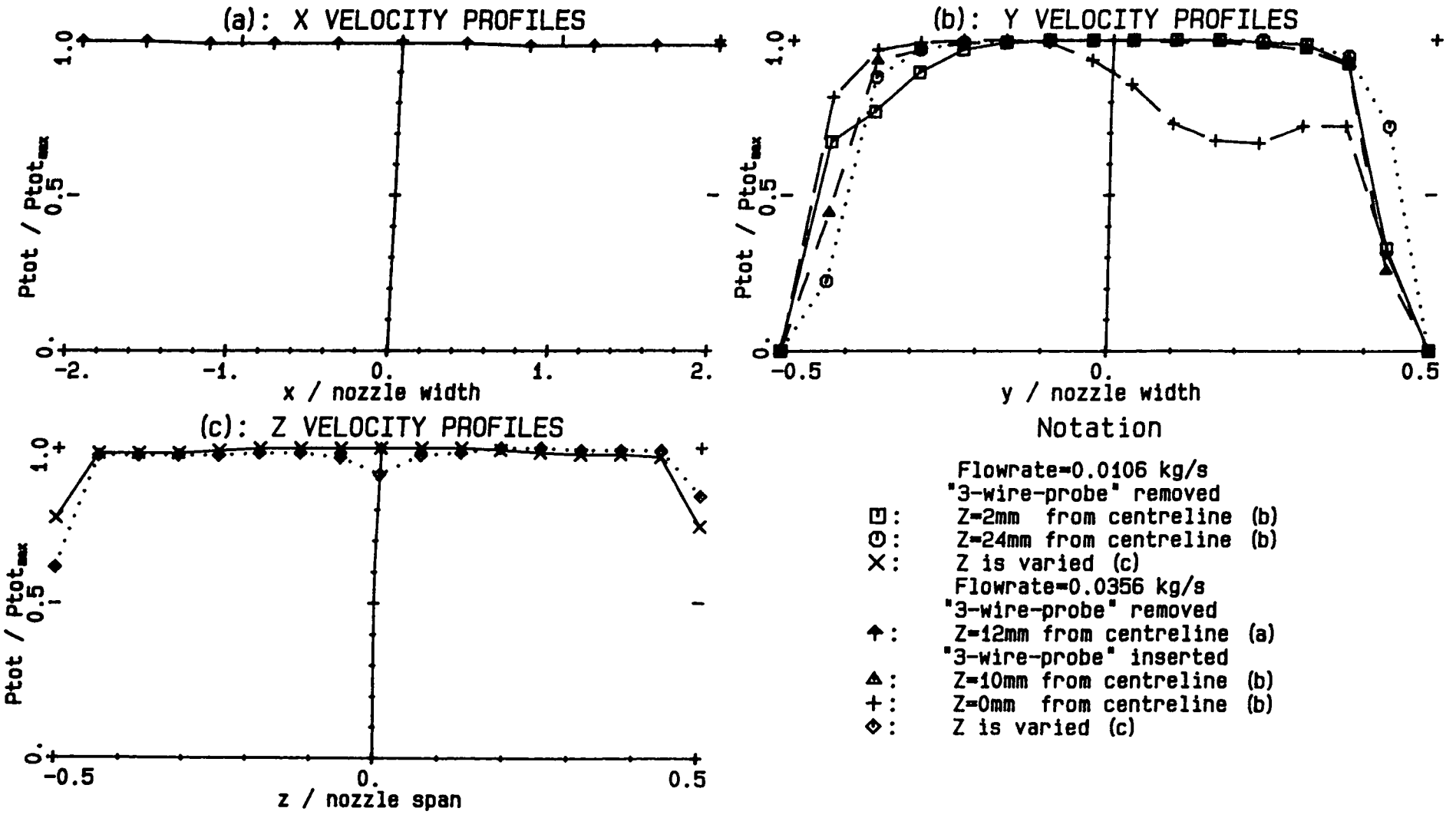

Figure 2.3: The pressure profiles of the calibration nozzle

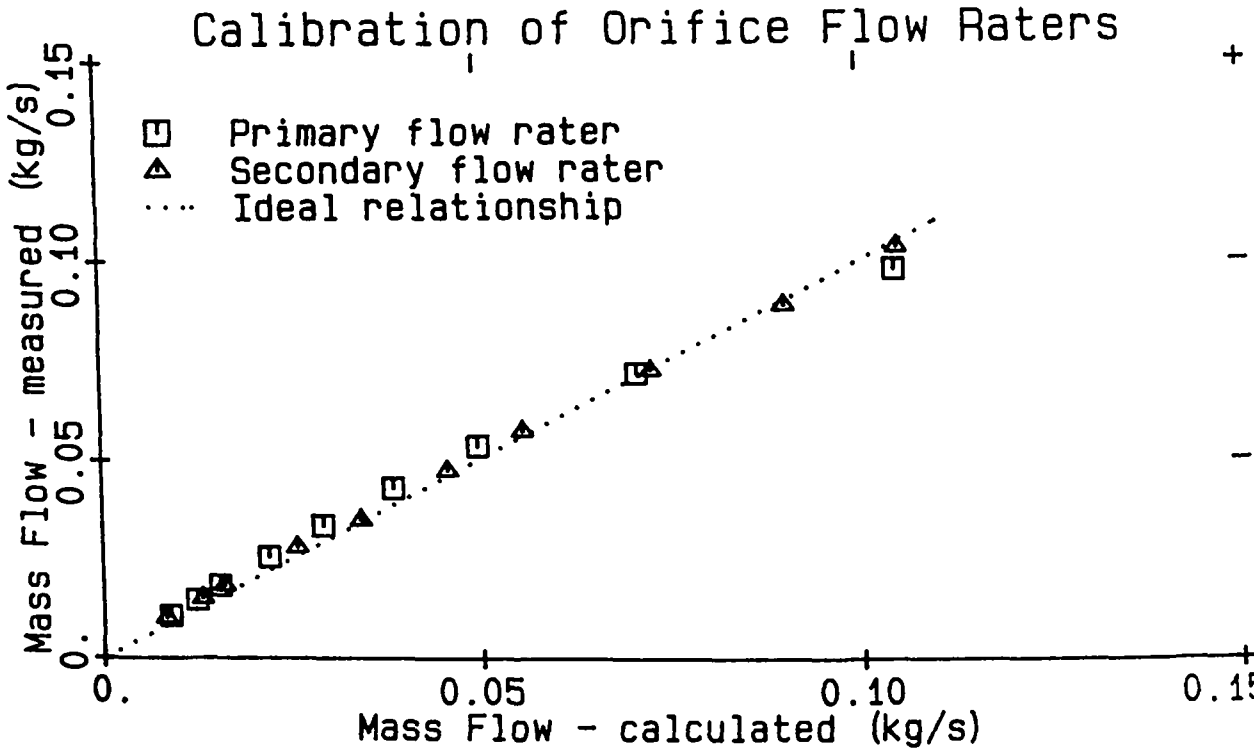

Figure 2.4: Calibration of the Orifice Flow-rater.

Figure 2.4. The discrepancy between the measured and calculated values is at least partly accounted for in the size of the orifice plate, d_0, relative to that of the pipe, d_p. The primary orifice flow rater, which deviates further from the calculated value than does the secondary flow rater, has a ratio, $d_0/d_p = 0.70$, that is right on the upper limit of acceptable BS1042 sizes. (Note that this ratio was selected to achieve minimum pressure loss). The secondary flow rater has a smaller orifice size ratio, $d_0/d_p = 0.43$, and so gives greater accuracy at the price of a greater pressure loss.

2.1.4 Combustion Apparatus

The combustion apparatus has been designed to enable the fuel (natural gas or liquid petroleum gas) to be safely premixed with either an oxidant (oxygen) and/or an inert (nitrogen or carbon dioxide). Dilution of the fuel with an inert is to enable the simulation of a fuel of lower calorific value. Premixing with an oxidant is often necessary in industry to improve flame stability, and so its influence was also investigated. The nozzle used in all of the detailed investigations has a cavity diameter of $D = 13$mm, which was small enough to limit the usage of bottled gas to a reasonable value. Detail drawings of this nozzle can be found in Appendix A.

The apparatus is shown in Figure 2.5. Safety features include

- A large capacity exhaust fan, which prevents unburned gas from collecting in the laboratory.
- An interlocking solenoid valve in the fuel line. The solenoid is only activated when a "leaf switch", placed in the exhaust duct, is switched on by an adequate flow of air within the duct.
- A flame trap to extinguish a flame in the line, in the event of flashback.
- Low internal volume variable area flow raters each metering individual gases only.
- Non-return valves on each line upstream of the mixing junction to prevent a mixture of gases occurring in any of the flow-raters.
- A low internal volume, high heat conducting, copper coil flow-rater for metering the gas mixture when the bypass dump was used. (See below.)
- A quick acting purge valve to purge the lines of air or oxygen thoroughly with an inert gas prior to the opening of the fuel valve. It can also be used to extinguish the flame.
- All apparatus is located behind a polycarbonate screen, and the flame is remotely ignited using a spark igniter.

The coil flow rater has been previously developed by Nathan (1983) and Nathan and Luxton (1984) for the safe metering of combustible mixtures. It has been found that the coiling of a pipe causes a strong secondary flow to stabilise the main flow [87], and to effectively eliminate the unpredictable pressure drop characteristics associated with the transition between the laminar and turbulent flow regimes. The pressure drop across the coil then gives a unique measurement of flow-rate. The coil is made of copper tubing of a smaller diameter than that of the nozzle. In the event of a flash-back, it acts not only to quench the flame because of the high heat transfer properties of copper, but also as a flame trap. Flash-back occurs when the flame speed of the mixture is greater than the mean exit velocity of the nozzle. However, at the coil, the flame front encounters an increased velocity of the mixture due to the reduction in cross sectional area. If the velocity ratio is sufficiently high, it will prevent the propagation of the flame. Note that the geometry of the MLC nozzle provides an inherent flame trap, because $d_1 \ll d_2$, and a further "pepper pot" trap and a non-return valve are placed between the coil flow rater and the burner.

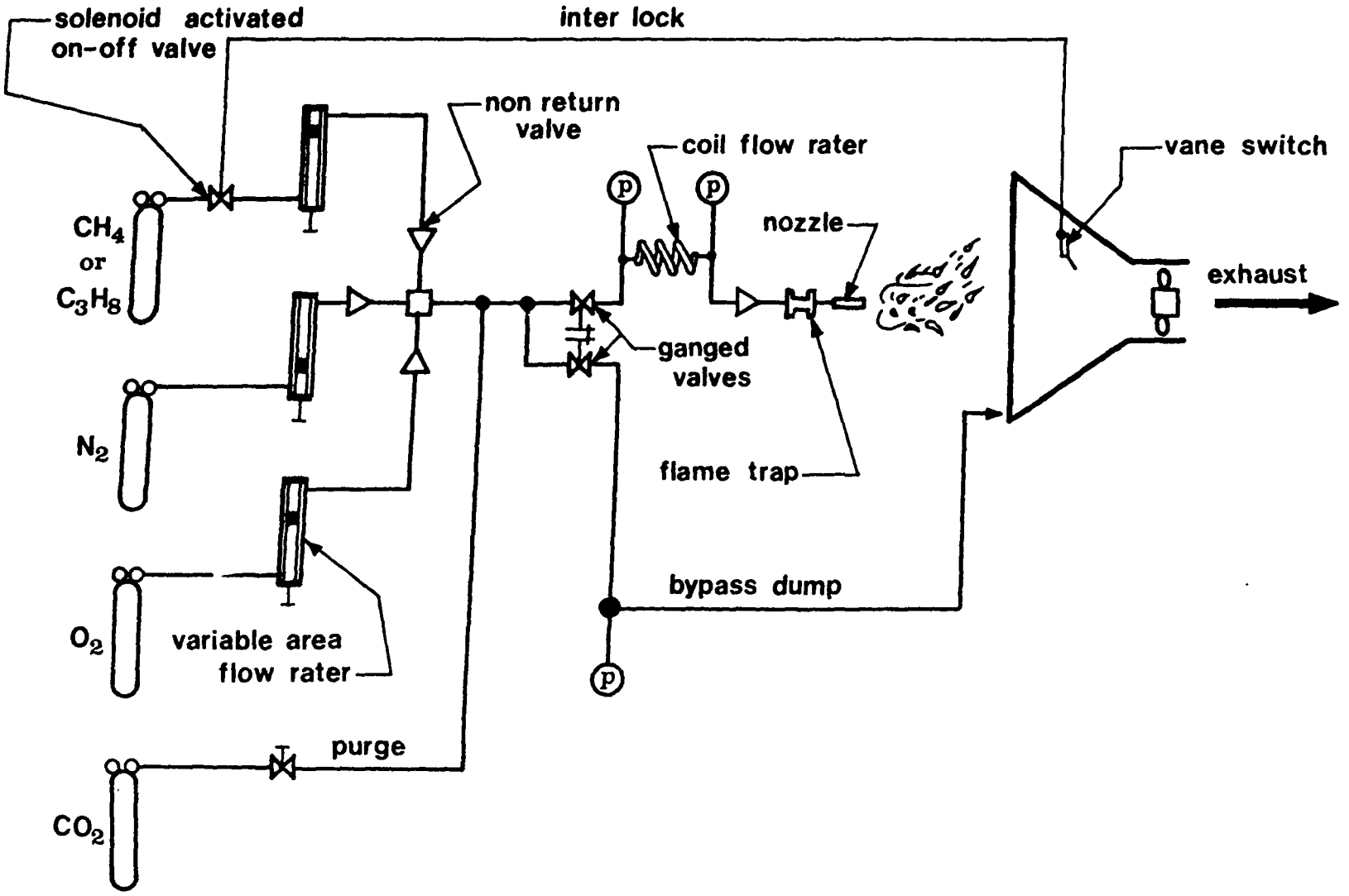

Figure 2.5: The Combustion Rig

Chapter 3

The Family of Enhanced Mixing burners

3.1 Introduction

A family of Enhanced Mixing Nozzles has been developed at the University of Adelaide, arising from the Abell nozzle [4,5,6]. All have the characteristic Orifice-Cavity-Orifice (O-C-O) geometry, shown in Figure 3.1, but generate different flow patterns and involve different mechanisms. Consequently the ratios of the characteristic dimensions, vis. d_1/D, d_2/D and l/D, are different in each case. Figure 3.2 illustrates the ratios of the dimensions associated with each nozzle.

The three nozzles are:

- Abell nozzle — which uses acoustic excitation.
- Mid Length Cavity (MLC) nozzle — which generates a precessing jet following an asymmetric reattachment of the instantaneous primary jet to the cavity wall within the nozzle. The instantaneous jet *does not* fill the exit plane of the nozzle, through which it leaves at a large angle.
- Long Cavity (LC) nozzle — which appears to generate a precessing jet similar to the MLC nozzle, except that it *does* fill the exit plane and it does not leave at such large angles.

It is well known that increased rates of mixing and increased spreading angles usually occur simultaneously. Such events will be accompanied by a more rapid decay in the centreline

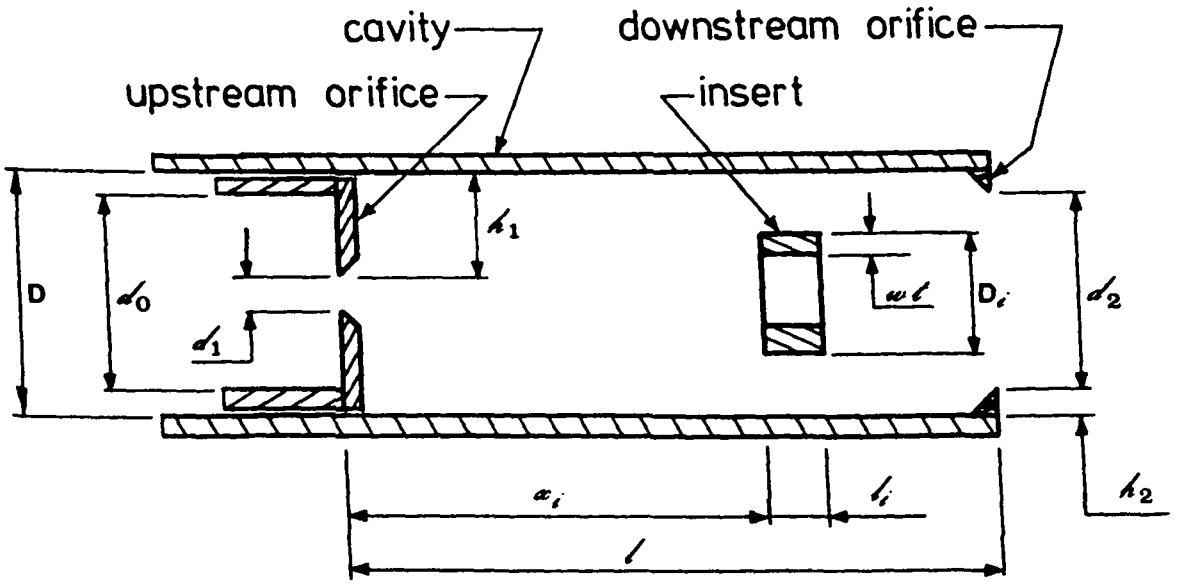

Figure 3.1: A Schematic diagram of all Orifice-Cavity-Orifice nozzles

velocity of the jet provided that the jet retains the bell-shaped velocity profile of a simple jet. Consequently, Hill and Greene (1977) and others (eg. [12]), measure centreline velocity to indicate the degree of improvement in the mixing rates of their nozzle. The simplicity of this technique allows a wide range of configurations of the O-C-O nozzle to be scanned reasonably quickly to indicate their relative performance and operating ranges.

Figure 3.2 is based on a series of single point measurements of centreline "velocity". The centreline total pressure was measured at a fixed number of nozzle diameters from the exit plane, for five driving pressures, as the cavity length was varied for each combination of orifice plates. Sufficient total and static pressure profiles were measured and recorded to ensure that similarity of jet profiles was approximated for each range of geometries; see for example Figure 8.2. From such measurements it may be concluded that a more rapid decay in centreline velocity indicates a more rapidly spreading jet and stronger mixing.

Whilst the MLC nozzle has been found to have the best performance characteristics of the three nozzles compared in Figure 3.2, and thus forms the bulk of this presentation, the early part of the present investigation was focused on the other two versions. For this reason, and for the sake of completeness, the Abell and the LC nozzles are discussed below in relation to the MLC nozzle.

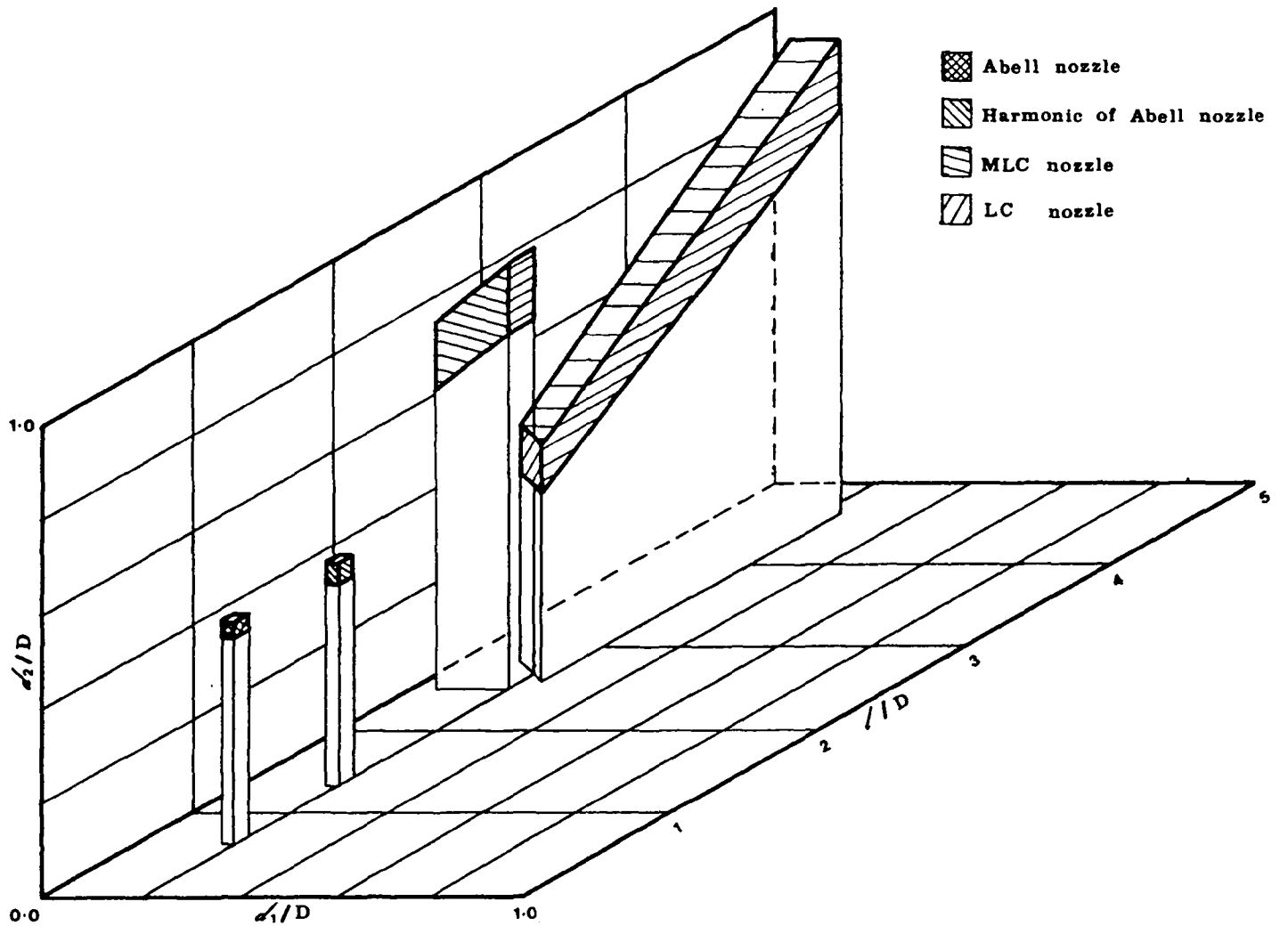

Figure 3.2: The Geometric Ratios of each member of the family of Orifice-Cavity-Orifice nozzles

3.2 The Abell Nozzle

The Abell nozzle was developed and documented by Abell and Luxton [4,5,6,58]. It utilizes the well known acoustic feedback mechanism [83,84], where a downstream acoustic source, in this case the cavity, couples with an upstream Strouhal shedding, in this case from the upstream orifice. The dimensions of the nozzle are ingeniously selected so that the Strouhal shedding from the first orifice will match and drive one of the resonant modes of the cavity, primarily the (0,1) radial mode. This resonance in turn reinforces and strengthens the shedding. These highly organised vortices then impinge on the second orifice, producing an extremely strong and self sustaining shedding. The resultant flow generates very strong mixing, which appears to be strong enough to induce reverse flow in the jet.

As can be seen from Figure 3.2, the Abell nozzle has a relatively short cavity. Its optimum dimensions, selected to give the best combination of mixing enhancement and turn-down ratio, are [58]:

$$d_1/D = 0.2, \quad d_2/D = 0.45, \quad 0.6 \leq l/D \leq 0.7$$

A detailed investigation of the effect which varying cavity length has upon flame stability revealed an important aspect of acoustically driven nozzles not covered by the research of Abell and Luxton. It is well known that the number of possible resonant modes of a "room" increases with the volume of the room [61]. Similarly, it can be seen from Figure 3.3 that as the length of the cavity is increased, to the order of twice the optimum length determined by Abell, so the number of resonant modes which are able to couple with the Strouhal shedding also increases. The effect of these extra resonant modes can be seen in Figure 3.3. As the flow rate is increased from zero, several zones of both stable and unstable combustion are encountered. Extensive acoustic spectra, taken in conjunction with the combustion experiments, revealed that all zones of improved flame stability within the range of acoustic nozzles ($0.45 \leq l/D \leq 1.5$) were accompanied by a strong acoustic resonance. This was detected by the appearance of a peak in the sound pressure level (SPL) spectrum at a discrete frequency. The results are archived in the department of Mechanical Engineering, the University of Adelaide.

Whilst the extra resonances which occur at longer cavities mean that a stable flame is possible for a larger operating range, the nozzle is still unsuitable for combustion applications. The various resonances are not of the same strength, and do not produce the same level of stabilization. Furthermore, the flame shapes which they produce are not identical. Consequently,

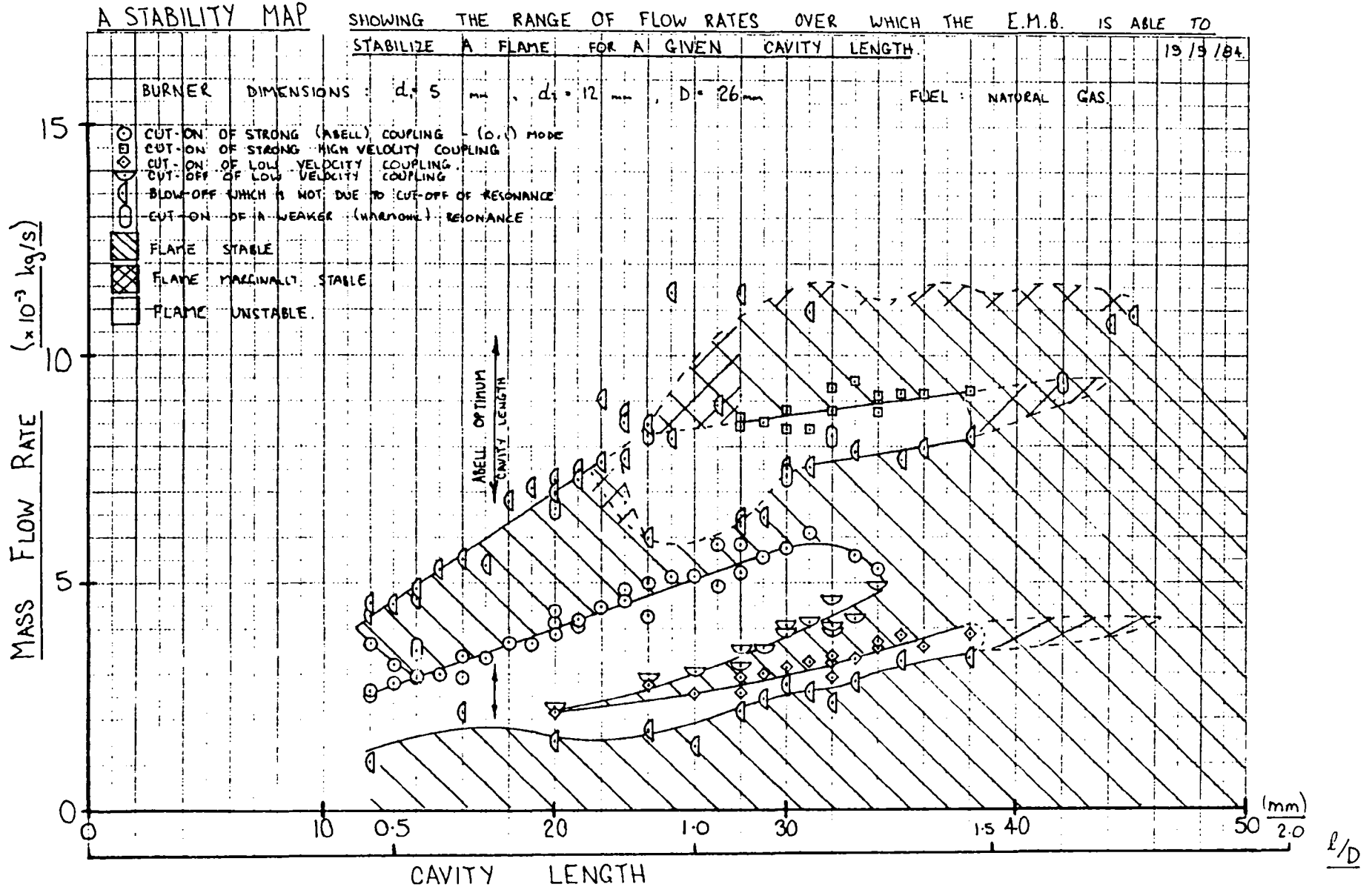

Figure 3.3: Flame stability zones of an O-C-O Acoustic Nozzle

even if it were possible to overlap the various zones of stability (which seems extremely unlikely) serious combustion oscillations would be likely to occur between the adjacent modes. It appears that limited turn-down ratios are an inherent feature of all acoustically excited nozzles.

A summary of the results of the present investigation associated with acoustic nozzles is given below, for $d_1/D = 0.2$ and $d_2/D = 0.45$.

1. Acoustically induced enhanced mixing occurs throughout the dimensional range: $0.45 \leq l/D \leq 1.5$.
2. For $l/D < 0.45$ acoustic resonances are detectable, but do not cause an improvement in flame stability.
3. For $0.45 \leq l/D < 0.8$ "cut-on" of an acoustic resonance (presumably the (0,1) mode with or without coincident modes as found by Abell and Luxton for $0.6 \leq l/D \leq 0.7$) occurred over a single operating flow range, and was associated with a dramatic improvement in flame stability.
4. For $0.8 \leq l/D \leq 1.5$ different acoustic resonance can be excited over different flow ranges. This results in several zones of stable and unstable combustion in the operating range of a single geometry. The flame shape in each range is different.
5. A "cut-on" of flow patterns which produce improved flame stability is always accompanied by an acoustic resonance.
6. Flame blow-out is not necessarily accompanied by a corresponding "cut-off" of an acoustic resonance.

3.3 The Long Cavity Nozzle

The Long Cavity (LC) nozzle generates intense mixing, and a rapidly spreading jet throughout its entire operating range. Detailed acoustic spectra indicate that the enhanced mixing is not generated by acoustic feedback. No dominant frequencies are present, and no sudden change in the spectrum, or jet (and flame) shape, occurs in any part of the operating range, as would be expected if an acoustic resonance is important. Thus the LC nozzle does not suffer from the problems of limited turn-down ratio associated with acoustic nozzles.

The nozzle is also insensitive to minor changes in dimensions, of the order of ±10%, giving it excellent wear characteristics. Furthermore, although optimum geometric ratios exist, the phenomena associated with these nozzles will occur for a large number of O-C-O dimensions. In retrospect it is probable that the discovery of the MLC nozzle, with its even greater enhancement and flame stability, led to the premature cessation of experiments on the LC nozzle. For this reason, although a large number of LC nozzles have been tested, the limits of geometric configuration have not been exhausted and it cannot be claimed that the nozzle has been optimised. Nevertheless, the dimensions shown in Figure 3.2 are representative of the LC nozzle.

The total and static pressure profiles shown in Figures 8.1 and 8.2 clearly show that there is no recirculation zone in the jet, and it behaves as a rapidly expanding simple jet with a bell-shaped velocity profile. This is in contrast to the pressure profiles obtained using the MLC nozzle, shown in Figure 4.7, whose profiles indicates that, on average, higher velocities occur at the jet edge than on the jet centreline in the region of the exit plane. The expansion angles of the LC nozzle can be determined using the velocity profiles based on r_{half}[1] because the true edge of the jet is very difficult to determine. The jet half width has been plotted at various distances downstream for twelve configurations of LC nozzle. The resulting jet profile is shown in Figure 3.4. Although insufficient profiles were measured for these results to be conclusive, they indicate that half jet spreading angles are of the order of 28 deg from the nozzle centreline. This is significantly greater than the spreading angles of a simple jet which are typically 4 deg. (See eg. [93] page 110.) Although not strictly comparable in terms of entrainment rate, its spreading angles are the same order as the 33 deg obtained by Badri Narayanan and Raghu (1982), who used a vibrating vane to excite a plane two-dimensional jet.

The optimum geometric ratios obtained from the combustion experiments agreed well with those obtained from the cold flow experiments (see Figure 8.8). The combustion experiments also showed that reductions in stand-off distance and of the fluctuation in standoff distance by factors of about 2.5 were achieved by the LC nozzle when compared with a simple nozzle. However this improvement was not nearly as great as that obtained with the MLC nozzle, which was more than an order of magnitude better. These results are shown in Figures 3.5 and 3.6. Neither of the EMB's produced a significant improvement in mean Blow-off velocity based on exit conditions, Figure 5.10. However, these combustion results must be interpreted

[1] r_{half} is the half width of the jet

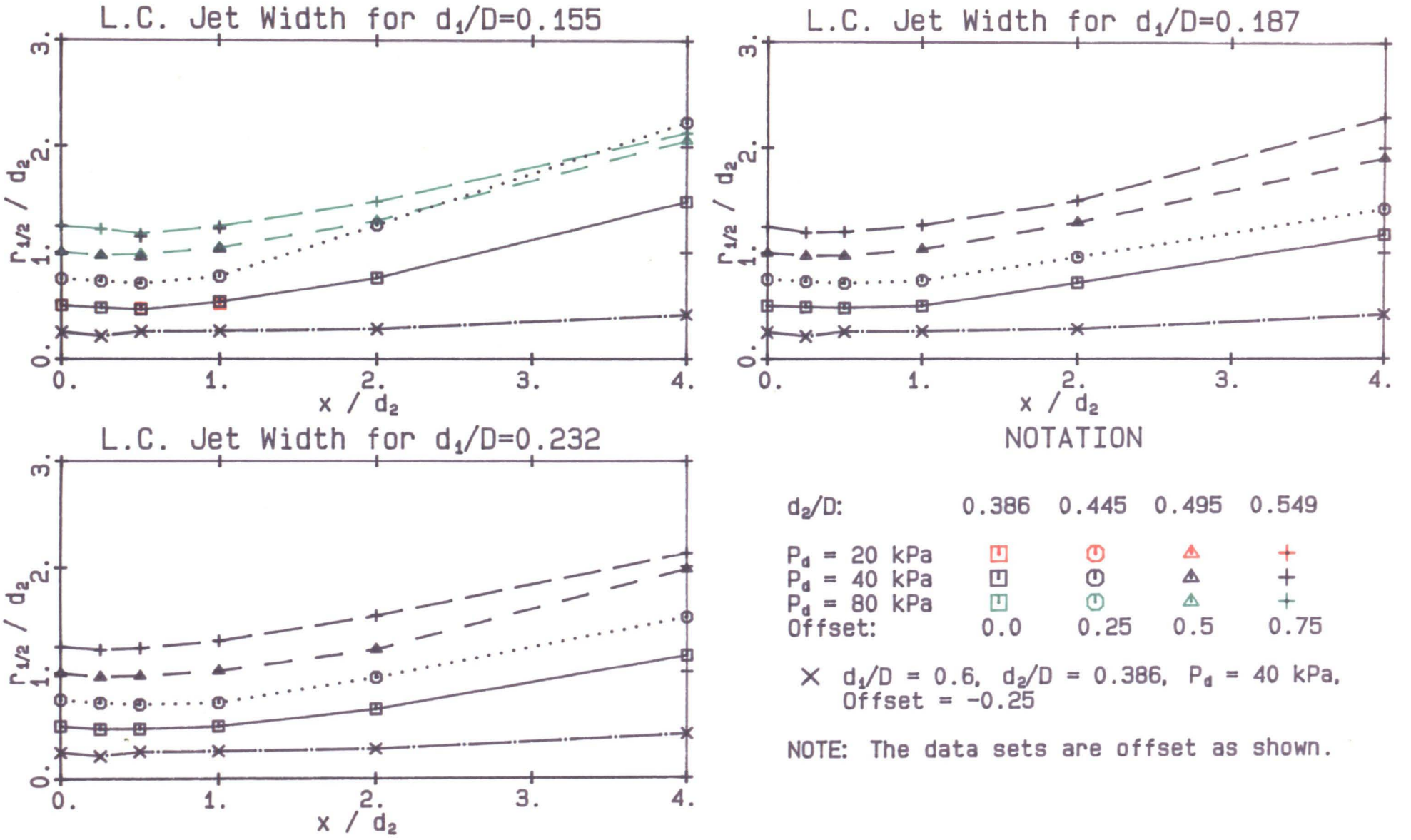

Figure 3.4: Half Jet Width profiles of LC nozzle

with caution as there is more than one choice of exit diameter and velocity scales. The search for the most appropriate scales is discussed in section 5.1. Photographs of the flames produced by each of the three nozzles are shown in Figures 3.7 to 3.9. It can be seen that the LC nozzle produces a shorter, more intense flame than does a simple nozzle, but that the MLC nozzle produces a flame of an entirely different character. Its flame is very short and bulbous in shape, and is extremely stable. Nevertheless, in applications where higher axial momentum is required, (eg. driving large scale furnace vortex motions), the characteristics of the LC nozzle may well prove to be more advantageous.

The mechanism whereby the LC nozzle produces the enhanced mixing is not fully understood. However it seems likely that an asymmetric reattachment is occurring within the cavity, as with the MLC nozzle (discussed in Chapter 4), leading to a precessing motion of the exiting jet. Because the LC nozzle has a longer cavity length, and/or smaller exit diameter than the MLC nozzle, the angle which the precessing jet makes with the nozzle axis is much smaller than that of the MLC nozzle. The LC nozzle is discussed more fully in chapter 8.

3.4 The Mid Length Cavity Nozzle

The MLC nozzle is the nozzle which is most fully discussed in the rest of the presentation. It is postulated that the MLC nozzle generates the enhanced mixing by means of an instantaneously asymmetric, precessing jet. The postulate has been derived from a large number of flow visualisation experiments, and a smaller number of pitot tube, hot-wire anemometry and acoustic spectra measurements. It is consistent with the results of other researchers who have investigated related flow phenomena and is unrelated to the mechanism of acoustical excitation.

The instantaneous jet leaves the exit plane of the nozzle at an angle of approximately 65 deg to the centreline of the nozzle, with the extreme edge of the jet being almost at right angles to the centreline of the nozzle. Consequently, it can be seen that when the asymmetric jet is precessing about the nozzle axis, on average it will produce a symmetrical jet with extremely large spreading angles. This produces an extremely short, bulbous flame as illustrated in Figures 3.10 and 3.11. The shape of the flame in Figure 3.11 is unusual, and appears to have captured in an instant the instantaneous jet at two positions.

However, because the instantaneous jet is continuously precessing, part of its linear mo-

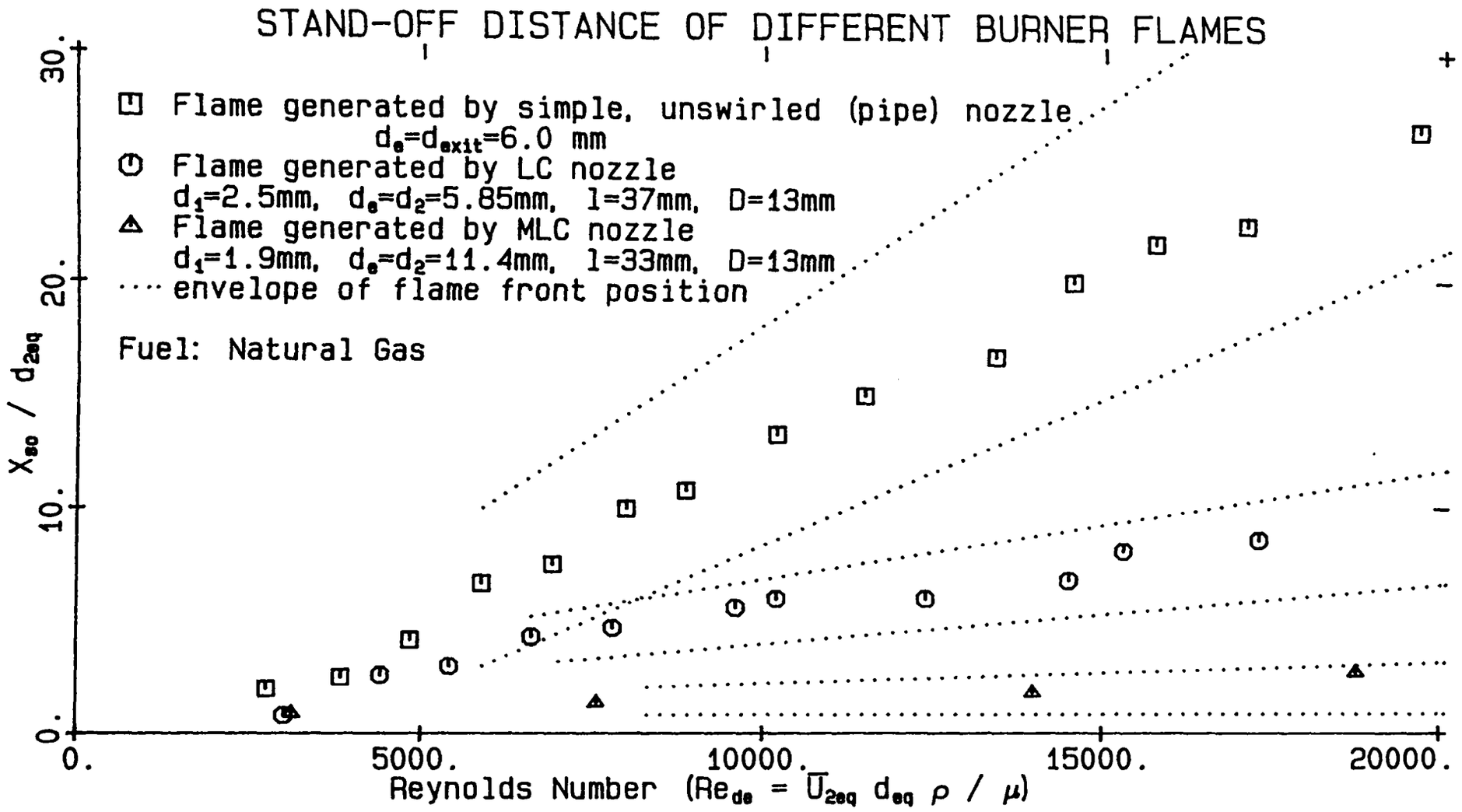

Figure 3.5: A Comparison of the Stand-off distance associated with various nozzles

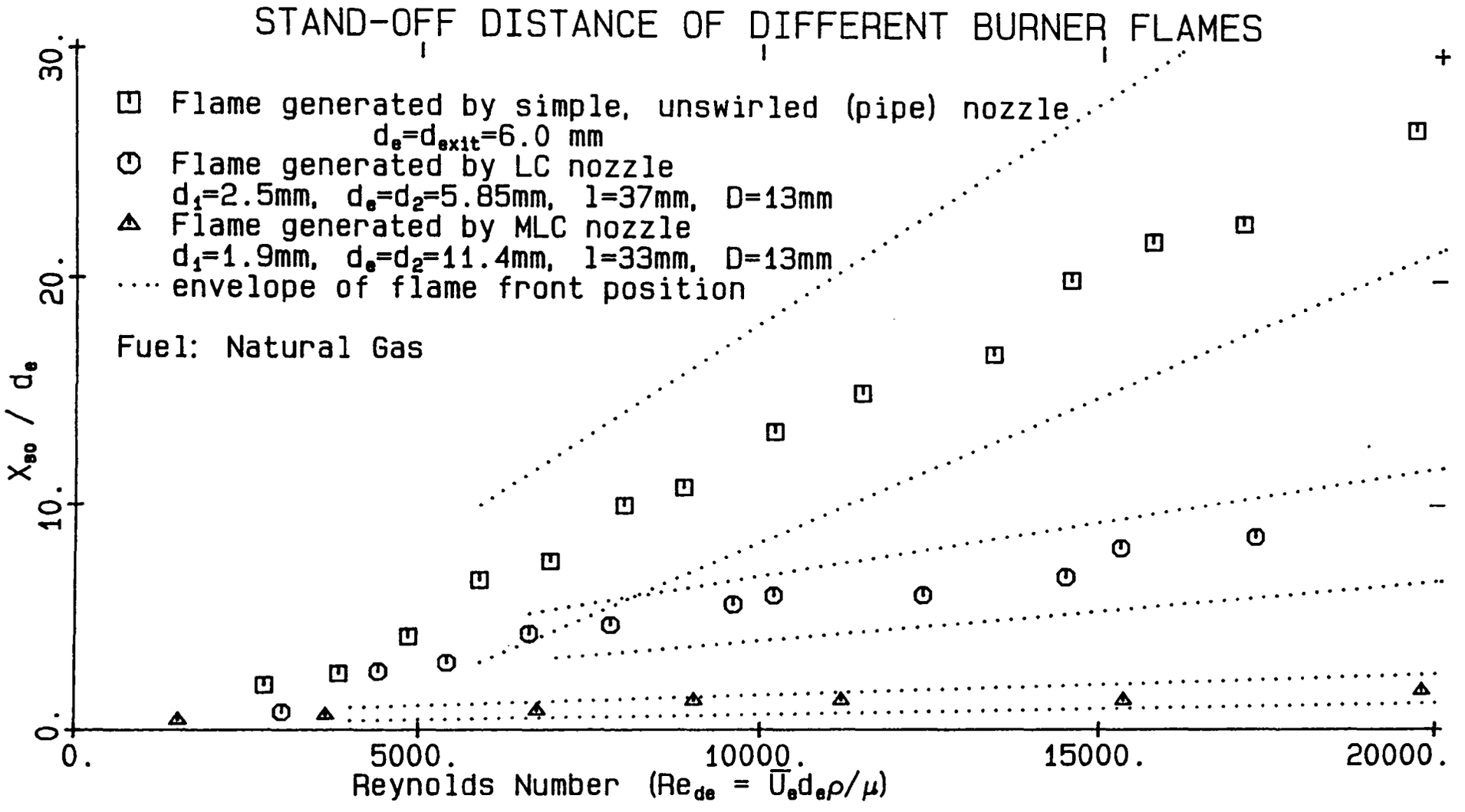

Figure 3.6: A Comparison of the Stand-off distance associated with various nozzles based on mean exit diameter

Figure 3.7: A Photograph of the flame produced by a simple, unswirled nozzle

Fuel:CNG, $\overline{u_e} = 34\text{m/s}$, $d_e = 11\text{mm}$, $\dot{m} = 2.64 \times 10^{-3}\text{kg/s}$.

mentum will be converted to angular momentum and extremely large scale vortex structures are formed. These structures have very long residence times since the jet does not continuously convect them downstream. Furthermore, the precession is generated fluid-mechanically, and so both the angle of the instantaneously exiting jet and the frequency at which it precesses are subject to variation about the predictable mean values. Such flow patterns can be expected to generate remarkably strong mixing.

These flow patterns support a highly stable flame with stand-off distances an order of magnitude lower than that produced by an unexcited, unswirled nozzle and blow-off velocities four times greater. Whilst these results were obtained in an unconfined (free air) environment only, they indicate that the nozzle has great potential in combustion applications. Furthermore, in cold flow applications, it produces entrainment rates five times that of an unexcited, unswirled nozzle[2].

[2]These values are based on an "equivalent diameter", d_{2eq}, discussed in Section 5.1.

Figure 3.8: A Photograph of the flame produced by a LC nozzle

Fuel:CNG, $\overline{u_e}$ = 89m/s, d_1 = 1.9mm, d_2 = 7.4mm, l = 44mm, $\dot{m}$ = 2.98 × 10^{-3}kg/s.

Figure 3.9: A Photograph of the flame produced by a MLC nozzle

Fuel:CNG, $\overline{u_e}$ = 39m/s, $\overline{u_{2eq}}$ = 150m/s, d_1 = 1.9mm, d_2 = 11.4mm, l = 33mm, d_{2eq} = 6.0mm, $\dot{m} = 3.27 \times 10^{-3}$kg/s.

Figure 3.10: A Photograph of the flame produced by a MLC nozzle showing bulbous shape.

Fuel:LPG, $\overline{u_e}$ = 14m/s, $\overline{u_{2eq}}$ = 50m/s, d_1 = 1.65mm, d_2 = 11.4mm, l = 32mm, d_{2eq} = 6.0mm, $\dot{m}$ = 2.61×10^{-3}kg/s.

Figure 3.11: A Photograph of the flame produced by a MLC nozzle whose shape is indicative of a precessing jet motion.

Details as for previous figure.

3.5 Conclusions

Three different modes of excitation have been identified for Orifice-Cavity-Orifice nozzles. Each mode corresponds to a characteristic range in the combination of primary dimensions, vis. d_1/D, d_2/D and l/D. The three modes of excitation are:

- Acoustic Excitation. The Abell nozzle uses strong vortex shedding from a primary orifice to stimulate a (0,1) radial mode in coincidence with one or more other resonant modes (eg. an organ pipe mode) to "pump" a very strong toroidal vortex at the nozzle exit.
- A partially understood fluid mechanic excitation. The LC nozzle appears to generate a precessing asymmetric jet, but with much smaller spreading angles than the MLC nozzle.
- A Precessing Asymmetric Jet, PAJ. The MLC nozzle generates intense mixing by means of a PAJ, and is the main subject of the present investigation.

Acoustic excitation has been investigated over a larger range of nozzle geometries than by previous researchers. It has been found that as cavity length is increased, jet excitation occurs over a larger part of the total operating range, through the excitation of different acoustic modes at different flow rates. Unfortunately, this does not overcome the problem of limited turn-down ratio associated with the Abell nozzle because the flow rates associated with adjacent modes do not overlap.

The LC nozzle has been found to produce increased rates of mixing throughout its entire flow range and to retain a relatively large flame momentum. Spread angles of approximately 28 deg were measured in a preliminary experiments. A detailed investigation of the LC nozzle was abandoned with the discovery of the MLC nozzle which has superior mixing characteristics. Details of the preliminary studies are given in Chapter 8.

Chapter 4

The MLC nozzle and its Mechanism

It is postulated that the Mid Length Cavity nozzle generates the enhanced mixing by means of an instantaneously asymmetric, precessing jet. The postulate has been derived from a large number of flow visualisation experiments, and a smaller number of pitot tube, hot-wire anemometry and acoustic spectra measurements. Good consistency has been found between those components of the mechanism which are discussed in the literature and the results of other researchers. These topics include: flow behind steps and abrupt expansions, fluidic nozzles and the mechanism of acoustic excitation of jets.

Chapter 4 begins with a qualitative description of the flow phenomena which occur within, and downstream from, the MLC nozzle. This outline is intended to orientate the reader, and consequently contains some unsubstantiated statements which are justified elsewhere in the thesis. The rest of the chapter deals with major experimental results which support the postulate; other experimental support is discussed as appropriate, and the comparison with the literature is discussed in Chapter 7.

4.1 A Qualitative Description of the flow patterns generated in and by the MLC nozzle

The following description of the flow patterns which appear to be occurring within the nozzle is illustrated by the wire and perspex model shown in Figures 4.1 and 4.2. Both the black and red wires indicate the instantaneous position of the *streamlines* of the fuel jet which enters the

cavity through the upstream orifice, while the yellow/green wires represent the instantaneous streamlines of entrained, ambient air which enters the cavity through the exit plane of the nozzle.

The jet emanating from the upstream orifice discharges into the cavity. The values of d_1/D and l/h_1 are selected so that naturally occurring pressure perturbations will cause the jet to deflect away from the axis of the nozzle, and to reattach asymmetrically to part of the inner surface of the cavity through a positive feedback mechanism which amplifies the asymmetries of the pressure field. At the reattachment point, conservation of momentum requires that most of the jet will continue in a generally downstream direction (as indicated by the black lines), but some will move in the upstream direction; the "reattachment reversed foot" (as indicated by the red lines). The main jet will then be forced to separate by the lip or discontinuity at the exit plane of the nozzle, inducing or amplifying an inward radial component of velocity directed towards the geometric centre-line of the nozzle.

The main jet does not occupy the whole of the available area of the exit plane of the nozzle, and ambient fluid from the surrounding atmosphere is induced to flow into the nozzle in the upstream direction through the remainder of the exit area. This occurs because pressure within the chamber is slightly sub-atmospheric due to entrainment by the main jet within the cavity.

On reaching the back of the chamber, the presence of the wall (of the primary orifice plate) causes the induced back flow to slew to one side, thus producing a swirling motion at the back of the cavity. Because the swirled flow must follow a concave curved path with an axis which is perpendicular to its instantaneous streamwise direction, it is possible that pairs of counter-rotating Taylor-Görtler vortices [92] are formed (as shown in Figures 4.1 and 4.2). It is important to emphasise that the occurrence of the observed flow patterns does not depend upon the presence or absence of the Taylor-Görtler vortices. Neither has it been within the scope of the present investigation to actually test for their existence. However it is speculated that their formation is likely at higher flow rates.

These Taylor-Görtler vortices are induced to spiral in towards the precessing jet because the entrainment appetite of the jet causes it to be at a lower pressure, in addition to the radial pressure field of the swirling flow. Conservation of mass also requires that the ambient air leave the nozzle. However, because the Taylor-Görtler vortices are very stable and retain their coherence for a long time, they tend to wrap themselves around the irrotational core of the jet

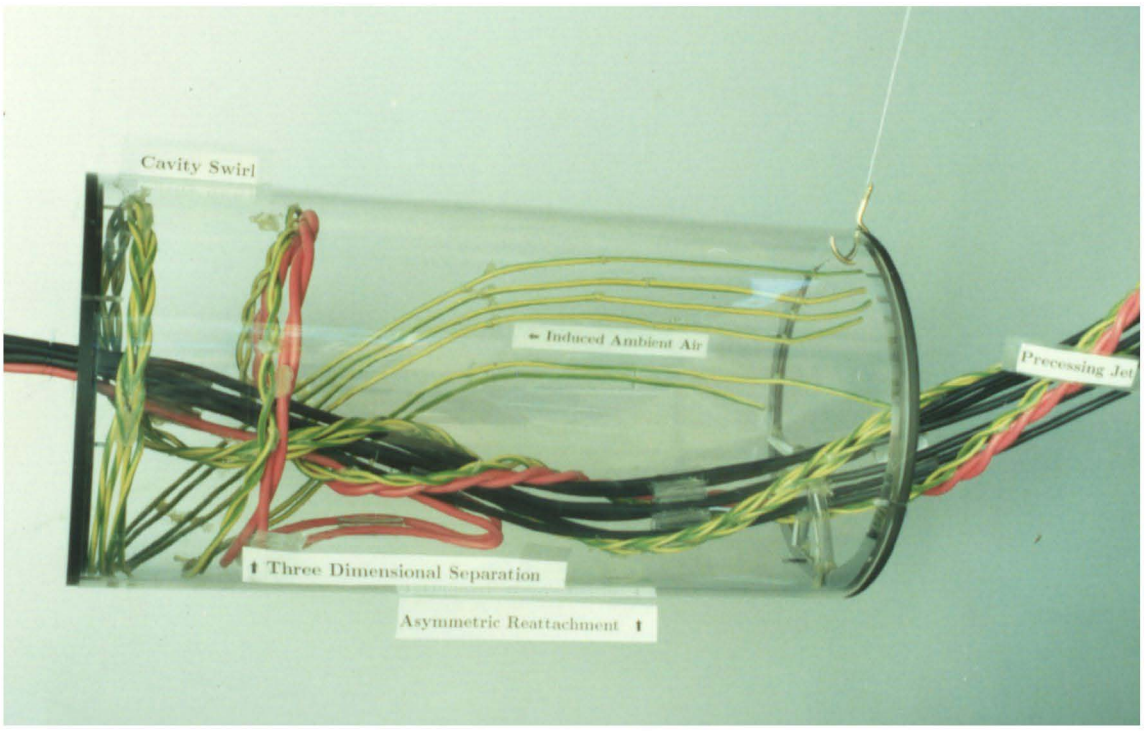

Figure 4.1: A Model of the proposed instantaneous flow patterns occurring within the MLC nozzle, viewing the plane of the reattaching jet.

The black and red streamlines represent fluid which enters the nozzle through the primary orifice, whilst the yellow/green streamlines represent ambient fluid entering the nozzle through its exit plane. At the asymmetric reattachment, the bulk of the jet continues in a generally downstream direction (black streamlines) whilst some of it moves in the upstream direction; the "reattachment reversed foot" (red streamlines). Simultaneously the induced ambient air moves toward the back of the cavity, where the presence of the wall causes it to slew to one side and generate a swirl. Because the swirling flow is moving inside a concave surface, pairs of counter rotating (Taylor-Görtler) helical vortices will may be formed which will spiral in toward the center of the nozzle and wrap themselves around the jet. At the place where the reattachment reversed foot interacts with the cavity swirl, a three dimensional separation will occur. This whole system of flow patterns will precess around the nozzle axis.

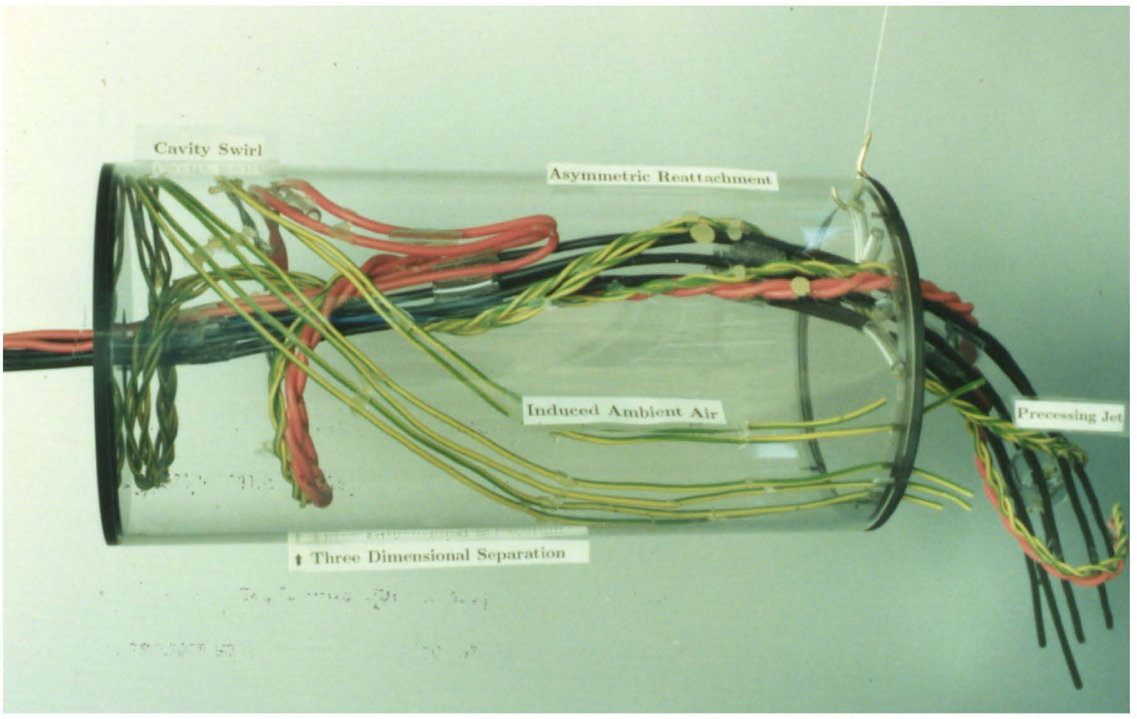

Figure 4.2: A view of the proposed instantaneous flow patterns within the MLC nozzle, from below the point of reattachment.

and probably retain their identity for some time after being entrained.

The total angular momentum into the nozzle is zero since both the jet entering through the upstream orifice and the ambient air induced through the exit plane are irrotational. Thus for angular momentum momentum to be conserved, the net angular momentum leaving the nozzle must also be zero. Now the Taylor-Görtler vortices are formed in counter-rotating pairs, and thus will have a net angular momentum of zero. Thus, it is necessary for the direction of swirl (ie. the swirling component of the flow which generates the Taylor-Görtler vortices) to be the opposite of the direction of the jet precession.

The flow patterns described above are also consistent with skin friction forces which are exerted on the wall when the instantaneous jet is asymmetrically attached. The azimuthal (swirling) component of thrust exerted by the Taylor-Görtler vortices between the wall and the jet will also be such that the jet is induced to precess in the opposite direction to that of the cavity swirl.

If the velocity of the entrained ambient air is insufficient for the Taylor-Görtler vortices to be formed, the cavity-swirl-fluid will spiral into the jet and be entrained by it, imparting a weak rotational motion to the jet. Angular momentum will still be conserved, and flow directions remain consistent.

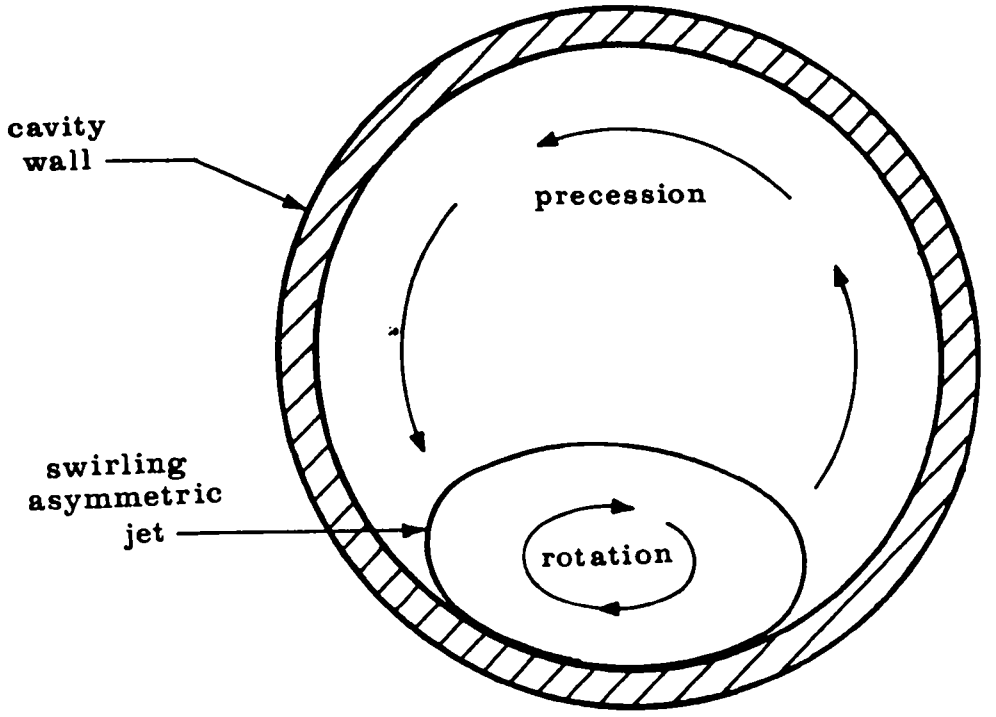

Figure 4.3: Rotational Directions within the nozzle chamber in the plane of reattachment when the flow upstream of the nozzle is pre-swirled.

The jet has no inherently preferred direction of precession, but will usually maintain a given direction once it has begun. However, for some reason which is not yet understood, a momentary cessation of the "enhanced mixing" flow patterns described above may occur. This phenomenon is referred to as "*intermittency*". When the flow patterns resume, usually after a fraction of a second, the direction of precession is frequently reversed. However insufficient observations have been made for this trend to be confirmed as typical. The introduction of an upstream swirl into the primary jet causes the reattaching jet to have a preferred direction of rotation, perhaps due to the skin friction at the wall in the plane of reattachment, or perhaps due to a preferred direction of slew of the reattachment reversed foot (See Figure 4.3). As such the incidence of intermittency is almost eliminated. It also appears to be much more likely that the Taylor-Görtler vortices are entrained into the primary jet so that they lose their identity more rapidly in this case. A suitably placed bluff body within the cavity is another geometric modification which has been developed with a view to eliminating intermittency.

It is interesting to consider in more detail the driving force for the precessing motion in terms of the circumferential thrust components exerted by the precessing jet and reattachment reversed foot. (It is a moot point as to whether these patterns and flow directions are initiators

of, or the result of, the precession.) The following interpretation cannot be conclusively confirmed from the experiments which have been conducted, but is compatible with the observed dynamics of the flow.

To cause the reattachment point to precess, a thrust must be exerted in the azimuthal direction on the jet prior to its reattachment. It is postulated that this thrust comes from an azimuthal component in the direction of the flows both upstream and downstream from reattachment, ie. in both the reattachment reversed foot and the in precessing jet. The streamlines of the jet are instantaneously moving in a skewed helical direction through the chamber, with the azimuthal component of the helix direction being the opposite of that of the precession. However, because the helix is a consequence of the precessing motion, the motion of the individual particles within the jet, viewed relative to the nozzle, will be mainly in an axial direction, but with a small radial component.

The same argument applies to the reattaching reversed foot. The azimuthal component in its velocity, being the opposite of that of the point of reattachment, must be the same as the azimuthal direction in the flow of the induced ambient air. Thus its motion is also consistent with Figure 4.3.

When the reversed flow from the main jet interacts with the swirling flow at the back of the chamber, a three dimensional bifurcation results and a bifurcation line, located between one quarter and one third of the cavity length from the inlet plane, forms on the surface around part of the chamber.

It is known that streamline curvature is caused by cross-stream pressure gradients, and that the pressure on the wall side of a wall jet is less than that on the free side [72]. Thus a perpetual imbalance exists in the pressure field within the chamber, as required by the perpetual rotation and by the precession of the asymmetric jet.

The main jet, on leaving the nozzle, is instantaneously travelling from one side of the cavity "across", and slightly behind, the geometric centre-line of the nozzle, about which it precesses. On average then, there is a very rapid initial expansion of the jet. Note also that because surrounding fluid is continually been drawn into the cavity and entrained into the main jet, some mixing has already taken place by the time the jet leaves the nozzle. Thus for combustion applications, the MLC nozzle provides some automatic premixing and preheating, since the furnace contains both unreacted air, and hot combustion products.

4.2 High Speed Schlieren Photography

Probably the most powerful experimental evidence to support the notion of a precessing jet, was obtained by high speed schlieren photography of the flame generated by the MLC nozzle. Because a schlieren optical system responds to density gradients, it not only enables the turbulent flame surface to be visualised (the flame is less dense than the surrounding air), but it enables the fuel jet to be seen since the fuel jet (natural gas) is also less dense than air but is more dense than the flame.

4.2.1 Apparatus

The apparatus, shown in Figure 4.4, consists of two twelve inch concave mirrors, with a focal length of ten feet (kindly loaned by the High Speed Aerodynamics Laboratory of the Defence Science and Technology Organisation, Salisbury), a mercury vapour lamp with associated lenses, a plane mirror, a knife edge and a high speed Hycam camera. The intensity of the light source was reduced as required by means of two rotating polarising filters. More details can be found in Appendix C.2.

4.2.2 Results

The high speed photography has been collated to produce the film which is included with this thesis. The film clearly shows that the jet is "flapping" at the nozzle exit. This flapping is a two-dimensional projection of a three dimensional motion, and is entirely consistent with the proposed precession of the jet. A more detailed discussion of the film is given in Section 5.3.4.

A large number of "still" schlieren photographs were also taken. Two of these, Figures 4.5 and 4.6, show the jet leaving the nozzle with an instantaneous component in the upward and downward directions respectively. They also show that the flame has a very bulbous shape indicating that, on average, the jet is spreading very rapidly, with approximate symmetry.

4.3 Total and Static Pressure Profiles

Total and static pressure probes are only accurate when used to measure steady flow of a known direction. Nevertheless, they provide a quick and easy method of indicating gross features of flow behavior in more complicated flows, if the results are treated with caution. More pragmatically, no suitable method for measuring true velocity profiles was available; the

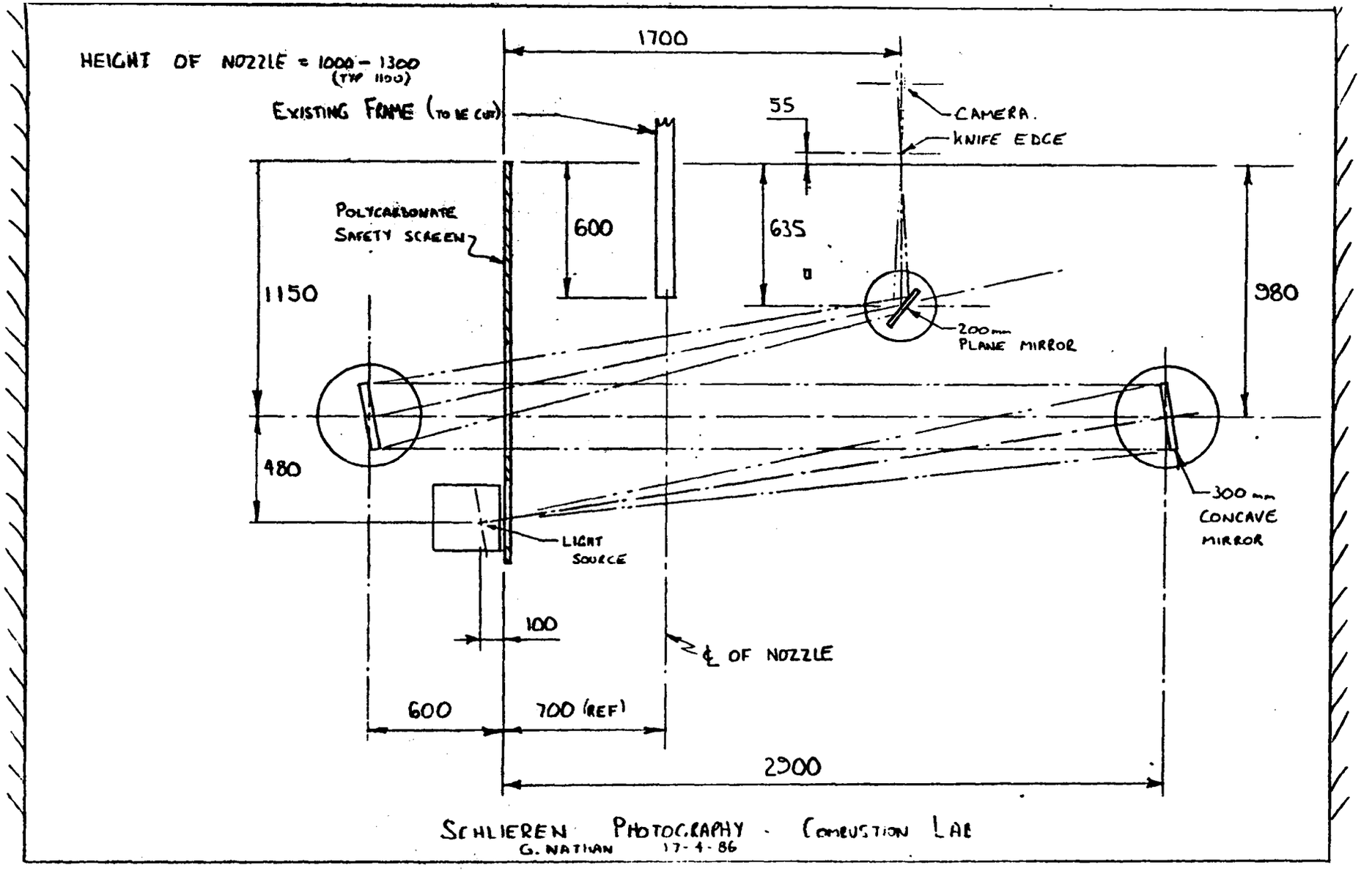

Figure 4.4: The Apparatus used for schlieren photography

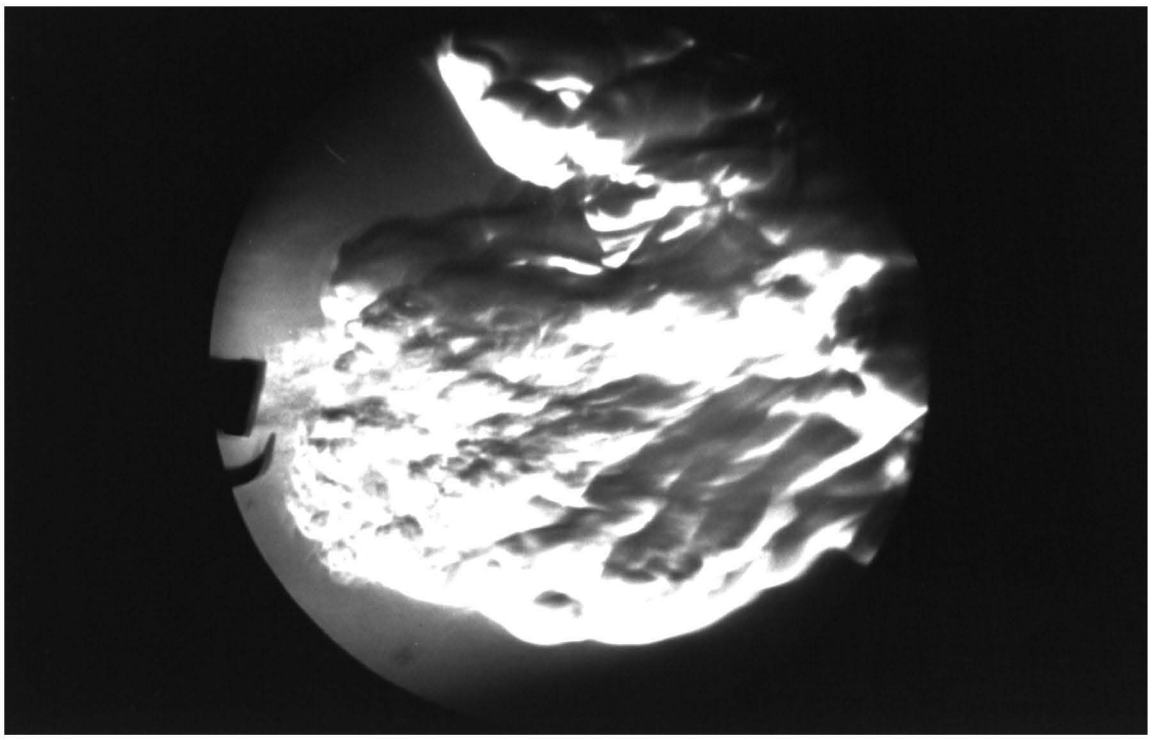

Figure 4.5: Schlieren photograph of the flame, showing the instantaneously asymmetric jet leaving with a component in the upward direction

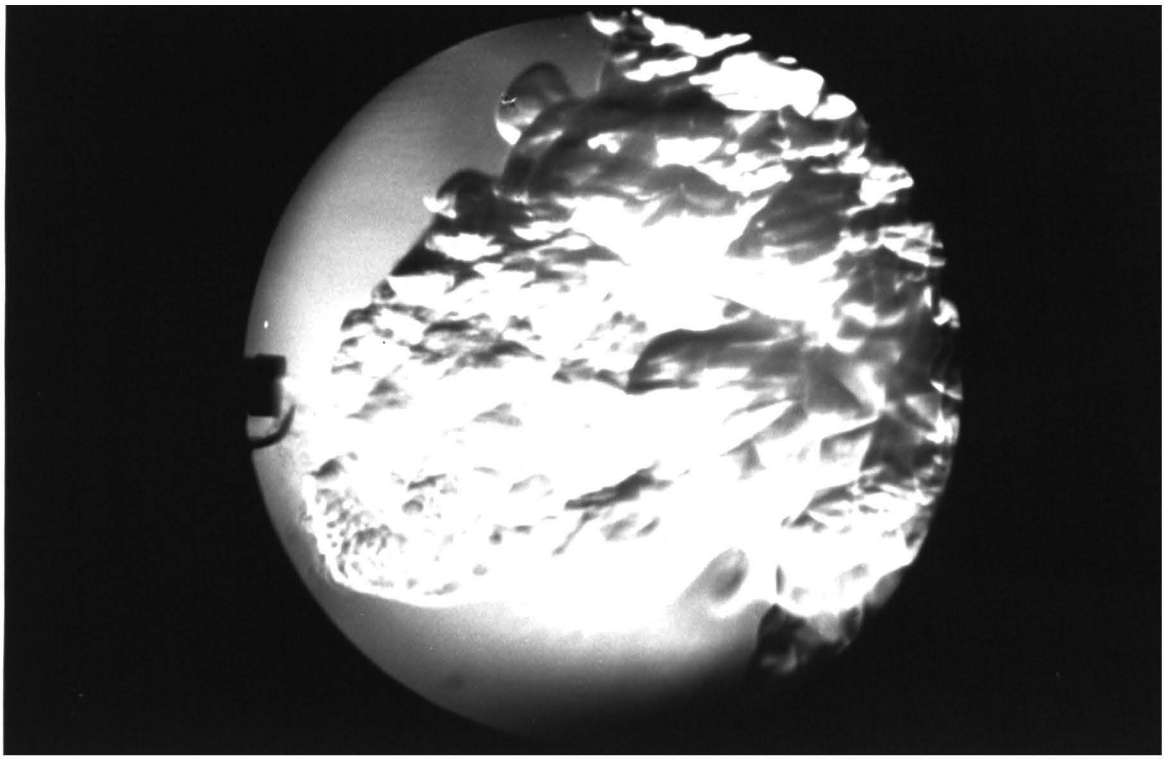

Figure 4.6: Schlieren photograph of the flame, showing the instantaneously asymmetric jet leaving with a component in the downward direction

rapidly changing flow direction and very strong three dimensionality of the flow field rendered the static hot wire anemometer probe unsuitable and neither a flying hot wire nor a multi-component Laser Dopler Velocimeter was available.

The results of the pressure profiles, although not precise, are valuable as a qualitative indicator of the velocity profiles in the the region of the exit plane.

4.3.1 Apparatus and Experimental Techniques

The total and static pressures were measured separately using 3mm diameter probes aligned with the geometric centre-line of the nozzle. This was done in spite of the fact that it was well known that neither the mean, nor the instantaneous flows are in this direction.

It would have been possible to improve the accuracy by aligning the probe with the directions of the strongest flow, indicated by the static pressure yaw meter (see Section 4.4). However, because the probe is in a precessing flow field, it would only be aligned with the strongest flow for a relatively short part of each cycle. Thus the probe would not only be subjected to large fluctuations in the *direction* of the flow, but also in the *magnitude* of its velocity. For both possible probe arrangements the response time of the probe is much slower than the dominant period of the oscillations. The resulting pressure measurement then, will be some form of "average", but weighted in a way which cannot be determined until the flow field has been adequately defined. Consequently, as the total and static pressure probes are only suitable for semi-quantitative measurement, the added complexity in aligning them with the estimated conical angle of the instantaneous jet was not considered to be worthwhile.

4.3.2 Results

The total and static pressure profiles are displayed in Figure 4.7. It can be seen that the total pressure[1] profile of the jet near the exit plane is not at all like the "top hat" profiles typical of a simple jet. On the contrary, it is a symmetric, but highly skewed profile, with very high total pressure at the edge of the jet and very low, though still on average positive, total pressure near the jet centre-line.

It is usual practice when measuring pressure profiles of simple jets to assume that the static pressure is equal to atmospheric pressure, and that no pressure gradient exists across the jet.

[1] Velocity = (total pressure − static pressure)$^{1/2}$

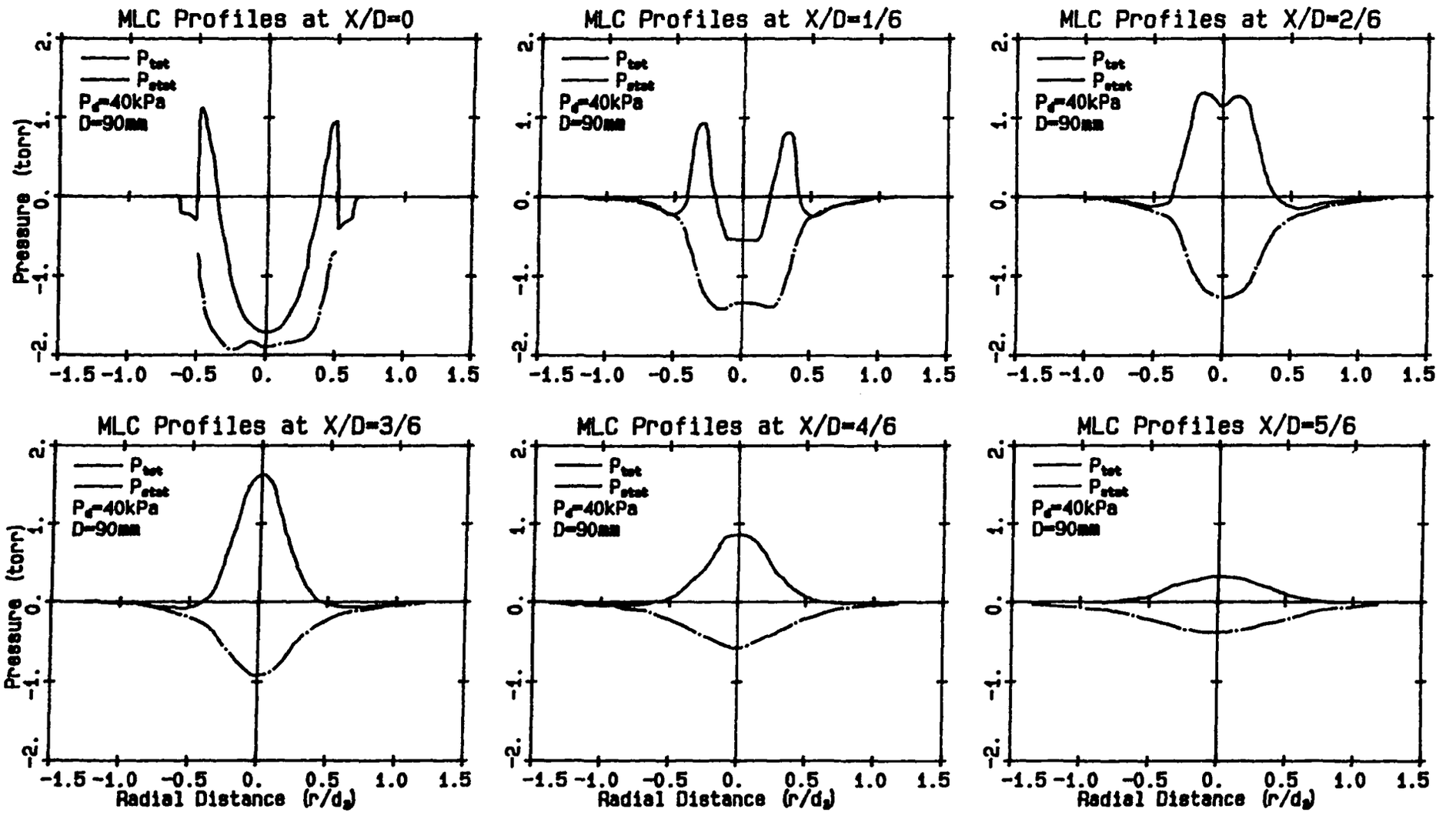

Figure 4.7: Total and Static Pressure profiles of the MLC nozzle

This yields reasonable results because the spreading angles are so small. However, in the case of the MLC nozzle, the *magnitude* of the (negative) static pressure, relative to ambient, near the nozzle exit is greater than that of the (positive) total pressure relative to ambient. Transverse static pressure gradients are always accompanied by a change in the direction of the streamlines. If the jet was instantaneously symmetrical, a low pressure core would indicate a *convergence* of the streamlines, which is clearly inconsistent with observed flow directions. However, this apparent dichotomy can be explained in terms of the proposed model. Because the jet at the exit plane of the nozzle is attached asymmetrically to the wall of the cavity, the very low pressure along the nozzle centreline is consistent with a rapid change in its direction towards and across the geometric centreline of the nozzle. Thus the very large static pressure gradient at the exit plane is further evidence of the rapid spreading of the jet. The very low pressure at the core of the mean jet is also consistent with the large entrainment appetite of the jet. Not only is the instantaneous jet caused to deflect towards it, the ambient fluid outside the jet is also drawn towards it.

Further evidence supporting the proposed model is found in the double-peaked shape of the total pressure profiles near the exit plane and the rapidity with which the profiles change shape. In fact, the shape of the profiles is changing so dramatically that by half a nozzle exit diameter downstream from the exit plane, the two total pressure peaks have merged. In the next one third of a nozzle diameter, the dynamic pressure ($P_{tot} - P_{stat}$) reduces by a factor of approximately four. The results also indicate that the jet, which is initially concentrated in the outer part of the exit plane, is directed radially inwards toward and across the geometric centre-line of the nozzle.

These results can be explained by an asymmetric, precessing jet in which the jet is instantaneously directed with a component toward the nozzle centre-line. Not only would such a jet have peaks in the mean velocity profile at the outside of the nozzle in the exit plane, but it would also produce very rapid spreading of the jet.

4.4 Measurment of mean flow direction by Static Pressure Yaw Meter

The results of the previous experiments indicate that the jet is spreading very rapidly, but do not give a quantitative measurement of the flow directions[2]. Several techniques exist for the measurement of flow direction when the flow is two dimensional and steady, but the accurate measurement of flow direction in unsteady, three dimensional flow is much more difficult and requires the use of sophisticated equipment such as a multi-component Laser Doppler Velocimeter which was unavailable for this research.

It was decided use one of the simplest 2-D flow direction measuring instruments, the static pressure yaw meter, realising that the results would need to be interpreted with caution in this highly 3-D flow. The results from these measurements not only indicate extremely rapid spreading (with the edge of the jet approaching 90 deg from the nozzle axis at the plane of the nozzle exit), but they support the postulate that the MLC nozzle generates a precessing jet. Indeed its readings can only be interpreted sensibly in the light of this postulate.

4.4.1 Apparatus and Experimental Techniques

The static pressure yaw meter, shown in Figure 4.8, consists of a long, thin tube (OD = 3mm) with two radial holes, spaced 90 deg apart, halfway along its length. These holes vent into separate cavities at either end of the tube.

The principal of its operation is as follows. The tube is placed with its axis at right angles to a known (or assumed) direction of flow. For example, when used in a wind tunnel to measure two-dimensional flow direction in the x-y plane, its axis is in the z direction. The tube is then rotated about its axis until the static pressures registered at the two holes are equal.

It can be seen intuitively that the static pressures will sum to zero when the mean flow direction bisects the angle between the two holes. However, there are also three other rotational positions of the probe at which the static pressures can be nulled. One of these occurs at the rear of the cylinder, where the mean stagnation point of the reverse flow is 180 deg behind

[2]Spreading angles are often determined from the jet width based on r_{half} at successive axial stations. Where the jet does not display similarity however, r_{half} is inappropriate. The jet produced by the MLC nozzle does not display similarity in the first half an exit diameter or so, and the velocity profiles downstream of this are so flat, and both the total and static pressures relative to atmosphere rapidly become so small, that it is difficult to measure r_{half} in the region where the jet does seem to display similarity with adequate accuracy.

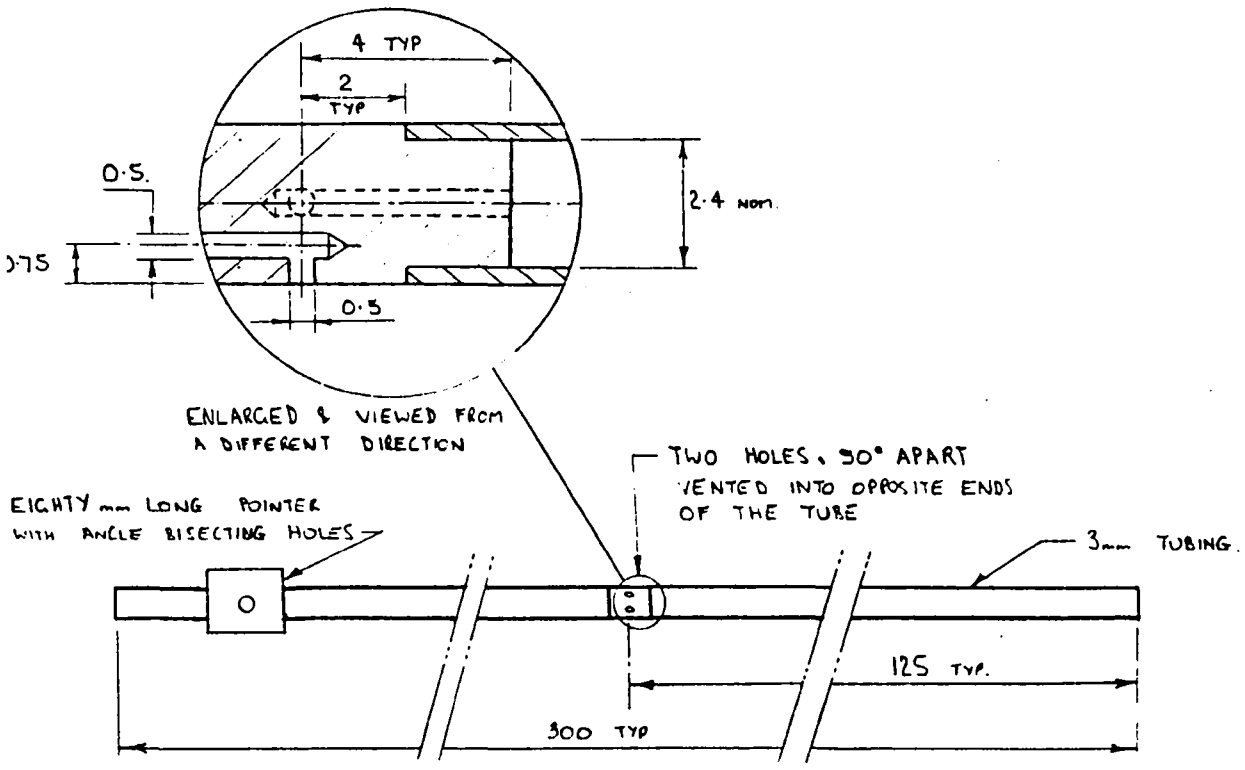

Figure 4.8: The Static Pressure Yaw-meter

the front stagnation point. Because the flow separates at approximately 80 deg from the front stagnation point, there is also . another angular position relative to the front and rear stagnation points at which the two pressures will be nulled. These two additional "null positions" were measured in a steady, two-dimensional flow of uniform direction produced by the two-dimensional calibration nozzle described in Section 4.7.2 to be at 106 deg from the front and rear stagnation points The results of the measurement are shown in Figure 4.10(a). It can be seen that that the measurement of all four null positions in steady, uniform flow will enable the flow direction to be uniquely determined.

The probe was traversed vertically through the geometric centre-line of the MLC nozzle, with the probe's axis held in the horizontal position, and perpendicular to the axis of the nozzle. The position of the probe could be measured to within ± 0.1mm in the vertical position, and ± 0.5mm in the horizontal direction. The pressure differential was measured directly using a 100 torr Baratron pressure transducer.

4.4.2 Results

The results of the flow direction experiments are shown in Figure 4.9 and a representative sample of the null positions is shown in Figure 4.10. It can be seen that, at the nozzle exit, on average the flow is moving with a large component in the radial direction directed towards the

geometric centre-line of the nozzle. However, it also indicates that immediately downstream from the exit plane there are very large spreading angles of up to 87 deg. Such a result cannot be explained by a steady jet as this would require either that the streamlines must intersect and cross or that there exists a uniquely organised system of flow surfaces with a form similar to layers of the iris of a camera. Whilst the latter flow pattern is a topological possibility, it is not possible from a fluid mechanical point of view. However, the observed unusual behavior does supports the notion of a precessing jet. When the probe is in certain positions, for each cycle of jet precession, it will be subjected to two strong flows of very different directions to as the jet sweeps past it. The probe will also be subjected to weaker secondary flows when the jet is in transit between these two positions, which are 180 deg apart in the circumferential position. The two different coloured direction vectors shown in Figure 4.9 represent these two strong flow directions which are sensed by the static-pressure yaw meter during the measurement. The same colours are used in Figure 4.10 to illustrate the interpretation of the results.

The results and their interpretation require some explanation. The actual null positions obtained by rotating the probe, shown in Figure 4.10, are very different from those which occur in uniform, two-dimensional flow. Except for the result obtained at the origin, the null positions cannot be interpreted sensibly in terms of a constant flow direction. However they can be explained in terms of the proposed mechanism.

Consider Figure 4.10(c)(i). The yaw-meter is located on the nozzle center-line, but 0.167 nozzle diameters downstream of the exit plane. The meter is subjected to an oscillating flow, where the oscillation is more rapid than the meter response. The meter, which only measures the two dimensional direction component in the radial plane in which it is situated, is thus effectively exposed to two flows simultaneously. For this reason, null positions occur at both the +53 deg and −47 deg locations. Weaker null positions also occur at 0 deg and 180 deg because on average the flow is moving in a generally axial direction.

All of the results *in the exit plane*, of which Figure 4.10(b)(ii) is representative, look like distorted versions of the steady state result. This seems to suggest that at the exit plane the yaw-meter is predominantly subjected to one flow direction (that which occurs when the jet is instantaneously reattaching at the wall on the same side of the centre-line as the yaw-meter), but slightly influenced by the presence of weaker flows. The weaker flows could either be the reversed flow of the ambient air induced into the cavity, or the lower velocity edge of the main jet, which exists when the jet has precessed to the opposite side of the cavity.

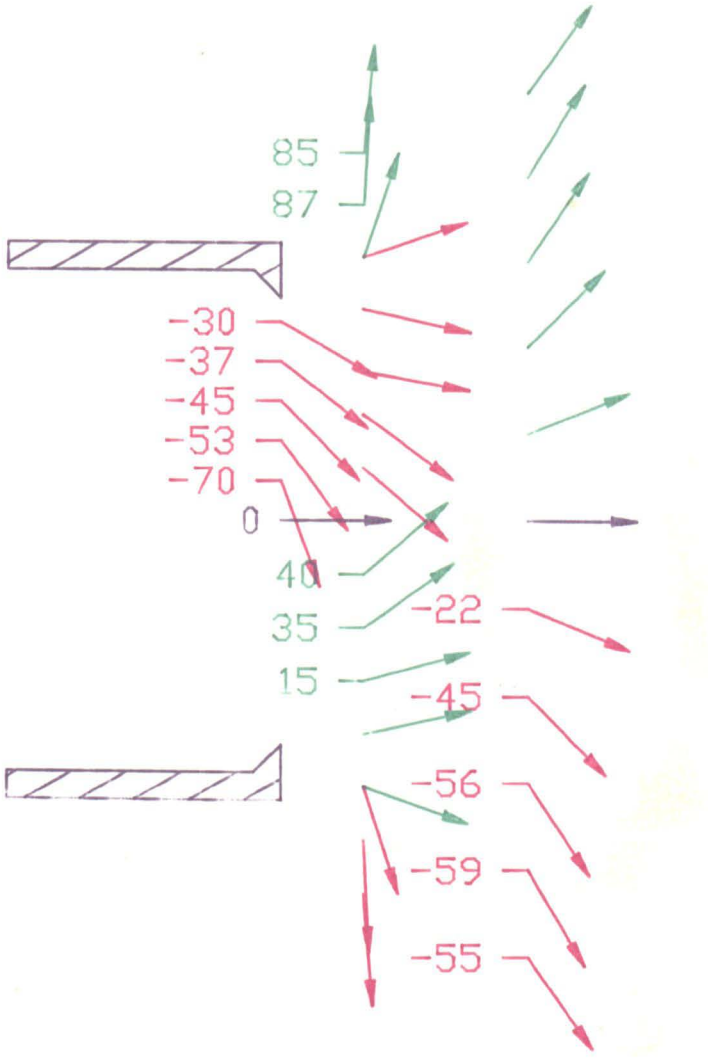

Figure 4.9: Average flow directions in the jet of the MLC nozzle, as measured by the Static Pressure Yaw Meter

Note that the horizontal tail at the root of some of the direction vectors is not part of the vector, but connects it to the label.

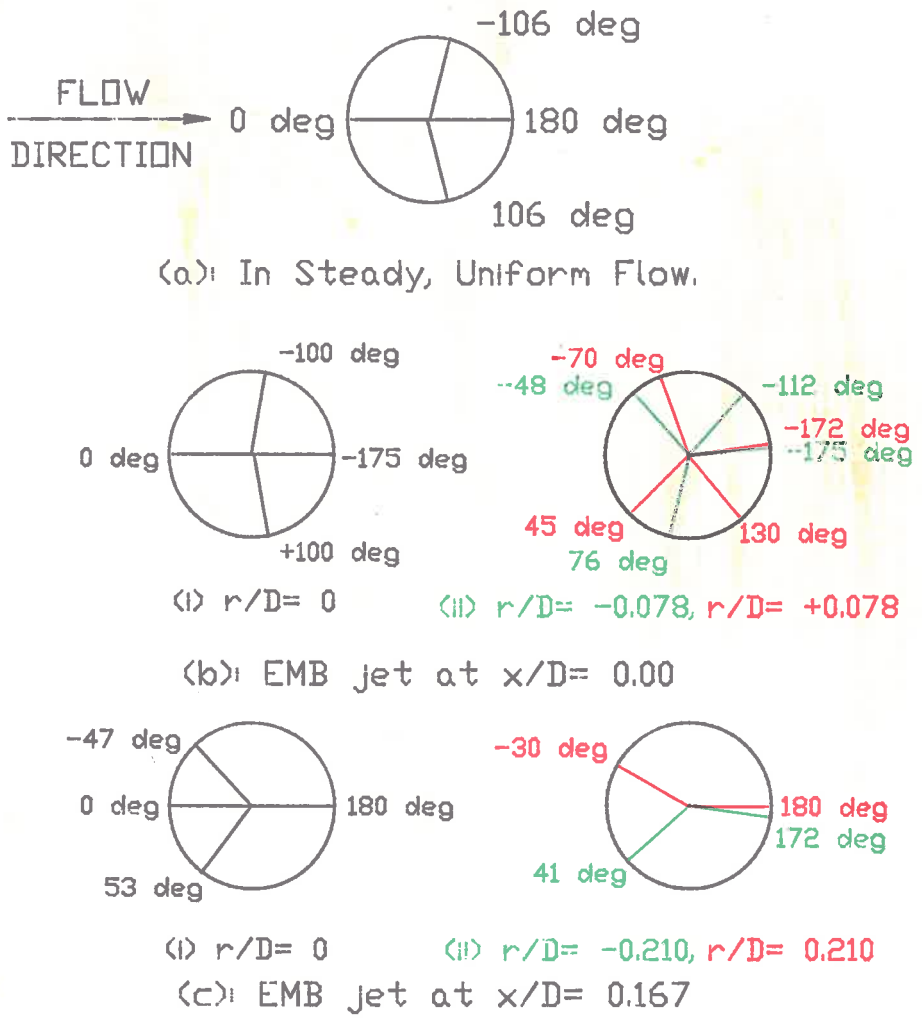

Figure 4.10: The null positions of the Static Pressure Yaw Meter

This shows typical angular positions of the static pressure yaw meter for which the pressure at the two holes were equal. The colours correspond with the flow directions in Figure 4.9.

When the yaw-meter is moved downstream from the exit plane, and radially away from the nozzle centre-line, the results are even more ambiguous. In some locations, of which Figure 4.10(c)(ii) is representative, only two identifiable null positions can be found, although zones of up to 90 deg of probe rotation exist where the pressure differential is very close to zero. This also suggests that the probe is subjected to highly oscillatory flow. The strongest null position was selected as representing the mean position of the instantaneous jet.

It is realised that directions indicated by the yaw-meter will necessarily be indicative only, because it is a two-dimensional instrument with a slow response time which is being used to measure a highly three-dimensional, turbulent flow. Never-the-less, the following conclusions can be drawn:

- Very large spreading angles (possibly up to 87 deg) occur at the exit plane of the nozzle.
- The jet leaves the nozzle with a large component of its velocity directed radially inward toward the geometric centre-line of the nozzle.
- These seemingly conflicting results can be explained by the proposed model of an asymmetrically reattaching, precessing jet.
- The rotational positions at which the static pressure at the two holes were nulled cannot be explained by a steady flow, but are sensible in the light of the proposed model.

4.5 The Wall Pressure in the cavity

To gain further insight into the behavior of flow within the nozzle, the static pressure on the wall of the cavity, P_w, was measured with air flowing through the large scale (D = 91mm) perspex nozzle. Tails for the pressure tappings were 15mm lengths of 1.5mm outside diameter thin tubing, flush mounted and glued into the cavity wall at 10mm intervals. A time average of the pressure was measured relative to ambient pressure using a multiple-tube inclined water manometer.

The results are presented in Figure 4.11, where P_w has been normalised by the driving pressure, P_d, and the distance from the upstream orifice, x, is normalised by the cavity length, l.

It can be seen that for the case of the short cavity nozzle, l = 150mm, P_w is approximately constant and sub-atmospheric along the entire wall. This is consistent with the notion that

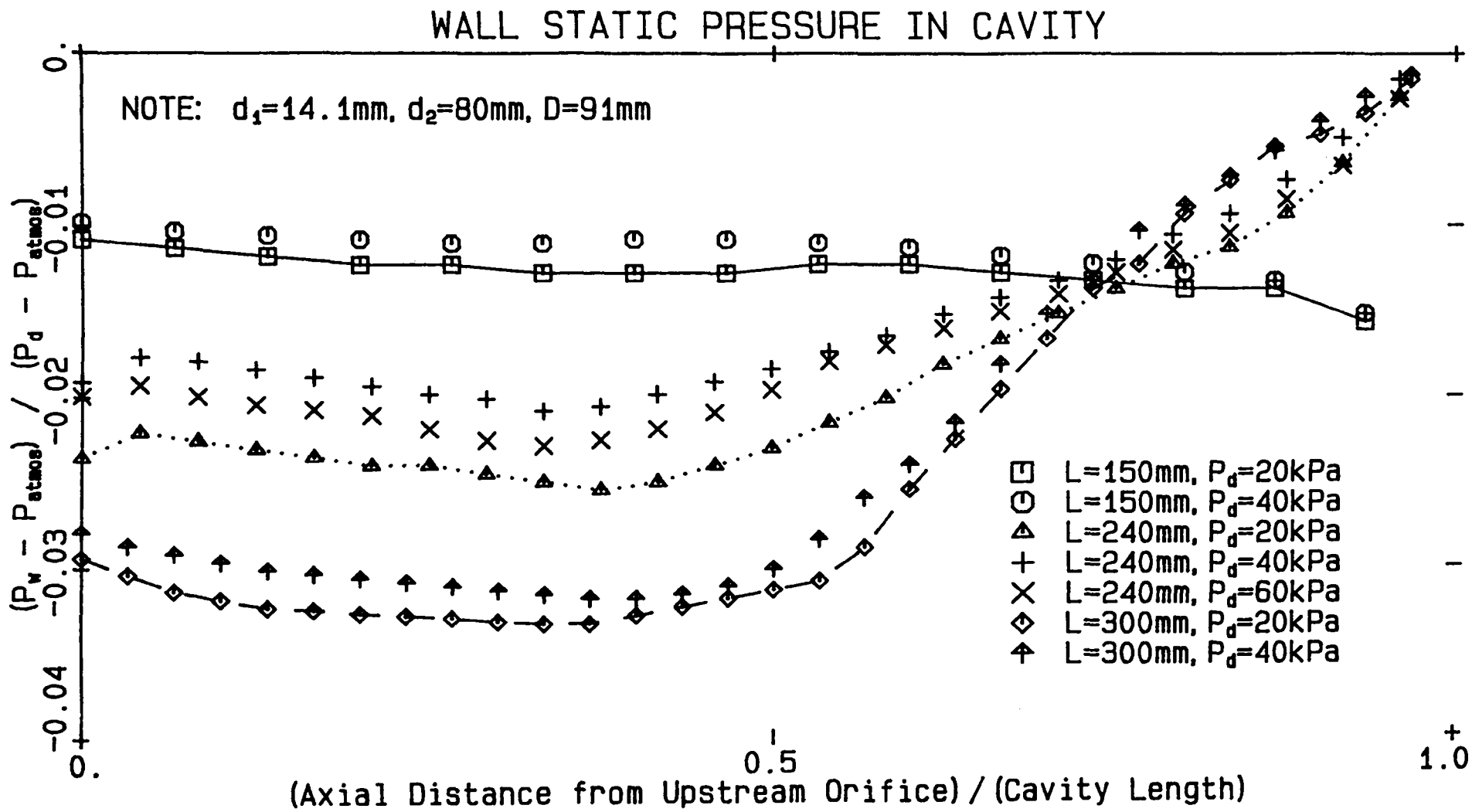

Figure 4.11: Axial distribution of average wall static pressure profiles in the cavity of the nozzle for three cavity lengths

the jet within the nozzle does not attach to the wall anywhere and, because of its entrainment appetite, is causing a negative pressure within the cavity. This interpretation is supported by the qualitative test of placing one's hand in the flow field and a small diameter, coherent jet whose diameter more closely approximates d_1 than d_2 at the exit plane.

By contrast, the wall pressure for the MLC nozzle, $l = 240$mm, shows two distinct regions. In the upstream part of the cavity, its behavior is similar to that of the short cavity nozzle, ie. P_w decreases slightly with increased x/l. However at $x/l \approx 0.38$, ie. $x/h_1 \approx 2.4$, where h_1 is the step height at the upstream orifice, an abrupt change in slope can be seen, and P_w *increases*, approximately linearly, to atmospheric pressure at the exit plane. It is suggested that this change in slope is caused by the presence of the instantaneous reattachment of the precessing asymmetric jet. It is slightly upstream of the positive bifurcation line measured using china clay visualisation, where $3 \leq x_p/h_1 \leq 4$, as can be seen in Table 4.4.

It is interesting to compare these results with those of Johnson (1986), who measured the wall static pressure downstream from an orifice plate in a long pipe carrying fully developed turbulent flow. In Figures 3.2.1 (b) and (f) of Johnson's report, it can be seen that P_w decreases very slightly as x increases from the orifice plate until it reaches the value which corresponds to the plane of minimum area at the vena contracta, or the "jet point". At the jet point, an abrupt change in the wall pressure gradient occurs, and P_w increases monotonically. The reattachment of the flow to the wall, downstream of the orifice plate, has no discernable influence on the gradient of P_w.

Johnson's tests were conducted with much smaller expansion ratios than exist in the present investigation. In his tests, $d_{orifice}/d_{pipe} = 0.72$ typically, whereas $d_1/D \approx 0.18$ in the present investigation. Furthermore, the end conditions are different. It is apparent that the change in the wall pressure gradient is not caused by the vena contracta in the present investigation. The distance from the orifice plate to the jet point, although depending on Mach Number and Reynolds Number, scales with the diameter of the orifice or jet. In Johnson's experiment, $x_{jp} \approx 0.5 d_{orifice}$. By contrast, in the present investigation as shown in Figure 4.11, the minimum wall pressure for the MLC and LC nozzles occurs at $x/d_1 \approx 6.5$ and 8 respectively. This is further evidence that the flow patterns in the present investigation are of a different character from those previously investigated through an orifice plate.

For the LC nozzle, $l = 300$mm, the wall pressure profile is qualitatively similar to that of the MLC nozzle, except that the change in slope of P_w vs l occurs further downstream; at $x/h \approx 4$.

The profile thus indicates that a reattachment is occurring in the cavity, but significantly further downstream. The amount of enhancement corresponding to this configuration of nozzle geometry is significantly less than that of the MLC nozzle.

4.6 The influence of a Downstream Separation

It has been found that the nature of the separation which occurs at the throat is crucial in determining whether the enhanced mixing flow patterns can occur. This section contains the primary experimental evidence for the conclusions which are drawn, but further evidence can be found in Section 6.3 which discusses the effect of varying the angle of a conical diffuser at the throat on entrainment.

The importance of achieving a *full* separation at the throat is investigated in the present experiments using a "bell-mouth contraction and expansion" (B-M-C-E). The bell-mouth contraction (B-M-C) ensures fully attached flow upstream of the throat, but three categories of flow are possible downstream from it, depending upon the shape of the bell-mouth expansion (B-M-E). *Fully attached* flow within the B-M-E can occur if the diffusion angles are sufficiently small. This is not possible for the expansion ratio of the MLC nozzle within the available cavity length, as discussed in Section 6.3. *Fully separated* flow downstream from the throat occurs when the expansion is sufficiently abrupt, as occurs for example with an orifice plate. Partially attached flow through the B-M-E occurs when an asymmetric jet is attached to it at every axial position, but only at one circumferential position. This jet cannot precess because the secondary flow patterns associated with the PAJ discussed in Section 4.1 can occur with this geometry. In this case, the asymmetric jet will leave the nozzle at a large angle to the nozzle axis, but will not precess.

This "non-precession" of the jet can be linked indisputably with the absence of separation at the throat. It is well known that if the pressure ratio across a single throat is greater than that required to produce sonic flow at the throat, then a shock will occur in the expansion downstream of the throat. This shock produces a very strong adverse pressure gradient which will lead to boundary layer separation unless the expansion profile is properly matched to the flow. Thus, for an imperfect expansion, by increasing the driving pressure sufficiently to cause the nozzle to choke, a full separation within the expansion will occur. If the onset of choking is sufficient to cause the non-precessing, partially attached jet to separate fully and then

commence precessing, it was reasoned that this would provide strong evidence to support the precessing jet mechanism postulated above. It is found that the onset of choking does indeed coincide with the onset of jet precession, as illustrated in Figures 4.20 to 4.21. The actual shape of the nozzle at the throat does not have a significant influence on the performance of the nozzle, provided that the recompression shock does in fact cause separation, and that the length of the expansion is not greater than the free reattachment length, (see Section 6.3.1).

Apparatus

The effect of using a bell-mouth at the throat was investigated using "smoke" to visualise the flow. A very intense smoke was required because of the high velocities of the jet. Furthermore it is necessary for the smoke to be injected into the pipe upstream of the throat which is at pressures of up to 120 kPa. The only technique available within the Department which satisfied these requirements was the production of ammonium sulphite smoke. This technique involved the introduction of ammonia and sulphur di-oxide through separate tubes into the region upstream of the nozzle. These two gases can be injected from a high pressure gas cylinder, and they react with atmospheric water vapour and each other as described by the equation below, to form a dense, white powder.

$$2NH_3 + SO_2 + H_2O \rightarrow 2(NH_4)SO_3$$

Both NH_3 and SO_2 are toxic however, and must be treated with caution. The laboratory in which the nozzle is situated is ventilated by a large exhaust fan. Two operators were used so that they could photograph the jet using only a very short burst of smoke, and then leave the laboratory whilst the smoke cleared. In this way, good photographs were obtained safely, although the technique is not well suited to conducting a large number of visualisation experiments. Details of the rig can be seen in Figure 4.12.

As described at the beginning of this section, it is possible to obtain a non-precessing, partially attached, asymmetric jet using a B-M-C-E throat. However, because the nozzle is axi-symmetric, there is no preferred circumferential position for this attachment. To obtain a good photograph of the asymmetric jet, it is necessary for the viewing direction to be perpendicular to the plane of symmetry. Furthermore, the bell mouth nozzle which was used did not always generate a non-precessing, partially attached jet. Both of these experimental problems were solved by placing a small "tooth" asymmetrically in the throat. A piece of brass

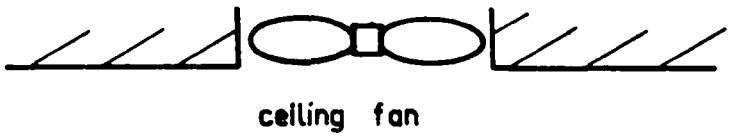

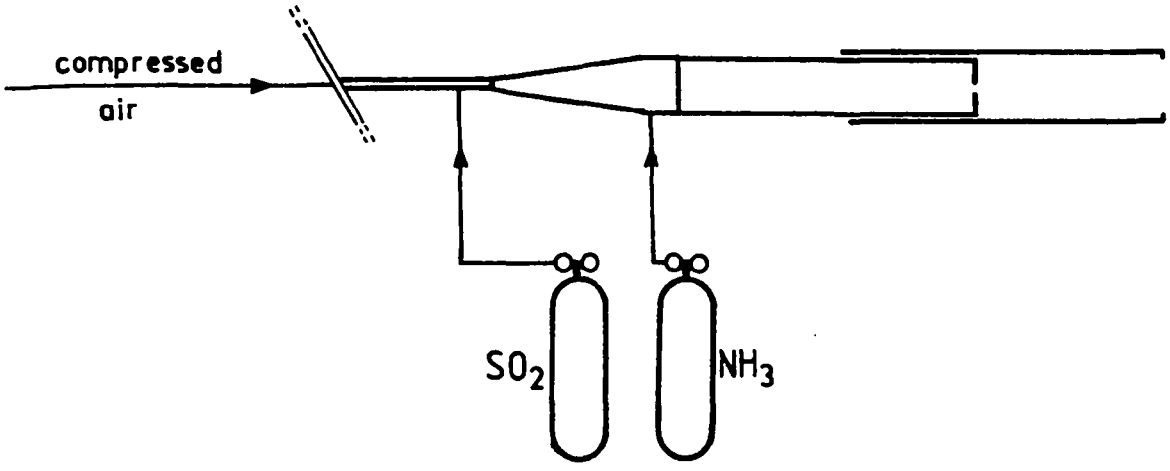

Figure 4.12: NH_3–SO_2 smoke injection apparatus

shim was clamped between the expansion and contraction, so that a small triangle protruded into the throat, Figure 4.14. This slight asymmetry was sufficient to cause the jet to always attach to the wall on the opposite side of the throat to the tooth. Consequently, it was possible to ensure that the image plane of the camera was parallel to the desired viewing plane.

To avoid the misconception that buoyancy may be responsible for the jet deflection, the patterns were inverted by placing the tooth on the opposite side of the throat. The result of this modification is shown in plate 4.13 which verifies that the influence of buoyancy is indeed negligible.

The bell-mouth nozzle, machined on a numerically controlled lathe, has the profile of a modified cosine curve. Modified cosine profiles are used in wind-tunnel contractions to ensure non-separated flow at the test section. The actual shape of the bell-mouth is given by:

$$y = 38sin^{1.5}(9/8)x$$

where y and x are in mm. Detailed drawings of it can be found in Appendix B.6.

The bell-mouth contraction and expansion was used in all tests recorded in the photographs , but the other dimensions in the nozzle were varied as indicated in the captions.

Figure 4.13: The asymmetric jet leaving the bell-mouth nozzle with the nozzle inverted – visualised using smoke. Nozzle dimensions: $d_1 = 14.1$mm, $d_2 = 80$mm, $l = 240$mm, $P_d = 20$kPa, shutter speed = 1/15sec.

Results

The photographs of smoke through the MLC nozzle with a bell-mouth contraction and expansion to produce a non-precessing asymmetric jet give clear evidence supporting of the postulated flow mechanism. The following observations are easily seen.

- The asymmetric jet leaves the nozzle at an angle which typically exceeds 45 deg.
- The asymmetric jet leaves the nozzle with a radial component in the direction opposite from that with which it enters the nozzle cavity along the wall of the bell-mouth expansion.

The latter point can be verified in two ways. First, because the "smoke" is actually a fine, white powder, it leaves a deposit on the surfaces over which it passes. Thus, when the tooth is placed at the top of the throat, the deposit reveals that the jet is attached to the lower surface of the expansion, and the smoke shows that the jet is leaving the nozzle with a strong component in the upward direction, Figures 4.14 and 4.15. Second, by removing the cavity section from the nozzle, so that the jet exhausts directly from the bell-mouth expansion into

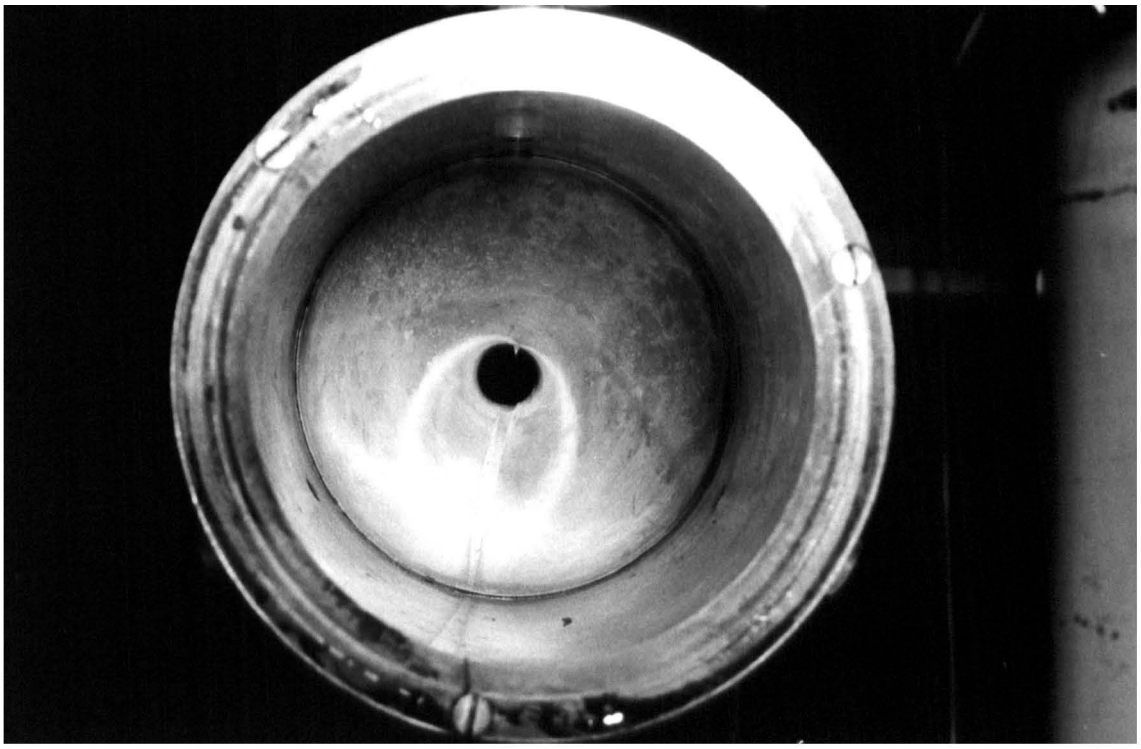

Figure 4.14: The bell mouth nozzle, showing the "tooth" which has been inserted into the throat, and the fine deposit of powder left by the "smoke" passing over the surface. Nozzle dimensions and operating conditions as for Figure 4.13

the atmosphere, without changing the position of the tooth, it can again be seen that the jet is asymmetrically attached along the lower surface of the expansion, as shown in Figure 4.19.

There is very strong evidence that the enhanced mixing phenomenon is in fact the precession of this asymmetric jet. It has already been mentioned that the jet can be made to precess by causing a separation in the throat when the nozzle is choked. Separation can also be caused if deposits of the smoke powder are allowed to build up in the throat. This in effect causes many small "teeth" to be present. Such a condition sometimes leads to intermittent precession, or to the jet oscillating between several preferred positions of attachment. The intermittent precession can be seen in Figure 4.16 which shows characteristics similar to those of the enhanced mixing shown in Figure 4.21. Unfortunately, time did not permit more detailed flow visualisation experiments using techniques such as strobing, or high speed photography to be performed. Such extensions of the experiment would have required a major rework of the ventilation system used in the laboratory because of the longer run times required.

The above flow visualisation experiments also reveal the function of the downstream orifice-plate, or lip. The asymmetric jet has a "natural" tendency, independently of the presence of

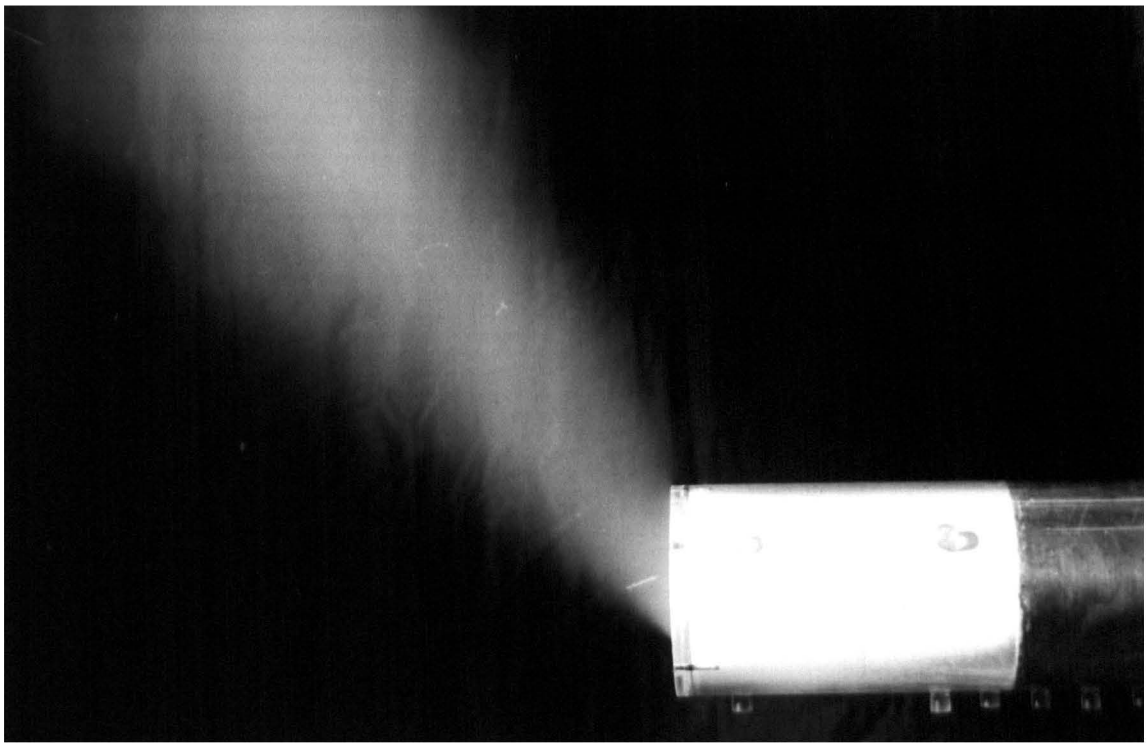

Figure 4.15: The non-precessing asymmetric jet leaving the bell-mouth throated nozzle - visualised using smoke. Nozzle dimensions as for Figure 4.13, shutter speed = 1/8sec

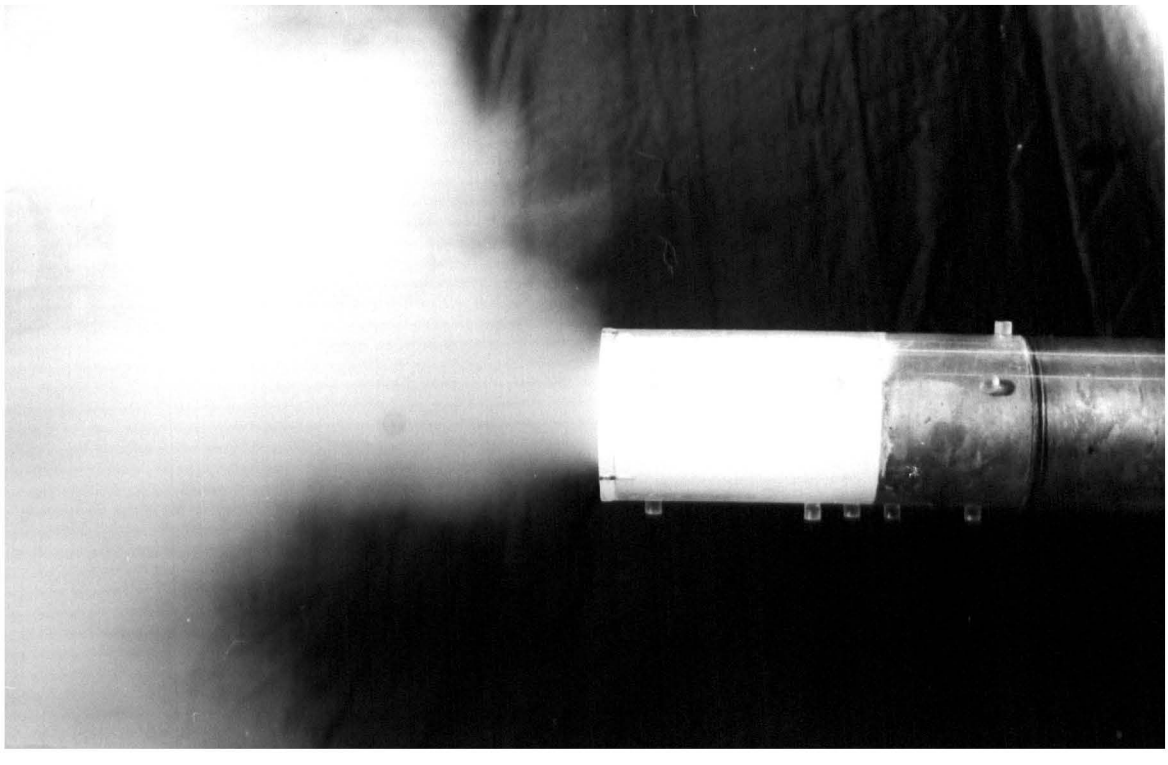

Figure 4.16: Intermittently precessing asymmetric jet visualised using smoke injection. Note that the throat was partially clogged by a deposit of Ammonium Sulphite powder. Nozzle dimensions: $d_1 = 14.1$mm, $d_2 = 60$mm, $l = 240$mm, $P_d = 40$kPa, shutter speed = 1/8sec.

a downstream lip, to leave the nozzle with a radial component directed away from the wall to which it has been partially attached. This can be seen in Figure 4.17 which shows the flow which occurs when no orifice-plate is used at the nozzle exit. The deflection of the jet centreline from the nozzle axis in this case is approximately 25 deg. As the size of the lip is increased, the jet is forced to leave the nozzle at a larger angle. Maximum deflection occurs at or near $d_2/D = 0.6$ where the angle between the nozzle axis and the centreline of the asymmetric jet is approximately 60 deg. Were this jet to precess, the edge of the mean jet would correspond to the outside edge of the instantaneous jet. The half jet spreading angle based on the this edge is about 75 deg. The character of the flow is the same in both cases, but the lip clearly causes much larger spreading angles. It is known that an axial pressure gradient exists at the exit plane of the nozzle in that part of the exit area not occupied by the exiting jet, due to entrainment by the instantaneous jet within the nozzle[3]. Immediately downstream of the exit plane, the jet is exposed to ambient pressure around that part of its circumference furthest from the exit plane, but to subambient pressure over that part closest to the exit plane. Consequently a "radial" pressure gradient must also exist across the exiting jet which causes the marked streamline curvature at the exit plane. It is postulated that the effect of the lip is to increase the magnitude of the radial pressure gradient at the exit plane, thus increasing the angle at which the jet leaves the nozzle. This hypothesis implies that spreading angles should increase with lip size, as has been observed. If the size of the lip is increased beyond the critical value of $d_2/D \approx 0.6$, the nozzle exit plane becomes constricted, inhibiting the influx of ambient fluid into the cavity, and hence reducing the entrainment within the cavity. Thus, the expansion angle begins to decrease, Figure 4.18.

Although the trends exhibited by the non-precessing jet are expected to apply qualitatively to the precessing jet, it is not known by how much the precession motion and its accompanying secondary flow patterns influence the quantitative values. It is known that the absence of the secondary flow patterns enables much larger geometric ratios to be explored for the non-precessing jet than is possible with the precessing jet. For example, it is not possible to stabilise a non-precessing jet when $d_2/D < 0.66$, but it has been possible to stabilise a partially attached jet with even the smallest of the orifice plates which has been made; namely $d_2/D = 0.38$. The reason for this difference can be explained as follows. The criterion for a jet to be partially

[3]This pressure gradient also induces the ambient fluid to move into the cavity in the upstream direction as discussed in Section 4.9

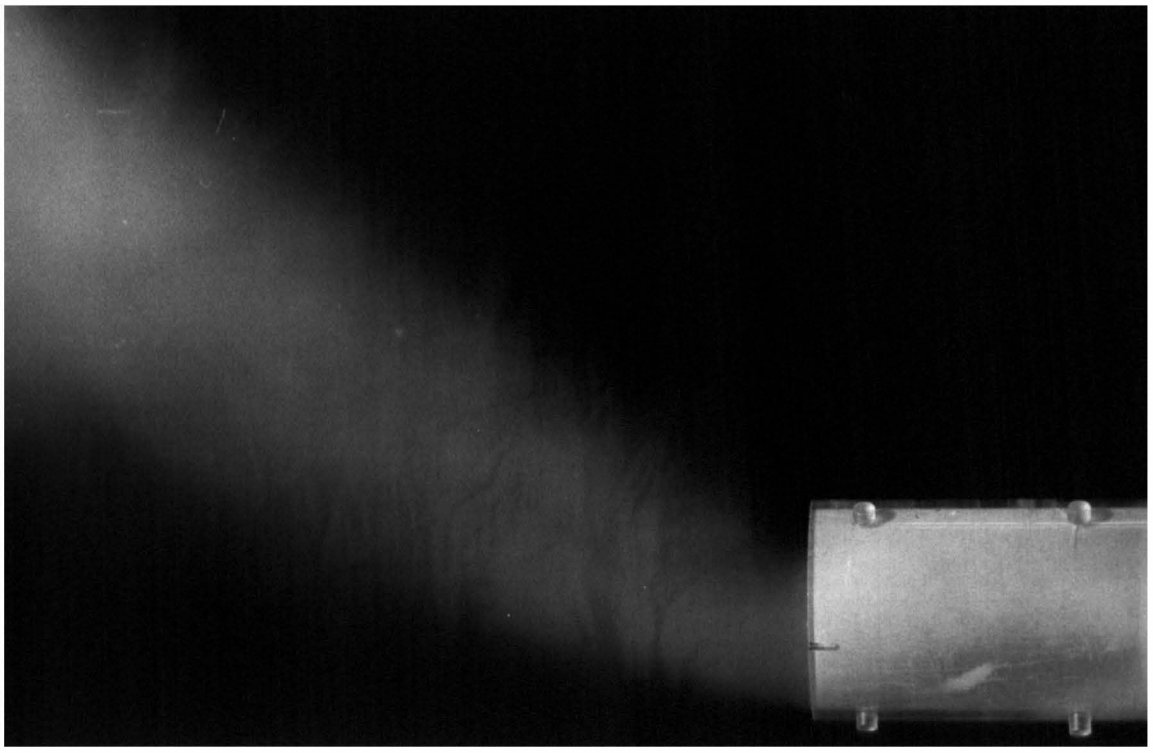

Figure 4.17: The non-precessing asymmetric jet exiting a bell-mouth nozzle which has no downstream orifice; d_2 = 91mm – visualised using smoke. Other nozzle dimensions and operating conditions as for Figure 4.13

attached depends only on the shape of the B-M-C-E and the presence of the tooth, ie. it is independent of the presence of a cavity wall or its length, and the presence and size of a downstream lip. By contrast, an asymmetric reattachment is very sensitive to nozzle geometry and a relatively minor reduction in, say, l or d_2 can cause the jet to fail to attach to the cavity wall, either permanently or intermittently.

The preceeding explanations aid in the interpretation of the investigation of the effects of cavity length and throughput on spread angles of the non-precessing jet. Figures 4.20 and 4.22 show that neither of these quantities influence the angle of exit of the asymmetric jet. It appears then, that, over a significant range, l/D only affects the stability of the asymmetric reattachment of the precessing jet, and does not change the amount of spreading. Similarly, the angle of exit of the asymmetric jet was found to be independent of driving pressure and throughput for sub-sonic conditions at the throat.

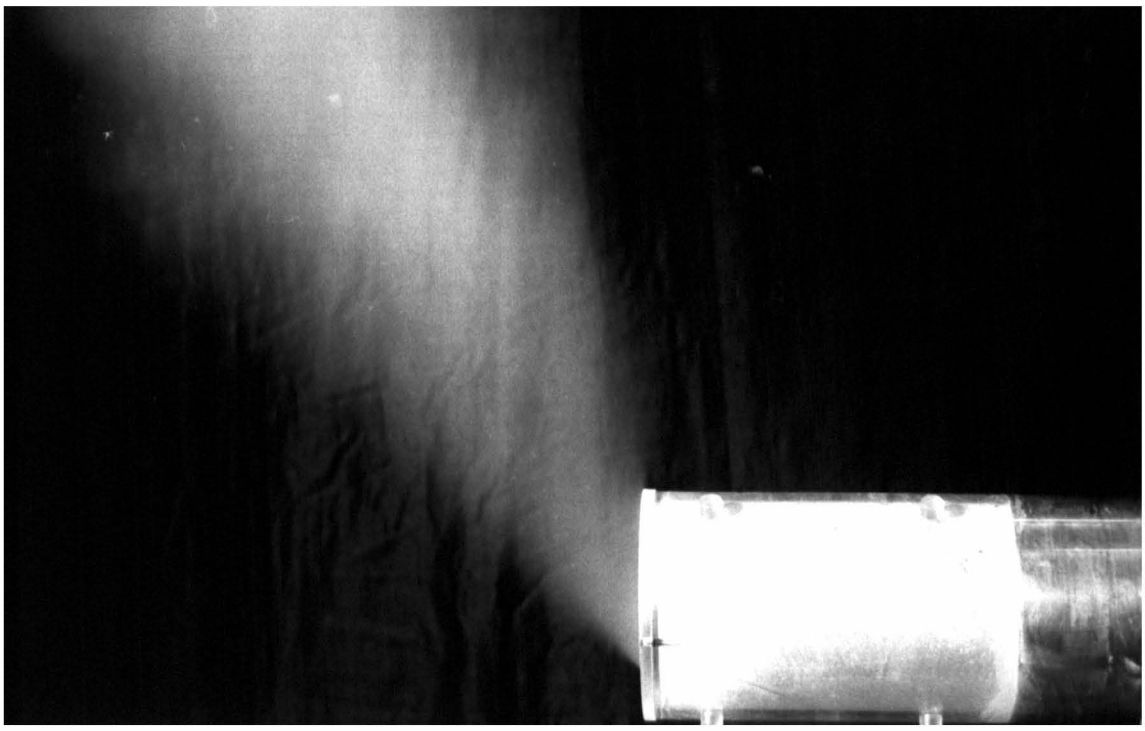

Figure 4.18: The non-precessing asymmetric jet exiting the bell-mouth nozzle which has a large downstream lip; d_2 = 50mm – visualised using smoke. Other nozzle dimensions and operating conditions as for Figure 4.13

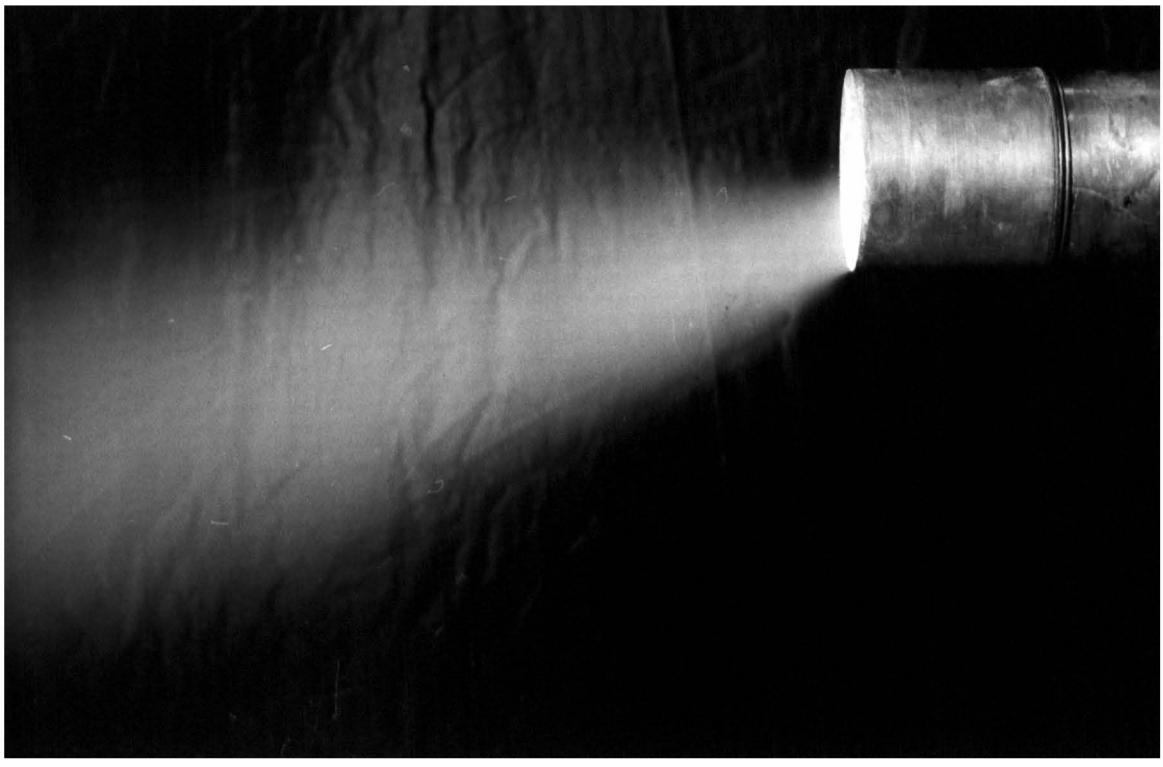

Figure 4.19: A smoke trace of the asymmetric jet leaving the bell-mouth nozzle when the cavity and downstream orifice are removed. Nozzle dimensions: d_1 = 14.1mm, P_d = 20kPa, shutter speed = 1/15sec.

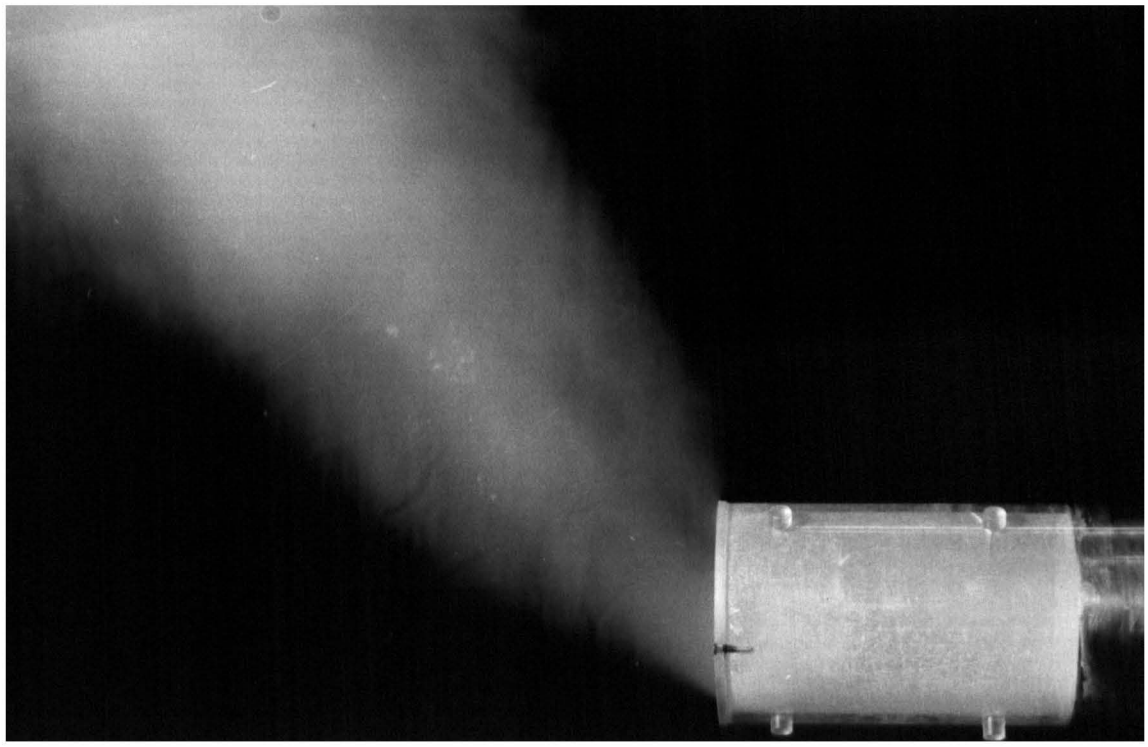

Figure 4.20: The asymmetric jet leaving the bell-mouth nozzle with driving pressure, P_d = 5kPa – visualised using smoke. Nozzle dimensions: d_1 = 14.1mm, d_2 = 80mm, l = 240mm, P_d = 5kPa, shutter speed = 1/15sec.

Application of the Non-Precessing Jet

The non-precessing jet appears to have considerable potential for application in the steering and automatic control of rockets and other jet propelled projectiles. Because the jet can be caused to leave the nozzle at a large angle, it generates a strong side thrust, assuming the structure is appropriately designed. Furthermore, the azimuthal direction of the thrust can be easily controlled by changing the position of the "tooth" in the throat. Alternatively, the azimuthal position of separation could be controlled fluidically, by means of small fluid jets, if temperature constraints made the mechanical system unsuitable. Both these systems are simple, and should be capable of very rapid response.

4.7 The Strouhal Number of the jet precession

The frequency of the precession motion of the asymmetric jet is a characteristic of the enhanced mixing phenomenon. If a characteristic length and a velocity scale can be found to normalise the frequency such that the resulting dimensionless parameter, the Strouhal Number is constant, then those characteristic length and velocity scales provide fundamental informa-

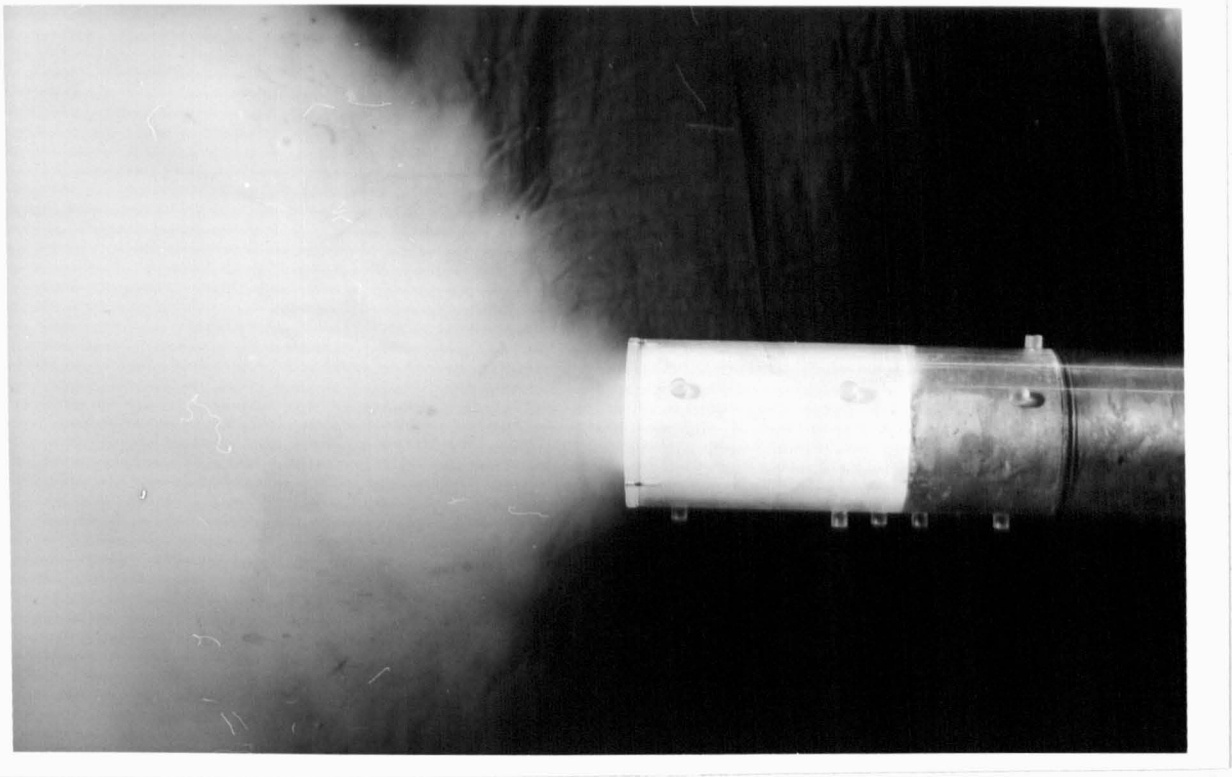

Figure 4.21: When the driving pressure is sufficient to cause the nozzle to choke, the non-precessing jet suddenly begins to precess. The photograph shows the nozzle with choked flow – visualised using smoke. Nozzle dimensions: $d_1 = 14.1$mm, $d_2 = 60$mm, $l = 240$mm, $P_d = 120$kPa, shutter speed $= 1/15$sec.

Figure 4.22: Varying cavity length has negligible influence on the exit angle of the asymmetric jet. Nozzle dimensions: $d_1 = 14.1$mm, $d_2 = 80$mm, $l = 190$mm, $P_d = 20$kPa, shutter speed = 1/15sec.

tion about the flow. In particular, the Strouhal number so formed can also be compared with the Strouhal numbers which characterise other flow phenomena described in the literature.

The precession frequency of the nozzle has been measured using two independent methods, and both yield similar results, with $St = fh/u_1 \approx 5 \times 10^{-3}$. One measurement was conducted in water, by measuring visually the period of a flapping motion of a dye trace. The other was conducted in air, using a hot wire anemometer and a frequency analyser.

The characteristic length scale of the motion has been found to be the "step height" of the upstream orifice plate, h_1, and the characteristic velocity is the mean velocity through the upstream orifice, u_1.

4.7.1 Frequency measurement using dye in water

Quantitative measurement of the precession frequency, f_p, can be obtained using a dye trace situated near the exit plane of the nozzle. When the asymmetric jet is instantaneously in the same circumferential position as the dye trace, the trace indicates a flow in the downstream direction. That is, the dye trace "flips" in and out of the cavity. As the jet precesses to another part of the cavity, the dye trace indicates flow in the upstream direction. The frequency of the

precession can be obtained by counting the number of times that the trace "flips" in a given time span, or by measuring the time span of, say, ten flips. These average frequency measurements are more accurate than trying to visually measure the period of each flip individually. The "flipping frequency" was also measured from ciné photography of the same experiment, and the results averaged. These results, however, are less accurate because the Hycam camera does not have a precision speed control mechanism. (More details of this experiment can be found in Section 4.9.)

The results of the frequency measurements are shown in Figure 4.23. It is clear that the precession frequency is directly proportional to the Reynolds No. (based eg. on d_1 & $\overline{u_1}$), and hence the mean velocity through the upstream orifice. The Strouhal No. of the precession is constant, with a value of $St = f_p h_1/\overline{u_1} \approx 5 \times 10^{-3}$, which is approximately the same as the value of Strouhal No. measured by hot wire anemometry in air.

The limited amount of scatter in the data indicates that the technique is adequate. Each data point of the real time measurements (data sets 1, 2 & 3) is averaged over at least one hundred and twenty cycles. That is the time taken for ten flips was measured at least twelve times, and the average of these results is plotted in Figure 4.23. By contrast, f_p as measured from the ciné film was obtained from an average of approximately fifteen cycles. Furthermore, the Hycam camera is only recommended for operation at framing rates of over twenty frames per second, (fps). Whilst the speed control, which is effected by a servo-controlled brake on the motor, is adequate from the point of view of photography, it is inadequate as an accurate time base for measurements, particularly at the low framing rates, down to 10 fps, necessary in the experiment to maximise depth of field. With this in mind, the conclusion that the relationship between f_p and Re is linear is not disturbed by the scatter in the data.

4.7.2 Frequency measurement using hot wire anemometry

The constant temperature hot wire anemometer, (CTA), is a small instrument with a very rapid response time making it ideally suited to the measurement of rapid fluctuations in velocity. However, used by itself, a single wire cannot give any information about the direction of the flow which is moving past it, although it measures the component of velocity which is normal to the wire (within a large range of yaw angles, Perry [74]).

In the present nozzle, the *predominant mean* directions of flow over the surface are known from the china clay experiments, which aid in determining a true velocity from the signal close

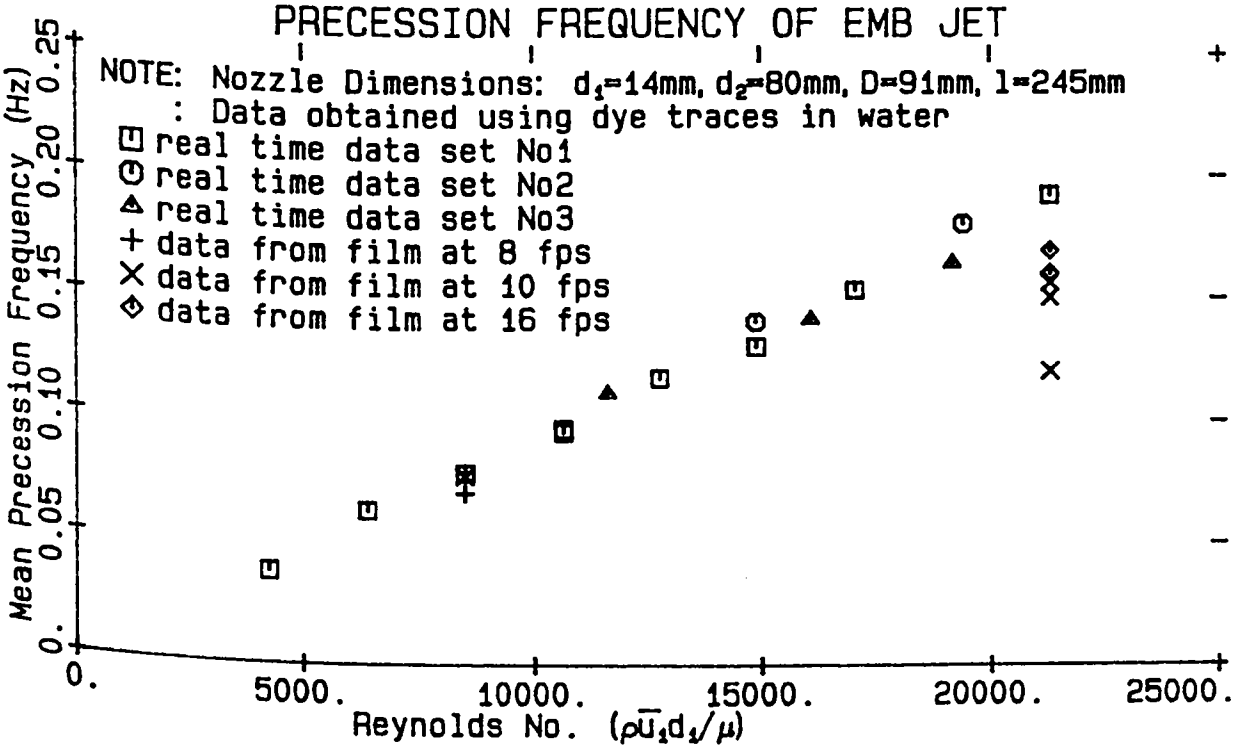

Figure 4.23: The Precession Frequency of the MLC nozzle as determined using a dye trace in water

Note:

- Real time data is averaged over at least 120 cycles.
- Data obtained from the ciné film is averaged over about 15 cycles.
- The framing rate of the camera is not guaranteed below 20fps.

to the wall. However, because the flow is highly three dimensional and complex, the hot wire anemometer is inadequate for giving accurate (and perhaps even meaningful) measurements of the velocity field within the body of the cavity or within the jet downstream from the exit plane. Nevertheless, the CTA is quite capable of measuring accurately the frequency of the velocity fluctuations, if not their direction. It is suitable, therefore, for determining the frequency of the large scale oscillations in the magnitude of the velocity which occur within the cavity, in the region downstream of the positive bifurcation line as the reattachment point precesses around the inside of the cavity.

To isolate the parameters on which the precession motion depends, the frequency spectrum of the flow near the exit plane was measured for a range of flow-rates and nozzle dimensions. eg. h_1, d_2, l and insert position, x_i. Only the mean frequency of the precession motion was measured. More detailed experiments such as ensemble averages, higher order moments and other frequencies in the asymmetric jet remain for further investigation.

Apparatus

The constant temperature hot wire probes were made of 5μm dia. tungsten wire of 3.2mm length. The probe holder was 3.2mm in diameter. The measurements were made using a TSI 4 channel hot wire anemometer, model IFA 100. The frequency response of the circuit was optimised, although this was hardly necessary because the frequency of interest was of the order of 10 Hz. The output signal from the IFA 100 was connected to a HP 3582A Spectrum Analyser from which a permanent record of the frequency spectrum could be obtained.

4.7.3 Results

The frequency spectra, Figure 4.24, clearly show a peak at approximately ten hertz, with much lower signal amplitudes at all other frequencies. The peak frequency corresponds to a Strouhal number, based on the step height of the upstream orifice and the mean velocity through the upstream orifice, of about 5×10^{-3}. This is a clear indication that the mechanism is not excited acoustically, because the Strouhal numbers associated with acoustic excitation are typically within the range 0.1 [96] to 0.6 [71].

The results of the frequency investigation are summarised in Table 4.1. The Strouhal number is calculated for a range of values of the characteristic velocity scale and of the characteristic length scale. Two of the velocity scales are calculated from a measured mass flow

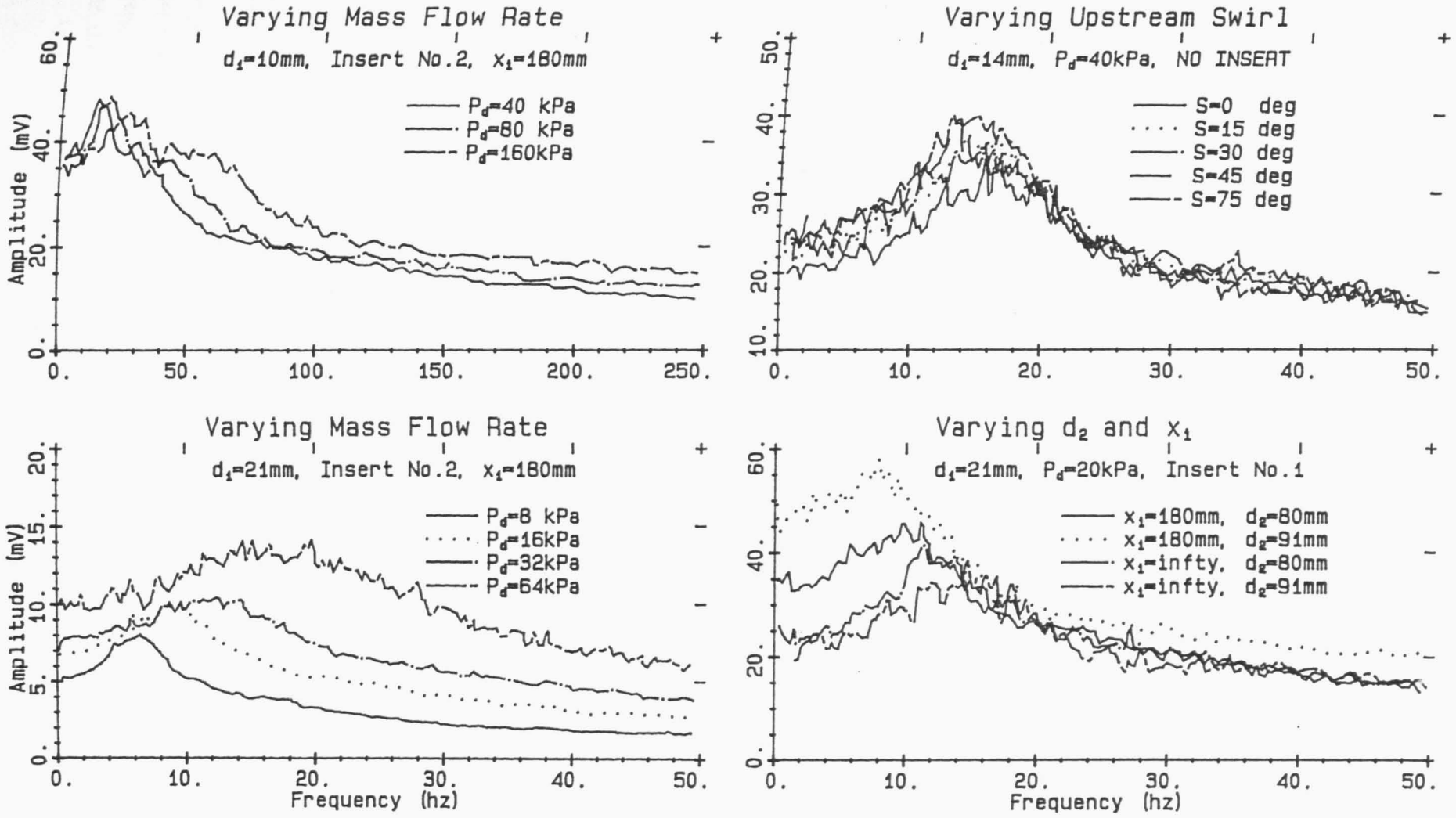

Figure 4.24: Typical frequency spectra of the flow inside the MLC nozzle obtained using hot-wire anemometry.

rate and an assumed density, while the third is calculated from a compressible flow analysis. Thus,

- $\overline{u_{1d}} = \dot{m}/\rho_d A_1$, ie. based on driving pressure and area of orifice plate,
- $\overline{u_{1a}} = \dot{m}/\rho_a A_1$, ie. based on atmospheric pressure and area of orifice plate,
- $\overline{u_{1c}} = \sqrt{[(\frac{p_0}{p_\infty})^{\frac{\gamma-1}{\gamma}} - 1](\gamma R T_t)(\frac{2}{\gamma-1})}$, ie. based on compressible flow analysis; independent of A_1.

It can be seen from Table 4.1 that neither d_1 nor d_2 are the characteristic dimensions on which f_p depends, because the Strouhal numbers based on them are strong functions of d_1. The Strouhal numbers based on h_1 show far less dependence on d_1, but their values are still vary. Those based on a velocity which has been calculated from the mass flow rate and an assumed density show a slight dependence on P_d, and that based on the velocity calculated using the compressible flow analysis shows a slight dependence on d_1. Furthermore, the relatively large changes in d_1/D correspond to much smaller changes in h_1/D. Consequently it is not possible to state conclusively from these experiments that $f_p \propto 1/h_1$, since it may be independent of both h_1 & d_1. However, the following explanation shows that it is plausible to interpret $St = f_p h_1/u_1$ as being the appropriate form.

It is probable that the calculation of the characteristic velocity from $\overline{u_1} = \dot{m}/\rho A_1$ contains an unknown function of P_d. Although the density at the throat is known reasonably accurately, the coefficient of discharge, and hence the area of the vena contracta, is a function of P_d. [4] By contrast, $\overline{u_{1c}}$ is independent of the throat area as its derivation assumes a large contraction ratio, and $St = f_p \times h_1/u_{1c}$ can be seen to be independent of P_d. Note that the assumption of a large contraction ratio is less valid for the larger orifice, and so a slight dependence on d_1 will result. It is worthwhile recalling that in the experiments where dye was injected in water (which is incompressible), the Strouhal numbers are independent of throughput, ie. $f_p \propto \overline{u_1}$.

It appears that the fluid-mechanic dimension on which the frequency scales is the "reattachment length", ie. the distance to the positive bifurcation line (see Section 4.8). Others

[4] The Engineering Science Data Unit [36] p 5 & 6, states that whilst c_d can be considered to be independent of Re (for thin plates with porosity < 0.5 and Re > 400), it does depend upon Mach Number, M. Increasing the pressure ratio across an orifice causes a gradual increase in M and consequent increase in the area of the vena contracta until the vena contracta chokes. Although further increase of the pressure ratio will not increase M, the vena contracta will continue to increase in area until it coincides with the edge of the orifice plate.

[5] Enhancement is very weak or negligible for this configuration

Nozzle Dimensions						Strouhal No.				
d_1/D	d_2/D	l/D	x_i/l	P_d (kPa)	f (hz)	$fh_1/\overline{u_{1d}}$ ($\times 10^3$)	$fh_1/\overline{u_{1a}}$ ($\times 10^3$)	$fh_1/\overline{u_{1c}}$ ($\times 10^3$)	$fd_1/\overline{u_{1a}}$ ($\times 10^3$)	$fd_2/\overline{u_2}$
0.231	0.88	2.69	0.75	8	6.6	4.7	4.3	2.0	2.6	0.15
"	"	"	"	16	9.0	4.6	3.9	2.0	2.4	0.14
"	"	"	"	32	12.8	4.9	3.7	2.1	2.2	0.12
"	"	"	"	64	17.9	5.6	3.5	2.1	2.0	0.11
"	"	"	"	20	10.9	4.8	4.0	2.1	1.6	0.13
"	1.0	"	"	"	8.2	3.6	3.0	1.6	1.2	0.15
"	1.0	"	–	"	15.2	6.7	5.6	3.1	2.3	0.21
"	0.88	"	–	"	12.0	5.3	4.4	2.4	1.8	0.19
0.110	"	"	0.75	8	7.4	4.9	4.5	2.7	1.1	0.57
"	"	"	"	19	11.0	5.4	4.5	2.6	1.1	0.57
"	"	"	"	40	15.0	5.5	3.9	2.0	1.0	0.50
"	"	"	"	80	19.0	6.0	3.2	2.4	0.8	0.41
"	"	"	"	160	28.0	8.0	3.0	2.7	0.7	0.38
0.155	"	2.42	–	20	9.2	4.0	3.3	2.0	1.2	0.22
"	"	2.69	–	"	11.5	5.0	4.2	2.5	1.5	0.28
"	"	2.86[5]	–	"	15.4	6.7	5.6	3.4	2.1	0.37
"	"	3.08[5]	–	"	20.8	9.0	7.6	4.6	2.8	0.50

Table 4.1: Summary of Strouhal numbers of the MLC nozzle, as measured using hot-wire anemometry

have found that the reattachment length behind an orifice plate scales with the step height, for example see Section 7.3. Thus it is anticipated that in the present nozzle also the step height of the primary orifice will have a predominating influence on f_p. However, the geometry of the present nozzle is more complicated than that of a simple orifice plate and so it is expected that the height of the *downstream* orifice plate, and the presence of a bluff body may also influence f_p. This is indeed the case, as can be seen from figure 4.24, and Table 7.1. Clearly f_p increases as h_2 increases when the insert is at $x_i/l = 0.75$, but this trend is reversed when the insert is removed.

Increasing l/D causes an increase in f_p, with a simultaneous reduction in the intensity of the peak for the longer cavities. The effect of decreasing x_i/l (ie. inserting the bluff body further into the cavity), is generally to decrease f_p, and at the same time to increase the intensity of the peak.

Whilst the Strouhal number based on d_1 is clearly not the parameter which describes the precession motion within the cavity, it is the parameter which must be used for comparison with other data in the literature. All fluidically and mechanically excited jets are characterised by the jet "diameter" (or jet width in the case of a plane jet). These values are listed in Table 7.1. It can be seen that the measured values of $f_p d_1/\bar{u}_1$ fit within the range of values of flapping two dimensional jets obtained by other authors – usually being toward the low end of the stated values. This is discussed more fully in Chapter 7.

4.7.4 The effect of insert position and geometry on Precession Frequency

The influence of the geometry and dimensions of the insert upon the precession frequency is shown in Figure 4.25, and the dimensions of the inserts are given in Table 4.2. The axial location of the insert, x_i, is normalised by the step height of the upstream orifice, h_1, because it is postulated that the insert influences the position of the three dimensional positive bifurcation line, x_p, and thus the precession frequency, f_p.

It is suggested that f_p will increase as the reattachment distance, x_p decreases. A decrease in x_p must be accompanied by an increase in the radial pressure gradient which causes the jet to reattaching and, because the flow patterns within the nozzle are three dimensional, a simultaneous increase in the axial pressure gradient will occur. This implies increased momentum in the reverse flow into the cavity, and, when it is deflected, increased swirl intensity. This in turn will lead to an increase in the skin friction force exerted by the attached jet on the wall,

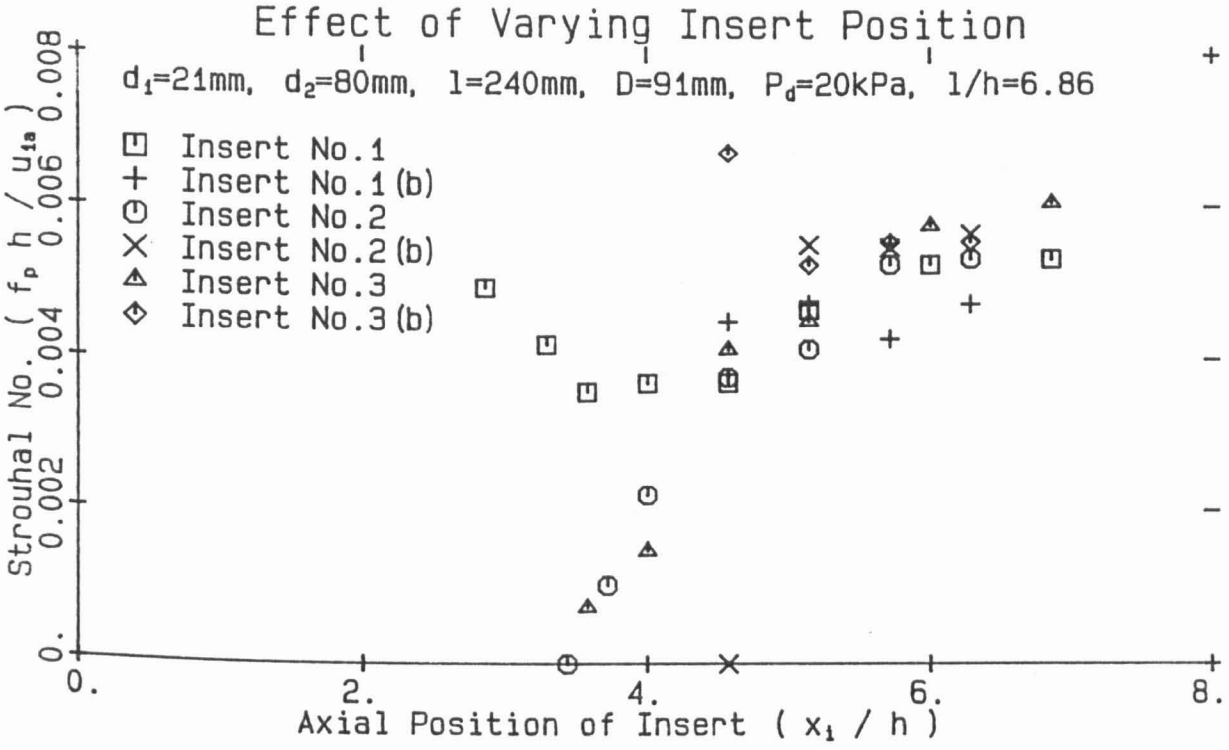

Figure 4.25: The effect of insert dimensions on the frequency of precession

and as illustrated in Figure 4.3, will tend to increase f_p.

It is clear that both the axial location of the insert, x_i, and its dimensions can have a large influence on the precession frequency, f_p, of the jet. When the insert is hollow, f_p depends strongly upon x_i and has only a secondary dependence upon the dimensions of the insert for a large part of the operating range. When the insert is solid, f_p is nearly independent of x_i for the range of inserts tested, and only the secondary dependence exists. The hollow inserts are able to be inserted much further into the cavity than are the solid inserts, before their presence destroys the flow patterns.

There appears to be a critical ratio of the outside diameter of the insert to the diameter of the cavity, D_i/D, for *hollow* inserts. Below this critical ratio, f_p decreases monotonically with x_i. Above this critical ratio, when the insert is introduced from the exit plane, f_p decreases with x_i to a minimum value, and then increases as x_i is further reduced. Insufficient experiments have been conducted for the occurrence of a critical value of D_i/D to be confirmed, or its value elucidated, however a conceptual hypothesis of its influence is tentatively proposed.

The locus of the motion of the instantaneous jet in the cavity will define a radius, r_{j-max}, of maximum instantaneous velocity, u_{j-max}. The presence of the hollow insert will cause a

Table 4.2: The dimensions of the various inserts

See Figure ?? for a description of the notation.

Insert No.	D_i (mm)	D_i/D_c	wt (mm)	l_i (mm)
1	55.0	0.604	3.30	20
1(b)	"	"	27.50	"
2	38.5	0.423	1.90	25
2(b)	"	"	19.25	"
3	31.5	0.346	1.60	20
3(b)	"	"	15.75	"

drag on the instantaneous jet, and so impose a radial pressure gradient on it. If the radius of the hollow insert is less than r_{j-max}, the pressure gradient will tend to move the jet towards the geometric centreline of the nozzle. Conversely, if its radius is greater than r_{j-max}, the pressure gradient will be radially outwards, tending to push the instantaneous jet towards the wall.

If $D_i \leq 2r_{j-max}$, decreasing x_i will have the same effect as will decreasing the cavity length, l, ie. the jet will be caused to diverge from the nozzle at a greater angle.This implies that a stronger axial pressure gradient will be imposed in the cavity, ie. the pressure on the upstream side of the diverging jet, within the cavity, must be lower relative to atmospheric pressure. However, this pressure gradient also implies that the pressure "above" the reattaching jet is reduced, or that the radial pressure gradient across the reattaching jet is reduced. This results in an increase in the reattachment distance, x_p, and a consequent decrease in f_p. It is anticipated that increasing the step height of the *downstream* orifice would have a similar effect.

It is interesting to observe that as the hollow inserts are inserted further into the cavity, the precession motion is eventually destroyed. The value of x_i/h_1 for which this occurs corresponds closely to the axial position, x_p/h_1, at which the asymmetric jet reattaches to the wall (cf. Table 4.4). It was also found that intermittency increases as x_i approaches x_p, and that for the smaller diameter inserts, f_p continues to decrease. It is proposed that the radial pressure

gradient described above, imposed by the presence of the insert in this sensitive region, is sufficient to prevent the reattachment from occurring, either totally or intermittently. With the larger diameter insert, as x_i approaches x_p, its effect on f_p changes, and f_p increases with decreasing x_p. It is suggested that this is caused because $x_i < x_{p1}$ and $D_i > 2r_{j-max}$ at that axial plane. Consequently its effect is to *decrease* the reattachment length and consequently to *increase* f_p.

This tendency throws further light on the limits of the nozzle geometry. It can be seen that decreasing the cavity length without the presence of an insert will lead to an unstable situation because the position of reattachment will get closer to the plane of the downstream negative bifurcation, x_{n2}. These two bifurcation lines will have a tendency to combine and cancel each other, thus eliminating the reattachment entirely. At a critical cavity length, l_{crit}, the jet will be bi-stable, and will oscillate between asymmetric reattachment, and no reattachment. This is the intermittency described earlier. If $l < l_{crit}$, then the mechanism will be unstable, and the enhanced mixing will not occur.

The effect of a solid insert is to force the asymmetric jet to flow around it, and thereby to prevent the instantaneous jet from intermittently flowing directly through the cavity without attaching anywhere to the wall. However, a solid body is quite capable of sustaining an axial pressure gradient across it, and so its presence tends to isolate the reattaching jet from any changes in pressure which may occur downstream of it. For this reason, x_p and hence f_p, are not likely to be greatly influenced by x_i.

4.8 China Clay flow visualisation

It is well recognised that if the flow patterns on the surface of a body are known, the character of the entire flow which is influenced by the body can be deduced [94,44]. Perry(1986) and Perry & Hornung (1984) have proposed the technique of experimentally determining the "critical points" (eg. points of separation and reattachment, or their three dimensional counterparts of negative and positive bifurcation lines respectively), and deducing a vortex skeleton of the flow because the streamlines can only be joined in a limited number of ways. From these, the complete velocity field can be approximated using the Biot-Savart law.

The type of surface flow patterns which can occur in three dimensional separated flow, are described and defined by Hornung & Perry (1984). The same definitions are used here,

because the two dimensional terms are inadequate and misleading. A positive bifurcation line (which in 2-D flow is equivalent to a line of reattachment), can be recognised by a component of flow moving away from it perpendicularly in both directions in the plane of the surface. Similarly, a negative bifurcation line (which in 2-D flow is equivalent to a line of separation), has a component of flow moving towards it from both sides of the line.

Various techniques exist for the visualisation of the flow over a surface, but obvious advantages exist in those which leave a permanent record. The method selected for the present study is a variation of the well known china clay technique.

4.8.1 Apparatus

The usual method of china clay flow visualisation consists of applying a thin layer of "china clay" (Kaolin) to the surface. When this is dry the surface has an opaque, white appearance. An oil is sprayed onto the surface which changes the refractive index of the clay, making it appear transparent, and then the flow is started. The mass transfer coefficient in the region of points of reattachment is high, which causes the oil to evaporate there first, returning the surface to its original colour. By contrast, points of separation dry most slowly. By photographing the surface at various stages in the drying process, it is possible to determine the critical points [19].

The technique used in this experiment, however, consisted of spraying the china clay on to the surface, and allowing it to dry *completely* whilst the surface is placed in the flow. The china clay then forms droplets which align themselves with the *average* streamlines over the surface. This permanent record yields far more information than does the other technique. (A theoretical and experimental discussion as to why the droplets align themselves with the mean streamlines is given by Ludweig and Hornung (1986) who investigated a very similar flow visualisation technique.)

To be able to examine the flow patterns inside the nozzle, a thin sheet of metal shim was rolled into a cylinder, and slid into the nozzle. This could then be removed when dry, unrolled for examination, and photographed. To improve the contrast, the surface of the metal was painted black, using a solvent-resistant paint. It was also found that if some of the oil was mixed with the china clay (about one-third oil), the mixture formed more distinct droplets – probably due to a change in surface tension. The flow over the downstream face of the upstream orifice was also able to be seen using this method, although its surface was not

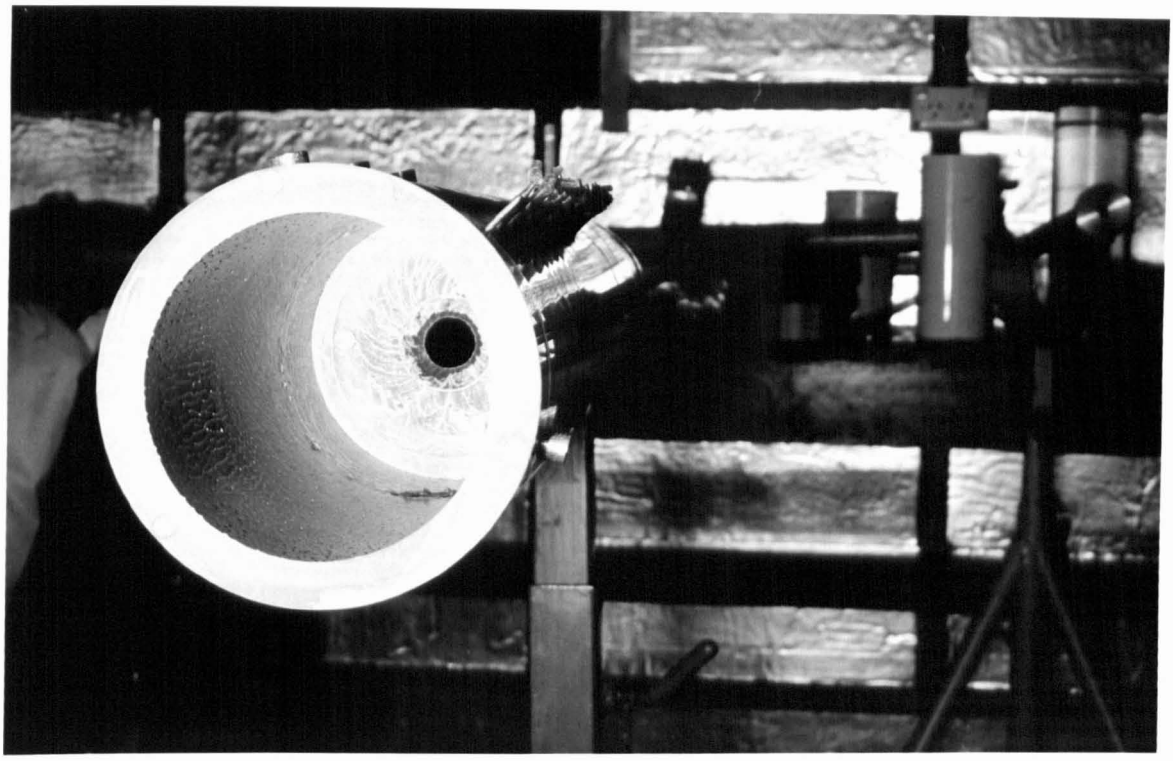

Figure 4.26: China clay flow visualisation — with the metal sheet in-situ. Nozzle scale: $D = 91\text{mm}$.

painted.

Figure 4.26 shows the dried flow patterns, with the metal sheet in-situ, ie. before being removed for photography. The other plates show the surface with the sheet unrolled.

Because the metal sheet is rolled around a horizontal axis whilst the experiment is being run, gravity exerts an influence on the motion of the fluid on the surface. If the mean velocity of the air within the nozzle is too low, then this influence can be significant, particularly on the surfaces which are most vertical. In these cases a circumferential component towards the "bottom" of the cavity will be superimposed upon the other flow patterns. It was found that for Reynolds numbers above 10^5, the influence of gravity was insignificant.

In all these experiments the large scale perspex nozzle with a cavity diameter of $D = 91\text{mm}$ was used, being large enough for the drop size of the china clay to be small relative to the flow patterns being visualised, and not too large for the compressor to supply air whilst the patterns were drying.

4.8.2 Results

The most important features can be seen in Figure 4.27, where the metal sheet has been unrolled. The mean flow direction is from bottom to top. The most obvious and important

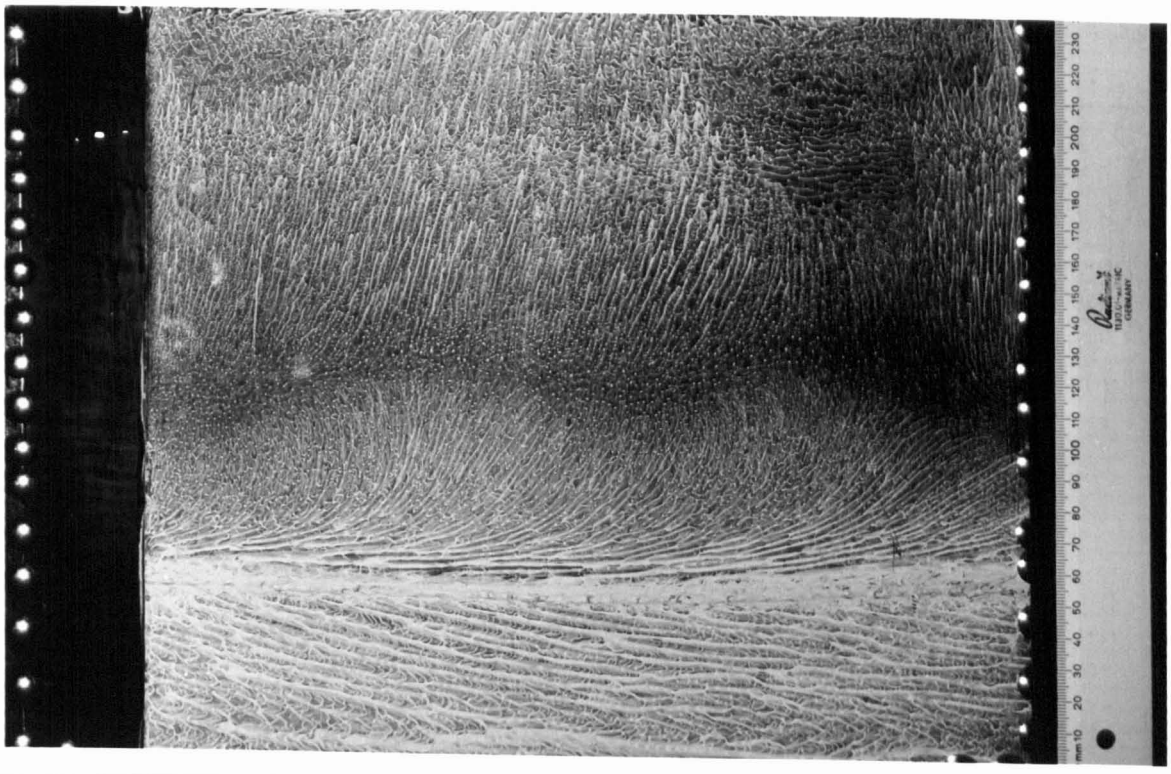

Figure 4.27: The flow patterns on the inside surface of the cavity, with the metal sheet unrolled. Mean flow direction is from bottom to top. Nozzle dimensions: $d_1/D = 0.155$, $d_2/D = 0.88$, $l/D = 2.7$, $D = 91$mm, insert No.1(b), $x_i/D = 2.2$, $P_d = 80$kPa.

features are:

- A transverse flow direction in the upstream part of the cavity, indicating a strong swirling motion.
- An upstream negative bifurcation line (ie. a three dimensional separation from the surface) where the transverse flow and the reversed "axial" flow combine.
- A positive bifurcation line (ie. a three dimensional reattachment line) approximately two-thirds of the distance from the entrance into the cavity.
- A downstream negative bifurcation line immediately upstream from orifice lip at the exit of the cavity.

A close-up of the upstream *negative* bifurcation line is shown in Figure 4.28, where it can clearly be seen that flow is moving towards the line from the upstream and downstream directions. It also shows the flow in the region of strong swirl in the upstream part of the cavity.

Figures 4.29 and 4.30 show the *positive* bifurcation in more detail. The flow is clearly moving away from the line in both the upstream and downstream directions. However, whilst the flow which continues in the downstream direction is in a purely axial direction, the streamlines on the surface generated by the reversed flow foot are curved. Curved streamlines indicate that there will be a gradient in the direction away from the surface of the azimuthal component of velocity. Thus the azimuthal thrust component exerted by the flow away from the surface of the reversed flow foot (described in Section 4.1) on the point of positive bifurcation will be greater than indicated by these mean surface stream lines.

There is some variation in the azimuthal component of direction of the reversed flow foot with nozzle configuration and operating conditions. In some cases, of which Figure 4.30 is typical, it seems clear that the reversed flow foot has an azimuthal component at the plane of the positive bifurcation. However in other cases, eg. Figure 4.29 and more clearly Figures 4.48 and 4.49, the flow appears to be entirely axial there. In the case of the latter two photographs, the enhancement was greatly weakened by the insertion of probes into the cavity (as discussed in Section 4.8.7). This could imply that the presence of an azimuthal component in the direction of the reversed flow foot, indicates higher precession frequency and/or more stable enhancement. Nevertheless, it should be recalled from the discussion in Section 4.1 that even when the flow along the surface is purely axial, the reversed flow foot must be moving in a helical path.

Examination of the flow over the upstream orifice plate (see Figure 4.31), reveals that swirling flow in the upstream part of the cavity (hereafter referred to as the "cavity swirl") is spiraling radially inward toward the nozzle centreline where it will be entrained into, or wrap itself around, the precessing jet. This is consistent with the observed static-pressure measurements on the cavity wall (see Figure 4.11) which shows that the pressure immediately downstream of the primary orifice plate is very low. Were the flow spiraling outward from the precessing jet, this would be required to be a region of high pressure.

4.8.3 Discussion of Results

The flow patterns indicated by the surface flow visualisation are highly three dimensional, and cannot be described by a two dimensional model. Neither can they be explained by a steady state flow model. They can only be explained by a a non-steady, 3-D model, such as that of the precessing, asymmetric jet described herein.

Figure 4.28: Enlarged view of the surface flow patterns of the upstream, negative bifurcation line. Mean flow direction is from left to right. Nozzle dimensions: $d_1/D = 0.155$, $d_2/D = 0.88$, $l/D = 2.7$, $D = 91$mm, insert No.1(b), $x_i/D = 2.2$, $P_d = 80$kPa.

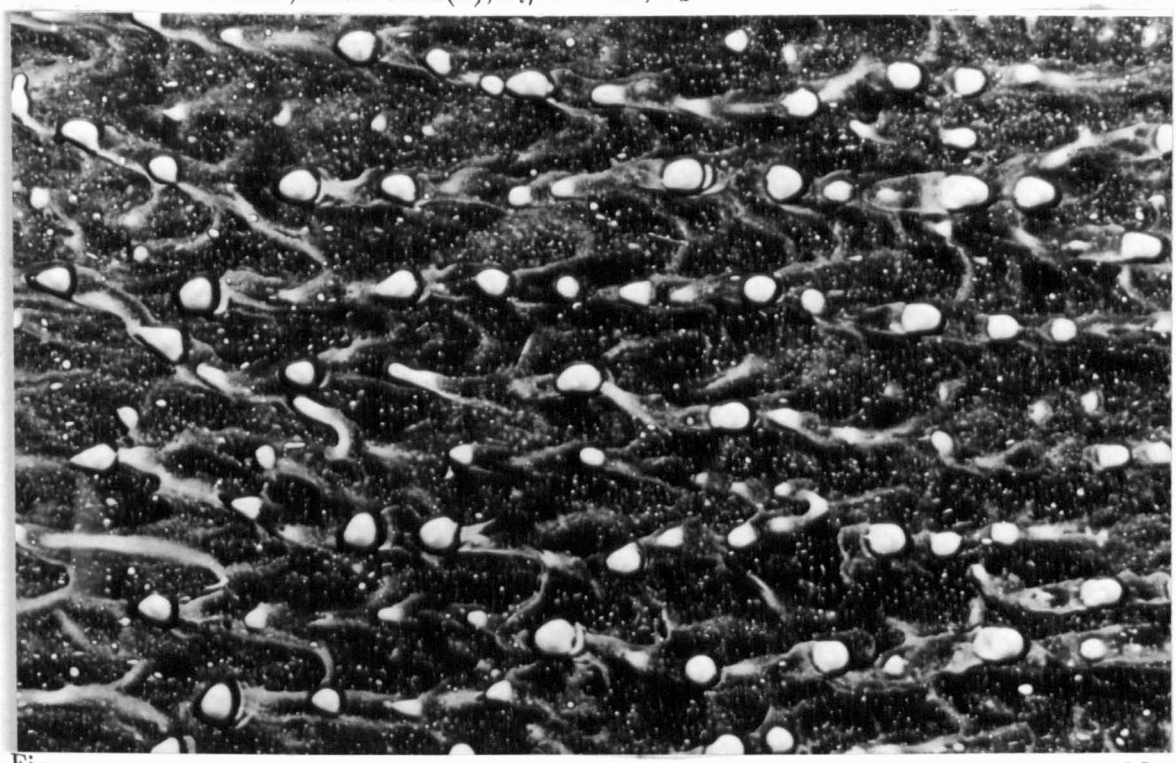

Figure 4.29: Enlarged view of the surface flow patterns of the positive bifurcation line. Mean flow direction is from left to right. Nozzle dimensions: $d_1/D = 0.187$, $d_2/D = 0.88$, $l/D = 2.7$, $D = 91$mm, $P_d = 60kPa$.

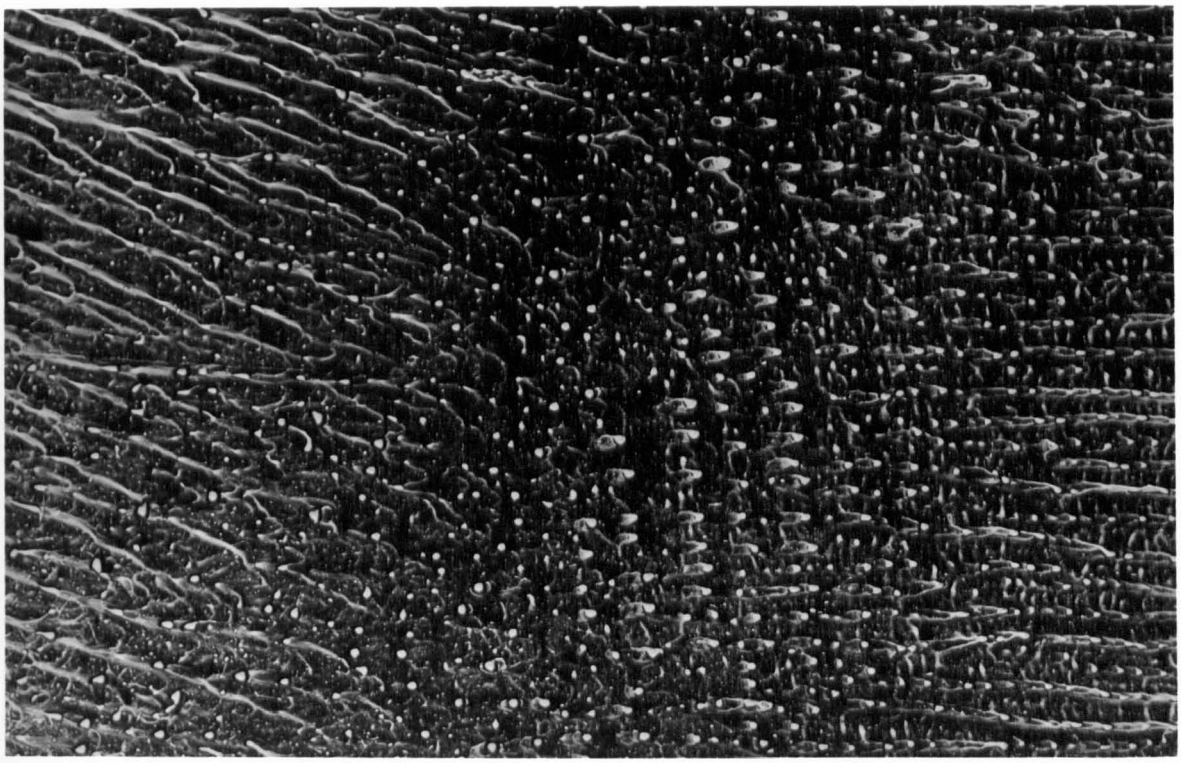

Figure 4.30: Enlarged view of the flow patterns up and down-stream from the positive bifurcation line. Mean flow direction is from left to right. Nozzle dimensions: $d_1/D = 0.110$, $d_2/D = 0.88$, $l/D = 2.7$, $D = 91$mm, $P_d = 160kPa$.

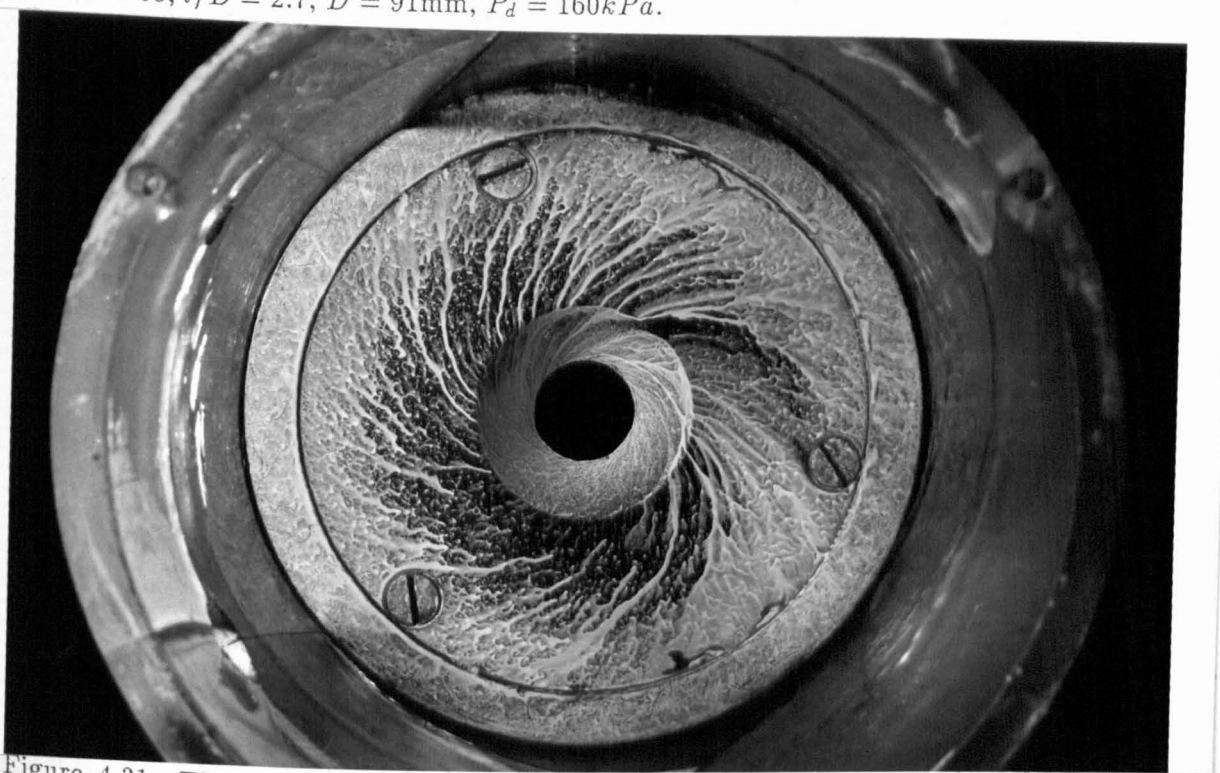

Figure 4.31: The flow over the surface of the upstream orifice plate. Nozzle dimensions: $d_1/D = 0.155$, $d_2/D = 0.88$, $l/D = 2.7$, $D = 91$mm, Insert No. 1(b) at $x/D = 2.2$, $P_d = 80$kPa.

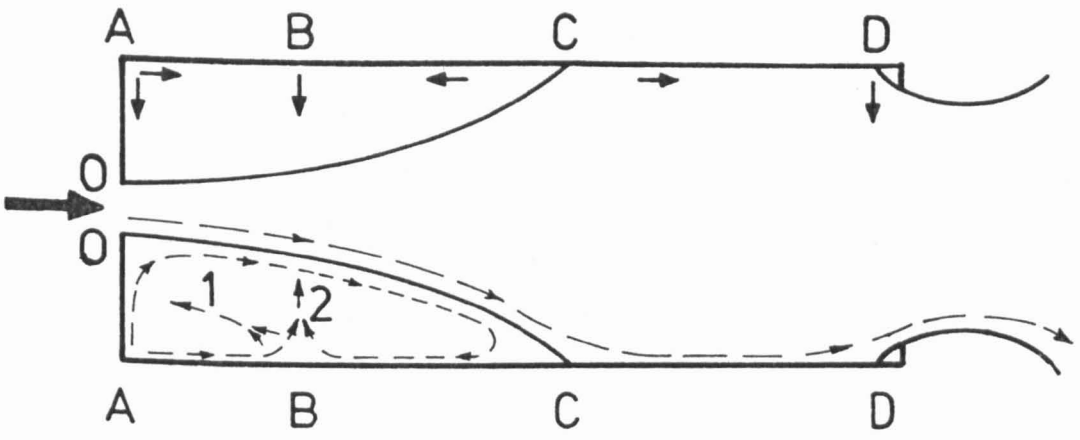

Figure 4.32: A two-dimensional, steady-state model of the flow patterns is unable to explain the observed flow directions. The arrows on the surface indicate the axial component of the flow directions on the surface, as determined by the china clay results.

Figure 4.32 shows the inadequacies of an axi-symmetric, steady-state model in explaining the observed flow directions. A strict axi-symmetric model entirely ignores the swirling flow in the back of the cavity, and so cannot be used. However even a pseudo-two dimensional model, upon which a swirling component would be superimposed on the flow upstream of the known negative bifurcation line, will be shown to be inadequate.

The steady state, axi-symmetric model requires that the flow reattaches symmetrically, in a manner similar to that of the flow downstream of an orifice with a small expansion ratio. This is consistent with the flow directions observed at point C in Figure 4.32. However the model cannot explain the observed flow directions at points A and B.

The flow is observed to be moving away from point A in both the axial and radial directions. This requires that point A be an infinite source, which is clearly impossible. Furthermore, topological rules exist, as described by Hunt et. al. [44], which require that the point of separation at B has a corresponding point of reattachment. Agarwal [7], who investigated the flow through orifice plates with small expansion angles, also found a "secondary" separation downstream of the orifice plate. However he found a corresponding reattachment point on the

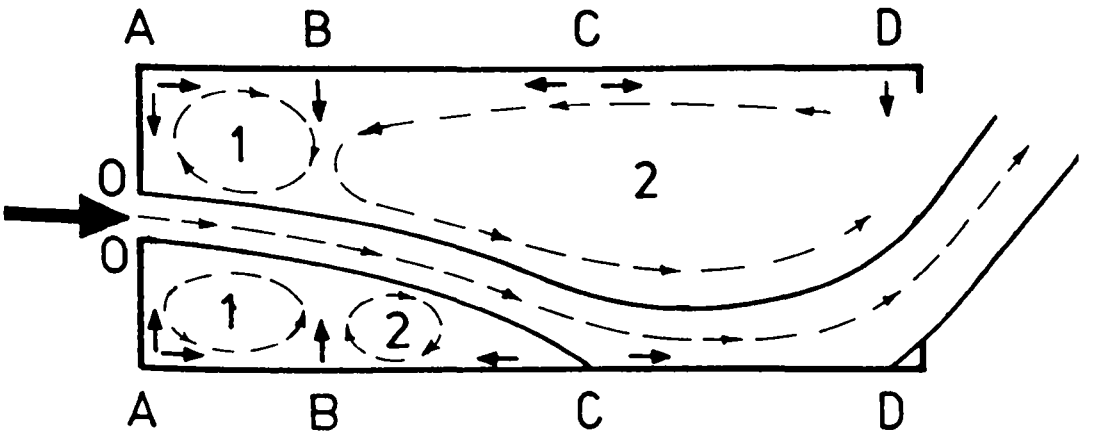

Figure 4.33: A two-dimensional, quasi-steady-state model of the flow patterns is unable to explain the observed flow directions. The arrows on the surface indicate the axial component of the flow directions on the surface, as determined from the china clay results.

downstream face of the orifice plate, ie. the flow moves along path B1. The results of the china clay experiments however, show that no reattachment occurs on the face of the orifice in the present nozzle (see Figure 4.31). The alternative flow direction – along path B2 is also not possible, being inconsistent with the flow along the streamline O–C on the edge of the jet.

The steady state model is able to explain the weaker, downstream separation which occurs just upstream of the downstream orifice (see point D of Figure 4.32) in terms of flow patterns which are topologically possible. However, these flow patterns would produce a definite vena-contracta, and so are not consistent with the rapid expansions observed in other experiments (see Figures 4.7 and 4.9).

Neither can the flow directions which are observed using the china clay experiments be explained using a quasi-steady, non-precessing asymmetrically reattaching jet. One such model is shown in Figure 4.33, but this does not resolve the discrepancies found in the steady state model.

A key to the explanation lies in the fact that china clay dries very slowly, and thus only reveals the strongest, or predominant, flow directions. It is postulated, then, that all three bifurcations only occur at one circumferential location in the cavity at any instant, and that

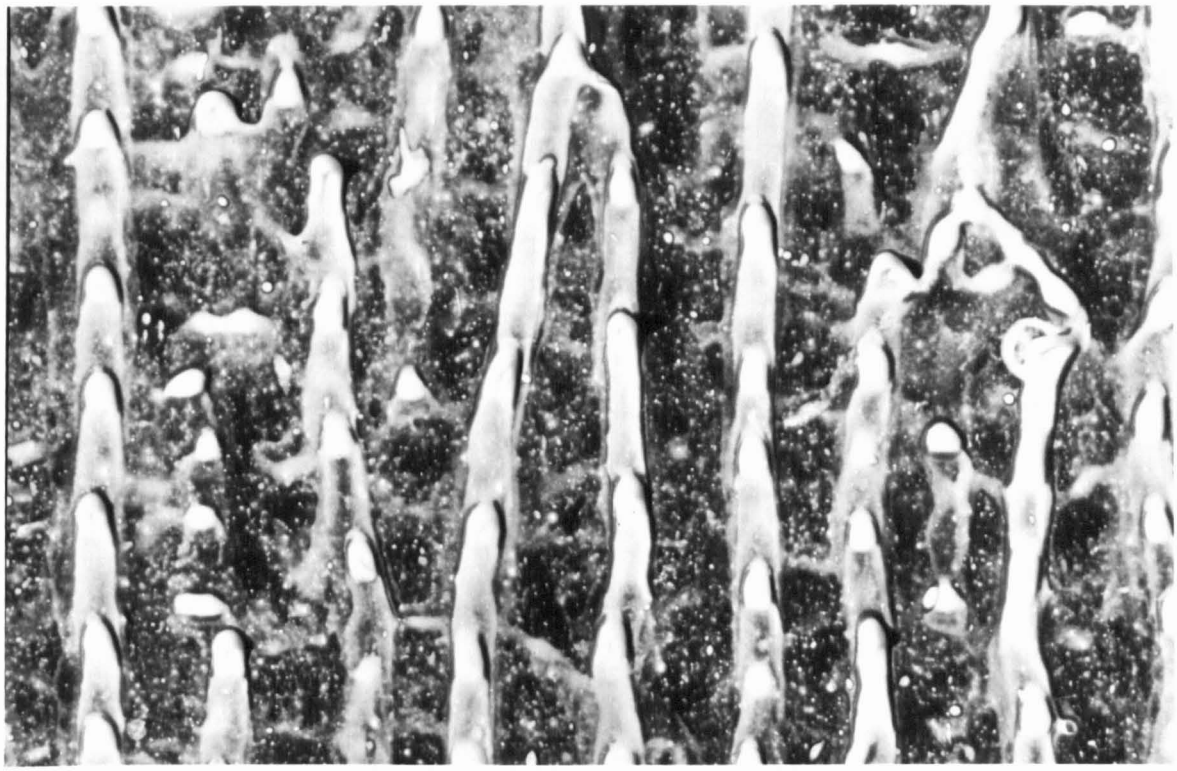

Figure 4.34: Enlarged view of the surface pattern downstream of the positive bifurcation line. Mean flow direction is from bottom to top. Nozzle dimensions: $d_1/D = 0.187$, $d_2/D = 0.88$, $l/D = 2.7$, $D = 91\text{mm}$, $P_d = 60\text{kPa}$.

they all precess around the cavity. Because these flow patterns are much stronger than the secondary flow patterns which occur over the rest of the surface, they dominate the response of the china clay technique.

As has been observed in the flow visualisation using dye injection in water (see section 4.9), fluid is simultaneously expelled from the cavity through one part of the exit plane and drawn into the cavity through the remaining area. This entrained fluid has been observed to move right to the back of the cavity which explains how fluid can maintain the cavity swirl flow without requiring an infinite source at the corner, A.

As a consequence of the precessing jet model, a point on the surface downstream of the axial location at which the positive bifurcation occurs will be subjected to a flow which alternates between being strong in the downstream direction, and weak in the upstream direction. The droplet formation of the china clay on this part of the surface is consistent with such an oscillating flow, having the appearance of a "two steps forward and one step backward" type motion (see Figure 4.34).

The flow which moves upstream from the positive bifurcation does so with a circumferential

component of velocity which is in the same direction as that of the cavity swirl. On meeting, the two flows form the open negative bifurcation [43], and then spiral into the central jet.

The jet which is instantaneously attached to one part of the cavity separates from the wall immediately upstream of the lip at the exit plane. It then leaves the nozzle with a large radial component and "crosses" the axis of the nozzle.

The proposed flow patterns, which are consistent with the results of the china clay experiments, have been described more fully in the introduction to this Chapter.

4.8.4 Reattachment Lengths

Thus far, the china clay experimental results have been interpreted only in a qualitative manner. However, they do also contain very useful quantitative information about the distances to the bifurcation lines. The reattachment lengths, x_r , of several related geometries are well documented and a comparison with these, shown in Table 4.3, gives powerful evidence that the reattaching jet in the MLC nozzle is indeed asymmetric, and not symmetric.

Symmetric flow downstream of plane, 2-D abrupt expansions is only found if the expansion ratio is "small". Abbot & Kline have found that the critical expansion ratio for plane expansions is 1.5, and that larger expansion ratios cause the reattachment length on one side of the expansion to be larger than that on the other, because to two shear layers interact. Investigating the flow patterns in an "analogous" axi-symmetric flow (ie. when the shear layer at any one circumferential position is influenced by the shear layer at another circumferential position) is far more complex, because the flow patterns are, on average, symmetrical. It seems plausible that a precessing instability may exist, but an investigation of such an instability is not known to the present author. It is certainly true that the reattachment distance fluctuates with time, but this occurs even in the simplest of reattaching flows such as that behind a backward facing step [33], and so is not necessarily associated with a precessing asymmetric instability.

Agarwal, who investigated the flow through orifice plates with "small" expansion ratios giving symmetric flow on average, found $9 \leq x_r/h \leq 12$, with a slight dependence on Reynolds Number. However, as can be seen in Table 4.3, the distance to the positive bifurcation in the MLC nozzle is typically $x_p/h = 3.5$. This is much more comparable with the reattachment distance of the wall jet over a backward facing step investigated by Pelfry and Liburdy [72],

[6] Reattachment lengths on both sides of the expansion are equal

Source	Configuration	Re	d (mm)	$\frac{2h+d}{d}$	x_r/h	x_s/h	Comments
Agarwal	Axi-symmetric orifice plate, small exp-ratio	3×10^4 to 7×10^4	45 to 60	1.6 to 1.2	9 to 12	1.5	symmetric expansion
Abbot & Kline	Plane, double & single backward facing steps in water	2×10^4 to 5×10^4	300 to 600	≤ 1.5	6	1.2	single & double, symmetric exp.[6]
				1.5 to 6	6	NA	single step, "symmetric" exp.
					3, 11	1.3, 3	double step, asymmetric exp.
Pelfry & Liburdy	Plane wall-jet	2×10^4	12.5	14	2.0	–	asymmetric reattachment to wall
present research	Axi-symmetric MLC nozzle, large exp-ratio	4×10^4 to 2×10^5	10 to 21	6.5 to 9.1	3.5	1.3	instantaneously asymmetric reattachment

Table 4.3: Summary of reattachment distances

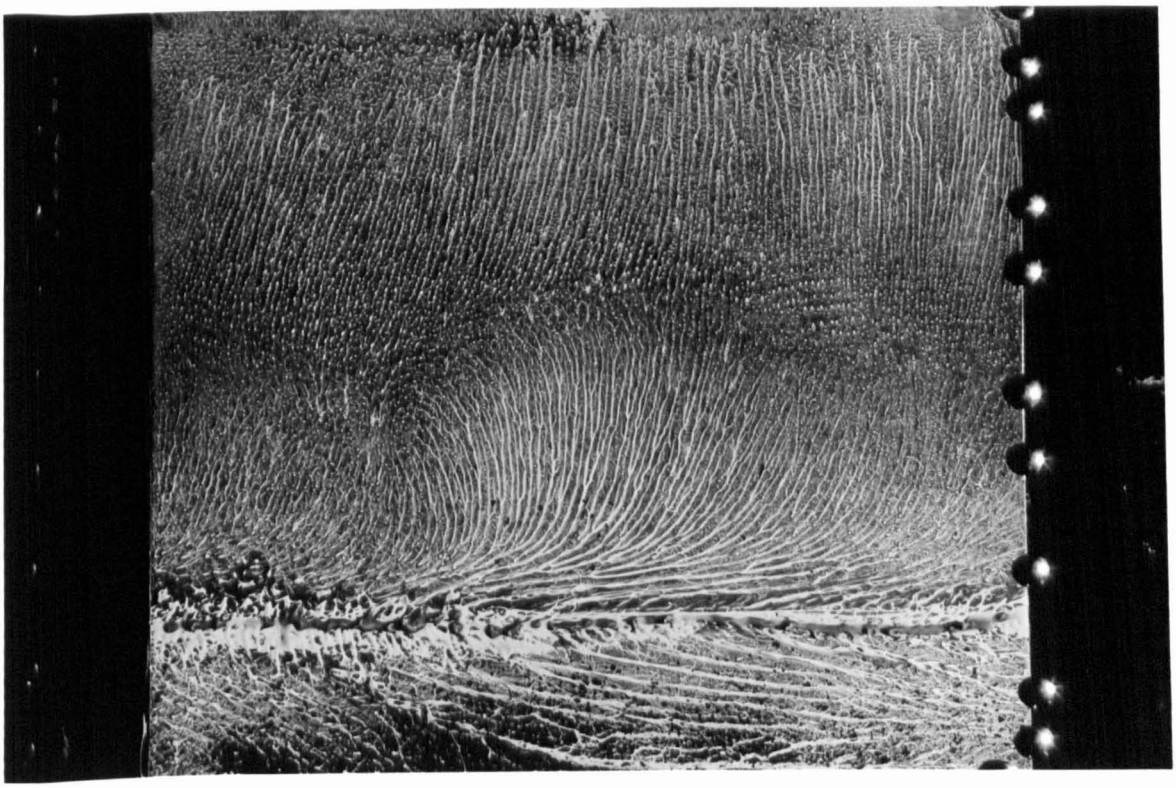

Figure 4.35: Variations in the axial bifurcation distances, with circumferential position, using china clay. Nozzle dimensions: $d_1/D = 0.110$, $d_2/D = 0.88$, $l/D = 2.7$, $D = 91$mm, $P_d = 160$kPa.

where $x_r/h = 2$. However reattachment distances are usually longer in an axi-symmetric geometry than in a plane geometry, as can be seen by comparing the results of Agarwal (orifice plate) with those of Abbot & Kline (plane expansion). These results strongly imply that the positive bifurcation line in the MLC nozzle is caused by an asymmetrically attaching jet, which is the axi-symmetric "equivalent" of a plane wall-jet.

The china clay experiments also reveal that the distances to the bifurcation lines vary slightly between runs, and even vary around the circumference of the nozzle for a given run. That is, the point at which the asymmetric jet reattaches to the wall may vary in the axial direction as the jet precesses. Examples of this are shown in Figures 4.35 and 4.36. This axial variation in x_r must be dependent on the azimuthal position of the jet; if it were random, it would not be detectable by the china clay technique, which averages the flow over a large number of precessions. This seems to indicate that there is some minor geometric asymmetry in either the nozzle or the position of an bluff body, which gives a bias to the reattachment distance at a particular circumferential location. A complete tabulation of results of bifurcation distances is given in Table 4.4.

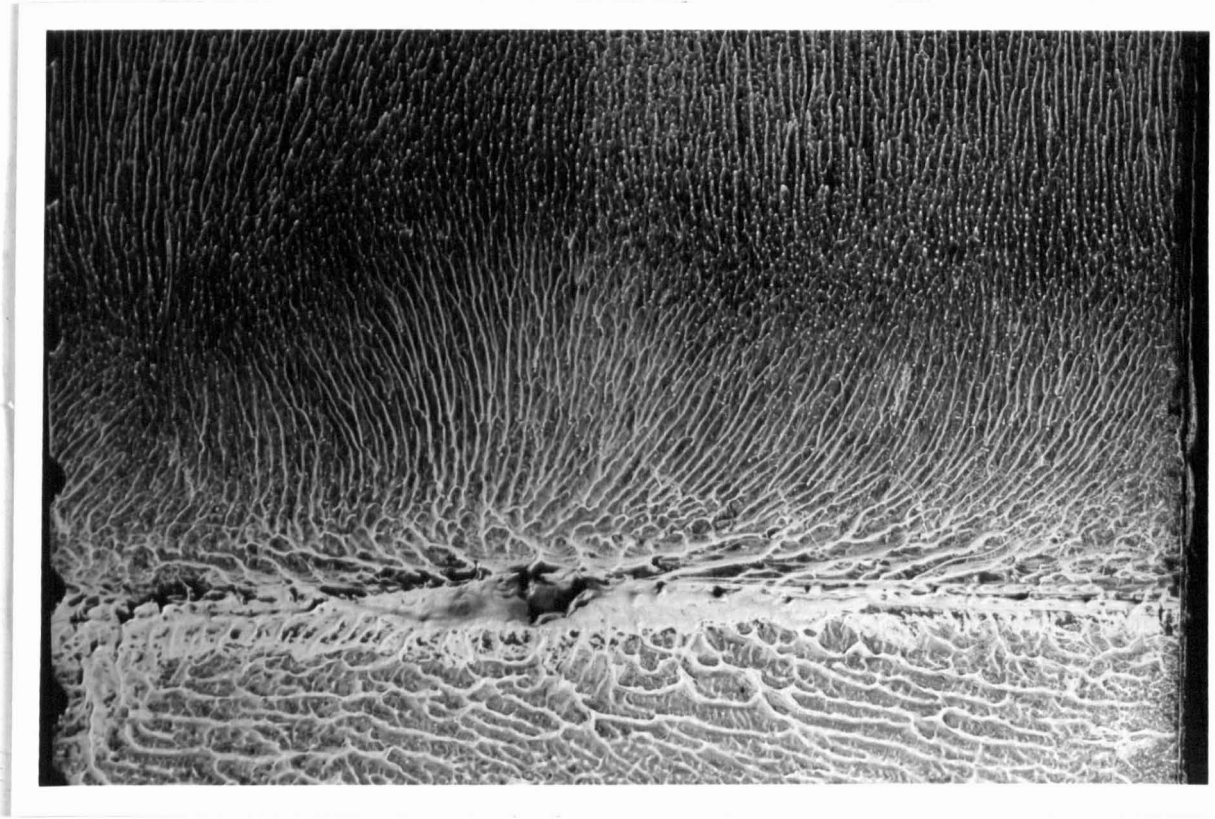

Figure 4.36: Variations in the axial bifurcation distances, with circumferential position, using china clay. Nozzle dimensions: $d_1/D = 0.187$, $d_2/D = 0.88$, $l/D = 2.7$, $D = 91$mm, $P_d = 60$kPa.

4.8.5 Intermittency and the directions of Precession and Swirl

By placing a non-hardening fluid into the clear, perspex nozzle (eg. water or oil), it was possible to observe visually the droplets moving on the surface. The fluid has a tendency to gather at the upstream, negative bifurcation, where the droplets can be observed to form a thin bead around the circumference of the nozzle, at a constant axial location. This bead slowly rotates around the inside of the cavity in a either the clockwise (CW) or counter clockwise (CCW) direction, without noticeable preference. For no apparent reason, the surface flow patterns are occasionally destroyed for a short time (of the order of a second or less) and then reappear. The new flow patterns usually restart in the opposite direction, but occasionally they restart in the same direction.

This abrupt cessation of the surface flow patterns is accompanied by a cessation of the "enhanced mixing" flow patterns, (the rapidly spreading, low velocity jet was replaced by a narrow, high velocity jet), and a drop in the pressure upstream of the nozzle (see section 4.10). This is the "intermittency" referred of earlier, and is obviously undesirable for practical applications of the nozzle. A schlieren photograph of a flame which is generated when the flow is

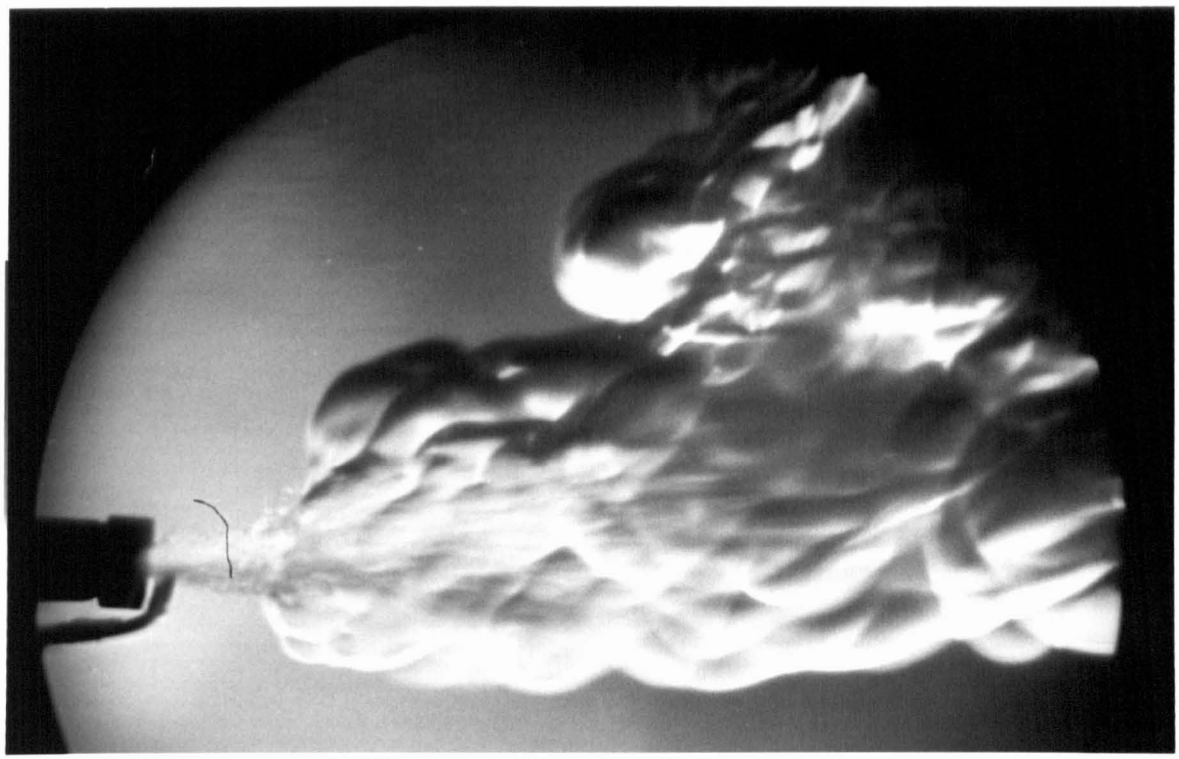

Figure 4.37: Schlieren photograph of flame shape when the flow is instantaneously unenhanced during a period of intermittent behavior. Nozzle dimensions: $d_1/D = 0.127$, $d_2/D = 0.877$, $l/D = 2.6$, $D = 13$mm, $P_d = 20$kPa, fuel:CNG.

instantaneously in this "intermittent" condition is shown in Figure 4.37 and 4.38.

In addition to the summary of the distances to the bifurcation lines, Table 4.4 gives the direction of cavity swirl, as obtained using the china clay experiments. It can be seen that there is a slight preference for the cavity swirl to rotate in the CCW direction. The reason for this is unknown, but may be due to minor asymmetries in the geometry of the nozzle.

It is possible to give the flow patterns a preferred direction of precession and rotation by introducing a swirl to the flow upstream of the nozzle, using swirl vanes (hereafter referred to as "vane swirl"). This appears to cause a significant reduction in the amount of intermittency[10]. The effect of such a bias on the rotational directions within the cavity is illustrated in Figure 4.3.

[7] positive swirl is in the clockwise direction, when facing downstream.

[8] direction as indicated when facing downstream.

[9] The distances to bifurcation lines are difficult to determine in this run

[10] A series of hot-wire anemometry experiments were planned in order to identify this intermittency, and measure the influence of vane swirl on it. Unfortunately, lack of time has prevented them being conducted at this stage.

Nozzle Dimensions			Insert			Re	Results			
d_1/D	l/D	S deg[7]	No.	x_i/l	l_i/l		x_{n1}/h_1	x_p/h_1	x_{n2}/h_2 (-ve)	Cavity Swirl[8]
0.155	2.69	0	–	–	–	1.5×10^5	1.40	3.0	–	CCW
"	"	"	–	–	–	1.5×10^5	1.29	3.0–3.7	1.5	CCW
"	"	"	–	–	–	8.2×10^4	1.4[9]	3.7	1.7	CCW
"	"	"	–	–	–	4.3×10^4	1.6[9]	3.9	1.9	CCW
0.187	"	"	–	–	–	1.5×10^5	1.5[9]	4.1	1.8	CCW
"	"	"	–	–	–	1.5×10^5	1.46	3.3–4.1	3.6	CW
0.110	"	"	–	–	–	1.3×10^5	1.22	3.0–3.6	1.9	CCW
"	"	"	–	–	–	6.9×10^4	1.48[9]	3.5	?	CW
"	"	"	–	–	–	1.8×10^5	1.25	3.1–3.7	2.2	CW
0.155	"	"	1(b)	0.82	0.081	1.5×10^5	1.45	2.9–3.5	1.2	CW
"	2.20	"	1(b)	1.15	0.081	1.5×10^5	1.19	2.5–3.4	0.2–3	CCW
"	1.68	"	1(b)	1.11	0.081	1.5×10^5	1.04–1.32	2.1,2.5	0.2–10	CCW
"	"	"	1(b)	1.10	0.081	1.5×10^5	1.04–1.32	2.1,2.2	0.6–10	CCW
"	2.69	75	–	–	–	1.5×10^5	1.22	3.2–4.2	2	CW
"	"	-45	–	–	–	1.5×10^5	0.91–1.22	3.0–3.8	1	CCW

Table 4.4: Summary of the distances to the bifurcation lines obtained using china clay techniques for various nozzle geometries

Note: $d_2/D = 0.88$ in all tests.

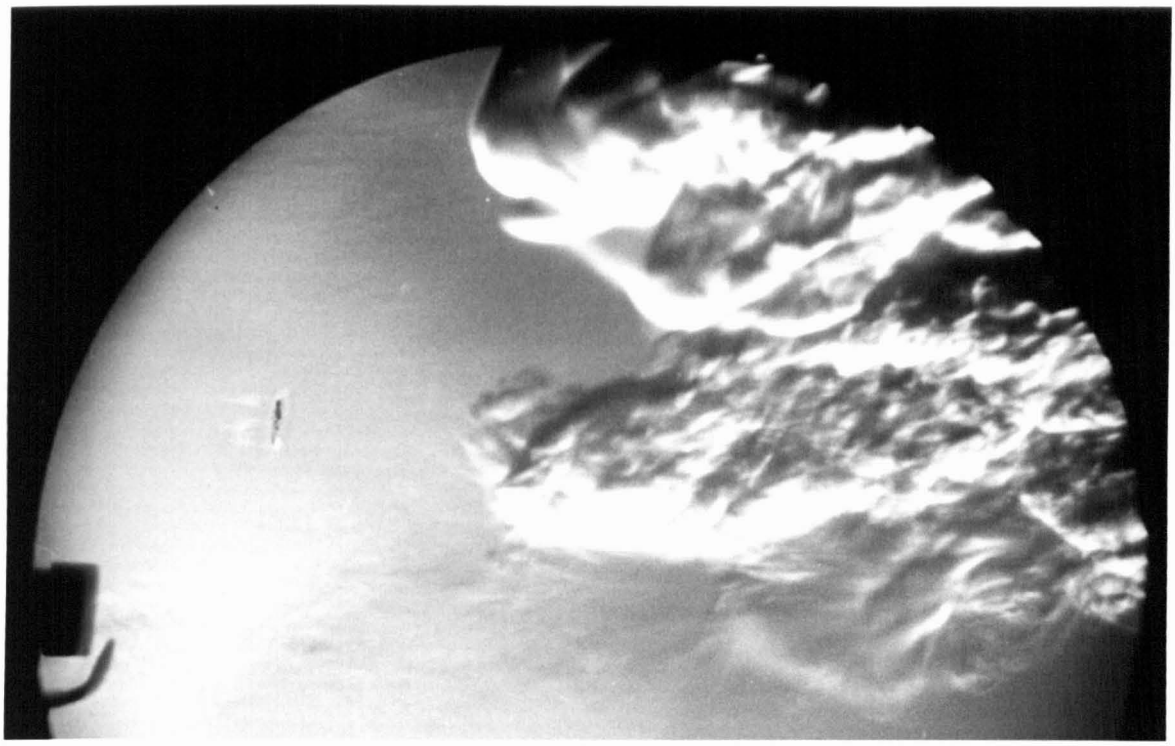

Figure 4.38: Schlieren photograph of the flame just prior to blow-off during a period of intermittent behavior. Nozzle dimensions: $d_1/D = 0.127$, $d_2/D = 0.877$, $l/D = 2.6$, $D = 13$mm, $P_d = 45$kPa, fuel: CNG-N_2; F=0.82.

Because the cavity swirl is strong, it will impart angular momentum to the central jet – either to a braid of helical vortices wrapped around an irrotational core, or to the jet into which it is entrained. When this jet reattaches to the cavity wall, it will tend to "roll" around the inside of the cavity in a manner analogous to one wheel rolling inside another, Figure 4.3. It can be seen that the direction of jet precession and the direction of jet rotation (and hence cavity swirl), must be opposite, and that the direction vane swirl, and cavity swirl must be the same.

It can now be seen that the effect of swirl vanes upstream of the nozzle, is to bias the rotational direction of the jet. This in turn biases the direction of precession, and also the direction of the cavity swirl. Although it is not possible to measure the direction of precession using the china clay experiments, it is possible to set the direction of the swirl vanes upstream of the nozzle, and to observe the direction of the resulting cavity swirl.

Two runs using the upstream swirl were conducted, and these both verified that cavity swirl and vane swirl directions are opposite (see the last two runs in Table 4.4). Further evidence was obtained from the flow visualisation experiments of multi-point dye injection in water, Section 4.9. In these experiments, not only were the rotational and precessional directions

able to be observed independently, but the flow in the upstream part of the cavity could be given an initial direction of rotation before the flow through the nozzle was turned on. This was done manually, by inserting a "paddle" into the nozzle, and physically moving it around the inside of the cavity to impart the required swirling direction to the flow.

It was found that when the cavity swirl was initially caused to oppose the vane swirl, the cavity swirl would abruptly change direction after five or so precessions of the jet. The change in direction occurred in every case, although in some cases the initial swirling direction would persist for significantly more than five precessions. If the paddle was not used to force an initial direction upon the cavity swirl, the cavity swirl would occasionally start in the opposite direction to the vane swirl, and then reverse as described above. Usually, however, it would always be identical to that of the vane swirl.

4.8.6 The effect of an Insert on the Flow Patterns

It has already been mentioned that the placement of suitably shaped "bluff bodies" or "inserts" into the nozzle can help reduce the intermit nature of the enhancement. On the basis of the proposed flow patterns, it is apparent that the effect of the bluff body is to ensure that the precessing jet takes the asymmetric path on its journey through the cavity. The china clay technique is ideally suited to confirming that the surface flow patterns are not influenced in character by the presence of the bluff body, and to investigating the influence of the insert geometry and position on the flow patterns within the nozzle.

Both a solid and a hollow insert were placed inside the cavity without otherwise altering the geometry of the nozzle. The configuration of the experiment is shown in Figures 4.39 & 4.40.

The resulting flow patterns are shown in Figure 4.41. It can be seen that character of the surface flow patterns are identical to those obtained without the insert and that the distances to the bifurcation lines are within the range of scatter observed when no insert was used (see Table 4.4).

The influence of the insert is so powerful that it can be used to stabilise the flow patterns at much shorter cavity lengths than would otherwise be possible. However, at very short cavity lengths, the insert must be placed *outside* the nozzle. Once again, the effectiveness of such a body can be explained by the proposed flow patterns.The exiting jet leaves the nozzle at a large angle to the nozzle axis from one side of the nozzle across the nozzle axis. The bluff body

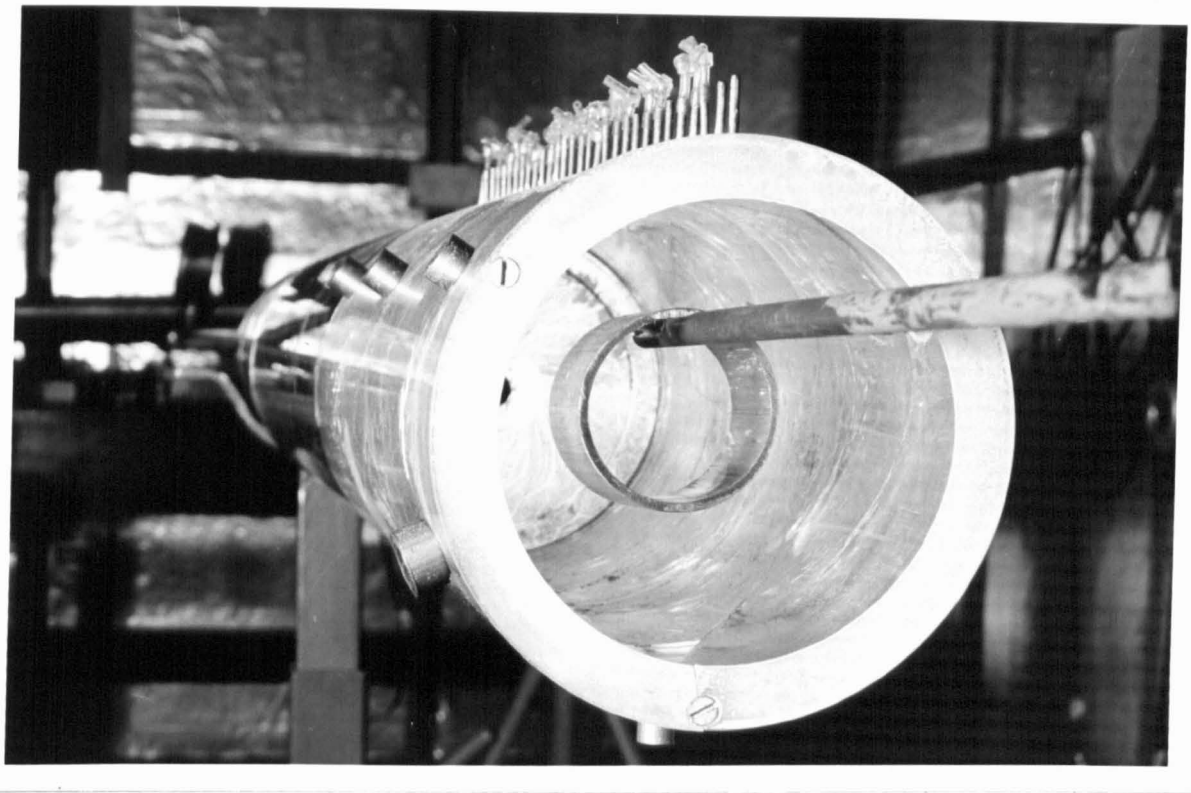

Figure 4.39: The experimental configuration of the china-clay experiments with an insert within the nozzle; hollow insert shown. Nozzle configuration: $d_1 = 10.0$mm, $d_2 = 80$mm, $l = 245$mm, $P_d = 160$kPa.

then provides a strong blockage to the axial motion of the exiting jet, and strongly encourages the flow directions associated with "enhanced mixing". This is illustrated in Figure 4.42.

However, the flow patterns *are* influenced by the shorter cavity lengths. It has already been mentioned that circumferential variations in the axial distances to a given bifurcation line exist. These variations become larger as the cavity length decreases, until a new phenomenon is observable in the surface flow patterns. The flow pattern obtained with insert No. 1(b) and $l/D = 2.2$ is shown in Figure 4.43. These show increased variation in x_p & x_{n2}, but the character of the flow patterns are unaltered. However, at a cavity length to diameter ratio of 1.7, the flow patterns are distinctly different, Figure 4.44. It can be seen that the downstream negative bifurcation line, x_{n2}, does not remain approximately parallel to the exit plane, but at one broad circumferential position moves upstream to "join" the upstream negative bifurcation line, x_{n1}. At this circumferential location, then, the positive bifurcation line is discontinuous.

At first sight, it appears that whole character of the flow has been altered. However, it must be recalled that the china clay produces a long time "average" of the surface flow patterns, and will only show a significant response to the strongest flow patterns. It is proposed then, that

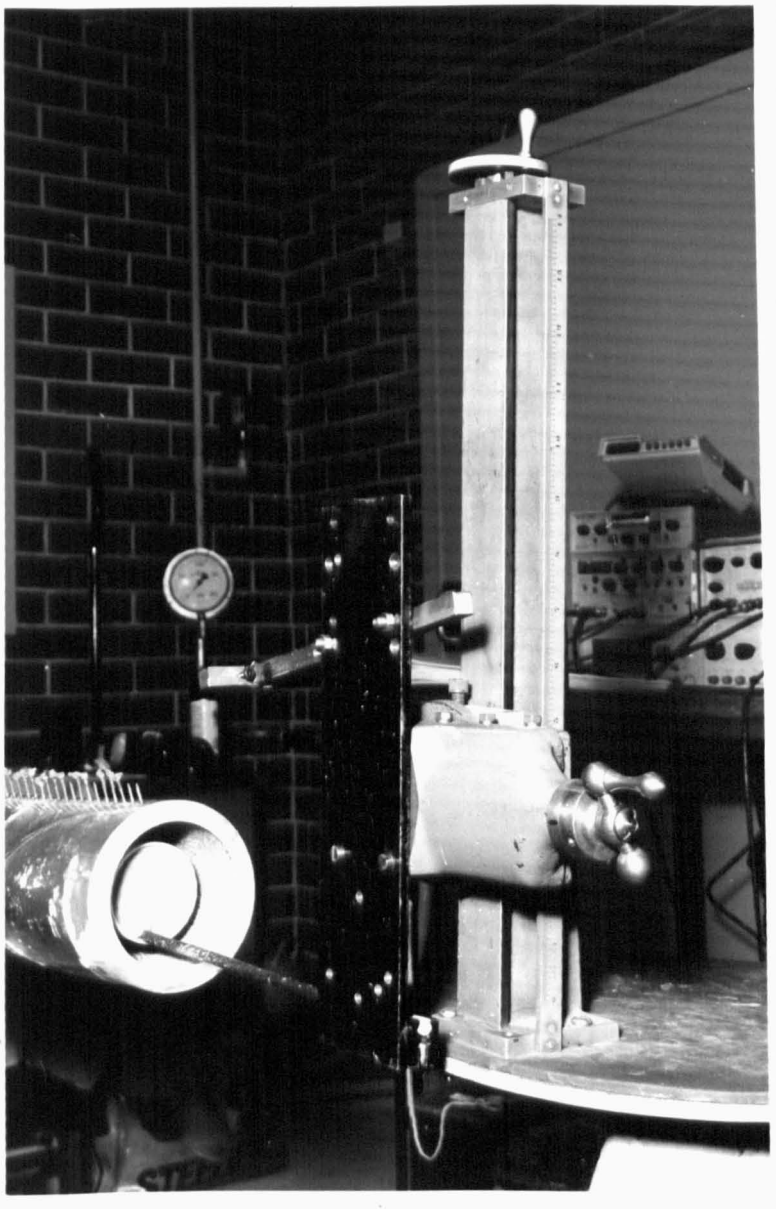

Figure 4.40: The experimental configuration of the china-clay experiments with an insert in the nozzle. Nozzle configuration: $d_1 = 14.1\text{mm}$, $d_2 = 80\text{mm}$, $l = 245\text{mm}$, $P_d = 80\text{kPa}$.

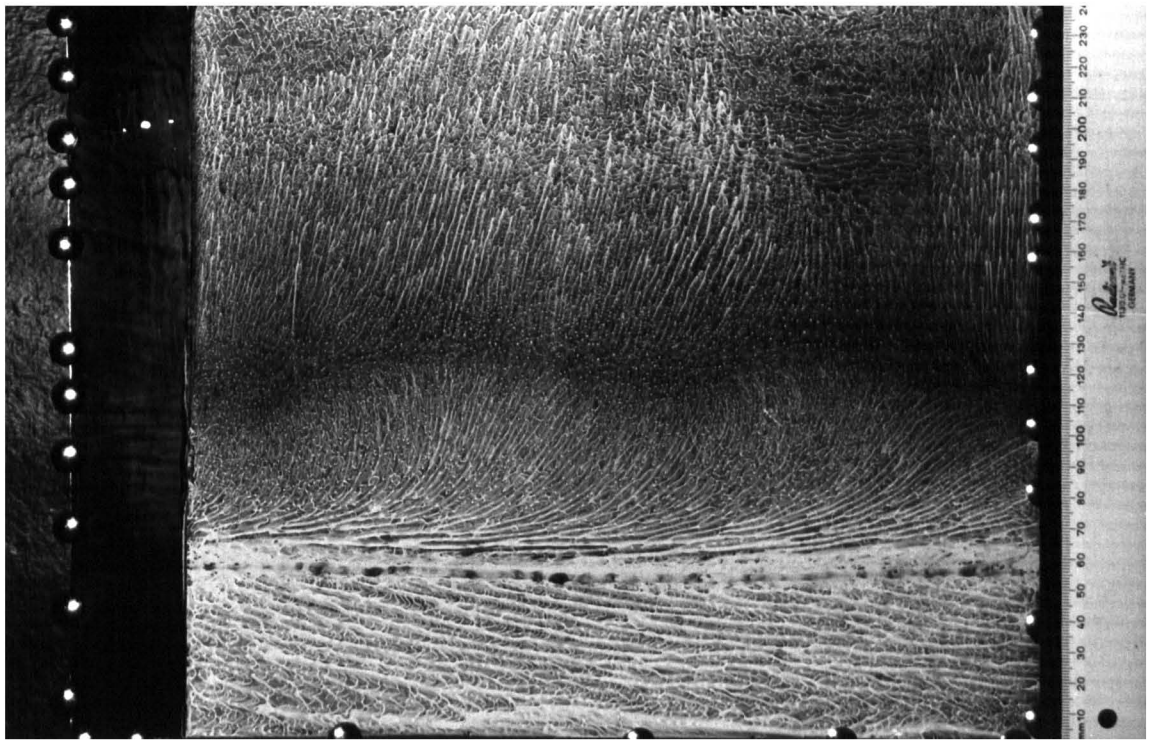

Figure 4.41: The flow patterns generated with a solid body insert within the nozzle. Nozzle configuration: $d_1/D = 0.155$, $d_2/D = 0.88$, $l/D = 2.69$, $D = 91\text{mm}$, $x_i/D = 2.2$, $P_d = 80\text{kPa}$.

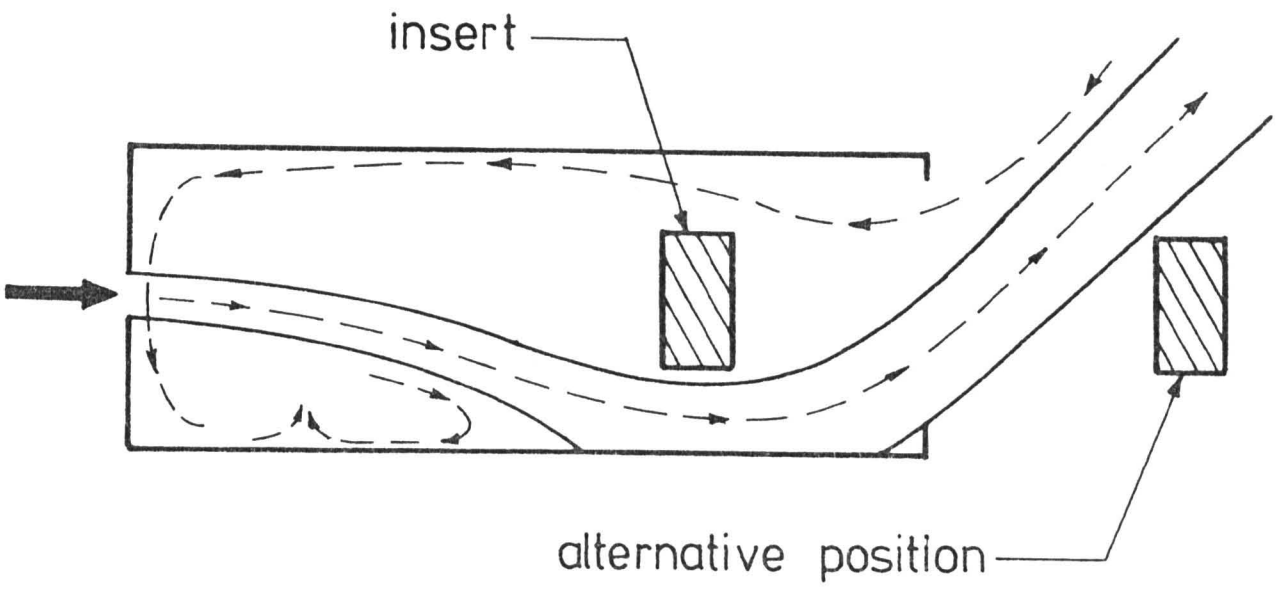

Figure 4.42: The stabilizing influence of a bluff body within the nozzle. The dashed lines indicate an alternative position for the bluff body.

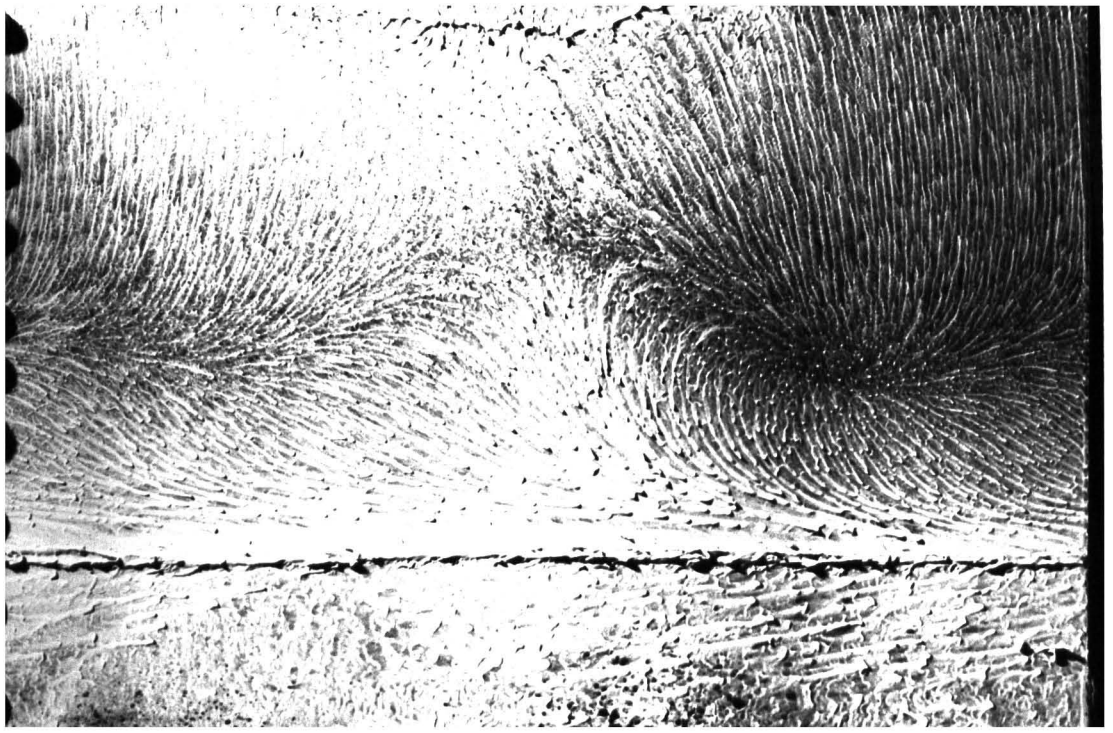

Figure 4.43: Cavity surface flow patterns with a bluff body just downstream from the nozzle exit plane. Slightly short cavity. Nozzle configuration: $d_1/D = 0.155$, $d_2/D = 0.88$, $l/D = 2.2$, $D = 91mm$, $x_i/l = 1.15$, $P_d = 80$kPa.

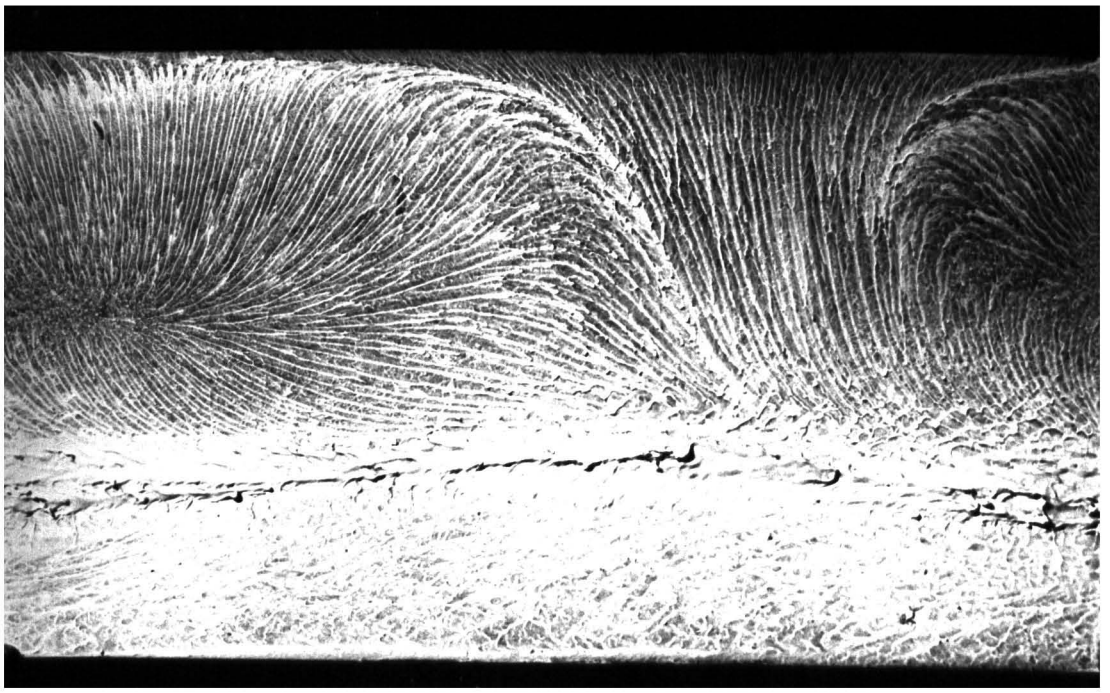

Figure 4.44: Cavity surface flow patterns with a solid bluff body just downstream from the nozzle exit plane. Short cavity. Nozzle configuration: $d_1/D = 0.155$, $d_2/D = 0.88$, $l/D = 1.68$, $D = 91$mm, $x_i/l = 1.11$, $P_d = 80$kPa.

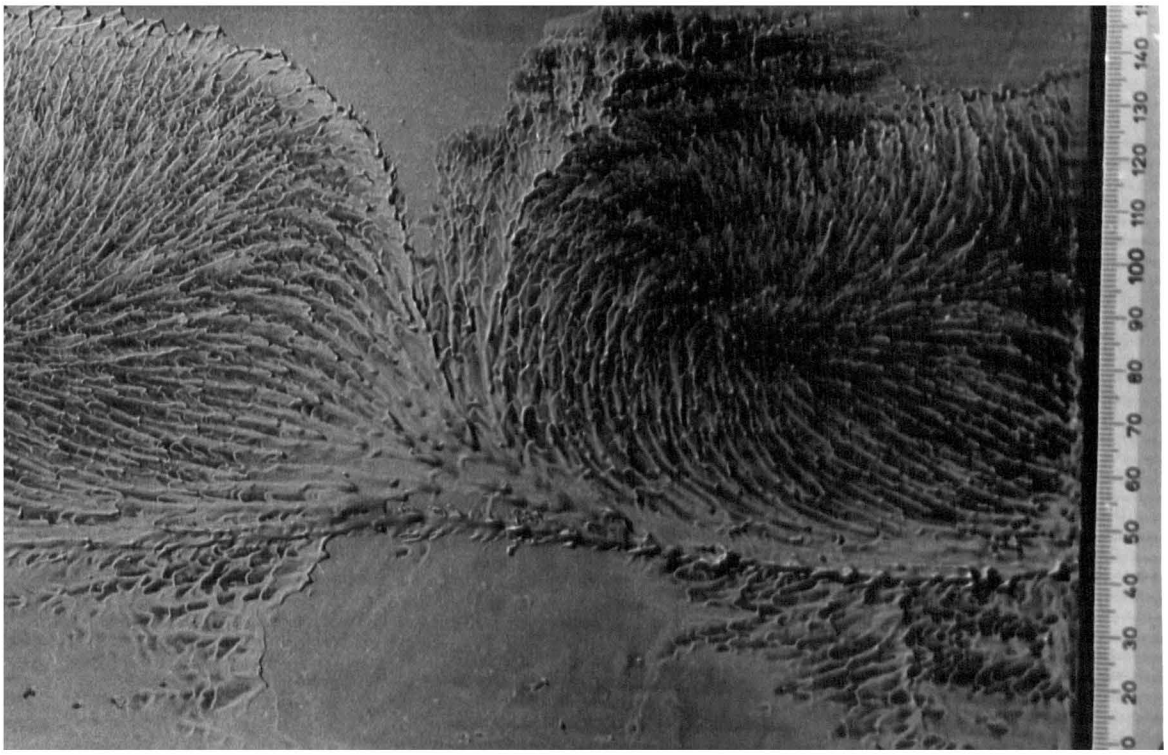

Figure 4.45: Testing repeatability of flow with short cavity and bluff body. Details as per previous figure.

the jet is still precessing, but that the precession is now strongly asymmetric. That is, the bulk of the reverse flow into the cavity is occurring at one circumferential position, and the bulk of the forward flow is probably occurring at another circumferential position. Furthermore, although the precession frequency is approximately constant, the precessional velocity may well not be. That is, the jet may be spending more time at some circumferential positions than at others.

Physical observation supported the contention that the flow patterns associated with the MLC nozzle were still occurring with this very short cavity. By placing one's hands in the flow, it is possible feel the large scale, low frequency pulsations in the exiting jet and its large spreading angles typical of the standard configuration of the MLC nozzle. These flow patterns are quite distinctive, and can be readily recognised, even though only in a qualitative sense.

To confirm these flow patterns, the experiment was repeated with an identical configuration, and special care was taken to ensure that the bluff-body was aligned as accurately as possible with the nozzle axis. The result was very similar, except that the quality of visualisation was poorer, because partial drying of the china clay occurred during the time taken in aligning the bluff-body. This is shown in Figure 4.45.

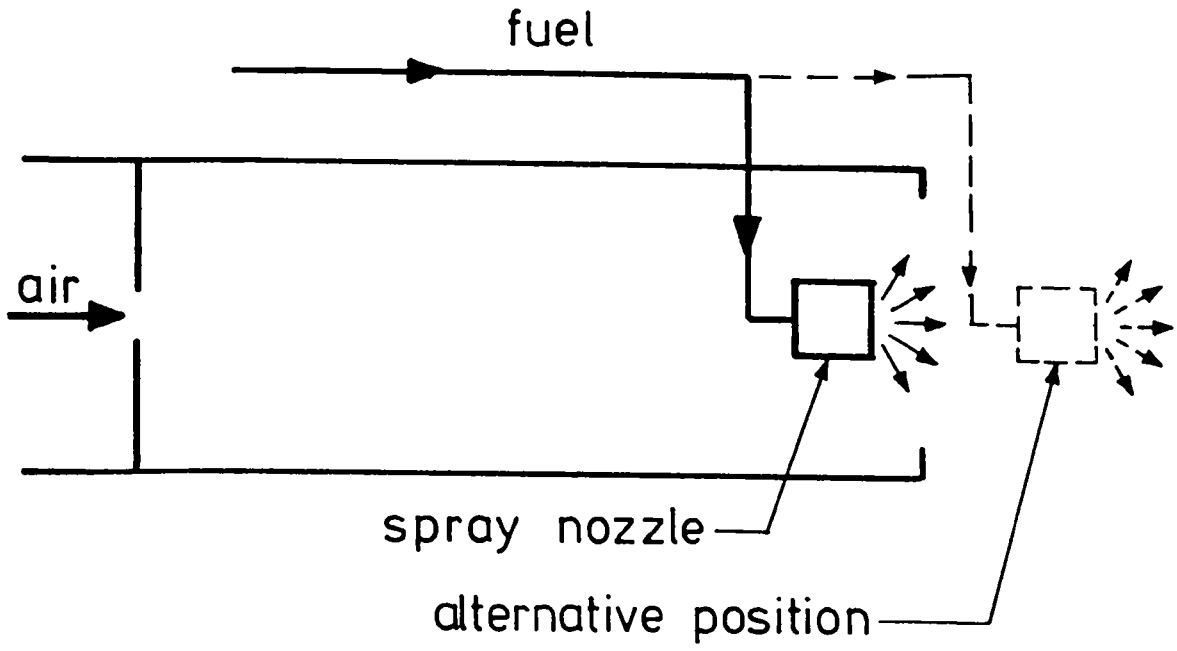

Figure 4.46: A possible configuration for combustion of pulverised solid, liquid or gaseous fuels.

4.8.7 The Influence of Probes on the Flow

China clay visualisation also provides a means of investigating the influence of protruding bodies, eg. a probe which supports a hot wire anemometer, in various parts of the nozzle. This is important, because it is essential to know the influence of the measuring device on the flow. Despite the fact that detailed hot wire anemometry experiments were not conducted as initially planned, the results are still relevant for any future investigation, and to provide further insight into the behavior of the flow patterns. This is important for some of the potential applications of the nozzle.

One such application which is envisaged is in the combustion of liquid or pulverised solids. In this case it may be convenient to introduce some or all of the combustion *air* through the present nozzle, and inject the fuel through a spray nozzle, located for example, on the axis of the present nozzle. The "spray nozzle" would then act as a bluff body in the flow, and the supply pipe through the cavity wall would introduce an asymmetric disturbance to the flow. Such a configuration is shown in Figure 4.46.

Apparatus

To simulate a probe support, short, threaded studs were glued to the surface of the metal shim sleeve. Cylinders of various diameters and lengths could be screwed onto the studs and the china clay experiment conducted. Alternatively, a cylindrical rod could be inserted into the cavity in the axial direction through the exit plane.

The rod diameters were either 6.4mm or 5.0mm, which is larger than the diameter of most hot wire probe holders and so is conservative in determining their influence, but is probably smaller than the required diameter of the supply pipe of a fuel jet.

Results

In general, it has been found that a protruding rod has most influence on the flow patterns if it is inserted into the region of highly swirling flow upstream of the first negative bifurcation line, ie. $0 \leq x \leq x_{n1}$.

When a rod of 6.4mm diameter is inserted axially into the cavity so that it extends right to the upstream orifice plate, at a radial position 0.22 cavity diameters from the wall, the enhanced flow patterns are entirely destroyed. However, if it is inserted to a position just downstream of x_{n1}, as shown in Figure 4.47, then it only has a very slight influence on the flow.

When a 5mm dia.. rod is inserted radially into the nozzle upstream of x_{n2}, as shown in Figure 4.48, whilst the surface flow patterns associated with the MLC nozzle are not entirely destroyed, they are dramatically altered, and measured subjectively, appear to be substantially weaker. First, the plane of positive bifurcation moves downstream to the plane of the downstream negative bifurcation, ie. x_p increases dramatically. In fact, the reversed flow can no longer be positively identified with the "reattachment" of an asymmetric jet, but could possibly be caused by induced, reverse flowing, ambient air. Secondly, the cavity swirl is greatly weakened, and the axial location of x_{n1} varies substantially around the nozzle. Thirdly, the reverse flow upstream of the reattachment is in a direction largely parallel to the nozzle axis for most of its journey upstream, beginning to slew to one side only in the immediate vicinity of x_{n1}. As discussed in Section 4.8.2, this implies that the reversed reattachment foot may be expected to exert a lower influence on the precession motion of the asymmetric jet than is the case when it has a circumferential component at the plane of reattachment.

The effect is even more dramatic if two rods are placed in this upstream flow region, with

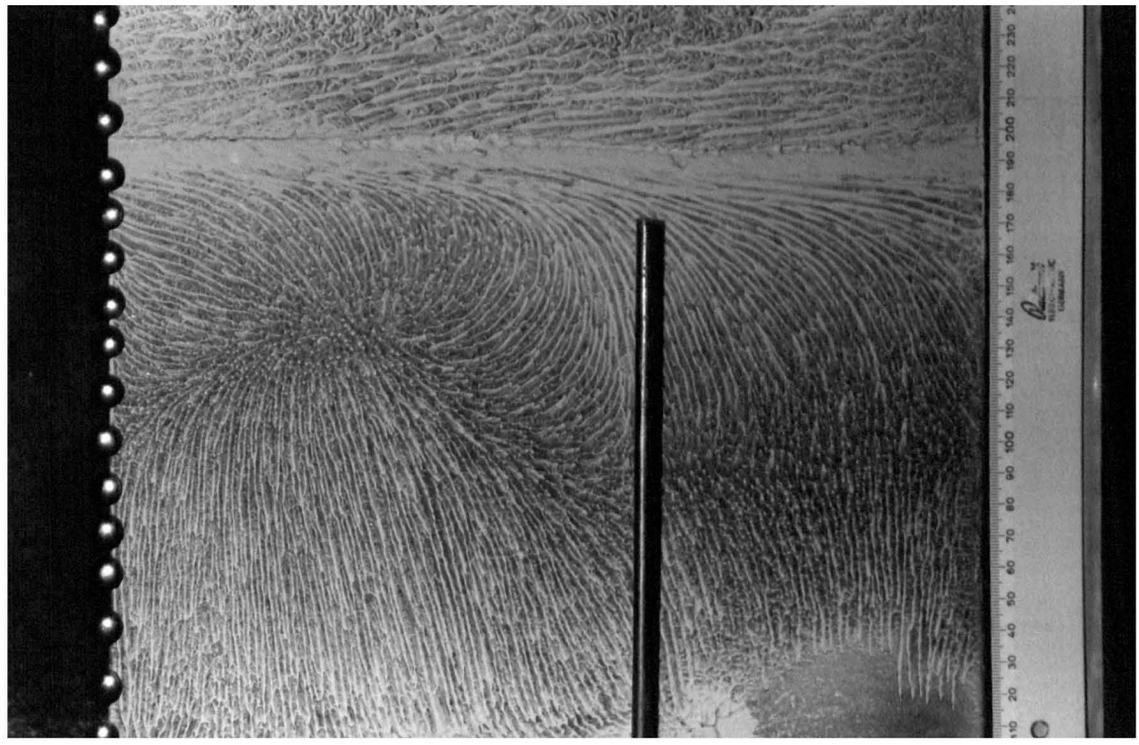

Figure 4.47: Surface flow patterns with a cylindrical rod inserted axially into the nozzle. The rod was positioned 0.22 of a cavity diameter above the surface in the position shown. Rod dia. = 6.4mm, nozzle configuration: $d_1/D = 0.155$, $d_2/D = 0.88$, $l/D = 2.7$, $D = 91$mm, $P_d = 160$kPa.

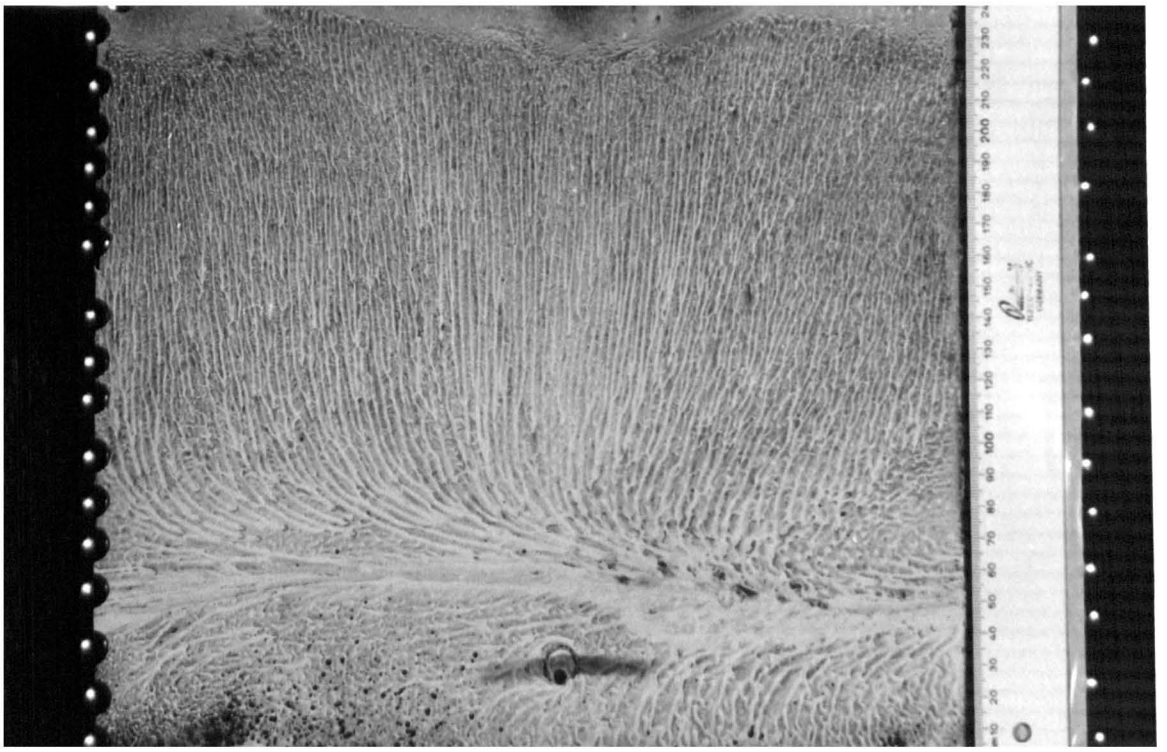

Figure 4.48: Surface flow patterns with a cylindrical rod inserted radially into the cavity at an axial location $x_r/l = 0.12$. Rod dimensions: $d_r = 5\text{mm}$, $l_r/D = 0.4$ nozzle configuration: $d_1/D = 0.155$, $d_2/D = 0.88$, $l/D = 2.7$, $D = 91\text{mm}$, $P_d = 80\text{kPa}$.

the second one being specifically placed at $x = x_{n1}$. As can be seen in Figure 4.49, the cavity swirl is now almost entirely destroyed, and the upstream negative bifurcation line is no longer a clearly defined feature.

These results imply not only that the cavity swirl is a sensitive region, but that there is a relationship between the angular momentum in the cavity swirl and x_p. On the basis of the conservation of angular momentum, it can also be expected that the precession frequency, f_p, will be reduced when the cavity swirl is damped. This implies that a relationship also exists between f_p and x_p. That is, as the damping on the cavity swirl is increased, so the precession frequency decreases and x_p increases.

4.9 Visualisation using Dye in Water

It is well known that most fluid mechanical phenomena scale with Reynolds Number. As a result, it is possible to investigate flow past one body using another body of a different size at a different flow velocity, and/or in a different fluid. This fact is used to verify that the enhanced mixing flow phenomenon is truly generated by a fluid-mechanical mechanism, and

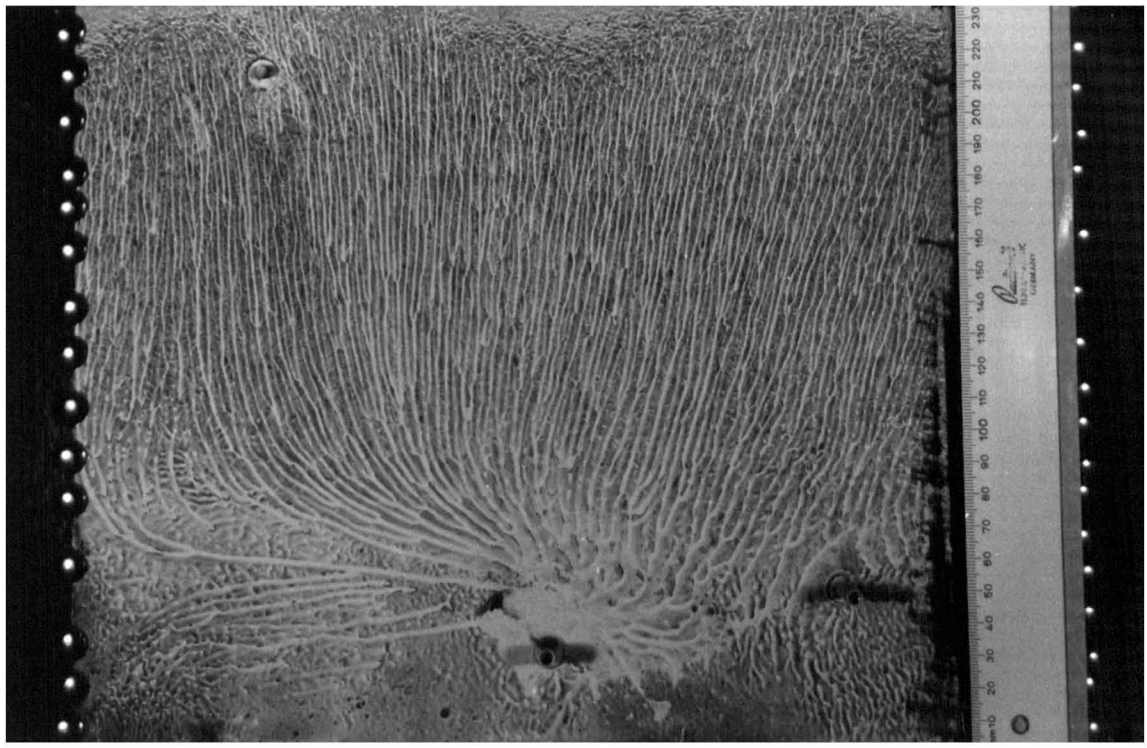

Figure 4.49: Surface flow patterns with two cylindrical rods inserted radially into the cavity at $x_{r1}/l = 0.12$ & $x_{r2}/l = 0.20$. Rod dimensions: $d_r = 5$mm, $l_r/D = 0.4$ nozzle configuration: $d_1/D = 0.155$, $d_2/D = 0.88$, $l/D = 2.7$, $D = 91$mm, $P_d = 80$kPa.

not by the acoustic coupling, discussed in Section 7.2.5. It also means that flow visualisation, or measurement, can be conducted in a more convenient fluid.

The velocities in water are about twenty times lower than those in air for a given length scale at the same Reynolds number. Furthermore, dye injection techniques are simple and readily available, and water flow rate is easily measured. Consequently there are significant advantages in using water instead of air as the medium for flow visualisation.

For these reasons a series of flow visualisation experiments were conducted in water. These yield further evidence which supports the mechanism proposed in section 4.1. Furthermore, they enable the precession frequency of the asymmetric jet to be measured visually. (As a matter of historical fact, water flow visualisation experiments provided the first insights which led to the postulate that mechanism of enhancement involves precession of the jet.)

4.9.1 Apparatus

The experiments were conducted in a glass-walled water flume, with a width of 300mm and a depth of 500mm. The large scale perspex nozzle ($D = 91$mm) was suspended in the water, and mains water was supplied to the nozzle, through a variable area Fisher & Porter flow rater,

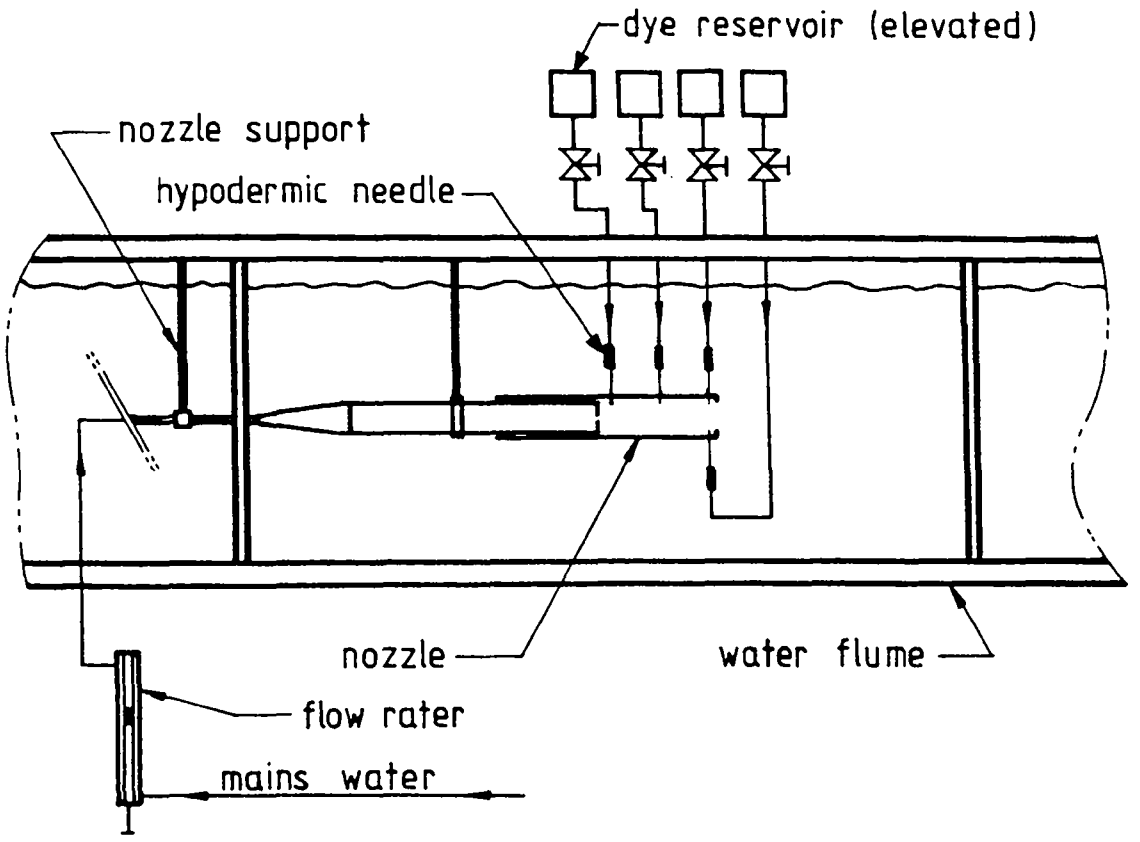

Figure 4.50: The rig used for dye-visualisation in water.

with a stated accuracy of ±2%. A small flow of water was constantly maintained through the flume in order to convect the dye away from the test section. This is illustrated in Figure 4.50.

Four different colours of dye were able to be injected simultaneously into the nozzle at different positions. Small plugs were made to fit into the nozzle at three circumferential positions in each of the three axial stations. Two of the axial stations were located at approximately one third of a cavity diameter from either end of the cavity, to enable visualisation of flow in the zone of "cavity swirl" and flow immediately upstream of the exit plane, whilst the third was in the middle of the cavity, to enable observation of the flow just upstream of the positive bifurcation line (where instantaneous reattachment of asymmetric jet occurs). At one of the circumferential positions, plugs were installed at another three axial positions to allow more detailed visualisation of the flow along the surface.

The dyes used were: Eosin yellow, Biebrich scarlet, Aniline blue and Flourescein. The dye was delivered through 1mm diameter "hypodermic needles" fed from reservoirs which could be raised or lowered to control the flow rate. Further fine tuning of the flow rate was provided

by a needle valve at the reservoir.

Ciné photographs were taken using a Hycam 16mm camera, and cuts from this film are included on the 16mm film enclosed with the thesis. Other experiments were conducted visually only.

Experiments were also conducted using the identical small scale brass nozzle, (D = 13mm), used for the combustion experiments. In this experiment, the gross flow patterns leaving the nozzle were visualised by injecting the dye into the flow upstream of the nozzle. This required that the dye be pressurised. To facilitate this, a small pressure vessel containing the dye was connected to the laboratory compressed air line.

4.9.2 Results

The precession of an asymmetric jet can be inferred from the motion of the dye trace of a single needle immediately upstream of the nozzle exit. The dye trace can be observed to "flip" periodically between the upstream and downstream directions. Flow in the downstream direction is consistent with the asymmetric jet being attached to the wall at the same circumferential position as the needle. Upstream flow can be inferred to correspond to the ambient fluid which is entrained into the cavity through that part of the exit area not occupied by the asymmetric jet. This occurs when the jet is attached to the wall at a different circumferential position from the needle.

The support for the proposed motion is even stronger when dye is simultaneously injected through three circumferential ports at the same axial position. The precession of the jet can now be observed, as the dye traces "flip" consecutively towards a constant circumferential direction. This motion can be seen on the enclosed ciné film of the motion.

Quantitative measurement of the precession frequency can be obtained from these experiments, as discussed in section 4.7.1. The results of the frequency measurements show that the precession frequency is directly proportional to the mass flow rate, and hence the Reynolds No. (based eg. on d_1 & u_1). The Strouhal Number of the precession is constant, with a value of $St = fh_1/\overline{u_1} \approx 5 \times 10^{-3}$, which is the same value as the Strouhal No. measured using hot wire anemometry in air.

The dye traces shown in the attached ciné film, clearly show that the rotational direction of the precession motion (indicated by observing the order which consecutive traces at the nozzle exit "flip") is the opposite of that of the cavity swirl in the upstream part of the cavity.

It can also be seen that the cavity swirl is continuous through a cross section of the nozzle by observing the upstream trace, which in part of the film is moved radially through the cavity.

The dye trace at the nozzle exit can occasionally be observed to move upstream right to the back of the cavity, where it joins the cavity swirl. This verifies the description given in section 4.1. More details of the axial flow patterns along a wall can be seen in that part of the film where four dye traces are inserted through the wall at four different axial stations at the same circumferential position. The dye trace immediately upstream of the plane of the positive bifurcation line can be seen to maintain an upstream component at all times. By contrast, the dye traces downstream of this plane exhibit the characteristic flipping motion, which agrees with the interpretation placed on the china clay flow visualisation experiments discussed in Section 4.8.3.

The results of visualising the overall motion of the jet through the small scale nozzle are summarised by Figure 4.51, which shows consecutive frames from part of the ciné film. The jet at the exit plane can be seen to be exhibiting a flapping motion, which is presumably a two dimensional projection of a three dimensional precession. Large scale structures with very long residence times can also be observed, as typified by the structure underneath the exit of the nozzle in frame (a). This is consistent with the large structures observed in the schlieren photography of the flame, and shows that they are not the solely result of the volume expansion which occurs in combustion, although this effect would enlarge these structures.

4.10 Mass Flow Rate – Driving Pressure Characteristics

The mass flow-rate through an orifice plate is influenced by the pressure ratio across it, and the contraction ratio [21], ie. its area relative to that of the upstream pipe. Thus it is to be expected that $\dot{m}$ will depend not only on the upstream driving pressure, but also on the pressure within the cavity, downstream of the orifice plate. It will also depend on d_1/d_0 (where d_0 is the dia. of the upstream pipe, which is constant).

It has been found for the same value of d_1/d_0 and d_1, that $\dot{m}_{MLC}$ is significantly higher than $\dot{m}_{LC}$, which is in turn higher than $\dot{m}_{orifice}$ (where $\dot{m}$ is the mass flow rate and the suffices MLC, LC and orifice refer to the Mid Length Cavity nozzle, the Long Cavity nozzle and the primary orifice discharging directly into the atmosphere). This can be seen in Figure 4.52. It is therefore apparent that the pressure at the throat for the MLC nozzle, p^*_{MLC} is less than

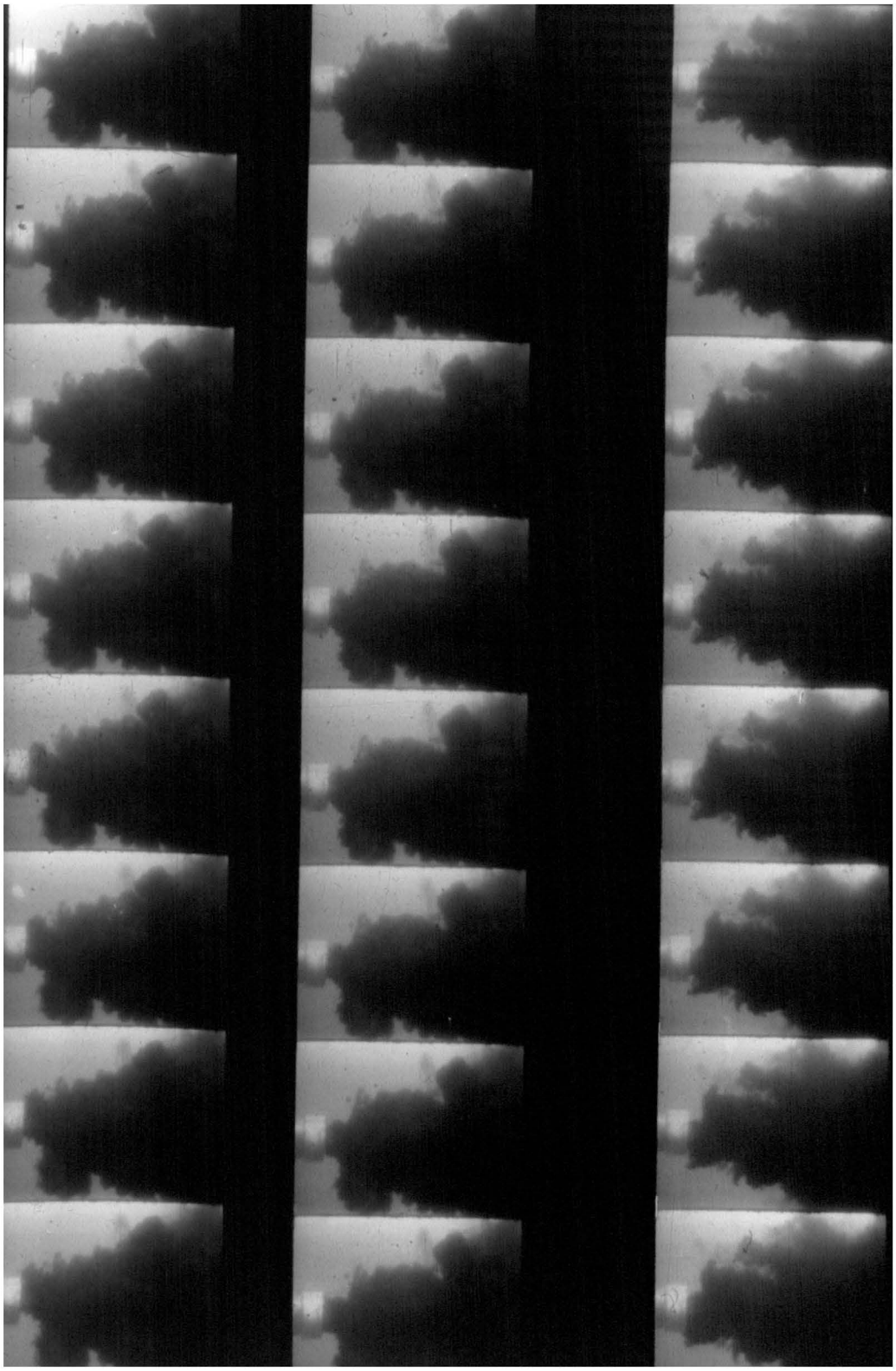

(a) (b)

Figure 4.51: Consecutive frames from a ciné film showing the gross motion of a submerged water jet from a MLC nozzle.

Nozzle dimensions: $d_1/D = 0.093$, $d_2/D = 0.75$, $l/D = 2.92$, $D = 13$mm.

Reynolds No. $= \rho u_1 d_1/\mu = 54 \times 10^3$. Framing Rate = 80 fps.

p^*_{LC}, which in turn is less than $p^*_{orifice}$ with the same upstream pressure.

It is known that the asymmetric jet within the cavity will entrain fluid. In the case of the MLC nozzle, the cavity is vented to atmospheric pressure through that part of the exit plane not occupied by the asymmetric jet, and so the pressure in the cavity must be sub-atmospheric. Thus $p^*_{MLC} < p^*_{orifice}$. However the LC nozzle is longer than the MLC nozzle and so the jet in it must have a correspondingly greater entrainment appetite. This supports the results of the static pressure on the wall, Figure 4.11, which show that $p_{w-LC} < p_{w-MLC}$. For the results of the two sets of experiments to be consistent, the MLC nozzle must have a much stronger *radial* pressure gradient in the upstream part of the cavity than does the LC nozzle. Indeed, a radial pressure gradient must exist here in the MLC nozzle because the streamlines are almost circumferential to the inside of the cylindrical cavity. For the swirling fluid to move radially into the centre of the nozzle and be entrained into the jet the radial pressure gradient must be greater than that required to maintain the circumferential streamline trajectories.

Unlike the MLC nozzle, the jet leaving the LC nozzle occupies all of the exit plane, and thus the cavity is not vented to atmospheric pressure. Furthermore, the mean velocity profiles of the LC jet show that it exhibits a vena contracta downstream of the exit plane (see Figure 3.4). This implies that the static pressure in the jet at the exit plane must be *greater* than atmospheric pressure. By contrast, the mean static pressure profiles through the exit plane of the MLC nozzle, shown in Figure 4.7, indicate that the mean static pressure of the jet is substantially *below* atmospheric pressure. Because the axial pressure gradients in a jet will be small (since the streamlines in it are nearly parallel), these results indicate that $p^*_{MLC} < p^*_{LC}$. They also indicate that fluid from the primary jet in the LC nozzle must be recirculated back towards the upstream orifice plate and re-entrained into the jet. Thus the "pre-mixing" of the jet fluid with ambient fluid which occurs within the MLC nozzle could not occur in the LC nozzle. This could partly explain the differences in the combustion characteristics of the two nozzle types.

In Figure 4.52, $\dot{m}$ is normalised by the assumed choking mass flow rate, leading to a Mach No. (M), and P_d is normalised by atmospheric pressure. Theoretically, if the orifice plate is considered in isolation from the nozzle, the normalising pressure should be the pressure at the throat, p^*. Because this pressure is not easy to measure and the p_w does not seem to be a valid indicator of p^*, p_{atmos} was considered to be the least ambiguous normalising term. Furthermore in practical application, the determination of $\dot{m}$ from one pressure, P_d, will be

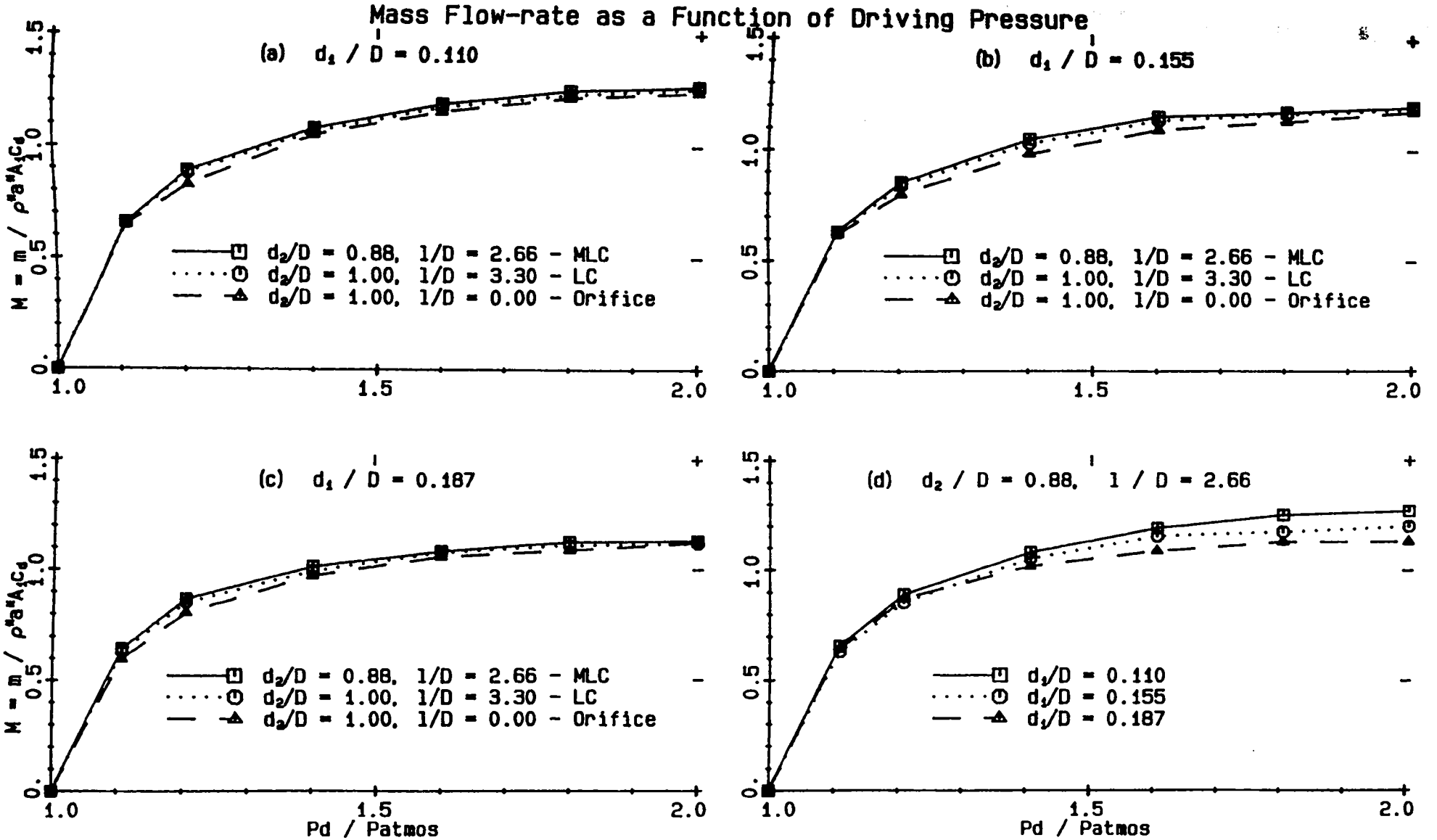

Figure 4.52: Mass-Flow-Rate as a function of Driving-Pressure for a range of different nozzles

much simpler than that requiring two measurements.

It can be seen that M asymptotes toward a constant value as the pressure ratio is increased, indicating that the flow is becoming choked, as expected. However, it asymptotes to a value of M which is larger than unity – a result which is clearly not possible. This is because Mach No. was calculated using the relationship $M = u/u^* = \dot{m}A_1/\rho^*$. Now $\dot{m}$ was measured, and so the discrepancy must be found in assumed values of the coefficient of discharge, c_d, and/or ρ^*.

The value of c_d was calculated using the British Standard, BS1042 (1964), for each orifice plate, which is accurate when M is small. This calculated value was found to be almost independent of d_1/D within the range of geometries used here, eg. $c_d = 0.592$ at $d_1/D = 0.110$, and $c_d = 0.596$ at $d_1/D = 0.231$. The throat density at choking was taken from the relation $\rho^*/\rho_0 = 0.634$. Now ρ^* depends only on the reservoir conditions, and so can safely be assumed to be accurate. However, as has already been mentioned in section 4.7.3, c_d *is* a function of M. As M begins to approach unity, the area of the vena contracta, and hence c_d, increases.

The graphs also indicate that the maximum flow rate appears to be occurring slightly above an absolute driving pressure of two atmospheres. Unfortunately data were not measured at sufficiently high driving pressures to determine this value accurately. The theoretical choking pressure ratio for air is $p^*/p_0 = 0.528$. If the throat pressure is assumed to be atmospheric, then choking of the *vena contracta* will occur at $P_d = 191kPa$ absolute, or 90 kPa gauge. However, choking of the vena contracta does not correspond to choking of the orifice. Further increase in driving pressure will cause the vena contracta to continue to increase in area, and to move upstream, until it coincides with the orifice. This will correspond to the nozzle being fully choked. Note that this will not be the maximum mass flow rate which can be passed through the nozzle, because increasing P_d will lead to a corresponding increase in the density at the throat, thus allowing more mass to pass through.

4.11 Analysis of schlieren photography

It is also possible to obtain semi-quantitative information from the high speed schlieren photography. That is, it is possible to digitize the motion of identifiable fluid features or structures on consecutive frames of the cine film. Because the scale of the photograph and the time between the frames is known, it is possible to measure a two dimensional projection of the magnitude

and direction of the velocity.

The technique is semi-quantitative only because:

- There is always some uncertainty in identifying the same point on a structure in two consecutive frames. However, with care and practice, reasonable confidence can be placed in the technique.
- It is only possible to measure a 2-D projection of the highly 3-D motion. This means that the measured velocity will always be less than or equal to the actual velocity.
- The HYCAM camera does not operate at constant speed, but uses an automatic control circuit to approximate the desired framing rate. Thus the calculated nominal velocity could be up to ±30% out.
- Only 177 vectors were measured, which is insufficient to give adequate confidence in the PDF.

Although the *direction* of each vector was calculated, the results are not presented here because they are too inconclusive. In addition to the above problems, the bias of having least measurements near the "edge" of the jet biases the results to give a predominance of vectors with a strong axial component of direction.

The Probability Density Function, PDF, of the *magnitude* of the velocity vectors is shown in Figure 4.53 for various distances from the nozzle exit plane. The velocity is normalised by the *mean* exit velocity, $\overline{u_e}$. Since the instantaneous jet does not fill the exit plane of the nozzle, it is clear that $\overline{u_e}$ will be substantially less than the average velocity of the instantaneous jet within the exit plane. That is it should theoretically be possible to have normalised velocities greater than one. However, it is clear from Figure 4.53 that the majority of measured vectors are only about 20% of $\overline{u_e}$, for $x/d_2 > 3$. This either indicates that the measured values of velocity are low, or that the velocity is decaying very rapidly within the region immediately downstream of the exit plane.

4.12 Conclusions

In this Chapter, the general characteristics of the enhanced mixing flow patterns produced by the mid-length cavity (MLC) nozzle have been summarised. The intention has been to

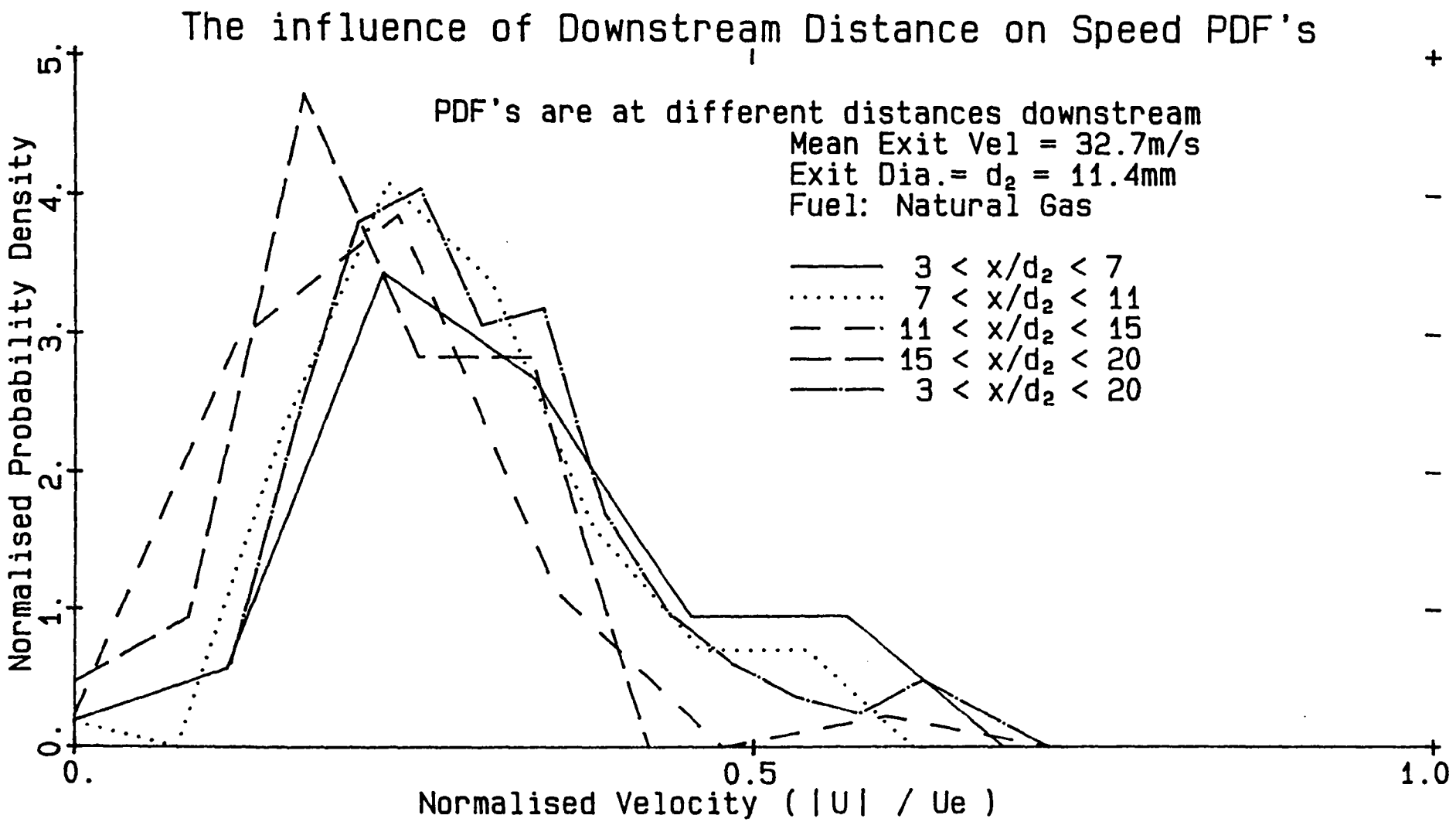

Figure 4.53: Probability Density Function of the fuel jet speed in the MLC flame, measured from high speed schlieren cine film.

introduce the phenomenon, the broad range of techniques used to determine the mechanism, and the essential data and qualitative interpretations which have led to the definition of that mechanism.

It is proposed that the mixing enhancement is generated by a precessing, asymmetric jet. The instantaneous jet from the primary orifice expands asymmetrically into the cavity, and attaches to the wall at one circumferential position. It then separates from the cavity wall slightly upstream of the downstream lip, and leaves the nozzle, without occupying the whole of the exit plane, with a strong radial component towards and beyond the geometric centreline of the nozzle. A secondary flow is induced into the nozzle from the ambient fluid through that part of the exit plane not occupied by the asymmetric jet. This reverse flow moves toward the back of the cavity, where it slews to one side, probably as a result of encountering the orifice wall, and forms a swirling motion. Eventually it spirals radially inwards and is entrained into the central jet. A negative bifurcation (three dimensional separation) is formed where the reverse flow, which originates the reversed flow foot of the instantaneously reattaching jet, interacts with the swirling flow at the back of the cavity. The separated and swirling flows are then entrained by the primary jet. The instantaneous jet and the secondary flow field all precess around the inside of the nozzle. The direction of the precession is the opposite of that of the upstream cavity swirl such that the total angular momentum through the exit plane of the nozzle equals the angular momentum of the primary jet as it enters the nozzle through the throat.

A large number of experiments have been used to verify the proposed flow pattern by which the MLC nozzle generates the enhanced mixing. The evidence for a precessing asymmetric jet is found in the following experiments.

1. The high speed schlieren photography shows the jet at the exit plane appearing to "flap" up and down. Because the nozzle is axi-symmetric, it is evident that the camera captures a two-dimensional projection of a three dimensional precession motion.
2. The visualisation experiments using dye traces in water show that the fluid motion near the cavity wall at the exit plane oscillates between an upstream and a downstream direction. This can be explained by the presence of a precessing asymmetric jet. When the jet is in the same circumferential position as the dye trace, it sweeps

it downstream. When it has precessed to a different circumferential position, the induced reverse flow moves the trace upstream. When three traces are equally spaced around the exit plane, the precessing jet can be observed to sweep past the needles in a constant rotational direction.

3. The visualisation of a *partially* attached jet using smoke shows a jet expanding asymmetrically from the throat of a bell mouth expansion and contraction at the upstream orifice. If the B-M-C-E is suitably shaped, the jet will partially separate, remaining attached to the wall of the cavity at at every axial station in only one segment of the circumferential position. This jet does not precess, and can clearly be seen to leave the nozzle at an angle of about 60 deg to the nozzle axis, in a manner which is postulated to be similar to that of the instantaneous precessing jet. This "frozen" asymmetric jet can be clearly linked with the precessing jet. It is possible to generate a *full* separation at the throat by forming a shock from near the throat, which occurs when sufficient driving pressure is used to take the nozzle to just beyond choking. The onset of choking was found to coincide with the generation of the characteristic flow patterns of the MLC nozzle.

4. The total and static pressure profiles show that the bulk of the mass flow rate in the exit plane is concentrated near the geometric edge of the exit plane. Furthermore, the jet spreads very rapidly, *without* a vena contracta near the exit plane. If the jet was symmetric, and conformed to the pattern of reattachment and separation indicated by the china clay visualisation, a vena contracta downstream of the exit plane would be expected. This matter requires further elucidation. However, both the double peaked total pressure profile, and the absence of a vena contracta can be explained by a precessing asymmetric jet.

5. The static pressure yaw meter experimental results can only be explained by an oscillating flow which has two predominant directions and a period of oscillation which is significantly greater than the response time of the instrument. Also the results show that the flow in the exit plane has a direction with a very strong radially *inward* component. This is clearly incompatible with a symmetric jet which does not have a vena contracta, but can be explained by a precessing asymmetric jet.

6. The surface flow directions indicated by the china clay flow visualisation experiments

cannot be explained by either steady-state flow, or by an asymmetric jet which is not precessing. A sensible interpretation requires that the jet be *both* asymmetric and precessing.

7. The distance to the line of positive bifurcation (reattachment) as indicated by the china clay experiments, is more comparable with that of a plane wall-jet than with that of a the symmetric flow through a large orifice in a pipe. This indicates that the jet in the MLC nozzle reattaches asymmetrically.
8. The success of the bluff bodies in significantly reducing the amount of intermittency can be explained by their physical position in relation to an asymmetric jet. Because the jet must flow around them, they help to ensure that it maintains its asymmetry.
9. The success of a pre-cavity swirl in reducing the amount of intermittency can be explained in terms of the proposed flow patterns.
10. The low frequency oscillation in the exit plane measured by the hot wire anemometer can be explained by a precessing jet. The Srouhal number of this oscillation is the same as that of the "flipping frequency" of the dye trace in the exit plane as measured visually and from the film records.
11. The distinction between the static pressure profiles on the wall for the MLC nozzle and a symmetric flow through a cavity in a pipe, clearly indicates that the flow in the MLC nozzle is very different from the symmetric flow in a pipe/large-orifice configuration.

Evidence for the described secondary flow patterns is found in the following experiments:

1. The dye traces in water clearly show a reverse flow from the exit plane which often can be seen to move right to the back of the cavity. The fluid in the back of the cavity can be seen to be spiraling inward to the jet core in a rotational direction opposite from that of the precession. They also show that the fluid upstream of the plane of the positive bifurcation (as determined from the china clay investigation) is always moving in a direction with an upstream component, whilst that downstream of the plane oscillates in direction.
2. The china clay surface flow visualisation experiments clearly show that there is a very strong swirl in the upstream part of the cavity, and that it is spiraling radially

inward. It shows a positive bifurcation line just downstream from the middle of the cavity, and two negative bifurcation lines. One of these is between the cavity swirl and the line of positive bifurcation, and the other immediately upstream from the exit plane. Because the flow patterns are formed whilst the clay dries, they show mainly the strongest flow patterns which move over them. The flow patterns formed in this way are consistent with the described secondary flow.

The characteristics of the flow patterns of the MLC nozzle which have been determined experimentally are given below:

1. The precession motion occurs at a constant Strouhal number of

$$St = f_p h_1 / \overline{u_1} \approx 0.005$$

2. The half jet spreading angles based on the smoke visualisation of the statically deflected jet are of the order of 60 deg to the centre of the asymmetric jet, and about 75 deg to the outside edge of the jet.
3. The static pressure yaw meter indicates that some fluid near the edge of the jet, and immediately downstream of the exit plane, is leaving the nozzle at nearly 90 deg to the nozzle axis. The flow through the exit plane is at an angle of between -30 and −60 deg (ie. with a radial component directed towards the centreline).

Chapter 5

The Mid Length Cavity Nozzle: Performance Characteristics

The Mid Length Cavity (MLC) nozzle has the best performance characteristics of the family of Enhanced Mixing Nozzles. In this chapter details of the experiments which have been conducted to determine these characteristics, and the apparatus on which they were performed, are given. Both cold flows and combusting flows are examined. Flame stability is indicated by the measuring of blow-off velocity and stand-off distance, with and without premixing with oxygen and/or dilution with an inert. The cold flow experiments utilized an "entrainment shroud" to measure directly the entrainment rates of the nozzle.

The first section of the chapter deals with the problem of selecting an appropriate diameter scale which can be used to compare these characteristics with those of a simple nozzle. An "equivalent exit diameter", d_{2eq}, is introduced and all results are discussed in terms of d_2, d_{2eq} and d_1.

It has been found that the entrainment rate of the MLC nozzle is an order of magnitude larger than that of an unexcited jet if the comparison is based on d_2, about five times as large if based on d_{2eq}, and about twice as large if based on d_1. The stand-off distance, normalised by d_2 and d_{2eq}, is an order of magnitude less than that of a simple flame at the same Re. If normalised by d_1 it is half that of a simple jet. The blow-off velocity of the MLC nozzle is about four times as large as that of the unexcited jet if based on d_{2eq}, approximately the same if based on d_2, and about thirty times as large if based on d_1. Of the three scales, it appears that the most consistent is the "equivalent exit diameter", d_{2eq}.

5.1 Selecting a length scale for the enhanced jet

The flow patterns of a simple jet with a bell-shaped velocity profile are usually non-dimensionalised in terms of the exit diameter of the nozzle and either the mean exit velocity or a centreline velocity. Unfortunately, these simple scales are inadequate for normalising the flow patterns from the MLC nozzle.

As described in Chapter 4, the instantaneous jet which leaves the the nozzle does not fill the whole of the exit plane. Consequently, the mean exit velocity, based on mass flow rate and *exit* area, will not adequately represent the instantaneous mean exit velocity. Likewise, a change in the size of the downstream lip, (within the broad limits of operation), whilst influencing the *direction* at which the instantaneous jet leaves the nozzle, does not cause a significant change in the *magnitude* of its velocity. This is in direct contrast to a simple jet, where the exit velocity for a given flow rate is inversely proportional to the exit area.

The diameter of the *upstream* orifice is also an inappropriate dimension on which to scale the flow patterns of the nozzle. The virtual origin of the rapidly expanding jet is less than half a cavity diameter upstream of the exit plane, while the upstream orifice is a further two cavity diameters upstream, making it remote from the virtual origin. Also, the diameter of the instantaneous jet at the exit plane will be more than twice that at the throat because the jet entrains fluid as it traverses the cavity. Furthermore, none of the fluid-mechanical motions associated with the MLC nozzle (eg. the precession frequency and mean centreline velocity decay rate) scale on the throat diameter. However the diameter of the throat does control the mass flow rate and hence the mean velocities through the nozzle.

The cavity diameter, although useful in comparing EMBs of different scales, is even less appropriate than the orifice diameters in providing a comparison with other nozzles. The instantaneous jet nowhere fills the cavity, and the flow patterns do not scale on this dimension.

It is desirable to introduce an "equivalent" exit diameter, d_{2eq}, which corresponds to the diameter of an equivalent simple nozzle. The "equivalent diameter" proposed is the diameter of the instantaneous jet at the exit plane. This diameter is directly related to the mass flow rate in the primary jet, and is physically situated near the virtual origin of the mean jet.

However, there are ambiguities associated with this term. The jet at the exit plane of an unexcited jet will have a "top-hat" shaped velocity profile, its edge is clearly defined and equal to the diameter of the nozzle. By contrast, the instantaneous jet within the MLC nozzle has

a "bell-mouth" shaped velocity profile at the exit plane of the MLC nozzle, and so its edge is not clearly defined and its diameter cannot be measured in absolute terms. Consequently, it was decided to follow the common practice of defining the edge of the jet as twice r_{half}, where r_{half} is the radius at which the time averaged velocity relative to the surroundings is one half of that at the centreline.

Because the instantaneous jet precesses, its diameter is difficult to measure. Consequently it was decided that a good approximation of d_{2eq} could be best obtained by measuring r_{half} of a non-precessing, simple jet emanating from the same throat as is used in the MLC nozzle and at the same axial station as the the exit plane of the MLC nozzle. This measured value of d_{2eq} is preferred to a calculated value because it includes the effects of the detailed geometry of the throat.

As mentioned at the beginning of the chapter, d_{2eq} provides the most consistent basis for comparison of the results. Nevertheless, because of the ambiguities associated with it, the results are also discussed in terms of d_1 and d_2. Whilst each comparison in itself is incomplete, together they provide an adequate description.

5.1.1 Measuring d_{2eq}

The measurement of the diameter of the instantaneous precessing jet is a formidable task which was deemed to be beyond the scope of the present investigation. As indicated above, the half width, r_{half}, of an unenhanced jet emerging into atmosphere from the nozzle throat was measured at $x = l$, ie. at the same downstream location as the MLC nozzle exit plane. The equivalent exit diameter for the MLC nozzle was then assumed to be twice this measurement.

The measurement of r_{half} was made using a pitot-static probe, as discussed in Section 5.2.5. Measurements were made for the four sharp edged orifice plates and for the nozzle with a bell-mouth contraction. The results of these measurements are displayed in Figure 5.1.

The measured value of d_{2eq} would only be the same as those of the precessing jet if: true. If it is assumed that

- the presence of the EMB cavity does not restrict the entrainment of the instantaneous jet,
- neither the curvature of the jet nor its contact with the wall, cause it to distort in shape,

Whilst neither of these conditions are likely to be satisfied, the departures of the actual

diameter of the precessing jet from the measured value of d_{2eq} for each of the throat configurations are likely to be similar for all cases. Thus it is concluded that the measured value of d_{2eq} is an adequate exit plane jet scale for the present purposes.

It can be seen that d_{2eq} is typically about 42mm, compared with $d_1 = 14.2$mm and $d_2 = 80$mm for the perspex nozzle where $D = 90$mm. However, the dependence of r_{half} on orifice diameter requires some discussion. One might anticipate that d_{2eq} would increase in proportion with d_1. This is far from the case. Over the range measured, d_{2eq} exhibits a minimum between $d_1 = 14$ and $d_1 = 17$mm. To validate the measurement technique, one data point (that which defied the expected trend; $d_1 = 10$mm) was measured four times. Repeatability was very good, with a maximum deviation from the mean value being 0.4%.

The explanation for the observed dependence of r_{half} on d_1 is related to the development length of a jet. It is well known that on leaving a nozzle, the velocity profile of the jet changes from a "top-hat" to a "bell-mouth" velocity profile. For the orifice plates a vena-contracta is also formed immediately downstream from the primary nozzle. The development length depends upon the specific nozzle geometry but is typically five nozzle diameters. The spread angle, and hence rate of entrainment, is lower in the developing region than in the similarity region. Now the jet from the smallest orifice, $d_1 = 10$mm, was measured at $d_1/D = 24$, whilst the jet from the largest orifice, $d_1 = 21$mm, was measured at $d_1/D = 11$. Thus it can be seen that over the same axial distance, the jet from the smallest nozzle will have the smallest percentage of its length entraining at the lower rates associated with the developing region.

Increasing d_1 generates two opposing influences of major consequence on the value of d_{2eq}; that of increasing the initial jet diameter and that of increasing development length. A third influence of lesser significance also operates; increasing the ratio of d_1/D_0, where D_0 is the diameter of the upstream supply pipe, will also cause an decrease in the necking associated with the vena contracta.

5.2 Entrainment Measurements

5.2.1 Introduction

The mass flow rate across planes at right angles to a jet is known to increase with distance downstream. This will be accompanied by a simultaneous decrease in jet velocity in order to conserve linear momentum, and this in turn will result in a spreading of the jet. The

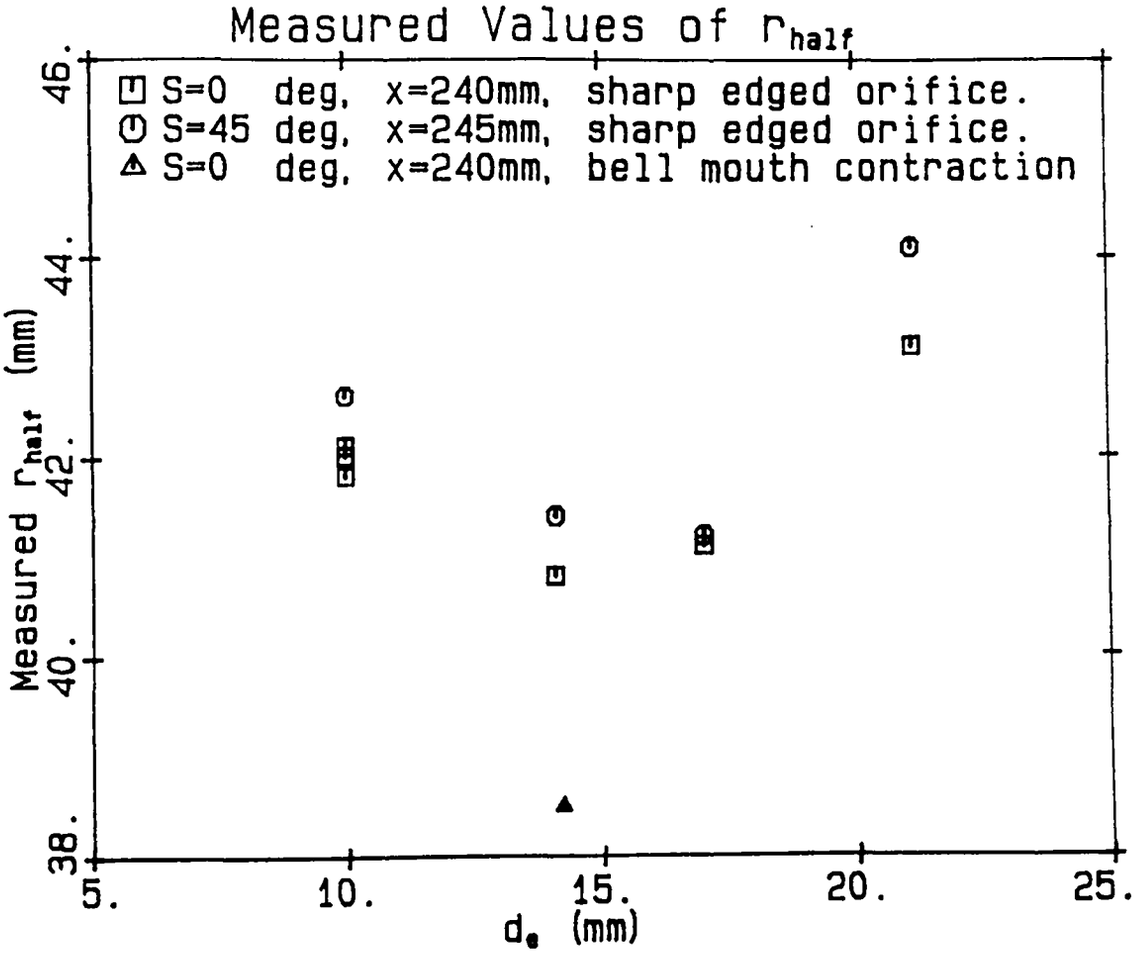

Figure 5.1: Values of d_{2eq} obtained by measuring r_{half} for an unenhanced jet at the same axial station as the exit plane of the MLC nozzle.

process by which the surrounding fluid is drawn into the jet is known as entrainment. It is largely governed by the large scale structures which engulf the ambient fluid [24,62]. Thus entrainment is a measure of the rate at which the jet mixes with its surrounds. Since most practical applications of jets utilise the jet mixing characteristics, (eg. chemical processes, stirrers and mixers, combustors, ejectors, etc.) entrainment is an important indicator of the usefulness of a jet.

Determining the entrainment rate, $d\dot{m}/dx$, is notoriously difficult and usually an indirect task. The usual method is to measure $\dot{m}$ at various axial locations by integrating velocity profiles, as per equation 5.1 [52]. Not only is this method laborious, but it is usually plagued by inaccuracies, due to the difficulty of measuring the intermittent, low velocity edge of the jet. These problems are compounded for the MLC nozzle because the precessing jet is instantaneously highly asymmetric and so the interpretation of the highly three-dimensional flow patterns is critical. Also, because the jet velocity decays so rapidly, it is impractical to measure it in the similarity region with a pitot tube. Consequently, low velocities and high intermittency occur throughout the jet, and not the exclusive province of the edge of the jet.

Ricou and Spalding (1961), (R&S), proposed an alternative method which enables the volume of fluid which has been entrained by the jet in a given length to be measured directly. The jet is surrounded by a porous-walled annular chamber. Air is injected through the inner wall of the annulus until the pressure at the downstream limit of the annulus equals the ambient pressure at which time the streamlines of the flow from the annulus to the jet are precisely radial. This condition indicates that the flow rate of air being supplied through the porous wall is the same as that which would be supplied from the surrounding atmosphere in the absence of the annular chamber. In this way, the mass flow rate through the primary jet, $\dot{m}_p$, and the secondary air, $\dot{m}_s$, can be measured directly using orifice flow raters upstream upstream from the rig.

These experiments indicate that in the first three exit diameters, based on the equivalent diameter, d_{2eq}, the MLC nozzle entrains approximately five times as much air as does a simple nozzle.

5.2.2 Mathematical Description & Notation

The mass flux, $\dot{m}$ across a section at right angles to the jet is given by

$$\dot{m} = \int_0^\infty 2\pi\overline{\rho u}\, dy \tag{5.1}$$

where the overbar denotes a time average.

Following R&S, the relationship between $\dot{m}$ and x is linear, provided that the jet displays similarity, and x, the distance downstream, is measured from the virtual origin. Assuming that density is constant, this relationship is given by

$$\frac{\dot{m}}{xM^{1/2}\rho^{1/2}} = K \tag{5.2}$$

where K is a proportionality constant and M is the excess axial momentum which must be constant and can therefore be calculated at the jet exit or at some other suitable location.

Alternatively, the relationship between the entrained fluid, $\dot{m}_s$, and the nozzle fluid, $\dot{m}_p$, can be expressed as

$$\frac{\dot{m}_s + \dot{m}_p}{\dot{m}_p} = K_T\frac{x}{d} \tag{5.3}$$

where K_T is another proportionality constant.

The relationship between K and K_T is given by

$$K = (\frac{\pi}{4})^{\frac{1}{2}} K_T \ .$$

R&S were able to use large values of x, and thus were able to approximate the origin of the jet as being at the exit plane. Since the velocity at the exit plane is uniform, M is given by

$$M = M_0 = \frac{1}{4}\pi d_0^2 \rho_0 u_0^2 \ .$$

In the case of the MLC nozzles, the velocity at the nozzle exit plane is not uniform, and so the mass flow rate is measured independently through the use of a calibrated orifice flow-rater. The origin of the EMB jet can still be approximated as occurring at the exit plane because, although the length of the shroud relative to its diameter is much smaller than is that of R&S, the large spreading angle of the jet means that the virtual origin is very close to the exit plane.

5.2.3 The Validity of Shroud Pressure as an Indicator of Equivalent Entrainment

It is necessary to verify the contention that when the pressure at the shroud exit is equal to the ambient pressure, that the shroud is supplying the equivalent amount of air which would be

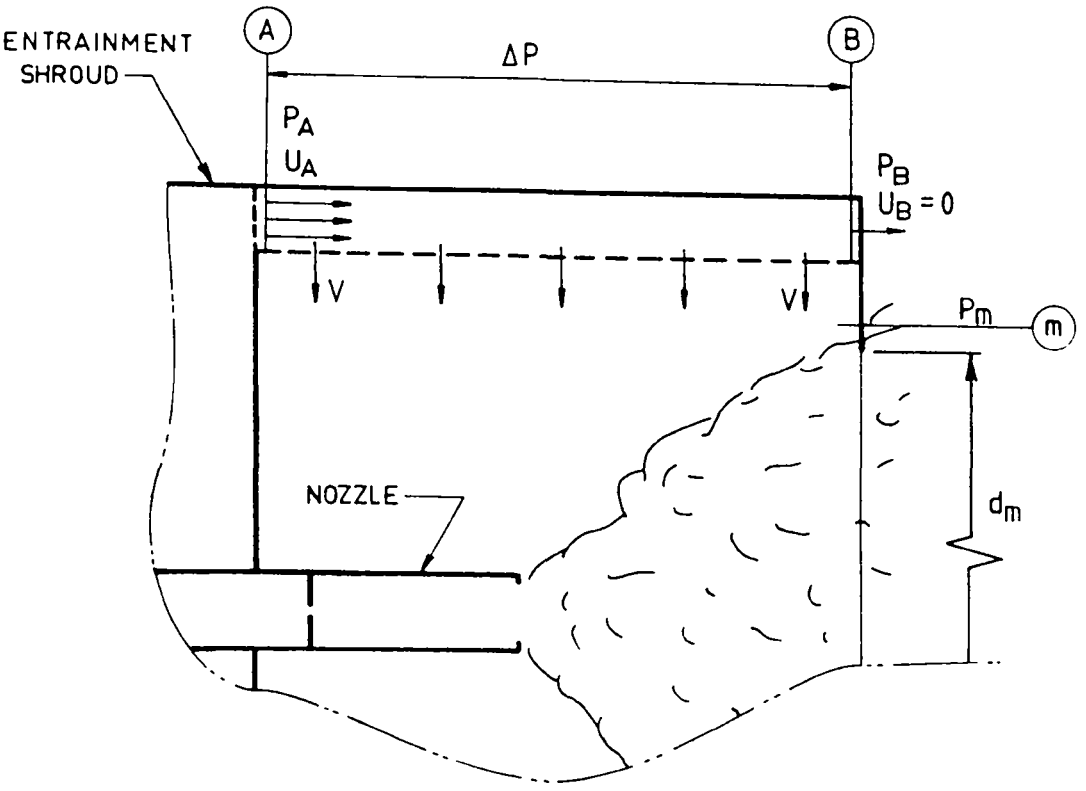

Figure 5.2: A schematic diagram of flow within the Entrainment Shroud. When the flow rates are balanced, $P_B = P_{ambient}$.

induced in the absence of the shroud. It can be seen from Figure 5.2 that if the flow through the porous wall, v, is uniform and perpendicular to the wall, then a constant velocity gradient of u_A/L_s, where L_s is the length of the porous wall in the x direction, will exist along the porous wall. Consequently a pressure gradient will also exist in the x direction, with $P_A > P_B$. (The influence of this pressure gradient on the jet is discussed in Section 5.2.5.) Similarly, a pressure drop will occur in the radial direction across the screen, so that $P_B > P_m$. Thus P_m is the static pressure which best represents the static pressure in the exit plane of the shroud.

Because the jet is entraining fluid from the surrounding atmosphere, it is acting as a sink, and its pressure will be lower than that of the surroundings. In an unconfined environment, this implies that the surrounding fluid will be drawn nearly radially toward the jet axis. If the pressure at the shroud exit, ie. P_m, is greater than ambient, there will be a tendency for the surrounding air to move out from the shroud with an axial component, and the shroud flow is larger than that that required to satisfy the jet entrainment. Conversely, if the pressure at the shroud exit is sub-atmospheric, then air will be induced into the shroud from the ambient surrounds, and the shroud flow will be failing to satisfy the jet entrainment. Thus it can be seen that when the pressure at the shroud exit is equal to ambient pressure, such that

the limiting streamline from the shroud is radial, the entrainment appetite of the jet will be satisfied precisely.

5.2.4 Apparatus

The Entrainment Shroud

The "entrainment shroud" is shown in Figures 2.1 and 5.2. A detailed drawing of the shroud is shown in Appendix C.1. The joints are sealed using "duct tape" and the shroud is sealed around the nozzle using a plate with a thick, felt "O-ring" sliding seal, thus enabling the position of the nozzle within the cavity to be varied. The porous cylinder is made of two different sized mesh screens. A screen mesh with an open area of 58% has been recommended [19,20] to minimise flow non-uniformities. In the present apparatus, a large and small sized mesh in series is used to provide the required pressure drop while maintaining uniform flow and reducing the scales of the turbulence generated upstream of the mesh.

Experimental Techniques

As stated in the introduction, the aim of the experiment is to measure the flow rates through the jet and the shroud, when the pressure immediately inside the shroud mouth is equal to the ambient pressure. This is done in two different ways. The first method uses a sensitive pressure transducer to measure the wall pressure in the shroud, and the second uses a smoke trace in the exit plane of the shroud to visually indicate when the shroud air is drawn radially into the jet.

Using the pressure measurement technique, the shroud pressure relative to atmosphere, P_m, is measured for a range of values of $\dot{m}_s/\dot{m}_p$ whilst m_s is held constant. The "zero crossing point" (the point at which this line intersects the abscissa) gives a good estimate of the value of $\dot{m}_s/\dot{m}_p$ for which $P_m = 0$.

Whilst P_m is easily measured for an unexcited jet, where d_m can be made small (see Section 5.2.5), it is much more difficult in the present rig when d_m is large enough to admit the enhanced jet. For example, it was found to be impossible to obtain sensible measurements of P_m when blowing the enhanced jet through the shroud having a mouth diameter, $d_m = 850$mm, and the static pressure tapping 25mm from the mouth. The reason for this is that the screens are fixed to the shroud wall using a 40mm "lip" which generates a local separation in the

secondary flow, causing the reading of P_m to be invalid. Rather than attempt to measure P_m directly, which would require a further reduction of d_m and so risk greater problems of jet impingement, it was decided when testing the MLC nozzle to infer P_m from a measurement of P_B. Because $\dot{m}_s$ is held constant in these experiments, the pressure drop across the screens will also be constant. By independently measuring the pressure drop, it was found that $P_m = P_B - 6\text{mTorr}$. This technique allows the shroud diameter ,d_e, to be set at its maximum value of 1000mm.

The shroud pressure relative to atmosphere is plotted against $\dot{m}_s/\dot{m}_p$ and the point at which $P_B = 6\text{mTorr}$ is obtained from the line of best fit. Because P_m depends on $\dot{m}_p$ and $\dot{m}_s$ as well as on the ratio between them, it is necessary to keep one of them constant if a continuous line is to be obtained. It was decided to hold $\dot{m}_s$ constant since $\dot{m}_s \gg \dot{m}_p$. Its value was selected as the maximum which could be supplied by the compressor/pressure-vessel without unacceptable supply pressure variations occurring in a run series.

The shroud pressures were measured using a 100 torr barocel pressure transducer with a heating element. Although this involved amplifying the signal 1000 times, and reading the smallest scale of the meter, this was found to be the most suitable instrument in the department. Provided that adequate time is allowed for the barocel to reach a constant temperature, (the instrument was left on continuously), it is found to be extremely stable. A 10 torr baratron, and a Combist micro-manometer graduated down to 0.0005 inches of water were found to be less suitable.

Three static pressure tappings spaced uniformly around the shroud's circumference were connected together to obtain a representative value of P_B. Although large fluctuations (of the same order of magnitude as the measurement) were encountered, acceptable results were obtained using the eye to select a suitable "average" value. The shroud pressures were of the same order of magnitude as the fluctuations in the ambient pressure in the laboratory, but this posed no problem if the zero was constantly monitored.

The validity of the results can be seen both from the minimal scatter within each line, and by the test for repeatability (see Figure 5.7(a)). Note that one of the lines in Figure 5.7(a) is inconsistent with the other three. The reason for this is unknown, but may have been due to an incorrect setting of one of the geometric ratios.

In the second experimental technique a smoke trace is used to determine the flow rates of P_m and P_s at which $P_m = 0$ from a single measurement. The smoke is injected vertically

downward past the outside edge of the shroud mouth, to avoid gravity bias, and the flow rates are adjusted until the trace is deflected neither into nor out from the cavity. This technique lends itself more readily to measuring K_T for a wide range of flow rates, and so enables the dependence of K_T on $\dot{m}_p$ to be investigated. Accordingly it is the recommended technique for future work.

5.2.5 The influence of the shroud on the jet

R&S were able to use a much longer shroud length to nozzle diameter ratio than is possible using the MLC nozzle, due to the much smaller spreading angles associated with the simple nozzle. Consequently, some of the experimental techniques necessarily differ. Two conflicting requirements exist; that of minimum influence imposed on the jet by the shroud, and that of maximum pressure differential across the shroud mouth.

As mentioned in Section 5.2.3, there is a negative axial pressure gradient in the shroud, equal to $(P_A - P_B)/L_s$, where the notation is defined in Figure 5.2. This tends to reduce the spreading angle of the jet relative to the unconfined case. However its influence on the jet will be small if the static pressure gradient in the shroud is small compared to the static pressure gradient in the jet. This is indeed the case. The shroud pressure gradient has been measured as $P_A - P_B \approx 10$mTorr (Figure 5.3), whilst the increase in static pressure along the jet centreline in the same distance is of the order of one Torr (Figure 4.7). Theoretical analysis indicates that to keep the shroud pressure gradient to a minimum, it is desirable to keep u_1 to a minimum, and so to make the shroud diameter as large as possible.

The importance of achieving a large pressure drop across the shroud mouth when the primary and secondary flows are unbalanced becomes obvious when it is realised that the shroud pressure relative to atmosphere is of the order of one millitorr, which means that even fluctuations in atmospheric pressure become significant. The shroud pressures can be increased by increasing the mass flow rate of the secondary air, and hence of primary flow, but this option is limited by the capacity of the compressor.

It can be seen intuitively that if the cross-sectional area of the annular space between the shroud mouth and the edge of the jet is large, the axial velocity through it (either into or out from the shroud) will be small, and so the pressure drop across the shroud mouth will also be small. As the area of the annular space decreases, the velocity through it must increase, with a consequent increase in measured pressure drop. Thus it is desirable to have the diameter of

the mouth only slightly larger than that of the jet.

R&S optimised the shroud geometry by altering the diameter of the shroud mouth. A decrease in aperture diameter always resulted in an increase in the magnitude of the shroud pressure. At the critical value of mouth diameter for which the shroud began to influence the jet, the value of K (ie. the zero cross-over point) was caused to decrease. This method was impractical for the present jet because its large spreading angles would have required a prohibitively large diameter of the shroud in order to have sufficient adjustment of d_m. Not only would this have been impractical, (since the shroud diameter was 1200 mm) but the already low shroud pressure would be further reduced because the velocity through it would be much lower for the same mass flow rate.

An alternative method by which the influence of the shroud on the nozzle may be determined is to find the *length* of the shroud, below which a further change in length has no effect on K. However, this technique assumes that K does not vary with axial distance, x, from the nozzle exit. Such an assumption is contrary to experimental evidence. Results indicate that the rate of entrainment of the jet generated by the MLC nozzle varies strongly with x over the first few exit diameters where its velocity profiles do not display similarity.

One very approximate method of determining whether the shroud is influencing the jet, was to feel the edge of the jet by hand. This indicates if the intermittent turbulent structures of the outer layer of the jet are impinging on the shroud. Some impingement is to be expected, because other experiments (see Figure 4.9) have indicated that the *initial* expansion half angles of the jet approach 90 deg. However, by using a large shroud diameter such impingement can be kept small so that the vast majority of the jet's mass is unimpeded by the shroud, and its influence is therefore small. It is should be pointed out that any errors which are induced by the jet impinging on the shroud will lead to a *reduction* in the value of K (see R&S). For this reason the estimated increase in entrainment rates for the MLC nozzle in comparison with simple nozzles are conservative. To test these predictions, the following experiments were conducted:

- A baffle was placed in front of the pressure tapping to ensure that the jet could not impinge on the pressure tapping, and was compared with the result without the baffle.
- The pressure drop along the shroud was measured to test the internal consistency of the measurements at varying values of primary jet flow rate.

These are discussed in the following sections.

The influence of the rapidly expanding jet on the pressure measurements

Two techniques exist for testing the internal consistency of the entrainment shroud measurements. If the rapidly expanding jet is impinging upon the static pressure tappings, it will superimpose a total pressure component upon the static pressure, causing the measured static pressure to be greater than the true static pressure. Such an occurrence is detectable in two ways;

1. The pressure differential between the upstream and downstream pressure tappings in the shroud (P_A and P_B respectively) will decrease with increasing $\dot{m}_p$, instead of depending only upon $\dot{m}_s$. This will occur because whilst the *true* static pressure differential must be a function of only the *secondary* mass flow rate, any *superimposed* total pressure component will be a function of P_d.
2. The zero crossing point of $\dot{m}_s/\dot{m}_p$, and hence the measured value of K, will change if a baffle is put over the static pressure tapping, preventing the jet from impinging on the pressure tapping.

To test for these events, the following experiments were conducted. The static pressures at both the upstream and downstream wall tappings were measured for varying values of $\dot{m}_p/\dot{m}_s$, with and without a baffle placed over the downstream pressure tapping. Two sizes of baffle were used; 80 x 100mm and 175 x 175mm. These were placed 100mm above the tappings, ie. on the inside of the inner screen.

The results of these experiments are shown in Figure 5.3.

The following two points are clear.

1. The presence of a baffle has only a minor influence on the measured value of K_T, the zero crossing point of $\dot{m}_s/\dot{m}_p$.
2. The pressure differential between the upstream and downstream pressure tappings of the entrainment shroud is approximately independent of $\dot{m}_s/\dot{m}_p$, although there is a lot of scatter in the results. This dependence is probably caused by the nonuniformities introduced when the shroud is either over-supplying or under-supplying

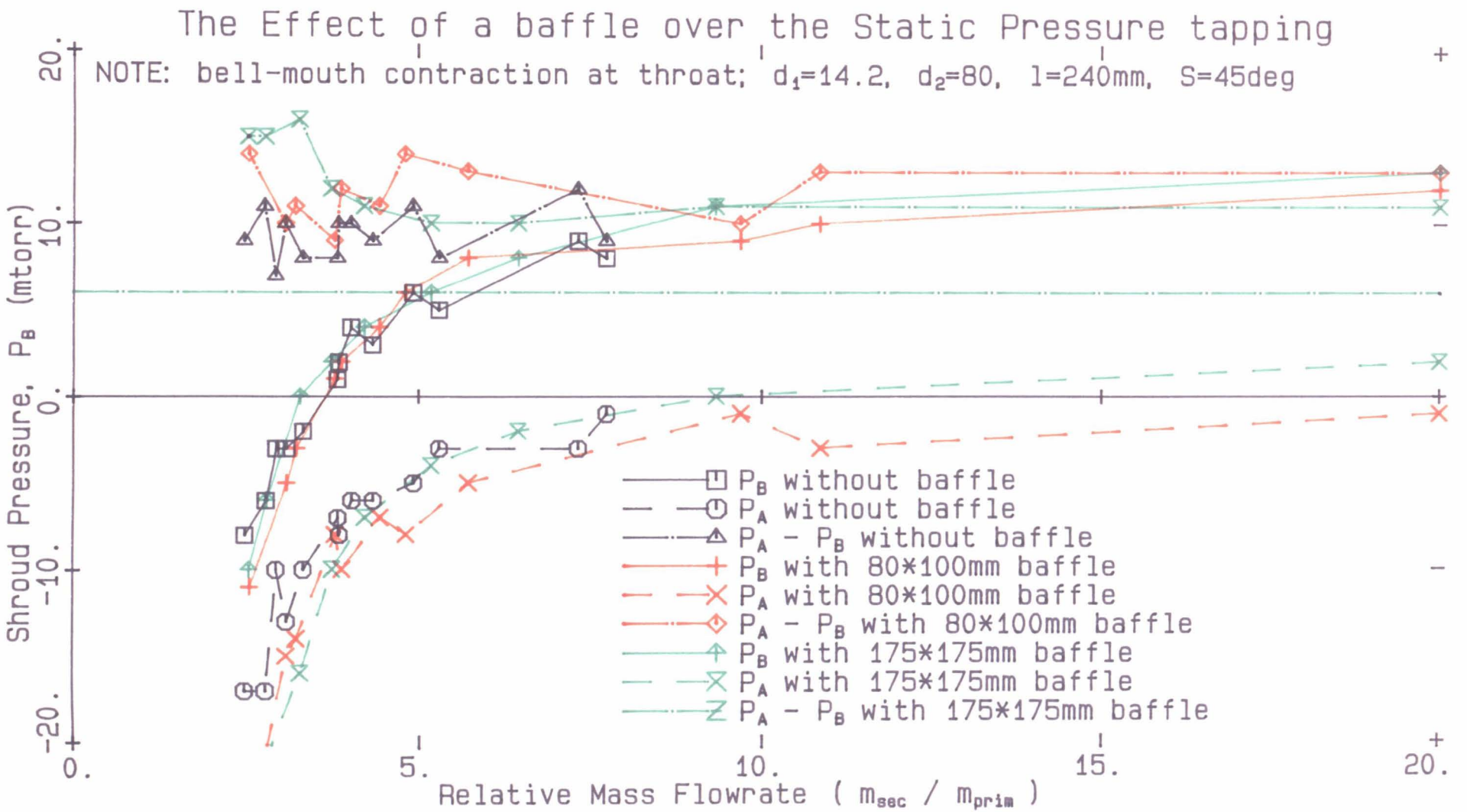

Figure 5.3: The influence of the jet upon the results of the entrainment shroud.

the jet, as discussed at the end of Section 5.2.5. Certainly the presence of the baffle does not reduce this dependence.

These results clearly indicate that impingement of the jet on the shroud does not significantly influence the results.

Note that no baffle was placed over the upstream pressure tapping because

- This tapping was well upstream of the nozzle exit plane, and hence impingement was impossible,
- If the downstream tapping has negligible influence, the upstream one will have even less.
- It is desirable to keep the baffle size to a minimum since it causes a reduction in the effective screen area.

Use of the shroud with an unenhanced jet

As a check of the accuracy of the measurement technique and the validity of the position of the static pressure tapping whose reading was to be compared with $P_{ambient}$, the entrainment of an *unenhanced* jet was measured. This is essentially repeating the experiment of R&S, except that the nozzle has a different profile, and the shroud a different geometry.

To do this, a shroud exit diameter of d_m = 400mm was selected. This diameter was approximately 100mm larger than the "true edge" of the jet at the same axial station as measured by the pitot-static pressure profiles. The results of these measurements are shown in Figure 5.4. Plotted on the same graph are P_B, $P_B - P_m$ and $P_B|_{dm=1000}$.

It can be seen that P_m, measured with d_m = 400mm, has a null pressure at $(\dot{m}_s/\dot{m}_p) = 8.19$. ie. $(\dot{m}_s + \dot{m}_p)/\dot{m}_p = 9.19$. This leads to a value of $K_T = 0.256$, compared with the value of $K_T = 0.26$ as measured using the pitot-static pressure profiles (see Section 5.2.5), and $K_T = 0.32$ as measured by R&S. The excellent agreement between the entrainment shroud and the pitot-static pressure profiles gives confidence that P_m is a valid measure of shroud pressure. The discrepancy between the present results and those of R&S suggests that there is a difference between the profiles of the two nozzles. However, the profile used by R&S is not specified. The present results are within the range of values found by other researchers, namely $0.24 < K_T < 0.50$, as quoted by R&S.

It can also be seen from Figure 5.4 that whilst $P_B - P_m$ is approximately constant, it is a slight function of $(\dot{m}_s/\dot{m}_p)$. The minimum of $P_B - P_m$ occurs near the place where

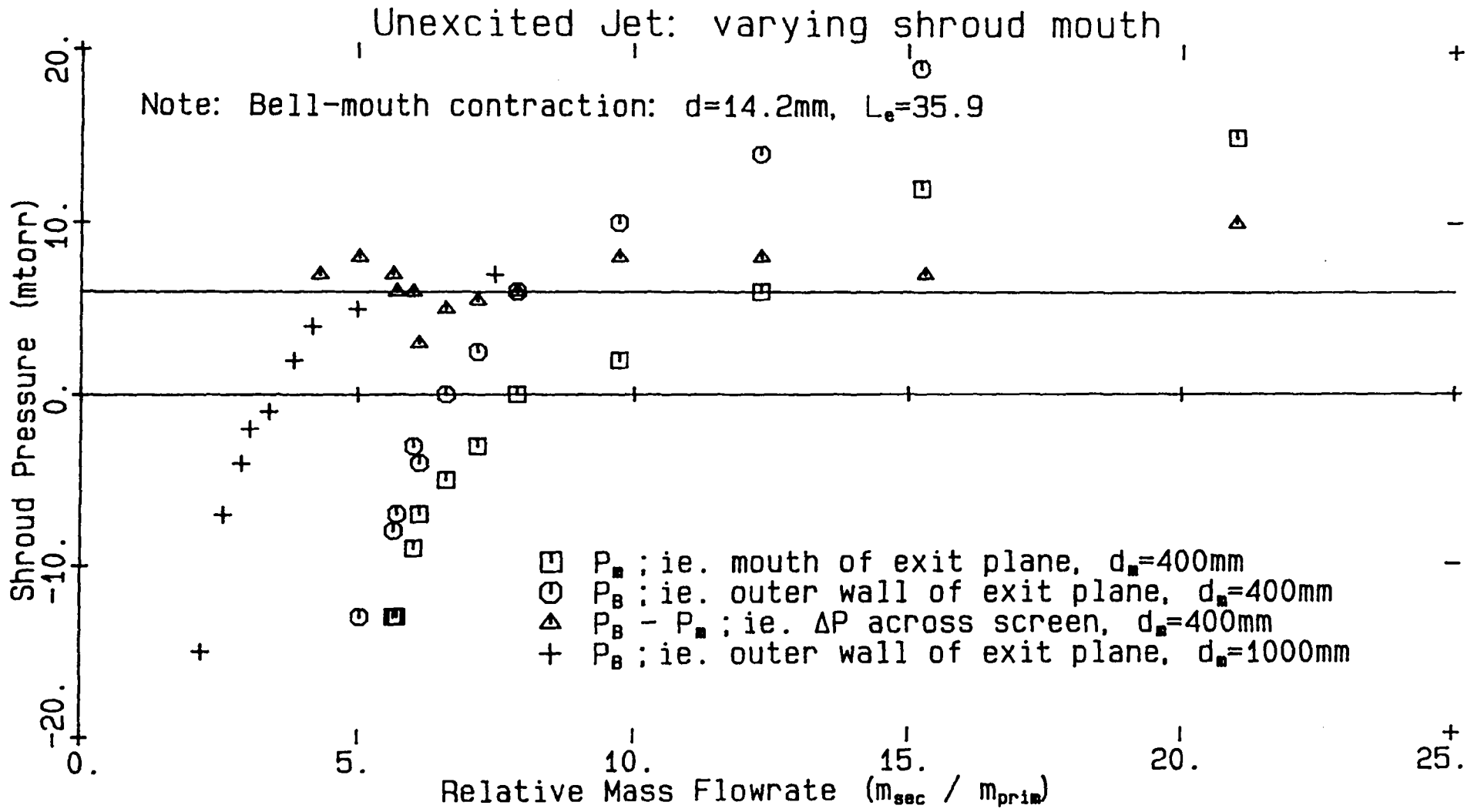

Figure 5.4: Measurements of wall pressure, P_B, in the entrainment shroud with an unexcited jet.

$P_B = 0$. This indicates that a secondary effect, probably caused by the tendency of the secondary streamlines to be non-perpendicular to the nozzle axis when the shroud is under-supplying or over-supplying the jet, is superimposed on the static pressure reading. The value of $P_B - P_m|_{Pm=0}$ is 6 milliTorr, ie. the pressure drop across the screens, at $\dot{m}_s = 0.06$kg/s. A horizontal line through $P_B = 6$mTorr is drawn on all plots of P_B against $(\dot{m}_s/\dot{m}_p)$, and the intersection of this shifted axis gives the true value of K_T. Note too that an attempt was made to calculate the pressure drop across the screens using the method prescribed by the Engineering Science Data Unit [35], but the Reynolds numbers through the screens were much too small to allow an accurate estimate of the Reynolds number correction factor.

Figure 5.4 also shows P_B for the unexcited jet, measured with $d_m = 1000$mm. In this configuration, the jet diameter is *much* smaller than d_m, and it can no longer be assumed that no axial pressure gradient exists within the shroud. Consequently the static pressure measured at P_B does not equal the static pressure at the edge of the jet in the exit plane. This is bourne out by the experimental results, where it can be seen that a large difference exists between P_B measured with $d_m = 400$mm, and P_B measured with $d_m = 1000$mm. However this difference is a minimum near $P_B = 6$mTorr, again indicating that the streamlines are approximately perpendicular to the nozzle axis at this flow rate, or that $\dot{m}_s$ equals the entrainment appetite of the jet.

The entrainment of the unenhanced jet measured by a pitot-static probe

In order to provide a check of the accuracy of the entrainment shroud in measuring K_T, it was decided to use an independent method of determining K_T. The most well known method is that of integrating velocity profiles, as discussed in Section 5.2.2. It is not possible to conduct these tests accurately using the MLC nozzle, because the velocities are too low. However an unexcited jet can be tested using both techniques.

The nozzle used was the bell-mouth contraction with a diameter, $d_e = 14.2$mm. A pitot-static probe was used to measure the dynamic pressure, and profiles were measured at $x/d_e = 10$, 15, 20 & 30, all of which are in the region where a jet displays self-similarity. The probe was mounted on a traverse which gives an electrical output proportional to the position of the probe. The probe is connected to a small reservoir, which damps out pressure fluctuations, and then to a pressure transducer. Both of these outputs are connected to a plotter, so that the profile is recorded directly. The profile was then digitized.

The accuracy of the results can be tested in at least three ways;

1. The momentum flux of each profile should be constant, and the normalised momentum flux, H/H_e, should be unity.
2. The jet should expand linearly with downstream distance once similarity has been reached, ie $(r_{half}/d_e) \propto (x/d_e)$. Any profile whose spreading rate does not lie on the same straight line can be considered suspect.
3. The normalised shape of the profiles should be similar, ie. (u/u_{cl}) vs (r/r_{half}) should cause all profiles to collapse onto the same line.

These comparisons, along with the normalised mass flux, are presented in Figure 5.5. The comparison of the shape of the profiles shows that most of the scatter occurs near the very edge of the jet and is probably associated with the digitization process. Nevertheless, the test of jet spreading rate shows that all data points lie on the same straight line, with a correlation coefficient of $R = 0.999$, and the momentum flux at each station remains constant with a maximum variation of 5%. These values are typically 4% less than unity, indicating that a slight error may have arisen in the measurements at the exit plane, possible because of the finite diameter of the probe. The momentum flux and the mass flux of each profile were determined by integration;

$$\frac{H}{H_e} = 8\int_0^\infty \left(\frac{u}{u_e}\right)^2 \left(\frac{r}{d_e}\right) d\left(\frac{r}{d_e}\right) ,$$

$$\frac{\dot{m}}{\dot{m}_e} = 8\int_0^\infty \left(\frac{u}{u_e}\right) \left(\frac{r}{d_e}\right) d\left(\frac{r}{d_e}\right) .$$

The normalised mass flux increases linearly with distance within the range $x/d_e > 10$. where the jet displays similarity. The line has the equation

$$\frac{\dot{m}}{\dot{m}_e} = 0.261\frac{x}{d_e} + 0.0662$$

with a correlation coefficient, $R = 0.996$. The mass flux at the axial plane corresponding to the distance to the exit plane of the shroud can thus be calculated. Using equation 5.3, $K_T = 0.26$, which compares well with that value obtained using the entrainment shroud set with $d_m = 400$mm (see Section 5.2.5).

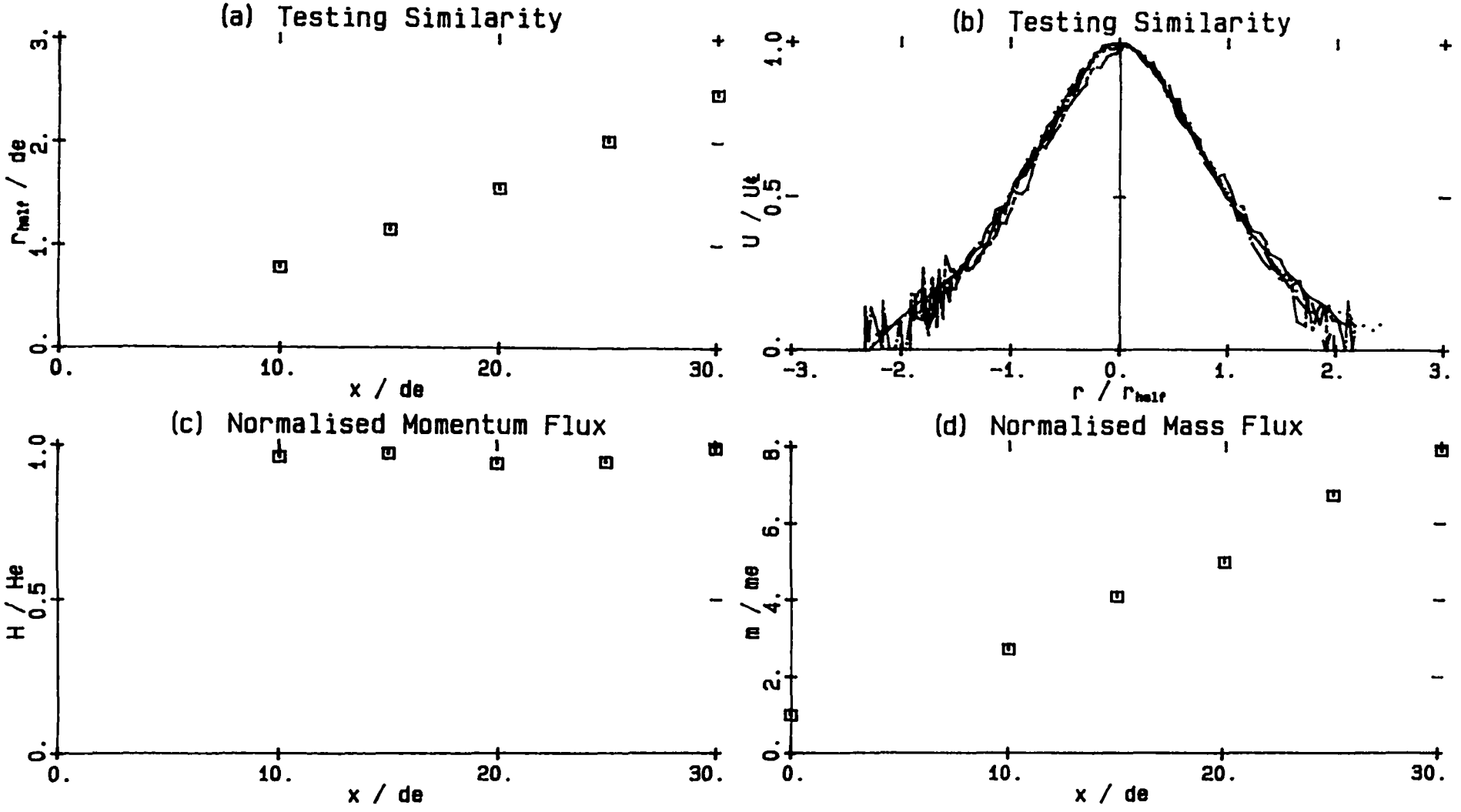

Figure 5.5: Pitot-static pressure profiles of the unenhanced jet; bell-mouth contraction: $d_e = 14.2$mm.

5.2.6 Results

The experiments conducted on the entrainment shroud can be broadly classified into two groups; those related to verifying that the shroud does not influence the results, and those used to determine the entrainment characteristics for the various geometric configurations of the nozzle. The former experiments have been discussed in Sections 5.2.4 and 5.2.5 and the latter have been briefly reviewed in Chapters 6 and 4. In the present section the entrainment characteristics of the nozzle are discussed in more detail. In particular the dependence of K_T upon x and $\dot{m}_p$ is tabulated. The results of the two measuring techniques, namely measuring the shroud pressure with a pressure transducer, and inferring the absence of an axial pressure gradient at the shroud mouth from a smoke trace, are also compared.

The results of the entrainment measurements obtained using the pressure transducer are displayed in Figures 5.6 & 5.7. The ratio of $\dot{m}_s/\dot{m}_p$ which is equivalent to that which would occur in the same axial distance in the absence of the shroud is found at the intersection of the line of best fit with the line P_B = 6mTorr, (ie. where shroud pressure, $P_m = 0$ re. ambient).

It can be seen that for some nozzle configurations the line of best fit approaches toward the line P_B = 6mTorr asymptotically but does not reach it within the range of experimental data. The trend whereby $P_B \rightarrow$ 6mTorr as $\dot{m}_s/\dot{m}_p \rightarrow \infty$ (either from below or from above) is to be expected. The pressure drop across the shroud mouth depends on the square of the velocity of the secondary or ambient air flowing through it. As such, it depends on both the mass flow rate of the air, and the cross sectional area between the edge of the jet and the edge of the shroud mouth, A_{j-m}. Thus, when $\dot{m}_p = 0$, there is no jet in the shroud, and $A_{j-m} = A_m$, which is so large that the pressure drop across it is imperceptible. Thus it is to be expected that there will be a minimum flow rate of the primary jet for which sensible readings can be obtained. Furthermore, evidence suggests that there exists a critical nozzle Reynolds Number, Re_c, below which no enhancement occurs. Thus for $Re < Re_c$ the cross sectional area of the shroud which is unoccupied by the jet will also be very large, resulting in an infinitesimal pressure drop through the shroud exit plane.

From the above comments it can be seen that measurement of the "zero crossing" point, and hence K_T, is subject to large error when $\dot{m}_p$ is small. In the present experiments $\dot{m}_s$ is kept constant, and so this problem will be most severe in the nozzles which generate the greatest enhancement. Nevertheless, trends in the influence of nozzle geometry upon entrainment rate

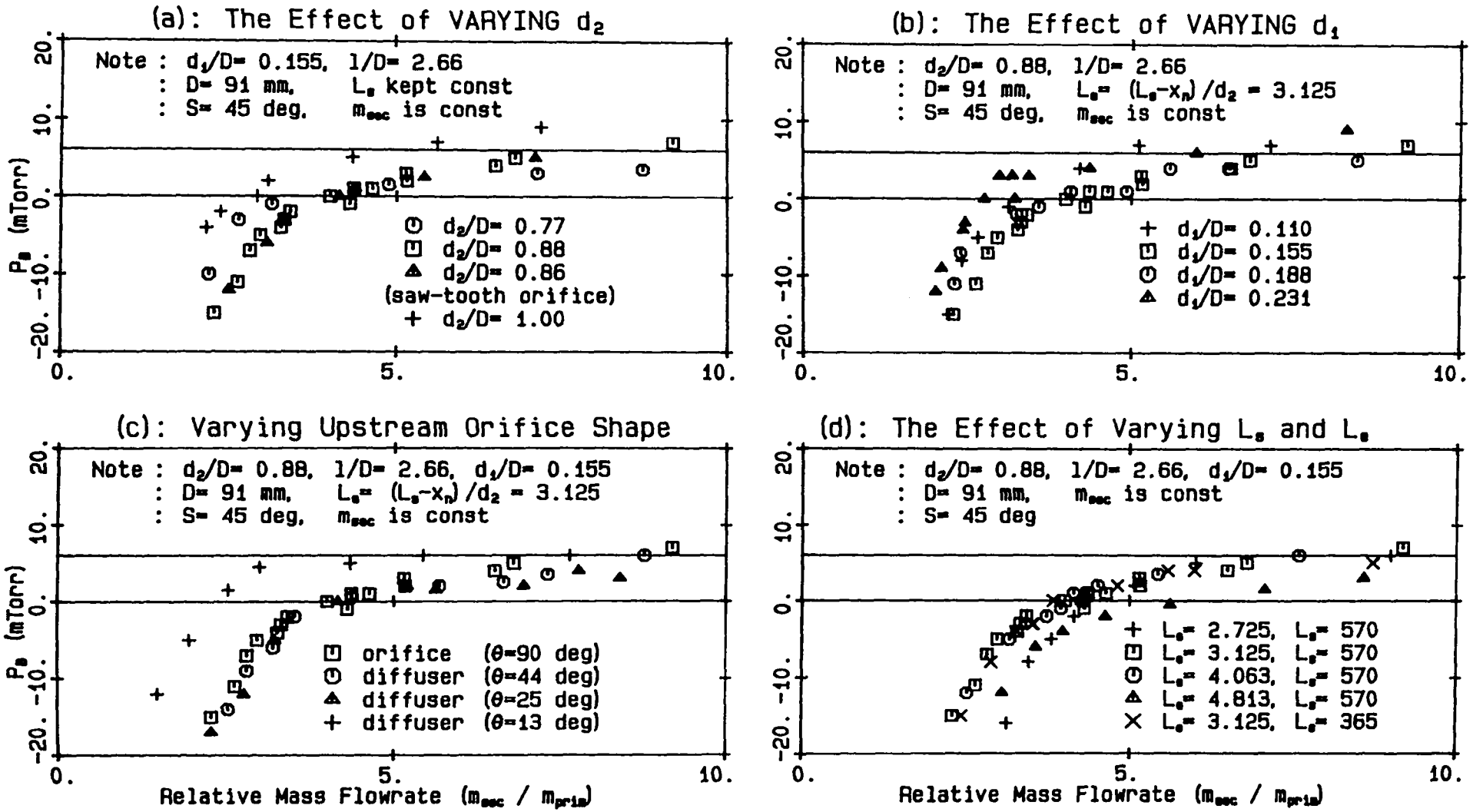

Figure 5.6: Entrainment rates determined using the Entrainment Shroud

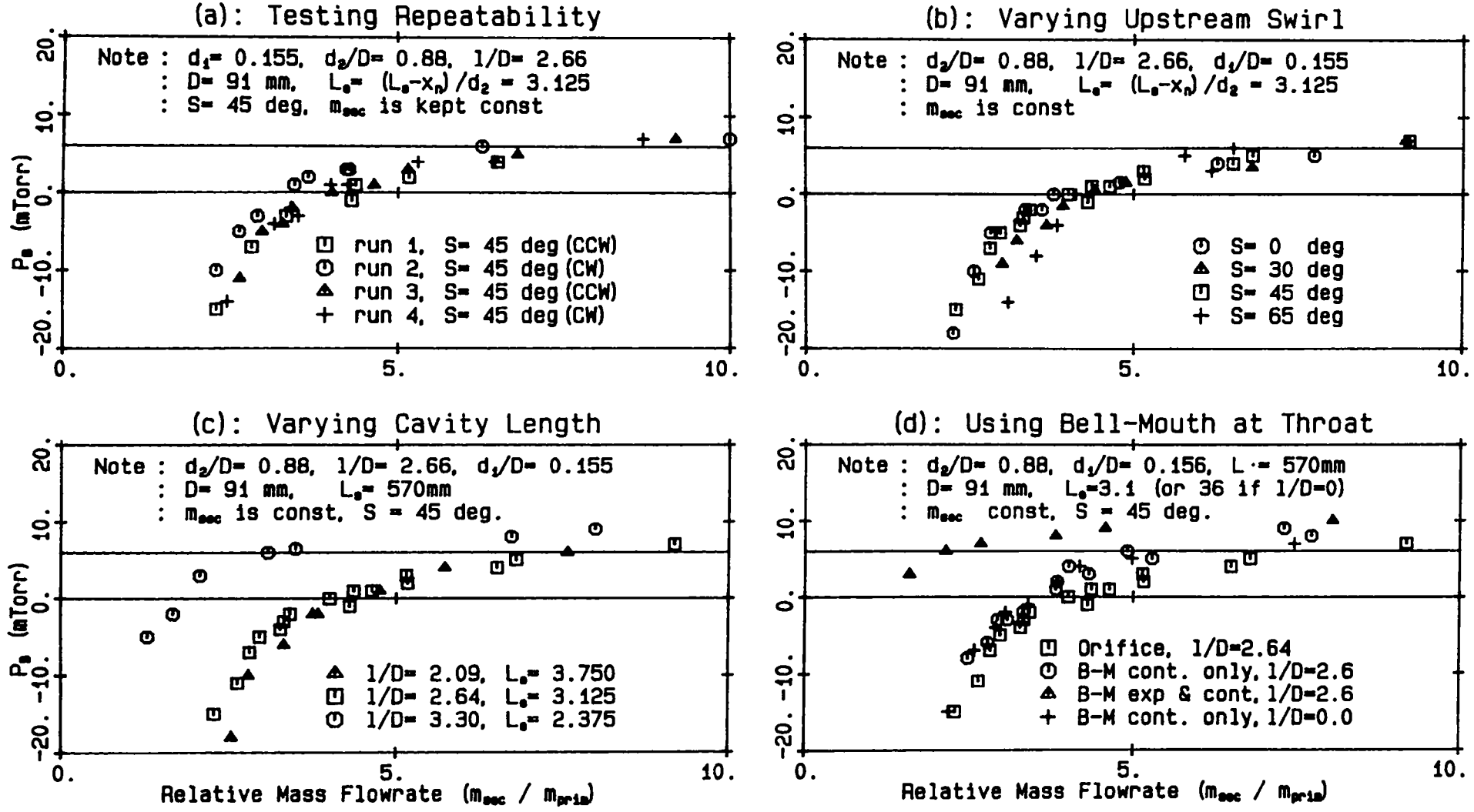

Figure 5.7: Entrainment rates determined using the Entrainment Shroud

can be inferred from the line of best fit even if the specific value of K_T cannot be measured.

The results of the entrainment measurements obtained from the smoke trace technique are shown in Figure 5.8. It is apparent that there is a large amount of scatter in the data, and that K_T is dependent upon $\dot{m}_p$. The scatter is to a large extent attributable to the intermittent nature of the enhancement. For some nozzle configurations and flow rates it is possible to balance the pressures so that the smoke trace descends vertically for either the higher or the lower rate of enhancement, between which the jet is switching intermittently. Those measured at the lower state of enhancement are shown by marking the symbol with a "/" tail as shown. Some of the scatter is also caused by the low pressure drop across the shroud mouth, causing the technique to be less sensitive than is desirable.

The smoke trace technique lends itself more easily to determining the dependence of K_T on $\dot{m}_p$ than does the pressure transducer technique, because $\dot{m}_s$ is not required to be held constant during the experiment and each data point can be obtained more quickly. Consequently the technique is less dependent upon the capacity of the compressor and a larger value of $\dot{m}_s$ can be used, although it does decrease slowly with time.

Figure 5.8 shows that K_T is, in general, inversely related to $\dot{m}_p$ within the range of experimental data. This suggests that the spreading angle of the jet decreases as the Reynolds Number through the nozzle increases. It also implies that there must be a discontinuity near $\dot{m}_p = 0$ because K_T must be zero there. Such a result indicates that there exists a critical Reynolds Number,Re_c, below which there is no enhancement. It can also be seen that the dependence of K_T on $\dot{m}_p$ decreases with increasing $\dot{m}_p$. A more detailed examination of some data sets, notably $d_1 = 21$mm, $d_2 = 80$mm, suggests that there may exist a transition Reynolds number, Re_t, between two characteristic dependencies of K_T upon Re. Below the transition the dependence approximates the relation $K_T \propto \dot{m}_p/\dot{m}_s$, whilst above the transition, K_T is nearly independent of $\dot{m}_p$. Unfortunately, the capacity of the compressor limited the maximum value of $\dot{m}_p$ and so the details of this part of the curve cannot be confirmed. However it is interesting that the transition appears not to have a strong dependence upon d_1. This suggests that the transitional Reynolds number may depend on the flow in the supply pipe upstream of the nozzle. Support for this is found in the fact that for the nozzle configuration $d_1 = 21$mm, the transitional Reynolds number based on the flow in the supply pipe is calculated as $Re_t = \rho u_0 D_0/\mu \approx 8 \times 10^3$, which is about three times the generally accepted value of transition from laminar to turbulent flow in a pipe. It is known that the reattachment distance

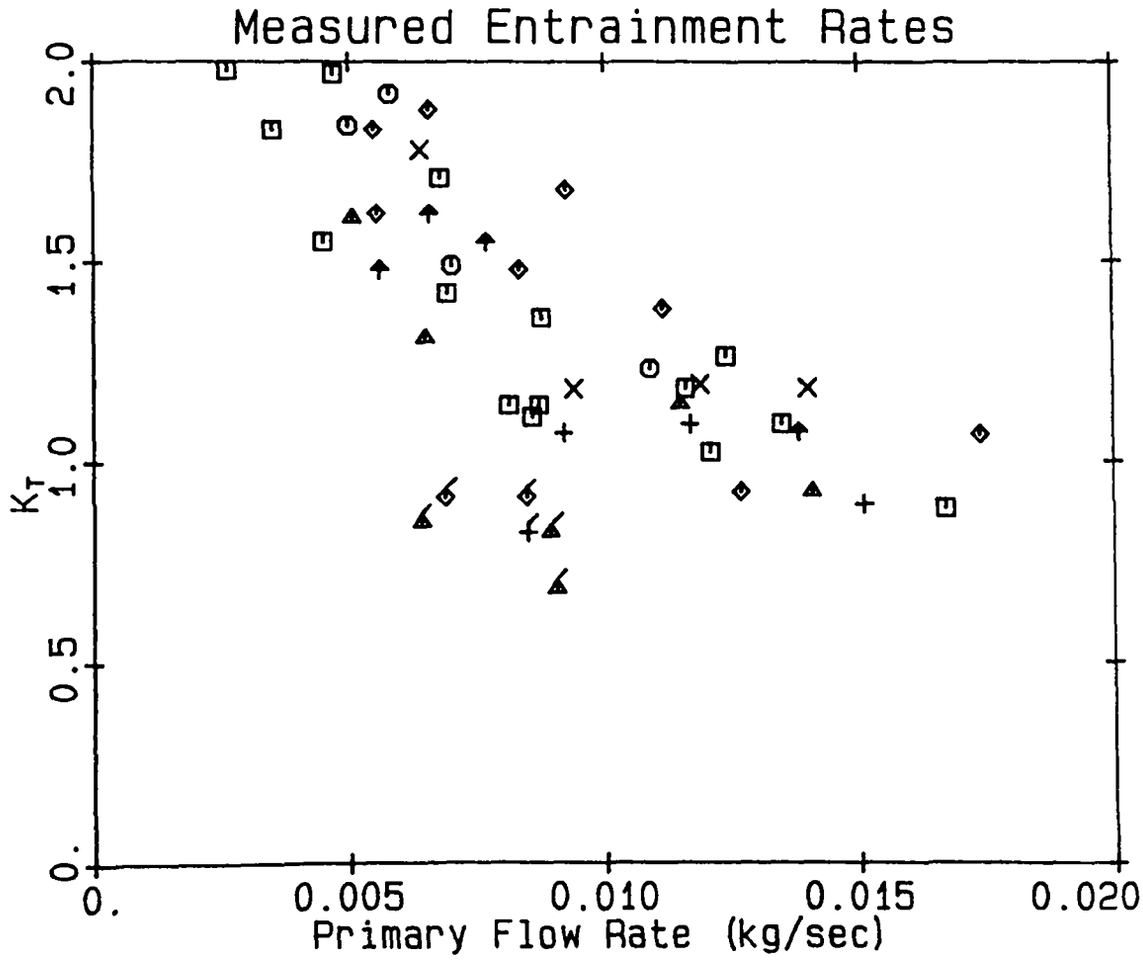

Notation of Symbols

	d_1 (mm)	d_2 (mm)
◇	10	80
↑	10	70
□	14.1	80
○	14.1	70
△	17.0	80
+	17.0	70
×	21.1	80

NOTE: P_s was determined using a smoke trace at shroud mouth.
: S= 45 deg, x_n-Ls= 250mm, x_n= 320mm, l= 245mm, D=91mm
: A "/" tail on a symbol (eg. ⊡/) indicates a lower level of mixing enhancement.

Figure 5.8: The entrainment rates of the MLC nozzle as determined using a smoke trace at the exit plane of the entrainment shroud.

downstream from a backward facing step is a strong function of Reynolds number in laminar and transitional flow [?], and it is likely that K_T will vary with the reattachment distance within the MLC nozzle. However the relevant Reynolds number for such flows is usually based on the diameter of the "throat", and the transition Reynolds number of the present nozzle, calculated on the throat conditions, it is some five times that in the supply pipe. From the preceeding discussion it is clear that a more detailed investigation is required to determine the dependence of the character of the flow patterns, and hence K_T, upon mass flow rate.

The results of the two techniques can be compared with each other, and with the entrainment measurements of an unenhanced jet measured by R&S and within the present investigation. In Table 5.1, it can be seen that the two techniques are in reasonable agreement with each other, yielding discrepancies of 2%, 11% and 18% for the same nozzle geometry and value of $\dot{m}_p$. This is comparable with the scatter obtained when using the smoke trace technique alone. For the above comparison, the value of K_T from the smoke method was obtained at the same value of $\dot{m}_p$ using a visually determined line of best fit.

The results of these experiments are most easily compared with those of R&S if equation 5.2 above is rewritten in the form

$$\frac{\dot{m}_s + \dot{m}_p}{\dot{m}_p} = K_T \frac{x}{d_e}$$

which applies for unity density ratio between the jet and its surroundings. R&S find that for air flow through a simple jet, $K_T = 0.32$, which is slightly larger than the independent measurement of the jet emanating from a simple, bell mouth nozzle in the present investigation, which yielded $K_T = 0.26$. (The details of this measurement are discussed in Sections 5.2.4 and 5.2.5). The Factor of Improvement, FOI, relative to the measured value of the unenhanced jet, $K_T = 0.26$, is also shown in Table 5.1. For a constant position of the nozzle within the shroud ($(L_s - x_n)/d_2 = 3.1$), values of K_T for the MLC nozzle are typically an order of magnitude larger than this value when based on d_2, and about five times larger when based on d_{2eq}. It is worth noting that the value of K_T is not greatly effected by minor changes in nozzle geometry, say of the order of 10%. This suggests that the nozzle should have excellent wear characteristics.

[1] Factor of Improvement: $(K_T|_{MLC})$ / $(K_T|_{unenhanced})$

[2] mean diameter of saw-tooth orifice

Nozzle Dimensions			L_e	x_n	$\frac{\dot{m}_s+\dot{m}_p}{\dot{m}_p}$	$\dot{m}_p$	K_T	FOI[1]	Measuring	Comments
d_1 (mm)	d_2 (mm)	l (mm)		(mm)		($\times 10^{-3}$ kg/s)	re. d_{2eq}		Technique	
14	80	240	6.039	320	8.91	7.6	1.48	5.7	transducer	Reference
					8.03	7.6	1.32	5.1	smoke	
10	80	240	5.952	320	6.66	10.6	1.13	4.4	transducer	
			5.952		8.21	10.6	1.38	5.3	smoke	Varying
17			6.068		7.94	11.5	1.14	4.4	smoke	d_1
21			5.669		6.79	10.5	1.20	4.6	transducer	
21			5.669		6.79	10.5	1.23	4.7	smoke	
14	70	240	6.039	320	8.4	10.9	1.23	4.7	smoke	Varying
	82[2]				8.8	7.8	1.46	5.6	transducer	d_2
	91				5.81	12.5	0.96	3.7	transducer	
14	80	240	7.80	248	8.57	8.1	1.44	5.6	transducer	Varying
			4.063	350	7.76	10.6	1.28	4.9	smoke	x_n

Table 5.1: The values of K_T found using the Entrainment Shroud.

In all cases, a sharp edged orifice plate was used and the upstream swirl vanes were set to 45 deg.

The affect of varying Entrainment Length

The non dimensional entrainment length, $L_e = (L_s - x_n)/d_{2eq}$, is a measure of the length of the jet, in nozzle diameters, contained within the entrainment shroud. Since d_{2eq} is only slightly dependent upon d_1 (see Figure 5.1) and is independent of d_2, L_e will depend upon the length, L_s, of the porous wall of the shroud and on the position of the nozzle within the shroud, x_n.

It can be seen from Table 5.1 and Figure 5.7(d) that K_T is inversely related to L_e when x_n is varied. This implies either that the amount of fluid entrained depends on the length of the porous wall, or that the entrainment appetite of the jet is a function of the axial distance from the nozzle exit plane. To determine which of these is the controlling influence, it is necessary to vary L_s and x_n independently. This is because a change in x_n alone will also change the percentage of secondary air which is supplied to the jet from behind the nozzle exit plane, and hence the flow patterns of the secondary air within the shroud.

As illustrated in Figure C.1, x_n can be altered by sliding the nozzle within the shroud. The length L_s of the porous wall, is altered by blocking the upstream part of the porous wall with a 200mm long sleeve.

The dependence of K_T on L_s is shown in Figure 5.6(d) and is very slight. It must be concluded then, that the entrainment appetite the MLC nozzle decreases with axial distance from the exit plane. This inference is consistent with other measurements of the jet, and the postulated mechanism which causes the rapid spreading.

By definition, similarity of velocity profiles implies that the jet spreads at a constant angle. Such a result occurs for both the LC nozzle (see Figures 8.2 and 3.4) and for a simple unenhanced jet [93], and leads to the result that K_T is constant (see R&S). However the total and static pressure profiles of the MLC nozzle (Figure 4.7) show that dramatic changes in the velocity profiles occur over the first exit diameter of the jet and it is thus reasonable to expect that K_T changes rapidly also.

In contrast with other nozzles, which experience either a vena-contracta or an initial zone of small expansion angles followed by similarity, the MLC nozzle has an initial region of very rapid expansion, which appears to be followed by similarity in velocity profiles. This initial expansion can be seen in Figures 4.7 and 4.9, as well as in the many photographs showing the flame shape. Although Figure 4.7 appears to indicate that the jet displays approximate similarity beyond one nozzle dimeter from the exit plane, profiles further downstream are very

difficult to obtain because the velocities are too low for a pitot tube to give accurate results, and directions too variable for the output from a single component, static hot wire anemometer to be interpreted with confidence. These problems also mean that it is not possible to determine the jet width or half width using conventional methods. Such details must await a future investigation.

The consistency of the entrainment shroud results with the proposed mechanism within the MLC nozzle has been discussed in Chapter 4.

5.3 Combustion Characteristics

5.3.1 Introduction

The most immediate application which is envisaged for the MLC nozzle is combustion of either natural gas or coal, where its enhanced mixing characteristics and reduced tendency to convect the flame front downstream provide improved flame stability. Two parameters have been selected to provide a measure of flame stability. These are "blow-off velocity", V_{bo}, the mean exit velocity which causes the flame to be extinguished, and "stand-off distance", X_{so}, the distance between the nozzle tip and the flame front.

In order to compare these measured values with another type of nozzle (eg. a simple, unswirled, "pipe" burner), it is necessary to normalise them, or to base them on equivalent conditions. Typically, standoff distance is normalised by the nozzle diameter, and the blow-off velocity is based on mean exit conditions. As discussed in section 5.1, these descriptions alone are inadequate for the MLC nozzle, and so the results are also discussed in terms of d_{2eq} and u_{2eq}.

The flame shape generated by the MLC nozzle is much shorter and more bulbous than those of either of the other two nozzles. This not only indicates that very strong mixing is occurring, but in practice it is likely that flame shape, size and combustion efficiency will be more important criteria than will blow-off velocity. This is because a given throughput can always be achieved by increasing the scale of the burner and hence decreasing the exit velocity.

In the remainder of the section, the experimental techniques and results of the these experiments are discussed.

5.3.2 Blow-off Velocity of the MLC nozzle

Combustion is a highly complex phenomenon which depends upon inherently random processes. Thus it is to be expected that there will be scatter associated with any measurement of the processes. Such difficulties are compounded when measuring flame blow-off because it is not a steady state parameter. For this reason special care must be taken in its measurement, and sufficient data points measured for the results to be used with confidence.

Blow-off velocity is not presented in a normalised form due to the absence of a suitable normalising velocity scale. Whilst flame speed would provide some collapse of the blow-off data generated using different fuels, it is not the only intrinsic fuel property on which blow-off depends. For example, the burning velocity of LPG is only about 10% higher than that of CNG, whilst its blow-off velocity is more than twice as high. Furthermore, the burning velocity depends greatly on the operating conditions, and quoted values vary substantially, depending upon both the experimenter and the technique used.

Experimental Techniques

The usual technique for measuring the blow-off velocity of an undiluted, non-premixed fuel, is to increase the flow rate of the fuel slowly until the flame is extinguished. The process is complicated by the addition of another gas however, because increasing the flow rate of either gas changes both the mean exit velocity and the ratio of the two gases. Provided that only two gases are used, and an exact, predetermined ratio is not required, it is still possible to obtain reasonable results by slowly increasing the flow rate of just one gas, provided that adequate care is taken. If, however, three gases are being mixed together before entering the nozzle, it is necessary to hold the ratio of two of the gases constant, and vary the third. This requires a technique known as bypass-dumping, which is also required for safe combustion when premixing the fuel with an oxidant.

Bypass dumping, as shown in Figure 2.5, enables any ratio of constituent gases to be selected at the flow-raters. The mean exit velocity can then be adjusted independently by dumping part of the mixture into the exhaust duct. The throughput of the remainder of the mixed gas is independently measured using the coil flow rater.

Results

The results of the blowoff velocity experiments are given here and are compared with the results of other researchers and for other nozzles. The effects of pre-mixing the fuel with oxygen, and of diluting it with an inert gas are included.

The calculation of V_{bo} highlights the problem of choosing a suitable nozzle diameter scale, since V_{bo} is proportional to the diameter squared. If V_{bo} is calculated from the mass flow rate and mean exit diameter of the nozzle, then the MLC nozzle has a blowoff performance almost identical with the simple nozzle. But the flow through the exit plane of the MLC nozzle does not fill the exit area of the nozzle and hence this area is not an appropriate basis for evaluating V_{bo}. On the other hand, if V_{bo} is calculated from the diameter of the throat, then V_{bo} is increased by approximately thirty times over that for the simple nozzle, which suggests that d_1 also may not be an appropriate basis for the blowoff velocity.

More sensible results are obtained when the "equivalent diameter", d_{2eq}, is used as a diameter scale. This requires an approximate calculation of the mean velocity of the instantaneous jet at the exit plane of the nozzle. The blow-off velocity calculated from the mass flow rate at the throat (which will be less than the mass flow rate of the instantaneous jet at the exit plane) and d_{2eq}, is approximately four times larger than that of a simple jet. The results are displayed in Figure 5.9. This improvement is very similar to the increase in entrainment rates when calculated using d_{2eq}, which supports the suitability of this scale for providing a basis of comparison with other nozzles.

A seemingly curious coincidence is that V_{bo} based on exit area is approximately the same for all three nozzles, vis. the MLC, LC and simple nozzles. This can be seen in Figure 5.10 and further suggests that the mean exit velocity is not a valid method for calculating V_{bo}. The results of the blow-off velocity experiments on the LC nozzle clearly indicate that increased jet spread angles and decreased mean jet velocities are accompanied by an increased blow-off velocity. Figure 8.8 and Figures8.4 to 8.7) show that excellent agreement exists between the optimum cavity length as determined by minimum centreline total jet pressure and V_{bo} for the LC nozzle.

The effect of premixing the fuel with oxygen is shown in Figure 5.11. It can be seen that pre-mixing with small quantities of oxygen has a negligible or slightly detrimental effect on the blow-off velocity when using a MLC nozzle. This is in contrast to the increased flame stability

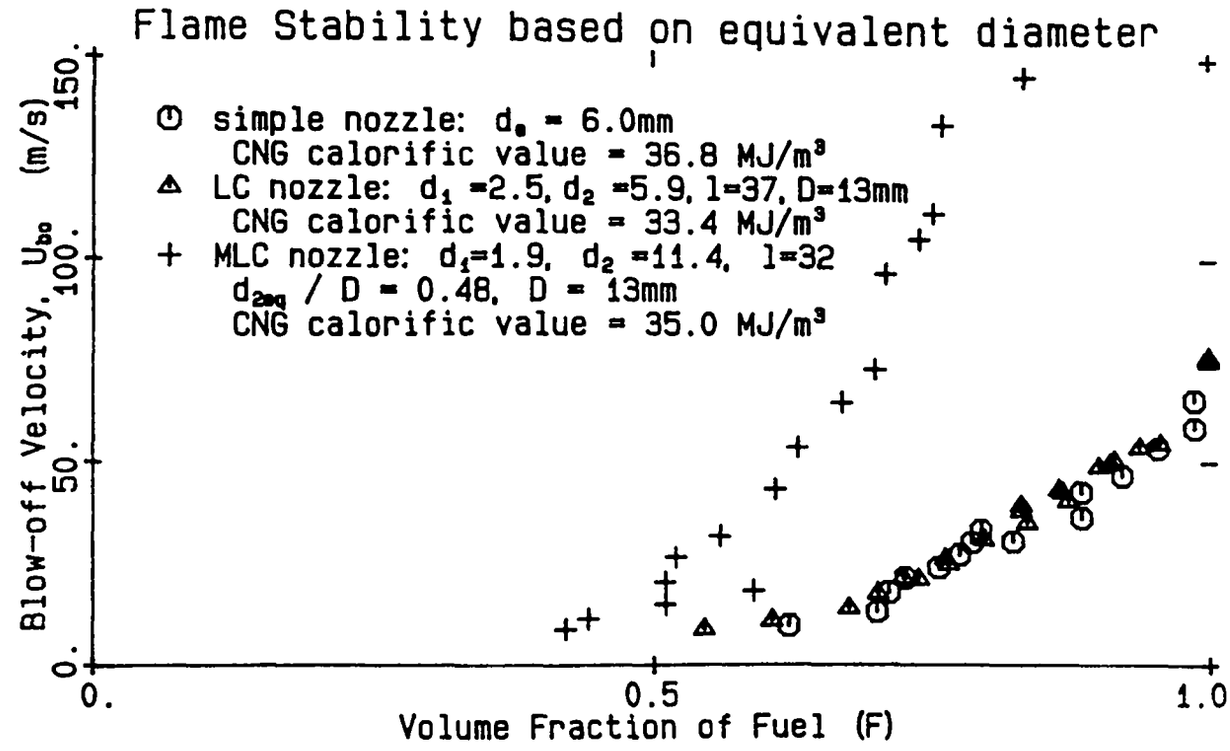

Figure 5.9: A comparison of the blow-off velocity of the three nozzles, calculated using the equivalent exit diameter

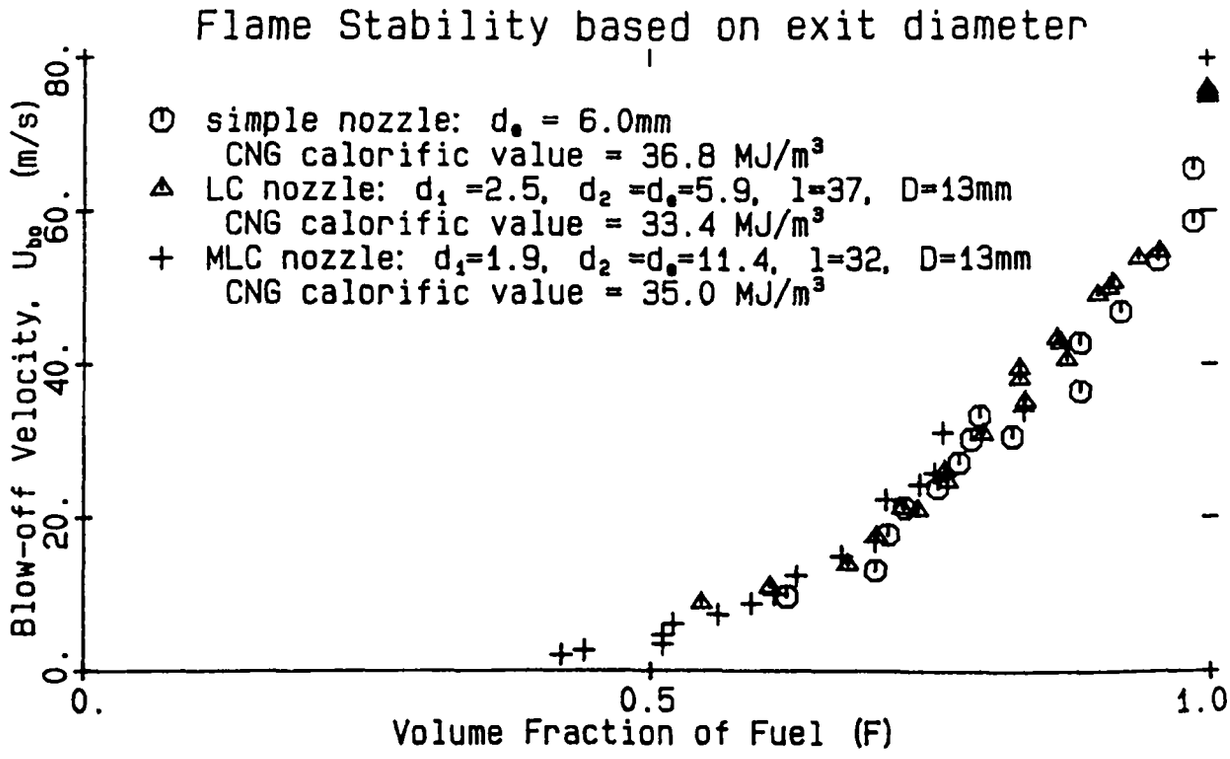

Figure 5.10: A comparison of the blow-off velocity of the three nozzles, calculated using the mean exit area.

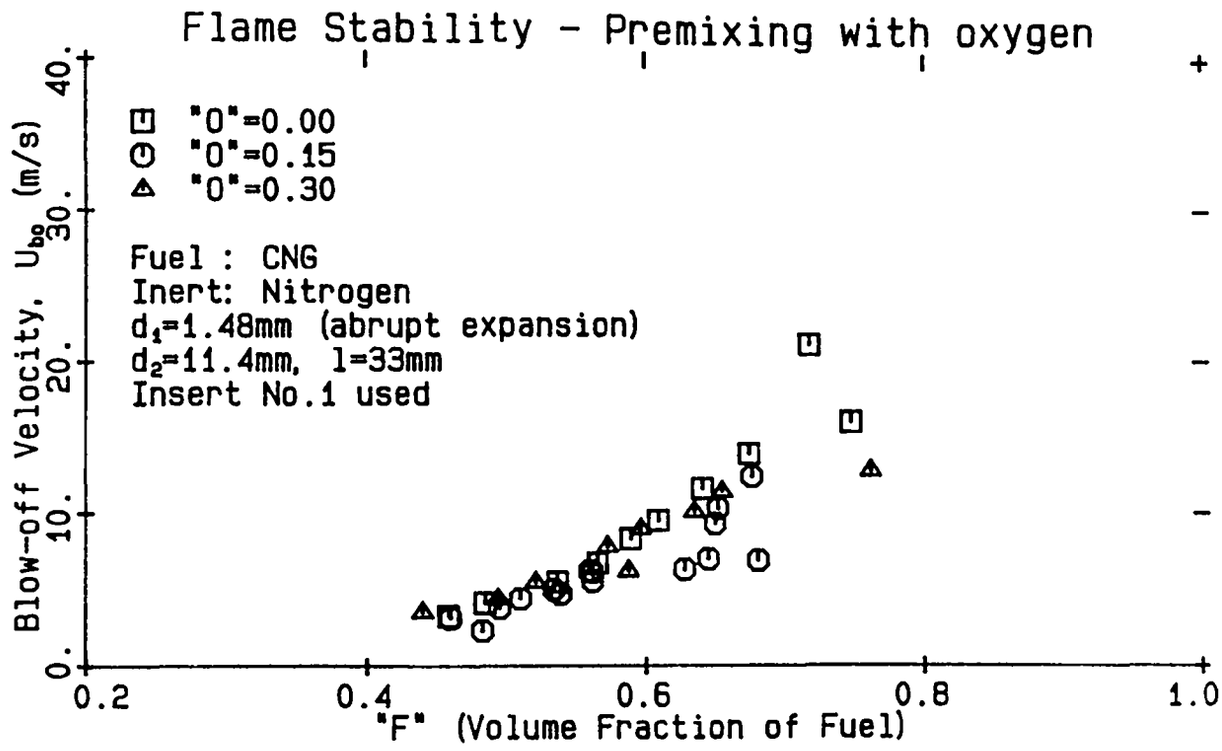

Figure 5.11: The effect of Premixing the fuel with oxygen on blow-off velocity

which occurs due to pre-mixing for most nozzles.

The reason for the result can be found in the dependence of flame speed upon equivalence ratio. Maximum flame speed occurs typically at an equivalence ratio of 1.2 [69], with the shape of the curve being flattest near the peak. Thus, increasing the specific volume of oxygen will cause an increase in flame speed if the mixture is fuel rich, will cause a decrease in flame speed if the mixture is fuel lean, and will have only a very small influence when the flame speed is near its maximum value. Figure 5.10 indicates that the MLC nozzle generates such intense mixing that the local equivalence ratio at the flame front is very near to that which gives maximum burning velocity. In this event, a small amount of premixing will have negligible influence on the burning velocity, but increasing the amount of pre-mixing will lead to a progressive reduction in flame speed, and hence of blow-off velocity.

Some discrepancy exists between the data obtained for O = 0.15, and O = 0.30, where "O" is the volume fraction of oxygen in the mixture. It is not possible for $V_{bo-O=0} > V_{bo-O=0.15}$ and $V_{bo-O=0.3} > V_{bo-O=0.15}$ simultaneously. It therefor appears that some of the data points in the line O = 0.15 near F = 0.65, where "F" is the volume fraction of fuel in the mixture, have a "low" value of V_{bo}, probably due to intermittency (see sections 4.1 and 4.7.4).

Fricker and Leuckel (1976) investigated the effect of swirl on blow-off velocity. They found

that increased swirl tends more to shift the "equivalence-ratio : blow-off velocity" curve toward the fuel rich side, than to actually increase the blow-off velocity. This has the effect of increasing V_{bo} when the burner is operated near stoicheometric conditions. The trend occurs as a result of the increased mixing generated by the swirling flow and so it is likely that the MLC nozzle will produce a similar trend. However, at this stage combustion experiments have only been conducted using unconfined flames (ie. open to the free air).

The other blow-off results are discussed in chapter 6 in which optimum geometric ratios are discussed.

5.3.3 Stand-off Distance

Introduction

Stand-off distance is a particularly important indicator of the likelihood of a flame driving "system instabilities". System instabilities arise when large scale oscillations in the position of the flame front couple with an acoustic resonance of the combustion chamber, or with a resonance within its associated supply or exhaust pipe network. Such gross combustion instabilities, known as "furnace chugging", can lead not only to "flame-out", if an in-phase fluctuation in the throughputs of the fuel or air is generated, but can also have a detrimental effect on the furnace structure.

A short stand-off distance is also indicative of a rapid decay in the velocity scales of the jet, since local jet velocities at the flame front cannot exceed the flame speed. Furthermore it implies high rates of mixing, since sufficient quantities of air must be entrained for local equivalence ratios to fall within combustible limits. These characteristics are synonymous with rapid spreading of the jet and very intense turbulence over a wide range of scales.

Experimental Techniques

The stand-off distance was measured visually. The nozzle and flame were placed between two etched scales, the front one having a transparent background, and the nozzle was aligned with the zero on each scale. By visually aligning the flame front with the same number on each scale, it is estimated that stand-off distance could be measured with a resolution of ± 0.5 cm. However, the position of the flame front is always oscillating, typically with a magnitude of at least ± 0.5cm, and the shape of the flame front is in a continual state of

flux. Furthermore, the visually determined position of the flame front depends slightly on the intensity of background light. Overall, the technique was considered to be compatible with the parameter being measured.

Results

The stand-off distance of the flame produced by the MLC nozzle is less than that of a simple nozzle. This is illustrated in Figure 3.5. The MLC nozzle supports a flame with a stand-off distance an order of magnitude less than that of a simple nozzle at the same Reynolds number when X_{so} is normalised by either d_{2eq} or d_2. This is because for a given mass flow rate, decreasing the normalising diameter will cause both the normalised standoff distance and the Reynolds number to increase in the same proportion. Standoff distance would appear to be improved by a factor of about two if it is normalised by the throat diameter. Similar reductions in the magnitude of the oscillations in X_{so} occur. These results indicate that system instabilities should be less likely to arise with the MLC nozzle than with a simple nozzle.

The flame generated by the EMB nozzle, and its oscillations, are of a different character from those of other nozzles. In a simple jet, the flame front is positioned where the flame speed and the jet velocity are equal. However, in the present nozzle, the flame "front" does not propagate into a coherent jet of fuel, but rather combustion occurs in a well mixed zone, analogous to a well stirred reactor (WSR). This well mixed region, and the associated high entrainment rates, are generated by the continuous variation in the *position* of the precessing fuel jet, as discussed in Section 4.1. Consequently, gross variations in the mean *velocity* of the jet, caused eg. by surging of the compressor or acoustic resonances within the supply pipes, will not directly generate a corresponding oscillation in the position of the flame front. Again, this type of flame is less likely to drive a system instability than is a conventional flame.

Because the mean frequency of the precession is well defined, it is possible that the precession itself could drive a system resonance. Whether or not this will occur, and the influence it will have, is not known at present. However, because both the precession frequency and the resonant frequencies can be predetermined in the design phase, it should be possible to ensure that such system instabilities do not occur. Furthermore, a precessing jet has the character of a higher order acoustic source, and hence is a less efficient radiator of acoustic energy than is the near-monopole character of a fluctuating flame front. Thus it seems unlikely that system instabilities of the type frequently driven by an oscillating flame front will arise.

5.3.4 General Characteristics

It is well known that flame stability is influenced by the turbulence of the flow field. Both the large scale flow patterns, which influence the gross mixing of the jet fluid with its surrounds, and hence the residence times, and the small scale turbulence which controls mixing at the molecular levels, are important. It has not been within the scope of the present investigation to measure the turbulence scales of the EMB jet. Nevertheless, the high speed schlieren photography of the flame, included as part of the thesis, does give a good indication of the flow patterns which are occurring.

As discussed in chapter 4, the MLC nozzle produces a precessing asymmetric jet. The structures, as opposed to the scale, of this instantaneous jet does not appear to differ greatly in character from that of a simple jet, and entrainment will be dominated by the large scale vortical structures typical of such a jet. Digestion of the entrained fluid will be via the fine scale turbulence superimposed on the large structures of the precessing jet. The very large scale turbulence associated with the flame front, the dominant feature of the MLC nozzle, is generated by the precession motion of the jet itself. This can be seen on the cine film as huge eddy structures with extremely long residence times. Note that the size of these structures is amplified by the volume expansion caused by the combustion. The short stand-off distance, and the bulbous flame shape can also be clearly seen in the cine film.

5.4 Conclusions

An equivalent diameter, d_{2eq}, has been defined for the MLC nozzle as the characteristic diameter of the instantaneous jet at the exit plane of the nozzle. Based on this diameter, the MLC nozzle produces a jet which entrains approximately five times the amount of ambient air as a simple jet. High rates of entrainment, combined with a greatly reduced tendency of the fuel jet to convect the flame front downstream, are expected to yield high flame stability in combustion applications, as is bourne out by experiment. Based on d_{2eq}, the nozzle produces a flame with a stand-off distance an order of magnitude lower than that of a simple nozzle and a blow-off velocity about four times higher.

5.4.1 The equivalent diameter, d_{2eq}

The "equivalent" diameter of the MLC nozzle is the diameter of a simple, unswirled and non precessing jet against which the performance of the MLC nozzle can be compared with some validity. This parameter has been shown to be necessary because no physical dimension of the MLC nozzle provides an adequate normalisation. More explicitly,

- The exit diameter, d_2, is an inappropriate dimension on which to normalise the flow patterns because the instantaneous jet which leaves the nozzle does not fully occupy the exit area of the exit plane, and does not control the mass flow rate or exit velocity.
- The throat diameter is inappropriate because the velocity through it is much higher than the velocity through the exit plane, and the mass flow is lower than that of the instantaneous jet in the exit plane.
- The cavity diameter is inappropriate because it is completely unrelated to the velocity scales in the exit plane.

The equivalent diameter is defined as the r_{half} diameter of the instantaneous jet in the exit plane of the nozzle. This definition causes no change in the normalising diameter scale of a simple nozzle, for which $d_{eq} = d_e$. The diameter of the instantaneous jet is based on r_{half} because it is a quantity which is able to be measured reliably. Consequently is has become the accepted method of normalising jets with a bell-mouth shaped velocity profile. A pitot-static probe was used to measure r_{half} of a non-precessing, simple jet issuing from the throat of the MLC nozzle at the same axial station as that of the exit plane of the MLC nozzle. This was taken as a good approximation of d_{2eq}. It was found that $d_{2eq}/D = 0.42$ for the Bell-Mouth contraction with $d_1/D = 0.156$. For the sharp edged orifice plates, d_{2eq} depends on d_1 and has a minimum at $d_1/D \approx 0.17$. A typical value for all sharp edged orifice plates is $d_{2eq}/D \approx 0.46$.

5.4.2 Rates of entrainment

The entrainment shroud, modelled on Ricou and Spalding (1961), has been verified to give accurate results for a simple, unenhanced jet, provided that

- the diameter of the shroud mouth, d_m, is only slightly larger than the diameter of the jet at the same axial location,

- the shroud pressure is measured in the exit plane of the shroud and as near to the mouth as practical.

The verification was conducted using a simple nozzle with a bell-mouth contraction. The entrainment was measured independently using the entrainment shroud, and by a series of pitot-static pressure profiles. The profiles were checked for similarity by comparing the shape of the normalised velocity profiles, and by testing for linear expansion of the edge of the jet. A check for conservation of momentum was also conducted on each profile. The agreement between this technique and that of the entrainment shroud was excellent, with both methods yielding a value of $K_T = 0.26$, compared with the value of $K_T = 0.32$ obtained by R&S. It is suggested that the difference between the present measurements and those of R&S is caused by any small differences between the profiles of the two nozzles.

It was verified that there was no adverse influence on results caused by impingement of the jet on the shroud by the following:

- Baffles were placed over the pressure tappings to prevent any jet impingement and this did not influence the measured value of P_B.
- The pressure difference along the shroud was shown to be independent of $\dot{m}_p$, ie. dependent only on $\dot{m}_s$.
- Good agreement was obtained between the two independent techniques for indicating a zero axial pressure gradient across the shroud mouth; namely using a pressure transducer connected to a wall tapping near the exit plane, and using a smoke trace in the exit plane.

The entrainment characteristics of the MLC nozzle

It has been found that the entrainment appetite of the MLC nozzle varies with both the mass flow rate through it, and the distance from the nozzle exit plane. The results indicate that K_T varies inversely with both x and $\dot{m}_p$ and suggest that there may exist a transition Reynolds number, above which, K_T becomes nearly independent of $\dot{m}_p$.

5.4.3 Combustion results

The two parameters used to indicate the combustion characteristics of the MLC nozzle are the blow-off velocity, V_{bo}, and the stand-off distance, X_{so}. If the MLC nozzle is compared

with a simple nozzle based on d_{2eq} at the same Reynolds Number (also based on d_{2eq}), then a reduction in X_{so} of an order of magnitude occurs, and V_{bo} is increased by about four times. If the comparison is based on the mean exit conditions, then a reduction in X_{so} of an order of magnitude is obtained, whilst there is no significant difference in the blow-off velocity. If the comparison is based on the the conditions at the throat, then X_{so} is reduced by a factor about two, whilst V_{bo} is about thirty times higher. It can be seen that the comparison based on the "equivalent exit diameter" gives the most consistent results, but they all indicate a definite improvement in flame stability, which is consistent with the increased rates of mixing and spread angles observed in the cold flow experiments.

Premixing the fuel with oxygen has very little influence on V_{bo} when only small ratios of oxygen to fuel are used. As this ratio is increased, a progressively detrimental influence is observed. This is in striking contrast to the trends observed with an unexcited jet, and is further evidence of the extremely rapid rate with which the fuel jet mixes with the surrounding air.

Chapter 6

The Optimum Geometric Configuration of the MLC nozzle

The Mid Length Cavity (MLC) nozzle is a member of a family of Orifice-Cavity-Orifice (O-C-O) nozzles, as discussed in Chapter 3. However it is not necessary for the MLC nozzle to conform to a strict O-C-O configuration. For example the upstream orifice can be replaced by a pipe of the orifice diameter discharging directly into the cavity, or the downstream orifice replaced by a "saw-tooth" orifice. These and other changes in the geometric configuration give valuable insights into the nature of the mechanism. For example, how important are the separations which occur upstream and downstream of the primary orifice?

A large number of experiments have been conducted in order to determine the optimum geometric ratios of the simple O-C-O MLC nozzle, and tests have also been conducted to examine the effect of upstream swirl and of a bluff body being inserted into the nozzle cavity. These latter modifications to the simple O-C-O nozzle were stimulated by the desire to eliminate the "intermittency" discussed in Chapter 4, by promoting or amplifying the existing flow instabilities responsible for the enhanced mixing.

6.1 The Geometric configuration

The notation of the MLC nozzle with a "bluff body" insert is as shown in Figure 3.1. The flow direction is from left to right. The bluff body can be placed either inside or outside the cavity, and the origin for streamwise measurement is taken as the plane of smallest geometric diameter in the nozzle. In practice a sharp edged orifice plate will produce a "vena contracta",

and so the true throat will occur downstream from this point.

6.2 Optimum diameter of the Primary Orifice

The expansion ratio from the throat into the cavity is of critical importance in determining the stability of the flow patterns which generate the enhanced mixing discussed in Chapter 4. It appears that if the expansion ratio is too small, the jet which is emanating into the cavity through the throat will not expand with sufficient asymmetry to generate a stable asymmetric reattachment. On the other hand, if the expansion ratio is too large, the cavity wall will tend to be too remote from the jet, and so will not influence it to reattach at all within the available cavity length. In the latter case, the jet will flow through the nozzle as if the surrounding cavity were not present. This upper limit of expansion ratio appears to be a strong function of Reynolds number, but was not investigated in detail because of its limited practical application. Such nozzles would require either extremely large driving pressures to achieve typical flow rates, or inordinately large cavity diameters. It has been found that the flow patterns associated with the MLC nozzle can be obtained for a range of values of d_1/D, with the optimum value being approximately $d_1/D = 0.15$.

6.2.1 Results from Entrainment Shroud

The influence of Throat Diameter

The entrainment shroud is used to measure the amount of ambient air entrained by the MLC nozzle. These experiments are described and discussed in Section 5.2.

The primary results of these experiments which show the effect of d_1 on entrainment are presented in Table 5.1, and more details can be found in Figure 5.6(b). These results indicate that maximum entrainment occurs for $d_1/D = 0.155$ ($d_1 = 14.1$mm). However, it must be bourne in mind that K_T, the proportionality constant indicating the entrainment appetite of the jet, varies with the mass flow rate through the nozzle (see Section 5.2.6). It is expected that this dependence will be able to be described in terms of a Reynolds Number, but determining this relationship is beyond the scope of the present investigation.

Nevertheless, it can be seen that K_T does not vary greatly with d_1 for a given value of $\dot{m}_p$. Thus it is likely that in practice the selected value of d_1 will be optimised in relation to the limiting values of operating pressure and nozzle size, rather than with a view to achiev-

ing maximum entrainment rates. The size of the upstream orifice also appears to effect the degree to which the nozzle is influenced by intermittent enhancement. This requires further investigation.

6.2.2 Results from single point total pressure measurements

The total pressure measurements, taken at a single point and a fixed number of exit diameters from the exit plane (typically between two and four), were designed to give a simple indication of the rates of mixing which occur over a large range of different geometries. They not only allow the nozzle to be classified in terms of the broad class of flow pattern being generated, but also enable a crude comparison of performance to be made. This is because maximum spread angles are indicated by minimum total jet pressure at an equivalent number of nozzle diameters from the exit plane.

The results of these experiments can be seen in Figures 6.1 to 6.5. It can be seen that minimum jet pressure occurs consistently over the whole operating range when $d_1/D = 0.157$. However the mechanism can be produced for seemingly any value of $d_1/D \leq 0.23$. Whilst very small values of upstream orifice diameter (eg $d_1/D \leq 0.05$) enhance mixing rates, the amount of enhancement decreases and the enhancement does not operate consistently throughout the operating range. Furthermore, the flow rates through such small orifice plates becomes so small that it is unlikely that any practical application for them will exist, and measurement also becomes very difficult.

The single point experiments also allow the nozzle to be optimised with regard to sensitivity to changes in nozzle geometry. It can clearly be seen by comparing Figure 6.3 with Figures 6.1— 6.5, that enhanced mixing can be generated for the largest range of d_2/D when using the same upstream orifice which has been found to give optimum performance using the other techniques (ie. $d_1/D = 0.157$).

6.3 Optimum shape of the Primary Orifice

It has been found that the precise shape of the nozzle in the region of the upstream throat is not of critical importance in influencing whether or not the the enhanced mixing flow patterns will occur, *provided* that the jet *fully* separates *downstream* from the throat. The initial configuration of a simple orifice plate at the throat, which generates both upstream and

Captions and Notation for Figures 6.2 to 6.5

Figures 6.2-6.5 show the results of single point measurements of total jet pressure, measured at $x/d_2=2$ (or $x/d_2=4$, denoted by **) for the value of d_1/D shown with each graph.

In each graph the effect of varying d_2/D for a given value of d_1/D can be seen. Each nozzle geometry was tested for four different driving pressures. Each driving pressure is given a different symbol, and each nozzle geometry a different colour.

The following table shows the notation for the symbols used in Figures 6.2-6.5. In each case the line was drawn through the data points corresponding to Pd = 60 kPa.

$d_2/D=$	-	0.66	0.77	0.88	1.00	(Figure 6.2)
$d_2/D=$	0.49**	0.66	0.77	0.88	1.00	(Figure 6.3)
$d_2/D=$	0.55**	0.66**	0.77**	0.88	1.00	(Figure 6.4)
$d_2/D=$	0.55**	0.66	0.77	0.88	1.00	(Figure 6.5)
P_d=20 kPa	□	□	□	□	□	
P_d=40 kPa	○	○	○	○	○	
P_d=60 kPa	△	△	△	△	△	
P_d=80 kPa	+	+	+	+	+	
P_d=100kPa	×	×	×	×	×	

Figure 6.1: Captions and Notation for the plots of Variation of Total Jet Pressure with Cavity Length in the following figures

Note: total and driving pressures are measured relative to ambient pressure.

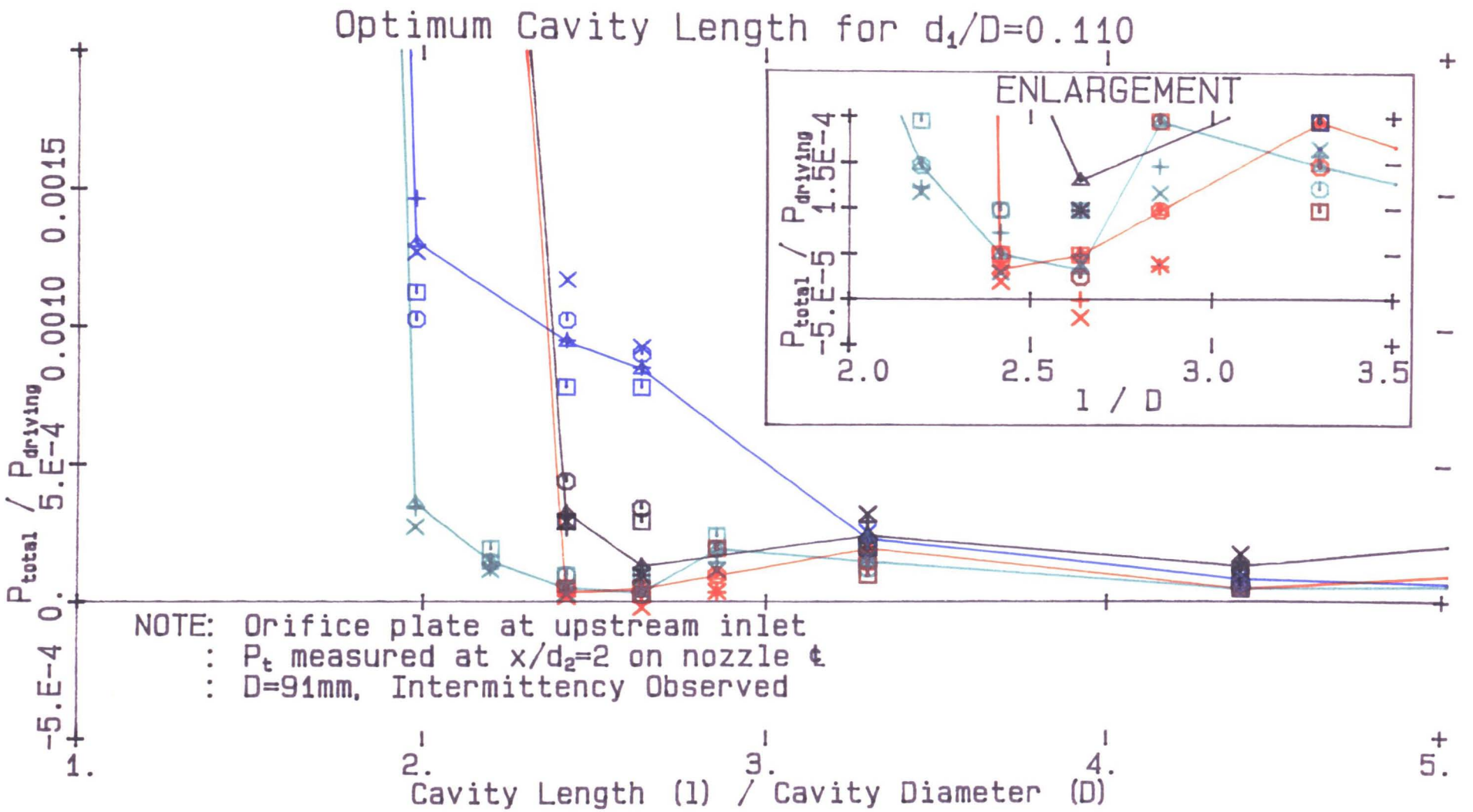

Figure 6.2: The Variation of Total Jet Pressure on the nozzle centreline with Cavity Length for $d_1/D = 0.110$

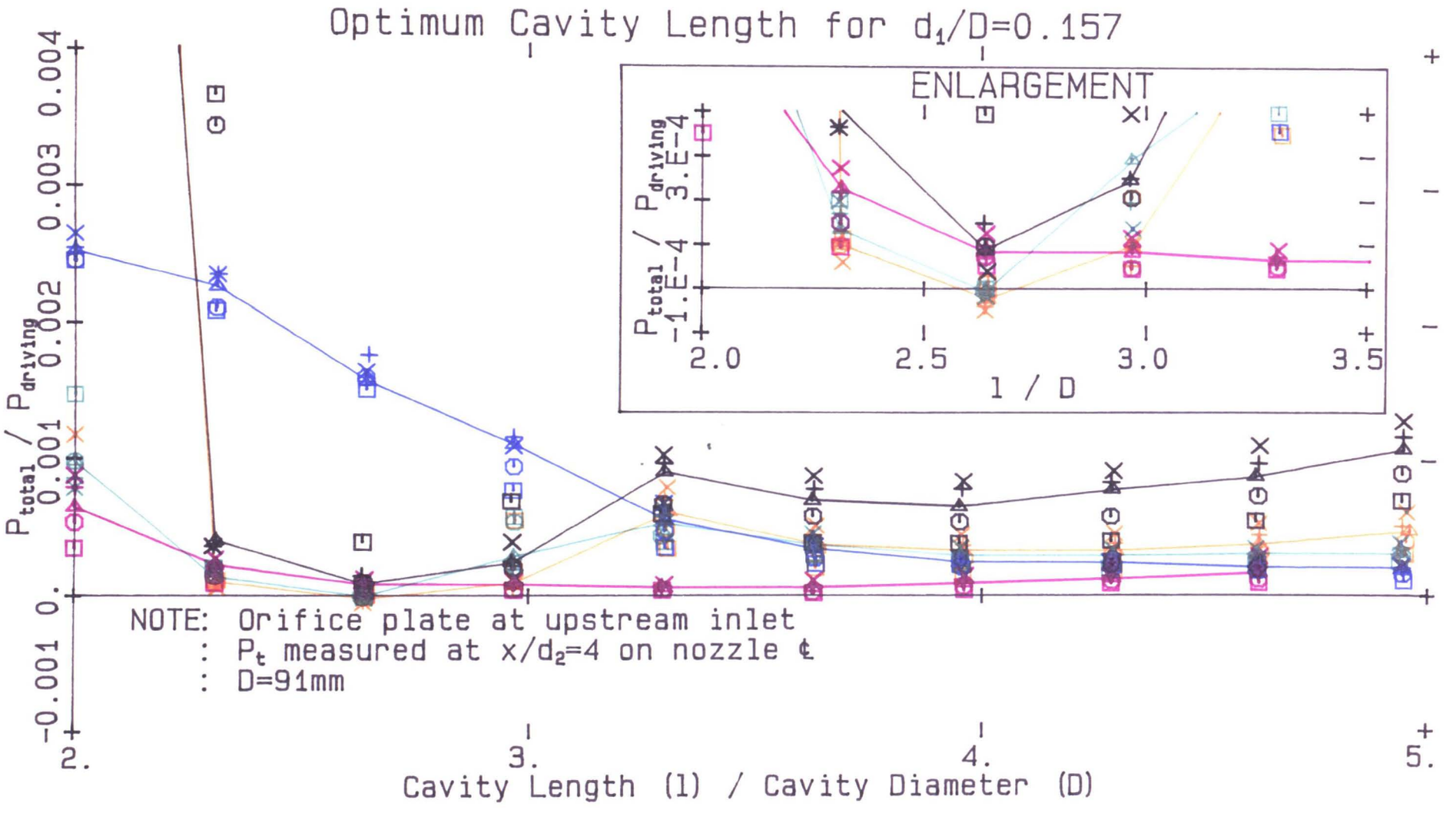

Figure 6.3: The Variation of Total Jet Pressure on the nozzle centreline with Cavity Length for $d_1/D = 0.157$

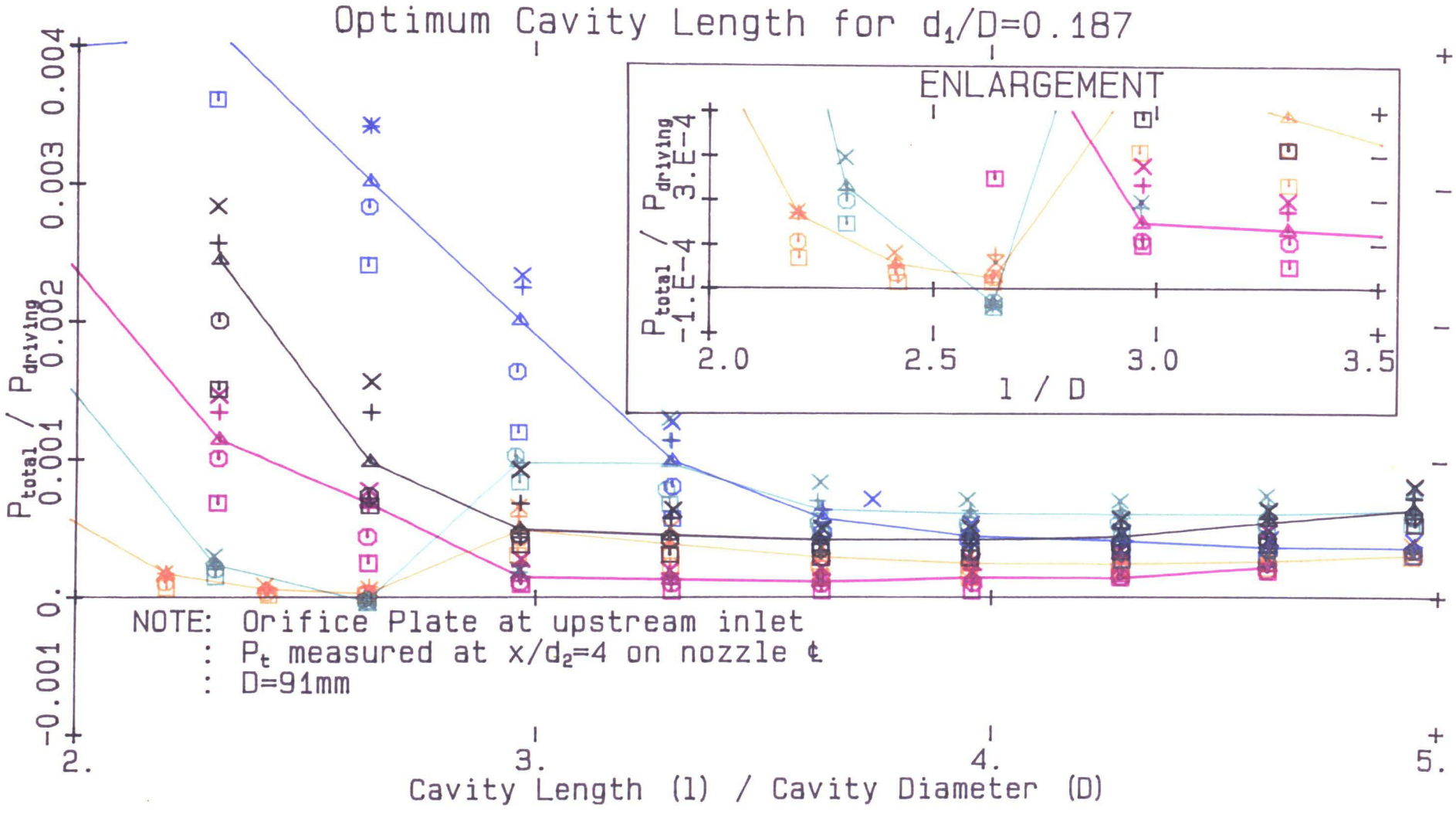

Figure 6.4: The Variation of Total Jet Pressure on the nozzle centreline with Cavity Length for $d_1/D = 0.187$

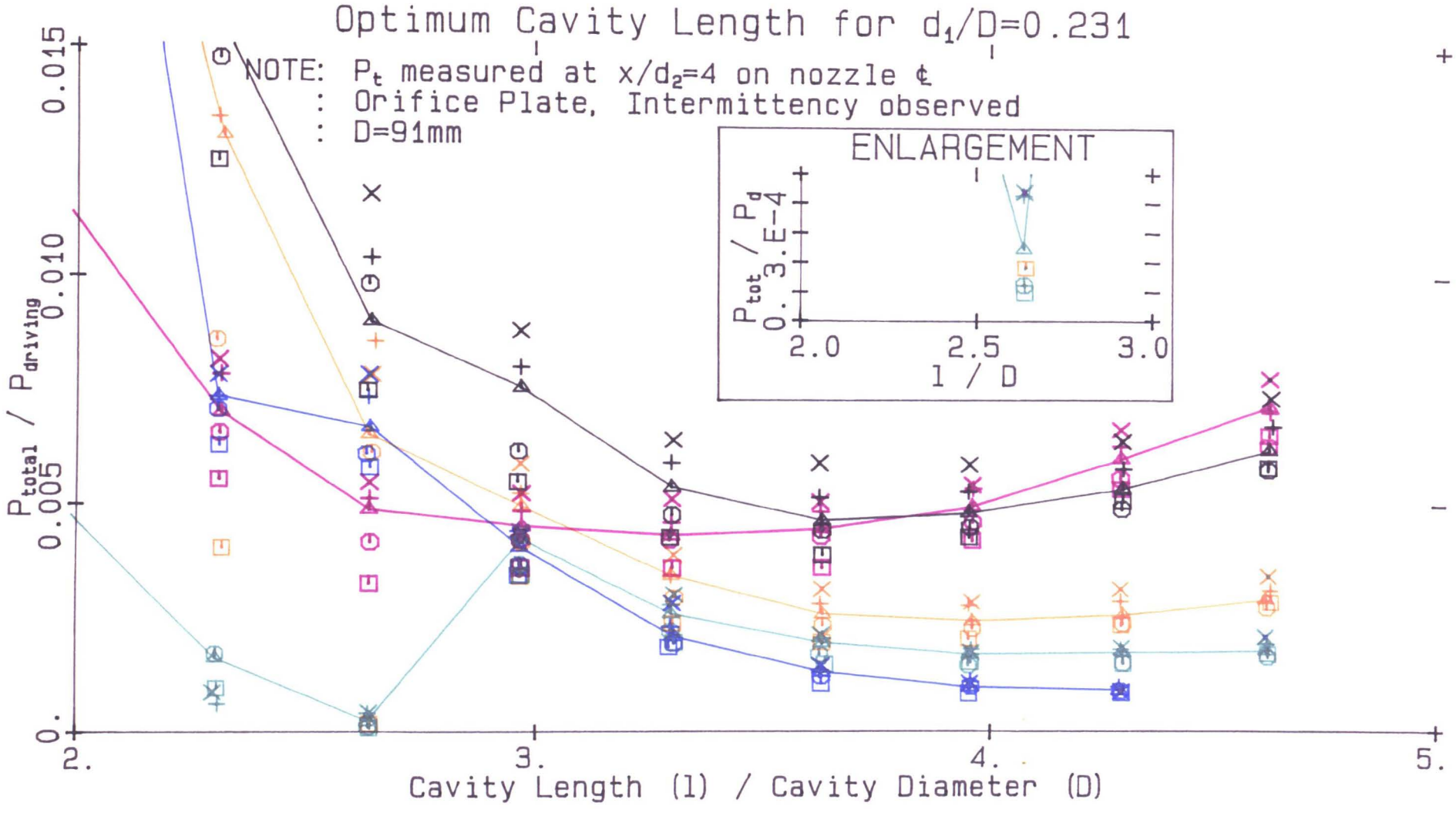

Figure 6.5: The Variation of Total Jet Pressure on the nozzle centreline with Cavity Length for $d_1/D = 0.237$

downstream separations, was modified to examine their influence independently.

First the separation upstream of the throat was eliminated by replacing the orifice plate shown in Figure 3.1 with a pipe of the same diameter, discharging through an abrupt expansion into the cavity. Alternatively, the simple orifice plate was replaced by a "bell-mouth" contraction to a throat of the same diameter (see Appendix B.6), again followed by an abrupt expansion into the cavity. The entrainment characteristics of the latter configuration are shown in Figure 5.7(d), where it can be seen that its entrainment appetite is only marginally less than that of the orifice plate.

This result does not necessarily imply that the shape of the velocity profile at the throat has no influence on the flow within the nozzle. Indeed Restivo and Whitelaw (1978) have found that the reattachment lengths downstream of a symmetric, plane sudden expansion were influenced more by the initial mean velocity profile than by the expansion ratio. It is to be expected that the turbulence intensity of the central jet and its entrainment appetite will influence the axial distance to the reattachment plane, and hence the optimum dimensions of the MLC nozzle. However, because the mixing enhancement is dominated by the precessing motion of the jet at the exit plane, provided that a perpetual[1] asymmetric reattachment occurs within the nozzle, any other differences will be secondary.

The shape of the expansion downstream of the primary throat was changed independently of the upstream shape, thus enabling it to be tested with and without an upstream separation. It has been found that if a *full* downstream separation can be prevented, which usually requires the elimination of the upstream separation also, then the mechanism producing precession will cease to operate. It is possible to achieve a *partial* separation at the throat[2] if a suitable bell-mouth contraction and expansion are used. In this case the jet will partially separate, remaining fully attached along one azimuthal position of the expansion only. This jet cannot precess because the secondary flow patterns and imbalance in the pressure field which occur "under" the jet with full downstream separation are eliminated by the presence of the surface. Thus the enhanced mixing does not occur. The details of these experiments are discussed in Section 4.6.

Various other expansions shapes were used, but all caused a separation to occur at the throat, and thus did not significantly effect the performance of the nozzle. (See Section 6.3.1

[1] ie. non-intermittent

[2] see Section 4.6

for more details.)

6.3.1 The Effect of Throat Conical Diffuser Angle on Entrainment

The effect of cavity shape downstream from the throat on the entrainment characteristics of the MLC nozzle were explored. Investigations were carried out with a "conical diffuser" at the throat, comprising a conical expansion with a half angle θ, measured relative to the nozzle axis, between the throat and downstream cavity, and an abrupt contraction upstream of the throat. The diffusers were made both with and without a radius at the throat as shown in the detail drawings found in Appendix B.7.

The results of this investigation are shown in Figure 5.6(c). Although insufficient data points were collected for a definite value of Kt (ie. where P_B = 6mTorr) to be determined in each case, the relative entrainment appetite of various configurations can be compared by examining the position of the lines of best fit. It can be seen that the data points for all values of $\theta \geq 25$ deg lie approximately on the same line. Thus their entrainment appetites are indistinguishable. However, at $\theta = 13$ deg, the rate of entrainment is greatly reduced. This result occurs whether or not the sharp edge at the throat was radiused.

It is apparent that the mechanism which generates the enhanced mixing is not influenced by expansion angles up to a critical value. However, for expansion angles beyond the critical value the mechanism is destroyed and the degree of mixing enhancement is greatly reduced. The following three *alternative* explanations are proposed:

Either

- The critical expansion angle represents the diffuser angle at which there is transition from fully *separated* flow to fully *attached* flow within it, in which case the flow in the diffuser is symmetrical.

Or

- The critical expansion angle represents the diffuser angle at which there is a transition from a three dimensional *reattachment* within cavity to no reattachment within the cavity, in which case the behavior of the jet within the diffuser/cavity approximates that of an unconfined jet.

Or

- The critical expansion angle represents the diffuser angle at which there is a transition from *fully* separated flow to *partially* separated flow within it, in which case the flow patterns associated with the MLC nozzle will occur.

The former explanation is considered to be extremely unlikely, because the critical "diffuser angle" is too large to support fully attached flow. The ESDU handbook [37] page 11, indicates the boundaries of separation flow regimes for conical diffusers. The area ratio between the orifice and cavity is much larger that recommended values, and consequently beyond the range of plotted data in the ESDU handbook. Simple extrapolation of the data suggests that to maintain fully attached flow throughout the diffuser would require its half angle to be less than 0.5 deg, while to eliminate transitory separation would require its half angle to be less than 3 deg.

The second explanation is even more implausible. If the jet is influenced by the cavity wall which is more remote (as occurs with an abrupt expansion at the throat), it will certainly be influenced by the diffuser downstream from the throat which is in close proximity with the jet.

The last explanation appears to be the most plausible, particularly when it is realised that the 13 deg expansion meets the cavity wall at the same axial location as the plane of the asymmetric reattachment, determined from the china clay visualisation, with an orifice plate at the throat. It appears then, that the edge of the critical diffuser approximates the edge of the asymmetric jet, thereby hindering the strong secondary flow patterns which accompany the precessing asymmetric jet. It should be emphasised that the jet which leaves the nozzle with the critical diffuser in the throat is, on average, symmetrical. Thus its behavior is quite unlike that of the partially attached jet caused by the B-M-C-E, discussed in Section 4.6, whose behavior was highly asymmetric in the mean. This implies then, that a full separation occurs at the throat of the critical diffuser followed by a partial reattachment well upstream of the end of the diffuser, and the generation of very weak secondary flow patterns. The jet is precessing, since it is symmetrical in the mean, but does not instantaneously leave the exit plane of the nozzle at a large angle to the nozzle axis.

This result does not conflict with the conclusion made in Section 4.6, that it is necessary for there to be a *full* separation at the throat if a precessing asymmetric jet is to be generated.

6.4 Optimum Diameter of Downstream Orifice

All results indicate that the exact shape of the downstream orifice plate is not critical. For example, it is not possible to discern any difference between the performance of the nozzle when the bevel on the orifice plate is on the upstream or the downstream face. The orifice can also be replaced by a saw-tooth orifice plate without producing any significant difference in the amount of entrainment (see Figure 5.6(a)).

However, evidence indicates that it is highly beneficial for a "lip" of minimal height to be placed at the nozzle exit. The function of the lip is apparently to assist in directing the instantaneously asymmetrically attached jet with a radial component away from the wall and across the nozzle centreline in a direction indicated by the measurements in Section 4.4. The flow visualisation described in Section 4.6 indicate that the asymmetric jet will follow this general flow direction even when there is no lip, which indicates that a radial pressure gradient exists across the exit plane which has an independent cause. However, the angle with which the instantaneous jet leaves the nozzle axis increases with the lip height.

There is also a lower limit to the diameter ratio d_2/D below which the flow patterns characteristic of the MLC nozzle do not occur. This limit depends weakly upon d_1/D, but is approximated by $d_2/D_{min} \approx 0.7$. It appears that if the downstream orifice is too small, either the reattachment will be adversely influenced, or the hole will not be large enough to allow the surrounding air to be induced upstream into the cavity.

6.4.1 Results from Entrainment Shroud

The effect of varying d_2/D on entrainment is shown in Figure 5.6(a). It can be seen that maximum entrainment occurs with the orifice size $d_2/D = 0.88$. However, the difference between entrainment for this orifice and the orifice $d_2/D = 0.77$ is very slight. By contrast, a significant reduction in performance occurs when no downstream orifice plate is used at all.

6.4.2 Results from single point total pressure measurements

The single point total pressure measurements also indicate that $d_2/D = 0.88$ gives the lowest (or equally low) value of total jet pressure on the centre-line. They confirm that if no downstream lip is present the amount of enhanced mixing will be greatly reduced. It can be seen that no mixing enhancement occurs when $d_2/D \leq 0.6$. This lower limit is not clearly de-

fined, for although some enhancement occurs when $d_2/D = 0.66, d_1/D = 0.157$, it is strongly intermittent.

The size of the downstream orifice plate which is required to generate enhancement also depends upon the size of the upstream orifice. It has been found that the nozzle is least sensitive to changes in the size of the upstream orifice when the downstream orifice is of the size $d_2/D = 0.88$. This is also the optimum size as determined using the other techniques.

6.4.3 Smoke Visualisation using a Non-Precessing Jet

Flow visualisation experiments with a non-precessing jet, discussed in Section 4.6, suggest that the static deflection of the jet increases with lip size (ie. decreased d_2) for $d_2/D > 0.6$. This suggests that mixing enhancement for a precessing jet will likewise increase over the same geometric range. However experiments with the precessing jet indicate that enhancement becomes increasingly intermittent as the lip height is increased when $d_2/D \leq 0.7$. It appears then, that optimum performance is likely to result when the downstream orifice diameter is marginally larger than the diameter below which intermittent enhancement occurs. This optimum diameter must also be dependent upon other operating conditions which influence intermittency, such as upstream swirl, and the position of an insert.

6.5 Optimum Cavity Length

The ratio of cavity length to diameter is also of fundamental importance in the generation of the flow patterns associated with the MLC nozzle. If the cavity is too short, the jet within the nozzle will not reattach anywhere within the nozzle. If it is too long, the instantaneous jet will fill the exit plane of the nozzle, and the secondary flow patterns which occur within the MLC nozzle (described in Chapter 4) will no longer be possible. These are the flow patterns associated with the LC nozzle which is discussed more fully in Chapter 8.

The MLC nozzle without an insert or pre-cavity swirl, can tolerate small changes in l/D without affecting the flow patterns. Furthermore, there seems to be little effect on the degree of enhancement within the range $\pm 10\%$ from $l/D = 2.7$.

6.6 Conclusions

The optimum geometric ratios for the MLC nozzle without an insert or upstream swirl are:

$$d_1/D \approx 0.15, \quad d_2/D \approx 0.7, \quad l/D \approx 2.7$$

The expansion ratio at the upstream orifice is critical because it determines whether the jet will expand into the cavity symmetrically or asymmetrically. However the shape of the expansion is only important in as much as it influences whether or not a full separation occurs at the throat. It is possible to achieve a partially attached jet throughout the nozzle when a suitably shaped bell mouth contraction and expansion is placed at the throat. In this case the jet expands asymmetrically into the cavity, attached at only one circumferential position at all axial positions. This jet will not precess because the secondary flow patterns and pressure fields characteristic of the MLC nozzle are not present. However the jet has a static deflection similar to the instantaneous dynamic deflection of the precessing jet. The ratio l/D is critical in determining whether or not an asymmetric jet will precess. The downstream lip is less critical, but helps to stabilise the asymmetric reattachment and increases the angle at which the instantaneous jet leaves the nozzle.

Chapter 7

Comparison with other research

7.1 Introduction

Although to the best knowledge of the author, no other research has been conducted on a device which produces flow patterns similar to those of the MLC nozzle, many closely related flow patterns have been thoroughly investigated elsewhere. Such topics include the flow behind steps and abrupt expansions, the mechanism of acoustic feedback, and mechanically and fluidically excited jets.

In this chapter relevant aspects of some of the research reported in the literature are discussed in relation to the interpretation of the experimental results presented in this thesis.

7.2 Comparison of the proposed mechanism with acoustic feedback

Since Brown and Roshko (1974) demonstrated the presence of large scale eddy structures in a two-dimensional shear flow, and their importance in the mixing process, much effort has been invested in stabilizing and strengthening these structures. Subsequent research has verified the dominant role which the large scale structures have on the rates of entrainment. Where a feedback mechanism has been found to exist naturally or has been artificially stimulated, it has usually involved the presence of highly ordered, large scale structures. Probably the best known of such mechanisms is that of acoustic feedback (see eg. Long et. al. (1984)). It was considered necessary to determine conclusively whether or not this mechanism has any influence on the flow patterns produced by the MLC nozzle.

7.2.1 The characteristics of acoustic feedback

Rockwell and Naudascher (1979) and Rockwell (1983) have set out the four elements of an acoustic feedback loop, and the characteristics of such self-sustaining oscillations. If any element of this loop is missing, ie. if fundamental characteristics of any element are not present in a given flow, it is valid to conclude that the large scale structures are not stabilized by acoustic feedback.

The necessary elements of a feedback loop, as stated by Rockwell are:

- *Feedback* or upstream propagation of disturbances from an impingement region to the sensitive, separating region at the origin of a free shear layer.
- *Inducement* of localised vorticity fluctuations by the arriving perturbations.
- *Amplification* of these vorticity fluctuations in the shear layer between separation and impingement.
- *Production* of organised structures at impingement.

7.2.2 Apparatus

To investigate the characteristics of the acoustic spectrum produced by the MLC nozzle, a one third octave band B&K acoustic spectrum analyser type 2112 was used. The output from this was recorded on a B&K level recorder type 2305, as shown in Figure 7.1. It is possible for a slight offset to occur in the recorded levels of frequency, because the paper moves under the pen during the recording, and it is difficult to align the 20 Hertz mark accurately. The microphone was placed 1m from the centre of the exit plane, and 30 deg behind it, to ensure that the flow did not impinge directly on the microphone.

A background noise spectrum was measured with the flow off, and revealed peaks at approximately 50Hz, 100Hz and 150Hz. These almost certainly correspond to the frequency of the electricity mains, which is nominally 50Hz, and its harmonics. These tests are shown in Figure 7.2.

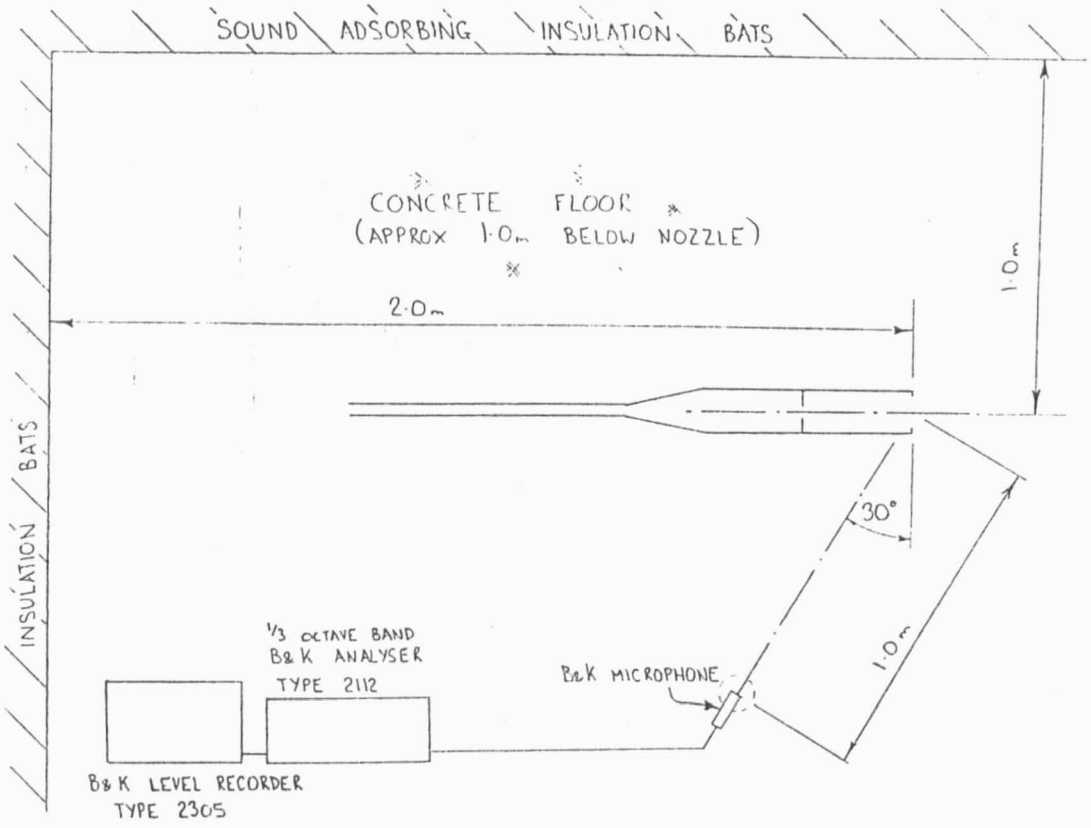

Figure 7.1: Experimental arrangement for acoustic frequency spectra measurements.

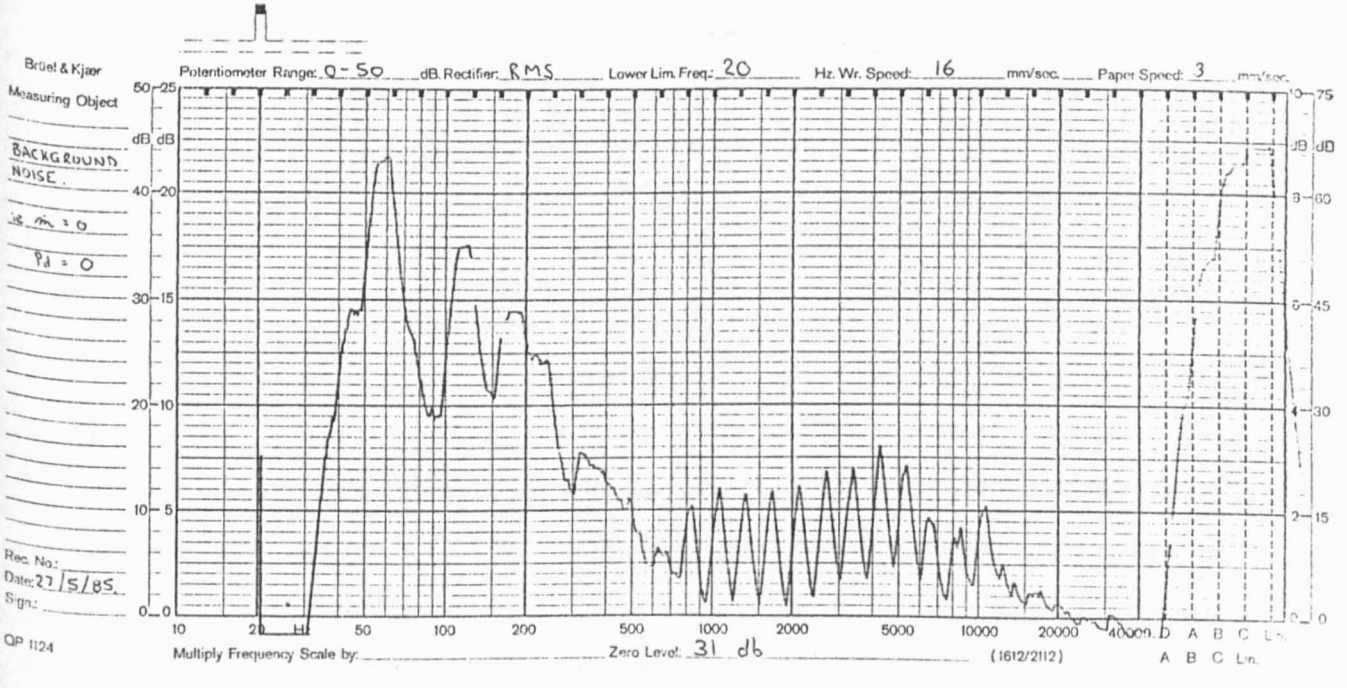

Figure 7.2: Background noise spectrum.

7.2.3 Comparing the characteristics of the MLC nozzle with the elements of an acoustic feedback loop

Consider first the element of acoustic feedback. The strength of the acoustic wave which is providing the feedback will determine the degree of influence it will have on the upstream separating shear layer. Furthermore, since the vorticity structures in the shear layer which it is reinforcing have a characteristic frequency, its energy will be concentrated about a discrete frequency. Thus any significant acoustic feedback will result in a peak in the acoustic SPL frequency spectrum. This result has been observed by many other researchers [96,97,42].

Welsh and Gibson (1979) and Welsh, Stokes and Parker (1984) investigated the effect of a duct resonance on the Strouhal shedding behind a plate in the duct. They found that improved organisation in the Strouhal shedding always implied a large increase in the SPL at that frequency, or at one of its harmonics, although a duct resonance did not necessarily imply improved organisation in the Strouhal shedding. They also observed that the shedding frequency would "lock onto" the resonant frequency for a range of velocities either side of the natural Strouhal velocity, corresponding to $St = 0.114$. This phenomenon was also observed by Abell and Luxton (1981) and produced greatly enhanced mixing in a jet and a very stable gas diffusion flame when used in a burner. However the "locking on" does not occur over a wide enough range of flow-rates to give an adequate turn down ratio for practical purposes.

The MLC nozzle can also be "de-tuned" so that *no* enhancement of the mixing occurs, by significantly reducing the cavity length. Thus the question of whether or not the enhanced mixing is accompanied by a change in the acoustic spectrum can be resolved by comparing the acoustic spectra of the tuned and de-tuned nozzle. If acoustic feedback causes the enhanced mixing, a peak should occur in the tuned nozzle spectrum which will be absent in the de-tuned nozzle spectrum for the same mass flow-rate.

The results of the SPL measurements, shown in Figures 7.3 and 7.4, clearly show that not only is there no clearly defined peak in any of the acoustic spectra of the MLC nozzle, but there is no significant difference between the spectra of the tuned and de-tuned nozzle, other than a slight *reduction* in SPL in the 500 Hz band. (Recall that the 50 Hz peak is also found in the background noise, Figure 7.2.)

Furthermore, the characteristic frequency of the vorticity fluctuations of the shear layer is proportional to the characteristic velocity, since it occurs at constant Strouhal number.

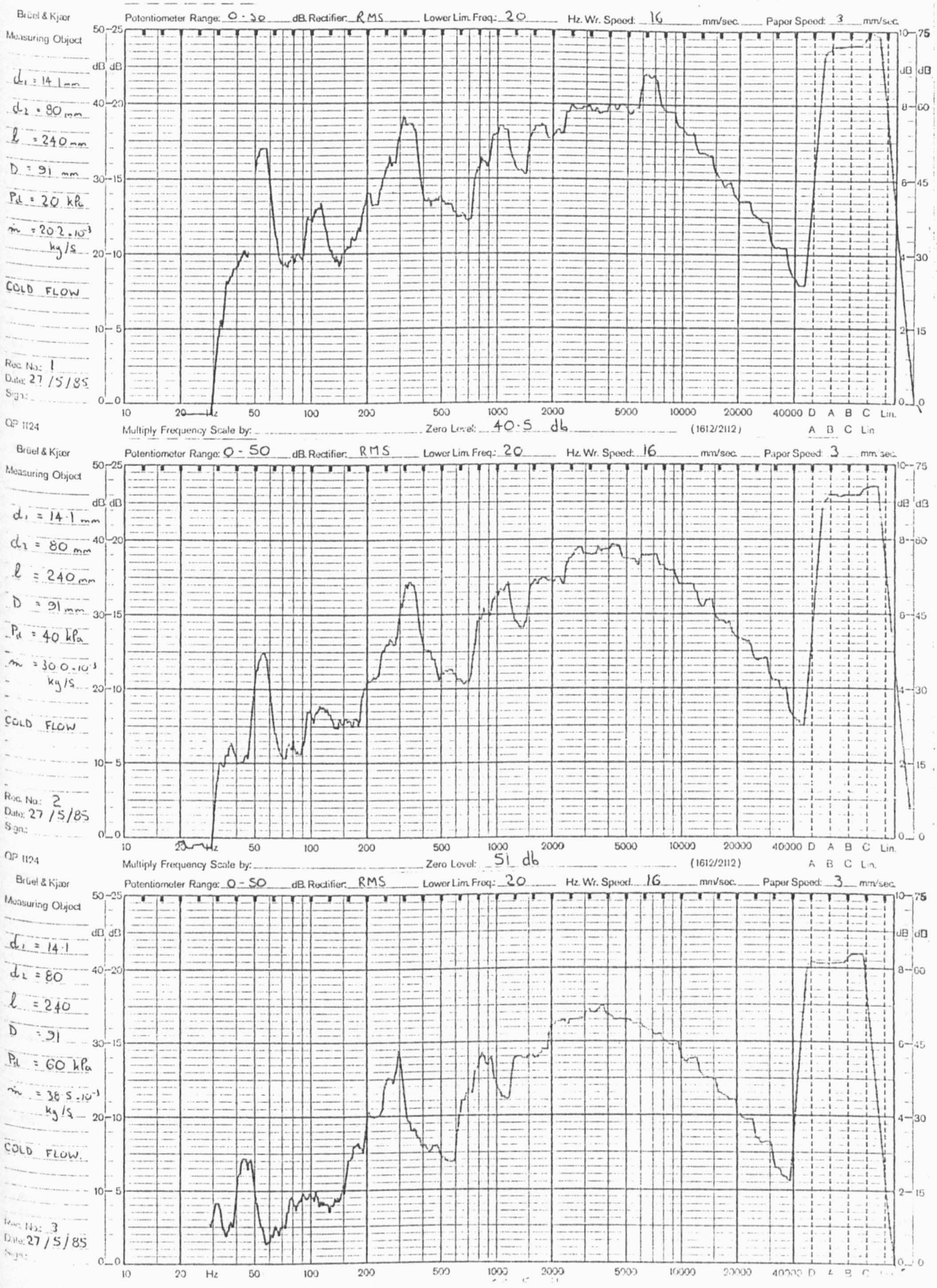

Figure 7.3: The acoustic spectra of a MLC nozzle during enhancement.

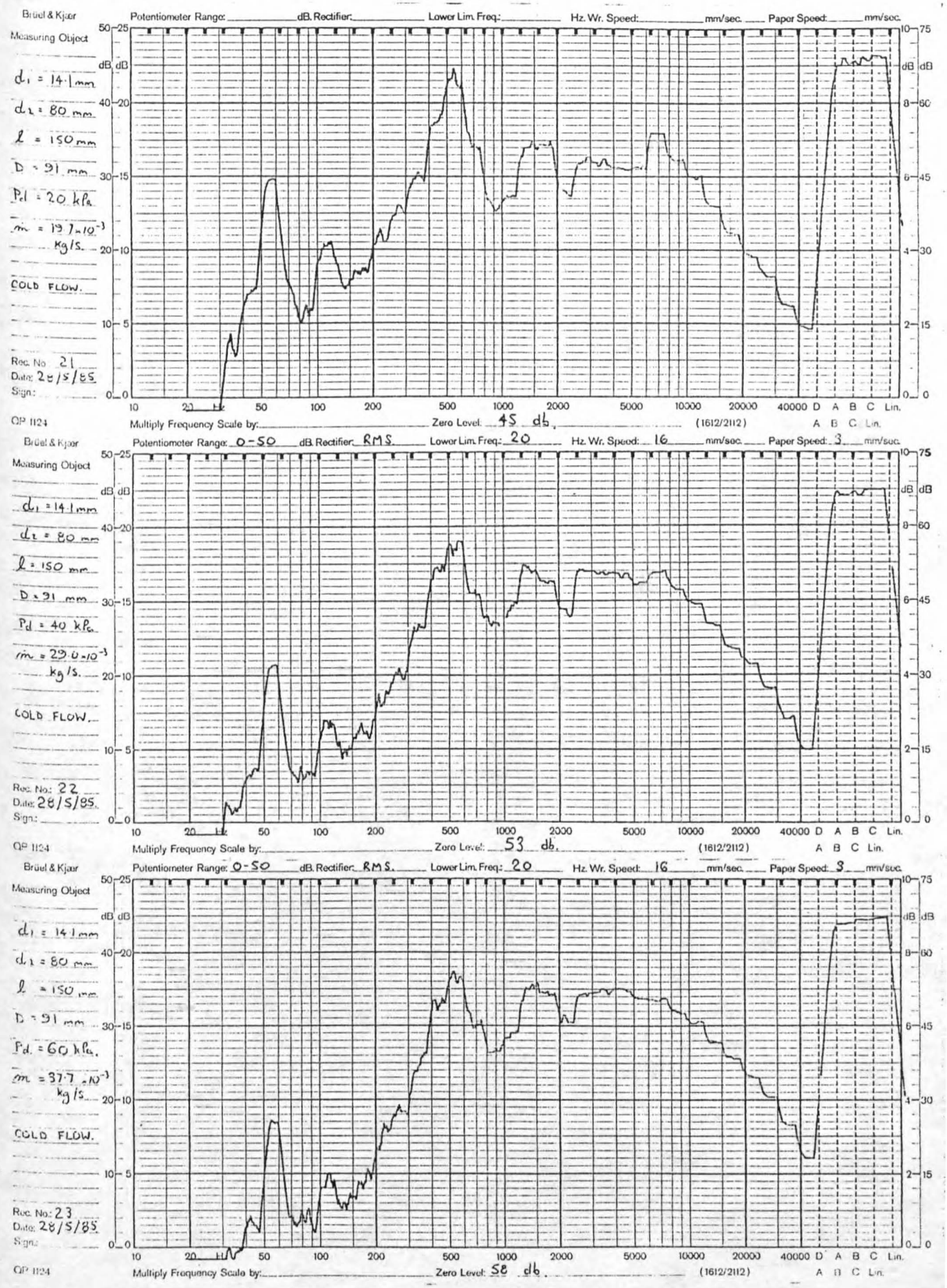

Figure 7.4: The acoustic spectra of a "MLC" nozzle with enhancement suppressed using a short cavity.

This implies that, if acoustic feedback is responsible for exciting these vorticity fluctuations, then the frequency of the acoustic signal must change with flow-rate. It can be seen from Figure 7.3, that no significant shifts in the frequency of the peaks in the SPL spectra occur as the throughput is changed.

Thus the acoustic SPL spectra of the MLC nozzle clearly indicate that acoustic feedback is not occurring within the nozzle, and thus cannot be responsible for the observed flow patterns.

Another element of the "feedback loop" is the conversion of the pressure fluctuations into vorticity fluctuations. Rockwell & Naudascher note that the magnitude of the local transverse pressure gradient plays an important part in this process and observe that for this reason a sharp edge produces stronger feedback. If the MLC nozzle utilised acoustic feedback to generate its flow patterns, then the Strouhal shedding at the upstream orifice would be an important element in the process, as was the case in the Abell nozzle. It has been found however, that replacing the upstream orifice by an abruptly expanding nozzle, without a sharp lip, does not cause any significant change in the flow within or beyond the nozzle. This result again suggests that acoustic feedback does not play an important part in the mechanism which generates enhanced mixing in the MLC nozzle.

7.2.4 Comparing the characteristics of the MLC and acoustic nozzles

The characteristics of a system which produces strong, coherent flow structures in a jet by amplifying the acoustic feedback signal through use of a resonance chamber have been extensively investigated [84,96,97,45]. The two most prominent characteristics are:

- A narrow operating range, ie. amplification of the oscillations occurs only within a narrow band of jet velocity.
- A dramatic rise in SPL at the resonant-excitation frequency, ie. as throughput is varied, the onset of jet excitation will coincide with the onset of a dramatic rise in SPL at a discrete frequency.

Both of these features were clearly observed in the Abell nozzle, the latter explaining the reason for its poor turn-down ratio. However neither of them have been observed for the MLC nozzle.

It can be seen in the acoustic SPL frequency spectra of the MLC nozzle shown in Figure 7.3, that there are no distinct peaks in the spectra. Furthermore, there are no dramatic changes

in SPL as the throughput is varied.

The wide operating range of the MLC nozzle has been verified in many experiments. For example, in the combustion experiments the flow patterns can be seen to be similar over a wide range of Reynolds number in the schlieren ciné film included with the thesis. The standoff distance can be seen in Figure 3.5 to vary smoothly over a wide range of throughputs. If the means of nozzle excitation was acoustic, improved standoff distance would only occur over a narrow range of Reynolds numbers. The single point measurements of total jet pressure on the nozzle centreline, shown in Figures 6.2 to 6.5, show that for the geometric configurations which give enhancement, $P_{total}/P_{driving}$ collapses well. This indicates that the flow patterns are similar at all five flow rates.

Thus it can be seen that the MLC nozzle has characteristics which are vastly different from those displayed by an acoustically excited nozzle.

7.2.5 The characteristics of the nozzle in Water

Finally confirmation that the mixing enhancement produced by the MLC nozzle is not stimulated by acoustic feedback was provided by operating the nozzle as a submerged water jet. The geometric configuration which will resonate at an acoustic frequency suitable for coupling with a fluid-mechanical vortex shedding in air, could not provide similar coupling in water. More specifically, to maintain Reynolds number similarity for the same nozzle, ie. $Re_{air} = Re_{water}$, we require

$$\frac{u_{air}}{u_{water}} = \frac{\nu_{air}}{\nu_{water}} \approx 16 \ ,$$

whilst the ratio of the speeds of sound is

$$\frac{c_{air}}{c_{water}} \approx \frac{330}{1540} \approx 0.23 \ .$$

This leads to a Mach number ratio,

$$\frac{M_{air}}{M_{water}} \approx 70 \ .$$

It can be seen then that it is not possible for an equivalent acoustic mode to exist in the cavity when a water jet is operated at the same Reynolds number as in air. The flow patterns in the jet were very similar when using the identical nozzle in the two fluids. Hence it is concluded that Mach number, the speed of sound and acoustic wave propagation are not important parameters in describing the flow patterns of the MLC nozzle. Thus these

experiments confirm the conclusion that the enhanced mixing generated by the MLC nozzle is not the result of acoustic coupling.

7.3 Flow behind Steps and Abrupt Expansions

A large body of research has been accumulated on the flow behind two-dimensional (2-D) steps and abrupt expansions which is of relevance to the present investigation. Despite the fact that the results of the 2-D investigations must be related with caution to the much more complex and highly 3-D flow patterns within and outside the MLC nozzle, the 2-D flows yield valuable insight into the behavior of the flow because they represent a simplified version of the 3-D case. Whilst a lot of work has also been done on the axi-symmetric flow through an orifice plate, frequently associated with flow rate measurement, much of this is of less relevance because the ratio of diameters of the orifice and the pipe in the present nozzles is much smaller than is typical for flow rate measurement devices.

7.3.1 Expansion Ratio

It has been found that for sufficiently small 2D expansion ratios[1], the shear layers on either side of the expansion are independent of each other. Consequently the flow on each side is similar to that behind an equivalent backward facing step. The reattachment length, x_r, then scales on step height, with a dependence on velocity which decreases with increasing Reynolds number.

Abbot and Kline (1962) found that the expansion is symmetric, ie. $x_{r1} = x_{r2}$, when x/b $\leq$ 1.5. This is illustrated in Figure 7.5. As shown in Figure 7.6, if the expansion ratio is greater than 1.5, the two shear layers begin to interact with one another, causing the reattachment length on one side of the expansion to be be larger than that of the backward facing step, and that on the other to be shorter [26].

As either the expansion ratio or the Reynolds number is increased still further, a third, and then a fourth, recirculation zone is introduced, and the flow behaves like that in a narrow

[1] expansion ratio = w/b (see Figure 7.5) for 2-D flows. Expansion Ratio is usually defined as ratio of downstream to upstream *area* of the expansion. For plane geometry, this is the same as the ratio of cross stream *lengths*. However, for an axi-symmetric geometry, the two ratios are vastly different. It is not known which ratio is most relevant in determining the onset of asymmetric flow for axi-symmetric geometries.

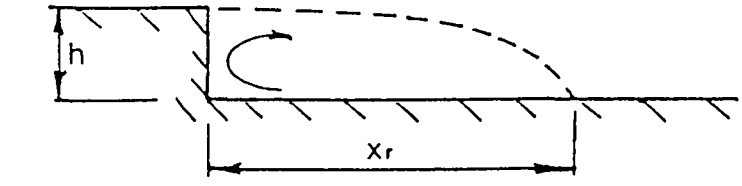

Backward Facing Step

- Brown, Roshko type vortex, vortex pairing observed (Eaton & Johnston, Troutt et al).
- Very low frequency oscillation of shear layer examined - its feedback mechanism is unknown (Cherry et al, Kiya & Sasaki).

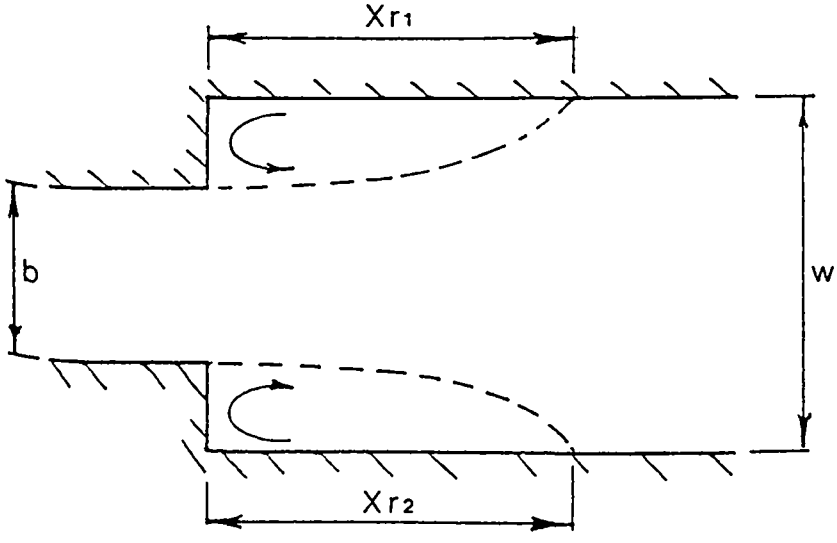

Abruptly Expanding Duct - Two shear layers independent

(Expansion Ratio = w/b)

- $x_{r_1} = x_{r_2}$
- Occurs for w/b $\lesssim$ 1.5 for fully turbulent flow (Abbott & Kline).

Figure 7.5: Abruptly Expanding Duct - two shear layers independent, and a Backward Facing Step.

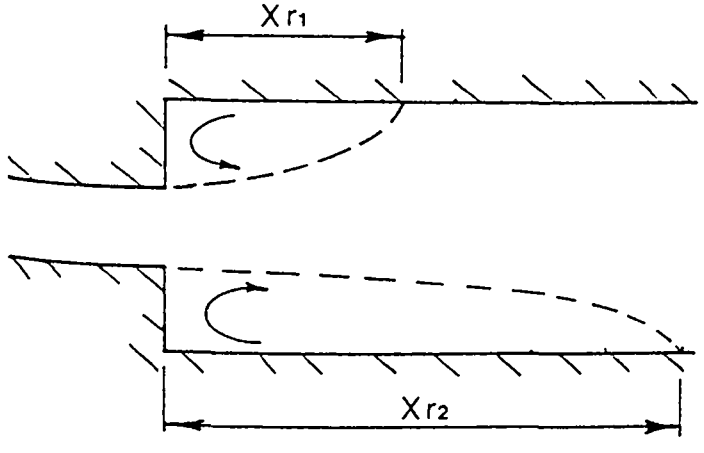

- $x_{r_1} \neq x_{r_2}$
- vortex shedding of the two shear layers is in antiphase (Cherdron et al).
- the expansion ratio required for the onset of asymmetry is a function of Reynolds number and aspect ratio (Cherdron et al).

Figure 7.6: Abruptly Expanding Duct - Two shear layers interacting

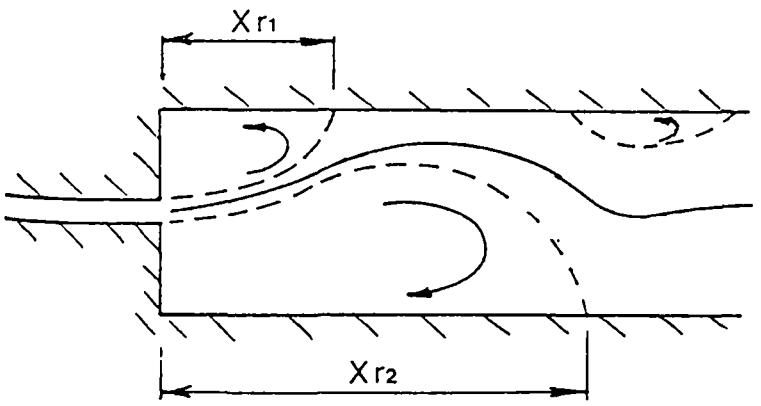

- A third (and fourth) recirculation zone observed for some Reynolds numbers (Armally et al, Cherdron et al).
- The third recirculation zone becomes more stable as w/b is increased (within reason) (Ouwa et al).

Figure 7.7: Abruptly Expanding Duct - Two shear layers strongly interacting such that flow behaves as an asymmetric jet.

jet expanding asymmetrically and attaching itself to one wall, and then the other, before eventually expanding to fill the section [70,8]. This is illustrated in Figure 7.7.

In other words, for plane, two-dimensional abruptly expanding ducts, the flow downstream of the expansion will be asymmetric if critical expansion ratios and Reynolds numbers (based on h) are exceeded. This asymmetry is quite strong. For example, Restivo & Whitelaw (1978), who used an expansion ratio of three, for which two unequal reattachment lengths were formed, found that there was a tendency for the maximum velocity in a given cross section to fluctuate from one side of the duct to the other with downstream distance, until symmetry was reached some 45 step heights downstream.

At larger expansion ratios, the transition from symmetric to asymmetric flow occurs at quite low Reynolds numbers. Ouwa et. al. (1981) found that for an expansion ratio of five, the transition occurred at $Re_h = 30$, and that this value depended upon the expansion ratio.

The MLC nozzle has a typical expansion ratio of seven, based on diameter, and thus of about fifty, based on area. This suggests that the flow entering the MLC nozzle through the throat will not expand symmetrically to fill the cavity, but rather will behave as a jet which will attach asymmetrically to one part of the cavity wall.

At this juncture, the distinction between plane and axi-symmetric jets becomes apparent. Whilst an asymmetric expansion of a plane jet is bi-stable and steady with time (bi-stable in the sense that there is no initial preference for the wall to which the jet will attach), an axi-symmetric expansion is inherently unstable as all reattachment points are equally probable. Thus, in the absence of a distinct geometric asymmetry, the reattachment "point" is free to precess. This distinction may be illustrated by the interpretation given by Pelfrey and

Liburdy [72,73], for the behavior of a plane, offset wall jet. The pressure underneath the reattaching jet is lower than that above it, because the wall below restricts the amount of air which can be entrained. It is this pressure gradient which causes the curvature in the streamlines of the jet. Such a condition is stable for a plane, two-dimensional jet, because the reattachment "bubble" is isolated from the flow on the other side of the jet by the jet itself and the wall. However this pressure imbalance "above" and "below" an axi-symmetric jet cannot be sustained because the jet does not separate the high and low pressure "zones". Even the most minor azimuthal asymmetry in the pressure field is sufficient to cause the jet to deflect sideways and the reattachment distance to change. Such a condition is inherently unstable, and is the cause for the precession of the jet and its reattachment point around the inside of the cavity.

The parameters which control the reattachment length behind a 2D backward facing step have been reviewed by Eaton and Johnston (1981). Five major influences were found:

- The initial state (laminar or turbulent) of the boundary layer (BL). Reattachment length, x_r, becomes independent of Re once the BL is fully turbulent.
- The initial thickness of the BL, δ, relative to the step height, h, ie. x_r/h decreases as δ/h increases.
- The intensity of the free stream turbulence. High levels of free stream turbulence decrease x_r .
- The stream-wise pressure gradient. This is determined by the geometry of the system. A trend of increasing x_r with increasing expansion ratio is apparent.
- The aspect ratio, ie. channel width / step height, of the apparatus.

As discussed in section 4.8.4, Agarwal (1986) found that the reattachment length behind an orifice plate in a long pipe appears to be a unique function of Reynolds number based on the radial step height of the orifice plate, Re_h. He also found that x_r/h was typically nine to twelve, depending on Re.

The reattachment length found in the MLC nozzle was typically three to four step heights (see Table 4.4). This value is more compatible with the results of Pelfry and Liburdy [72], who investigated a 2D wall jet over a backward facing step. They found x_r/h was typically two.

However, reattachment lengths for plane geometries appear to be shorter than those for axi-symmetric geometries. For example Eaton and Johnston found that x_r/h for a 2D backward facing step was typically between five and seven, compared with Agarwal's asymmetric values of nine to twelve.

However reattachment distance only becomes constant when the flow upstream of the step is fully turbulent. Armaly et. al. (1983) found a strong dependence of reattachment distances on Reynolds numbers, particularly in the transitional region for flow downstream from a 2D backward facing step. They found x_r/h varied between 18 and 6 for a particular geometric configuration over the range $1000 < Re < 6000$.

7.4 Mechanically and fluidically excited jets

Mechanically and fluidically excited jets are probably the most closely related flow phenomenon to those produced by the present nozzle. They operate by exciting a low frequency "flapping motion" of a plane, 2-D jet. This "flapping motion" appears to be a naturally occurring characteristic of all free jets, but is usually hidden in the randomness of the turbulent field. Cervantes de Gortari and Goldschmidt (1981), (C&G) used long time, statistical averages to isolate an apparent large scale flapping motion of an unexcited plane jet. The Strouhal number based on nozzle width and mean exit velocity varied with distance downstream, but was typically $0.01 < fd/U_0 < 0.08$. This is an order of magnitude lower than the Strouhal numbers associated with the large scale vortex structures generated in the region of high shear at the exit of a jet, which can be excited acoustically. Acoustically excitable structures typically have a Strouhal Number that lies in the range $0.3 < St < 0.5$ [54]. The similarity between the natural flapping frequency found by C&G and the mechanically or fluidically excited jets can be seen in Table 7.1, which shows that typical Strouhal Numbers are $St_{mech} \approx 0.05$ and $St_{fluidic} \approx 0.03$. C&G also found that the large scale structures become self preserving at large distances downstream, ie. when $x/d > 30$. The Strouhal number based on *local* velocity and jet half width in this region is constant, ie. $fr_{half}/u_{cl} \approx 0.11$.

Mechanically excited jets use an oscillating or vibrating vane, placed immediately downstream of the exit plane, to excite the large scale flapping motion of a plane jet [52,85]. Fluidic nozzles use a small, oscillating pressure gradient across a plane jet, immediately downstream of a separation plane but upstream of two alternative reattachment surfaces. The pressure gra-

dient, produced by fluid injection, is adequate to cause the reattaching jet to oscillate between these two bistable positions, and so triggers a flapping jet [95]. Both of these mechanisms give substantial gains in entrainment.

It is interesting to note that large scale, low frequency structures have also been observed in the wakes behind bluff bodies. Cimbala et. al. (1981) observed that these structures did not grow by the vortex pairing method, as do the large scale structures in the Karman Vortex Street (KVS), but result from an instability in the developing mean wake profile. Furthermore, Kawall & Keffer (1981) found large scale "turbulent bursts" at a Strouhal number of about 0.06 in the flow in the wake behind a cylinder. This is an order of magnitude below the frequency of the large scale structures in the KVS. Consequently, it appears that a motion analogous to the large scale flapping of a plane jet exists in the wake behind a plane bluff body.

It is apparent that large scale, very low frequency instabilities are present in plane jets and wakes, and in axi-symmetric wakes, with a Strouhal number of about 0.05. Because these Strouhal numbers are based on the width of the jet or bluff body, whilst the Strouhal number which best describes the motion of the present nozzle is based on the step height of the primary orifice, a comparison of the two must be treated with caution. Nevertheless, it is interesting to note that there is very close agreement between the Strouhal Number of the precessing jet in the present nozzle, $St = f_p h_1/u_1 \approx 0.005$ (see Table 4.1), and that of the mechanically and fluidically excited jets. It appears then, that the MLC nozzle is exciting an analogous motion, but in an axi-symmetric configuration.

Lai and Simmons (1985) state that transverse (and hence asymmetric) excitation of a jet is far more effective than axial (symmetric) excitation [85]. Similarly, Bradbury and Khadem (1975) found that entrainment of an axi-symmetric jet could be increased if the symmetry of the jet was partially destroyed by placing tabs asymmetrically in the nozzle. This trend also appears to apply with acoustically excited nozzles. Parekh & Reynolds (1987) found that combining a helical mode of excitation with an axial mode was a far more effective than axial excitation alone. Likewise, the Abell nozzle which generates very strong mixing has been found to excite predominantly the (0,1) radial mode [5] which, although symmetric, is a transverse mode.

These results and others displayed in Table 7.1 clearly indicate that entrainment is increased most effectively if a jet is excited asymmetrically. This gives credence to the notion that the highly asymmetric flow patterns generated by the MLC nozzle should give rise to high

rates of entrainment. These high rates of entrainment have been observed in experiments.

While acoustic excitation is readily achieved with axisymmetric configurations [6,?,42], it has the primary disadvantage of a limited operating range, as discussed in Section 3.2. A major disadvantage of the fluidic and mechanical modes of excitation is their two-dimensionality. Plane jets have less application than axisymmetric jets. Most configurations are also complicated in design, and would require constant monitoring and maintenance. Any system which is not fluid mechanically self exciting (eg. an oscillating vane), runs the risk of catastrophic failure of the excitation (eg. mechanical failure). This can have disastrous consequences in certain applications. By contrast the MLC nozzle is fluid mechanically self exciting, and axisymmetric. Furthermore, its geometry is extremely simple, and it is not critically dependent on dimensional accuracy, so its wear tolerance should be high.

It is interesting to compare the characteristics of the various means of jet excitation shown in Table 7.1. Typical maximum spreading angles, based on the angle between the centreline and the "edge" of the jet, are 35 deg for mechanically excited jets and slightly less ($\approx$ 25 deg) for fluidically excited jets. The MLC nozzle compares favorably with this, generating spreading angles of at least 60 deg.

7.5 Conclusions

7.5.1 Comparison with acoustic nozzles

The characteristics of the MLC nozzle have been compared with those of acoustically excited nozzles which have been described in the literature, and it has been shown that the MLC nozzle is not an acoustically excited nozzle. The following results have been found:

1. The elements of an acoustic feedback loop, as defined by Rockwell (1979) and Rockwell and Naudascher (1983), are not present in the behavior of the MLC nozzle. More explicitly:
   - *Acoustic Feedback* is identifiable as a strong peak at a discrete frequency in the acoustic SPL-frequency spectrum. No such peak exists with the MLC nozzle.

[3] angle between "edge" of jet, and jet centreline - determined using hot-wire anemometry

[4] angle between "r_{half} edge", and jet centreline

[5] based on maximum angle between the nozzle centreline and the centreline of flapping jet

[6] angle between "edge" of jet, and jet centreline - determined visually

Source	St (fd/U)	d (mm)	Re	Excitation Means	Comments
Acoustic Excitation of Axi-symmetric Jets					
Hill & Greene	0.25 to 0.65	25.4	9×10^4	pipe ring creating organ-pipe mode	Large increases in spread-angles and decay rate.
Hussian & Hassan	0.33 to 0.8	25 to 76	6×10^4 to 5×10^5	pipe ring creating organ-pipe mode	Large increases in spread-angles and decay rate.
Abell & Luxton [58]	0.48	9 to 12	6×10^4	radial, (0,1) mode in cavity	spread-angles[2] of up to 33 deg
Parekh & Reynolds	0.55	20	$\leq 1 \times 10^6$	Combined helical & axial modes	Spread-angles[3] of up to 35 deg
Mechanical Excitation of Plane Jets					
Lai & Simmons [51]	0.0001 to 0.003	5	11000	Axial pulsation of mass flow	Negligible difference between steady & excited jets
Galea & Simmons	0.0033 to 0.0125	5	10000	Transverse oscillation of exit area	50% increase in entrainment at $x/h = 20$
Simmons et. al. [86]	1×10^{-5} to 1.4×10^{-4}	0.38	1.4×10^5 to 3.9×10^5	Transverse oscillation of jet exit angle	Negligible difference between steady & excited jets
Simmons et. al. [85]	0.0008 to 0.0049	6	1.4×10^4	Transvese exitation – oscillating vane in potential core	100% increase in entrainment at $x/h = 20$
Badri Narayanan & Raghu	0.0006 to 0.06	20	6000 to 72000	Transverse excitation – oscillating vane in potential core	spread-angles[4] of up to 33 deg
Badri Narayanan & Platzer[10]	0.067	5	0 to 40000	Transverse excitation – oscillating lips on either side of the jet	spread-angles[5] of up to 35 deg incr. thrust by 1.2
Badri Narayanan	0.045	20	40000	Transverse excitation – twin oscillating vanes either side of the jet	entrained nearly twice the mass from surrounds as single vane excitation
Unexcited Plane Jets					
Cervantes de Gortori et. al.	0.08 at $x/d = 10$	6.35	7900 to 15100	Unexcited	Jet found to flap. $St = fr_{half}/u_{cl}$ is const for $x/d > 30$
Fluidic Excitation of Plane Jets					
Favre-Marinet et. al.	0.021 to 0.036	10	$\geq 10^4$	Transverse excitation of the jet by Coanda effect	spread angles[5] of up to 17 deg
Binder & Favre-Marinet	0 to 0.062	10	8500	Transverse excitation of the jet by the Coanda effect	spread angles[4] twice that of unexcited jet
Vietts	—	2.5	—	Transverse excitation – Flip-flop fluidic nozzle	spread angles[4] of up to 25 deg
Piatt & Vietts	0.0081 to 0.036	12.7	32000	Transverse excitation – Flapping of jet by Coanda effect	rapid decay in maximum velocity

Table 7.1: Literature review of the frequencies associated with different modes of jet excitation.

Note: "d" represents jet width (plane case) or jet diameter (axi-symmetric case).

Furthermore, if the MLC nozzle is "de-tuned" so that it no longer produces the enhanced mixing flow patterns, there is no significant change in the acoustic frequency spectrum.

- *Inducement* of localised vorticity fluctuations is strongly influenced by the magnitude of the local transverse pressure gradient, and hence a sharp edge is more effective at generating an acoustically excitable Strouhal shedding than is a smooth exit. However, the performance of the MLC nozzle does not seem to be greatly influenced by the shape of the throat, provided that a *full* separation was generated.

2. The characteristics of acoustic excitation are different from the characteristics of the MLC nozzle, ie.
   - Self excited acoustic excitation can only occur over a limited range of flow rates because the frequency of the Strouhal shedding is proportional to the velocity, and resonance can only occur at discrete frequencies. The MLC nozzle, by contrast, has continuous turn-down capability.
   - The onset of acoustic excitation (eg. as throughput is changed), is accompanied by a dramatic rise in acoustic SPL at the resonant frequency. The MLC nozzle has no dramatic changes in its acoustic frequency spectrum as throughput is varied.
3. Closely similar flow patterns are generated when the identical MLC nozzle is operated in water and in air, despite a factor of about 70 difference in the Mach numbers at the same Reynolds number. This would not be possible if the nozzle was acoustically excited because the resonant frequencies of the nozzle would be vastly different at the same Strouhal number.
4. The Strouhal number of the excitation is an order of magnitude lower than the Strouhal number of acoustic excitation.

7.5.2 Comparison with flow behind steps and expansions

The critical expansion ratio, which determines whether the flow behind a two dimensional abrupt expansion will be symmetric or asymmetric, has been found to be about 1.5 [1]. Although the critical expansion ratio which determines the onset of highly asymmetric flow, with

three or more recirculation zones, depends on Re as well as the expansion ratio, it is certainly less than five [70,81]. The MLC nozzle has an expansion ratio of about seven based on diameter, and of about 50 based on area, and thus, although it is geometrically axi-symmetric, it can be expected that its flow patterns will be highly asymmetric.

7.5.3 Comparison with mechanically and fluidically excited jets

Mechanical and fluidic excitation of a 2D, plane jet can promote a large scale flapping motion. The flapping motion appears to be an inherent instability of 2-D, free jets. There appears to be a strong similarity between this well known phenomenon and the proposed precession motion of the present axi-symmetric nozzle:

- The Strouhal Numbers of their motions are approximately the same, ie. $St_{fluidic} = fd/U_0 \approx 0.003$, $St_{mech} = fd/U_0 \approx 0.005$ and $St_{MLC} = f_p h_1/u_1 \approx 0.005$.
- The flapping motion of a plane, 2-D jet is conceptually a simplification of a precessing, axi-symmetric motion.

Research with mechanically excited jets has shown that asymmetric or transverse excitation is much more effective than symmetric or axial excitation in generating increased rates of mixing. This supports the notion that the very high rates of mixing found in the present nozzle are caused by the extremely high degree of asymmetry in the motion of the instantaneous jet.

Because axi-symmetric flows have an extra degree of freedom compared with plane flows, it is to be expected that they will be capable of greater asymmetry, and thus of more effective mixing. This is bourne out in a comparison of the plane nozzles with the present nozzle. The half jet spreading angles of the mechanically and fluidically excited nozzles are up to 35 and 25 deg respectively, whilst those of the MLC nozzle are certainly greater than 60 deg.

Chapter 8

The Long Cavity Nozzle

This chapter is essentially a continuation and expansion of the discussion the LC nozzle, which was introduced and briefly compared with the MLC nozzle in Chapter 3. Some of the results referred to earlier are presented in more detail and further inferences are drawn from them. For example, sufficient is now known about the flow patterns of the MLC nozzle to allow some deductions about the flow patterns within the LC nozzle to be made. However it should be reiterated that a thorough investigation of the characteristics and mechanism of the LC nozzle has not been completed due to the subsequent discovery of the MLC nozzle. Thus the results presented here are not conclusive, but provide an initial data-base for a subsequent investigation of either the LC nozzle itself, or a related topic such as flow through "small" orifice plates.

8.1 Pressure Profiles of the LC nozzle

In order to provide a basis for comparison of the characteristics of the LC nozzle, a large number of total and static pressure profiles were taken. For reasons of conciseness, only a representative sample are included here – the rest are archived in the Department of Mechanical Engineering, University of Adelaide. Figures 8.1 & 8.2 show the pressure and velocity profiles respectively. The velocity profiles are normalised using the maximum velocity and r_{half}[1].

It can be seen that reasonable similarity of the jet profile shape is attained downstream from $x/d_2 = 0.50$ in all cases, despite the fact that for $d_1/D = 0.187$ there is considerable asymmetry in the initial jet profile. This indicates that very high rates of mixing exist in the

[1] r_{half} is the radius at which the jet velocity is half of the maximum (centre-line) velocity at a given station.

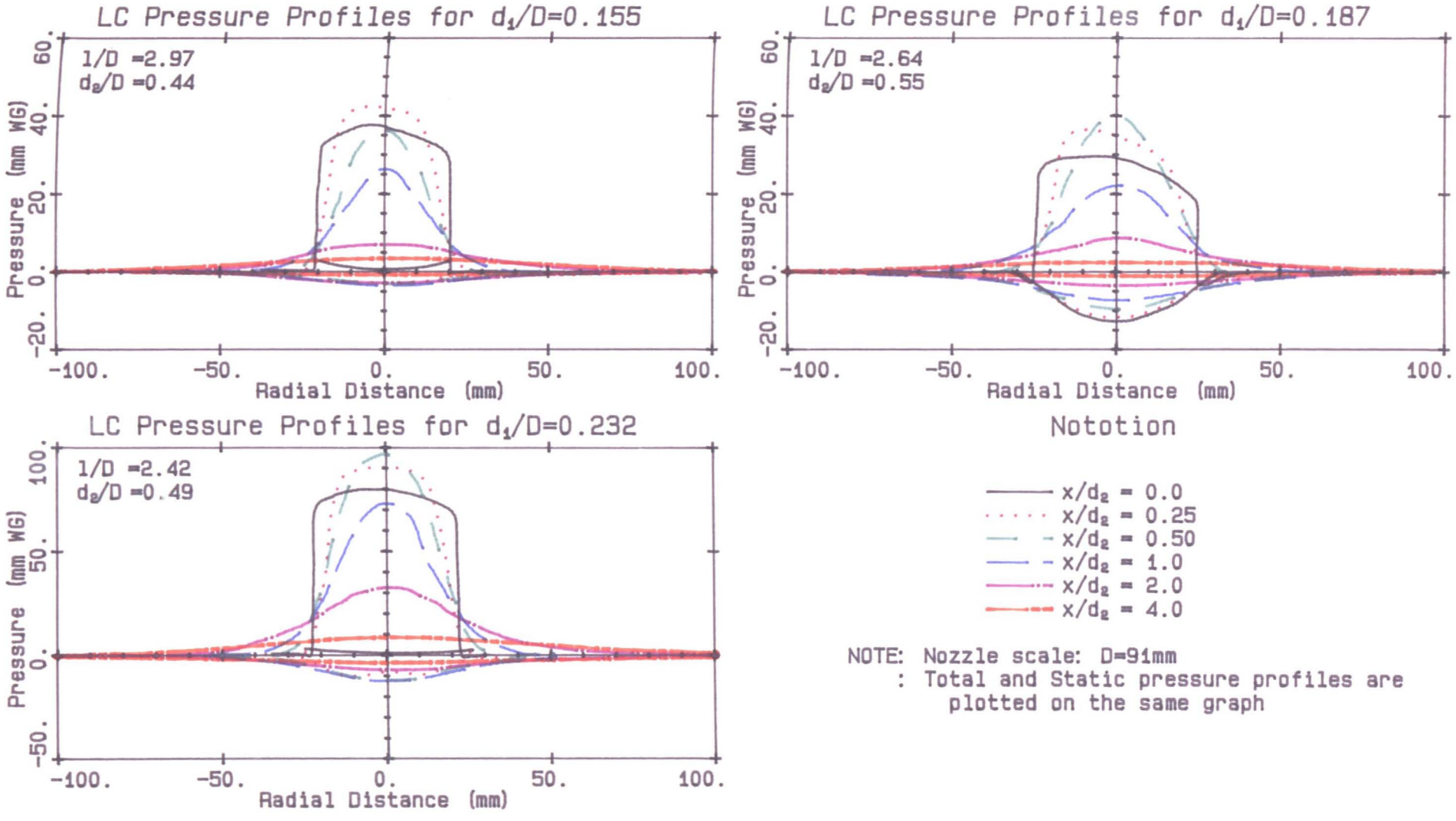

Figure 8.1: Total and Static Pressure profiles from LC nozzle

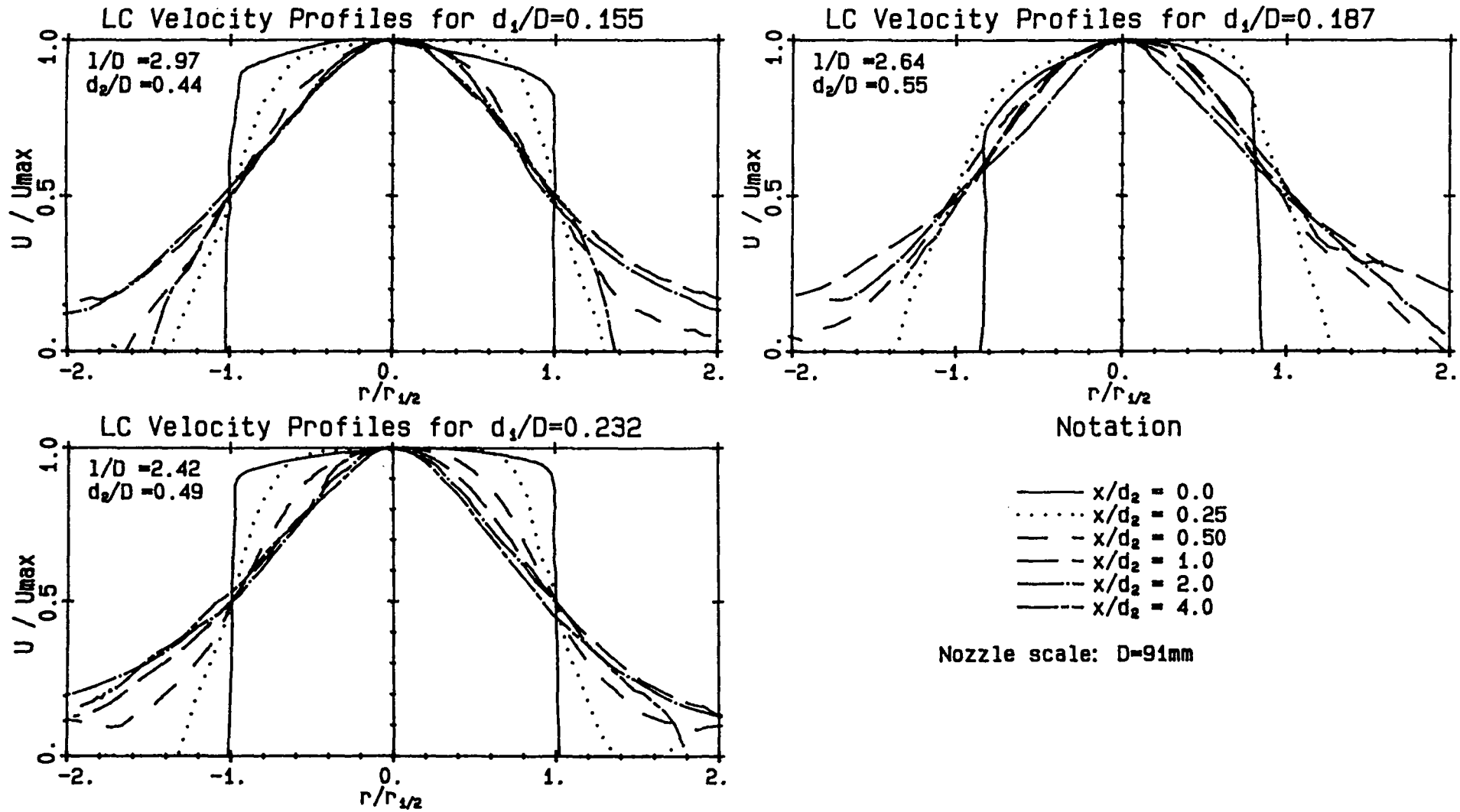

Figure 8.2: Normalised Velocity profiles from LC nozzle

initial region of the jet. The fact that the profiles show less similarity near the edge of the jet is to be expected because the velocities there are very low, and pitot tubes, which respond to the square of the velocity, have poorer resolution at low velocities. Furthermore, the velocity is obtained by taking the difference of two small numbers. Consequently, small errors are magnified near the edge of the jet.

Because the jet shows self-similarity, it is reasonable to compare single point measurements taken within the similarity region. It was decided to measure jet total pressure on the centre-line at a point four exit diameters from the exit plane. (A pitot-static probe was not used because a rapidly expanding jet experiences high static pressure gradients in both the axial and the radial directions (see Figure 8.1). Consequently, a pitot-static probe will measure the difference between the total pressure at one point, and the static pressure at another. Measuring total and static pressure would require doubling an already large number of experiments.) The single point measurements can be used to determine optimum geometric ratios because a lower centre-line velocity indicates more rapid spreading of the jet.

The results of these experiments are shown in Figures 8.3 and 6.1 to 6.5. It can be seen that if d_1/D and d_2/D are selected for a MLC nozzle, they can also be used in a LC nozzle if a longer cavity is used. However, the LC nozzle can operate over an even larger range of geometric ratios than is possible using the MLC nozzle.

8.2 Optimum Cavity Length using Blow-off Velocity

Because flame stability is influenced by the flow patterns produced by the nozzle, it is also possible to determine the optimum geometric ratios from combustion experiments. It was decided to measure the blow-off velocity (based on mean exit conditions) of flames stabilized by nozzles with a range of combinations of d_1, d_2 and l. Cavity length was varied for a systematically selected pair of orifice plates. At least three values of V_{bo} were measured for each configuration. The average of these values, along with representative values of scatter, are plotted in Figures 8.4 to 8.7.

8.3 Summary of optimum geometric ratios

The dependence of optimum cavity length on exit diameter for a given value of upstream orifice size can be seen in Figure 8.8 as determined using both these experiments and flame

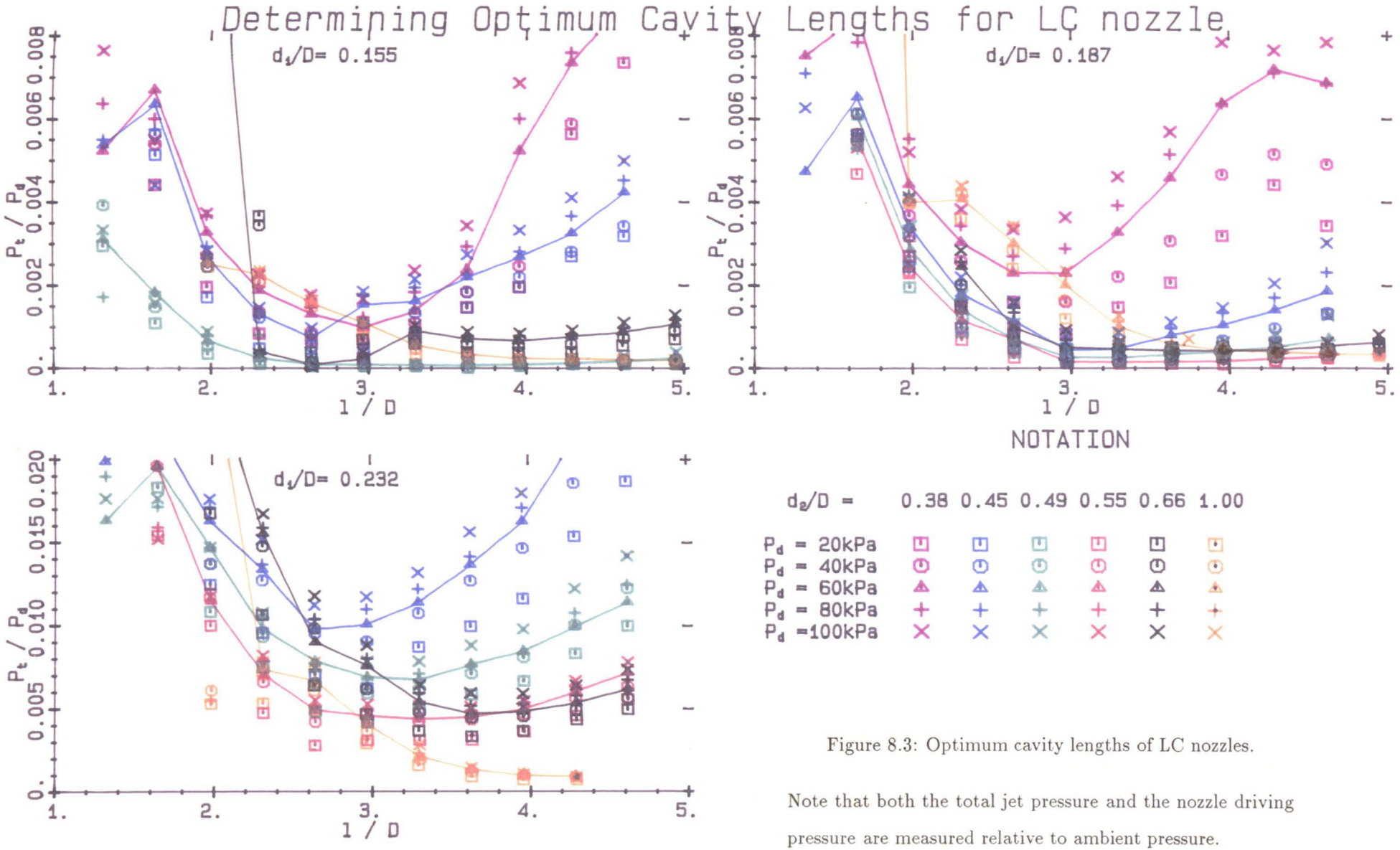

Figure 8.3: Optimum cavity lengths of LC nozzles.

Note that both the total jet pressure and the nozzle driving pressure are measured relative to ambient pressure.

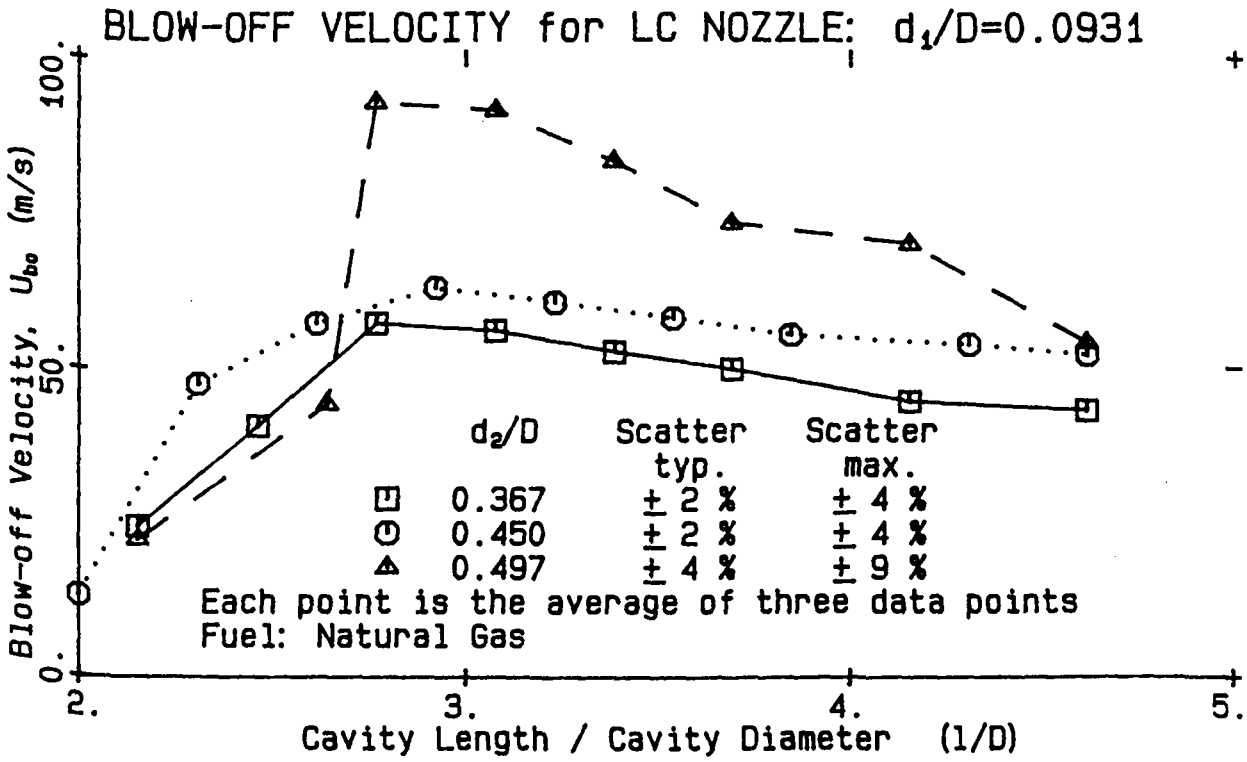

Figure 8.4: Optimum cavity lengths of LC nozzles determined from blow-off velocity; $d_1/D = 0.0931$

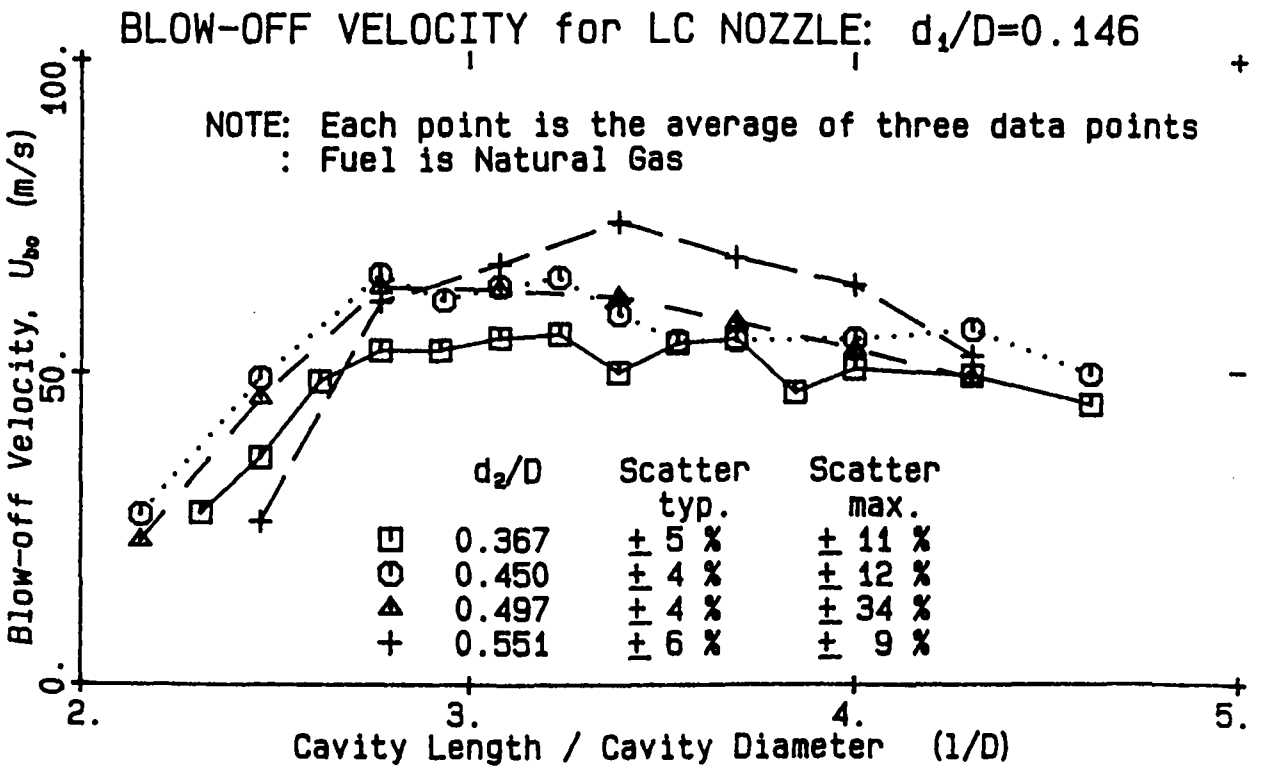

Figure 8.5: Optimum cavity lengths of LC nozzles determined from blow-off velocity; $d_1/D = 0.146$

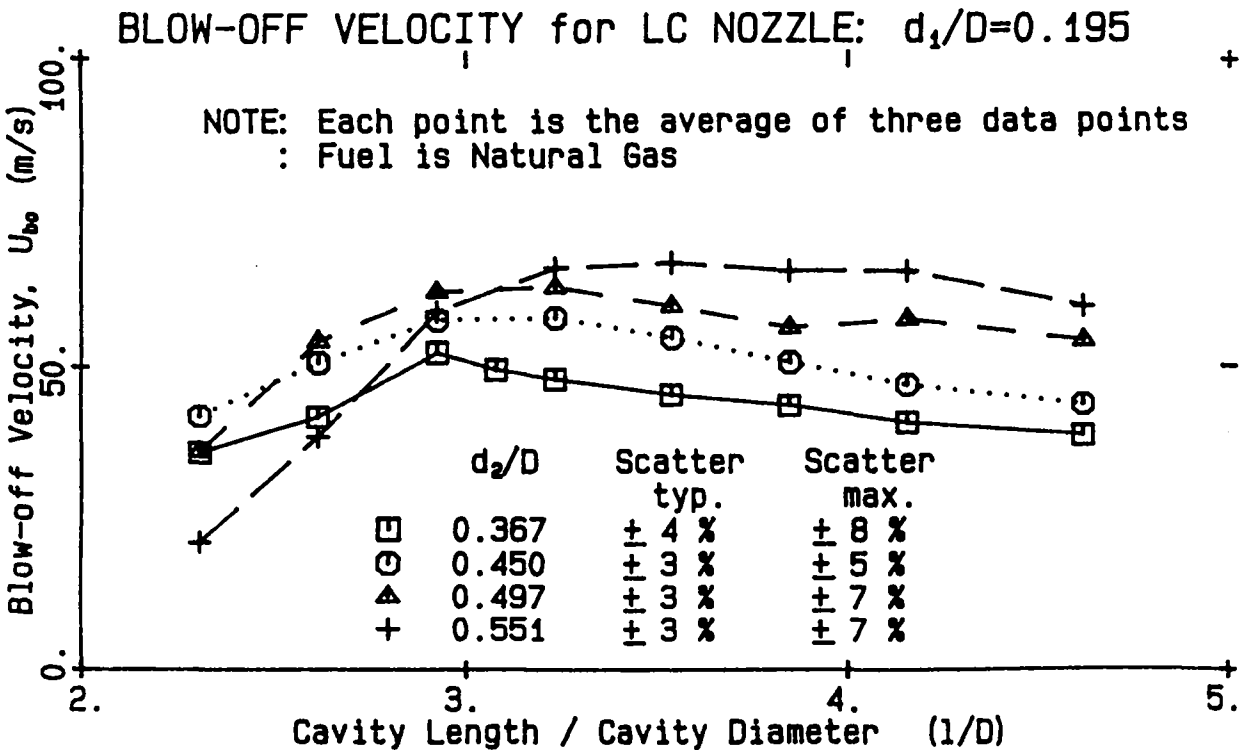

Figure 8.6: Optimum cavity lengths of LC nozzles determined from blow-off velocity; $d_1/D = 0.195$

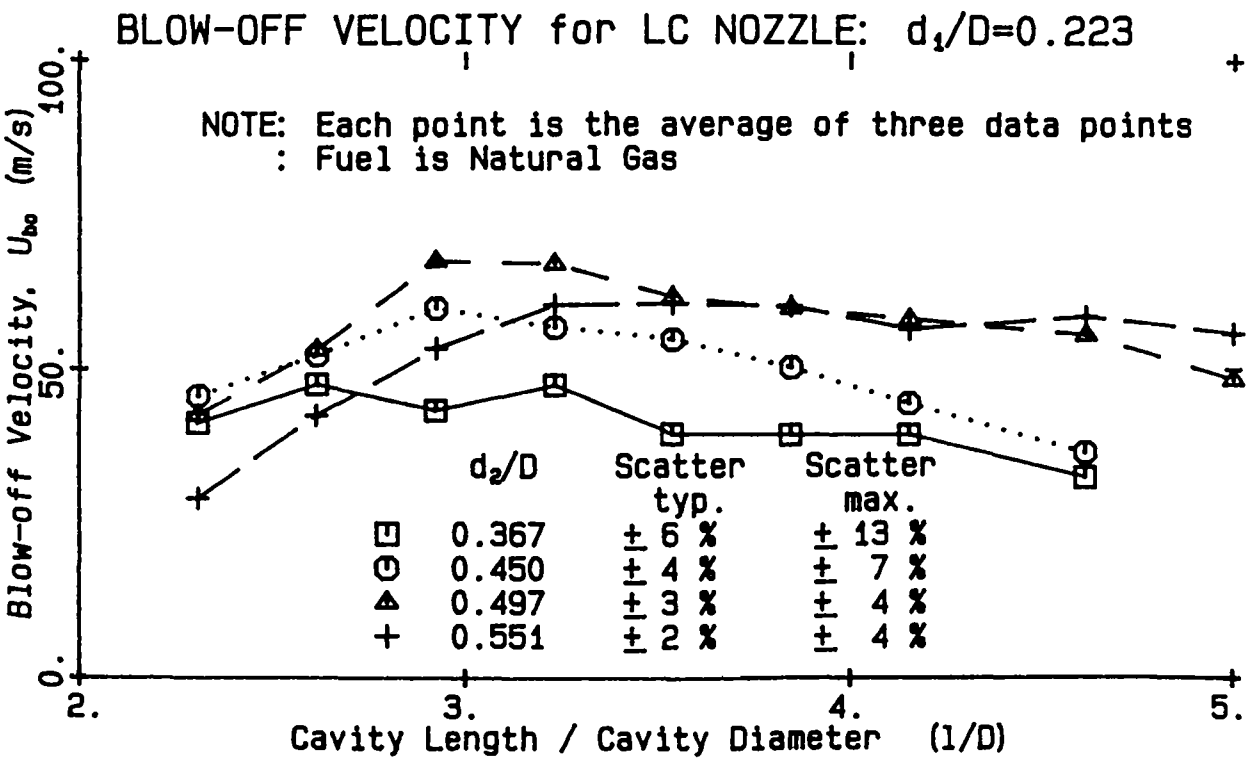

Figure 8.7: Optimum cavity lengths of LC nozzles determined from blow-off velocity; $d_1/D = 0.223$

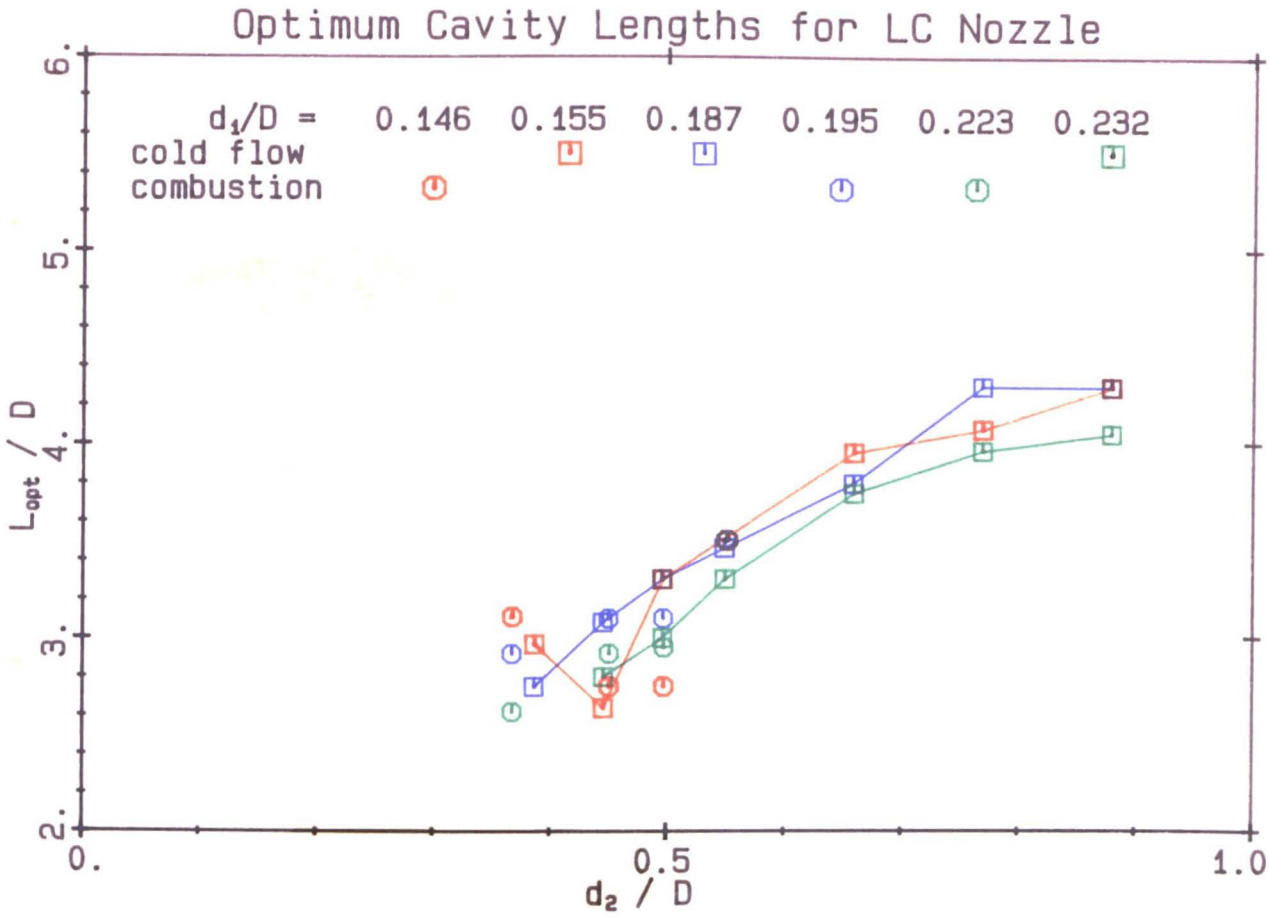

Figure 8.8: Optimum Geometric ratios of the LC nozzle determined from total pressure measurement on the nozzle centreline at $x = 3d_2$ from the exit plane.

blow-off velocity. It can be seen that cavity length increases nearly proportionally with exit diameter (except for part of the curve with the smallest value of d_1/D which shows a minimum at $d_2/D \approx 0.5$). Cavity length depends only weakly on d_1/D but there is a tendency for it to decrease with increasing d_1/D.

The latter result indicates that the important upstream geometric ratio is not d_1/D but h_1/D, which varies only slightly between the different nozzles. This is consistent with the results of other investigators [7], who find that the flow downstream of an orifice depends on h/D.

8.4 The Mechanism of the LC nozzle

8.4.1 Acoustic Frequency Spectra

Acoustic frequency spectra of the LC nozzle clearly show that it is not acoustically excited. The details of the characteristics associated with an acoustically excited nozzle are given in Section 7.2, where it is shown that the MLC nozzle is not acoustically excited. Consequently, in this section only the results are presented with a brief discussion.

The acoustic spectra of the LC nozzle for a range of flow rates can be seen in Figure 8.9. As found for the MLC nozzle, there are no distinct frequency peaks (other than those in the background noise), and the spectrum does not change significantly with flowrate, ie. there are no significant cut-on's of an acoustic resonance at a certain flowrate. As discussed in Section 7.2, this constitutes strong evidence that the enhanced mixing is not generated by acoustic excitation.

8.4.2 Flow patterns in the jet

In order to investigate the flow patterns produced by the LC nozzle, another flow visualisation technique was utilised; that of "smoke wires".

Apparatus

Four strands of 130 μm tungsten wire were suspended through the nozzle axis downstream of the exit plane. The wires are wiped with an oil impregnated rag. The oil, because of its surface tension, forms small droplets along the wires. The wires are then subjected to a short pulse (a few milli-seconds) of about forty volts. This heats the wire and causes the oil droplets to vapourise, so generating a smoke trace. A flash unit, positioned below and slightly behind the wires, is triggered by the pulse. A variable time delay exists between the pulse applied to the wires and the triggering pulse sent to the flash to allow sufficient time for the oil to vapourise and then be convected far enough by the flow to give an adequate picture of the streaklines. The experiments were conducted in darkness so that the shutter of the camera could be held open. The actual time of the voltage pulse, and the time delay between the pulse and the flash, were not recorded. The oil used was Concept Gene smoke oil.

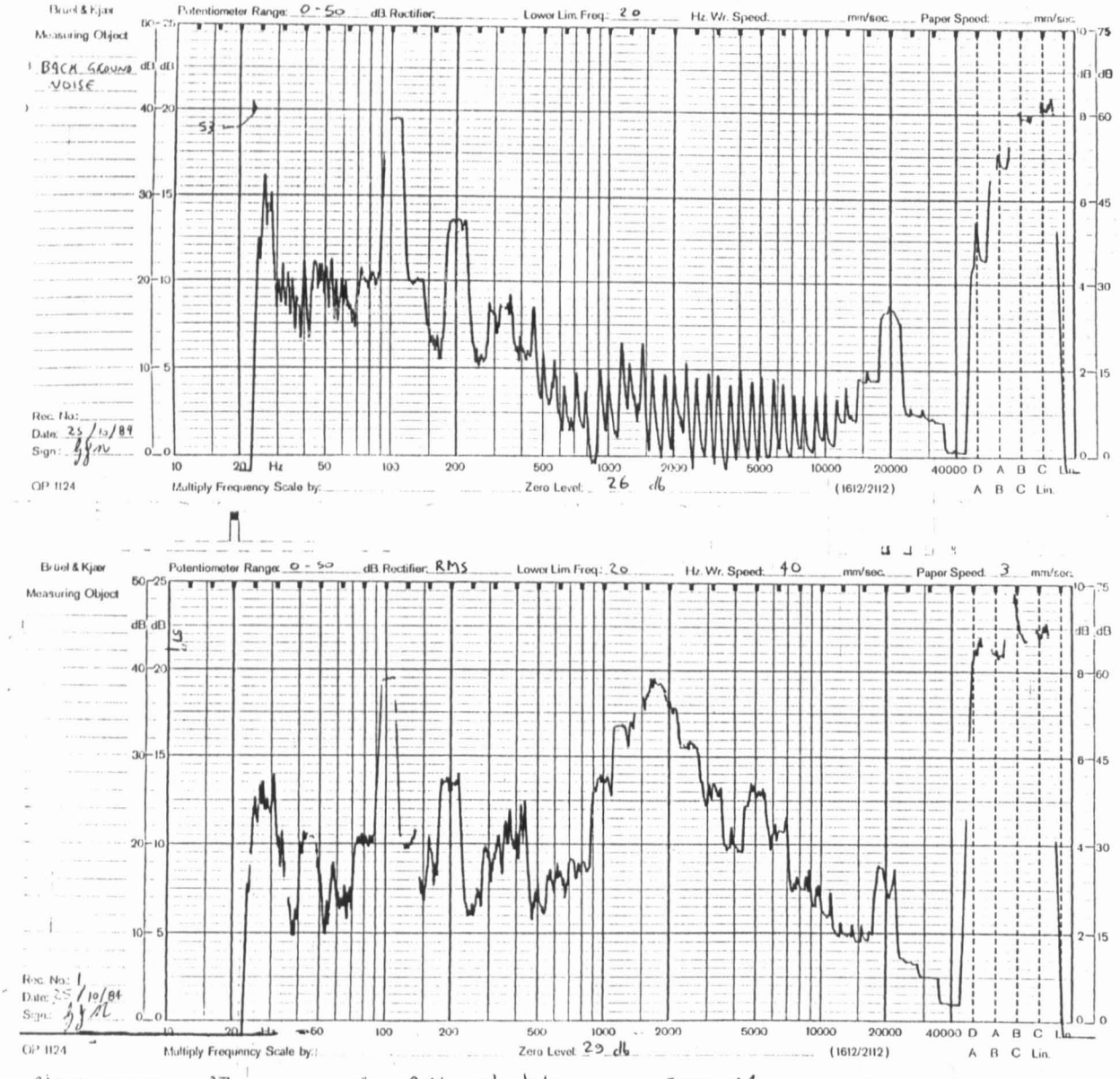

Figure 8.9: The acoustic frequency spectra of the LC nozzle.

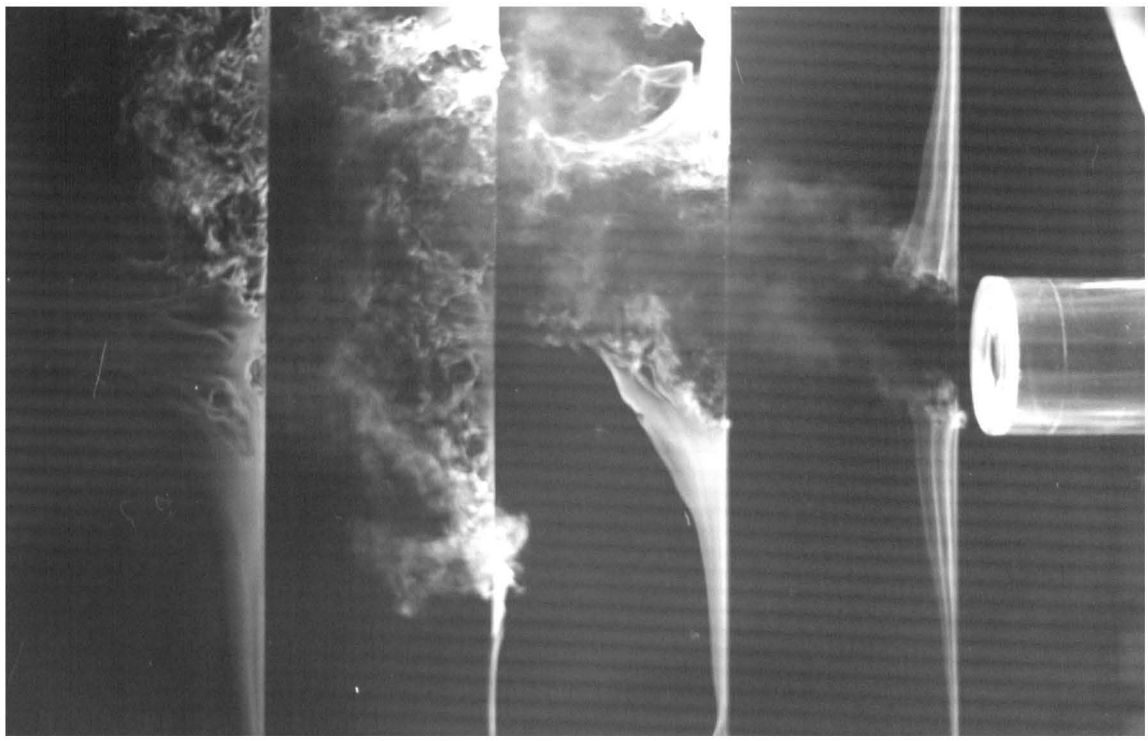

Figure 8.10: Smoke wire image of an instantaneous streakline pattern in the LC jet. – (a).

Results

The smoke wire traces shown in Figures 8.10 to 8.12 clearly show that the instantaneous jet leaving the LC nozzle is asymmetric. Because the trace captures a random event in the motion of the jet, it is to be expected that some photographs will display a greater degree of asymmetry than do others. Nevertheless, it appears that the instantaneous jet from the LC nozzle could well display a precessing motion analogous to, but not as asymmetric as, that of the MLC nozzle.

8.5 Conclusions

8.5.1 Apparent Mechanism

As has been mentioned, a detailed knowledge of the flow through the LC nozzle does not exist due to the limited investigation on this nozzle. Nevertheless, it is apparent that:

- The jet probably expands asymmetrically into the cavity. As discussed in Section 7.3, the expansion ratios are within the range expected for such an asymmetric expansion.
- l_{opt}/D depends upon d_2/D in such a way that if the jet within the cavity were to expand at a half angle of 4 deg from the upstream orifice, which is a typical value for a free

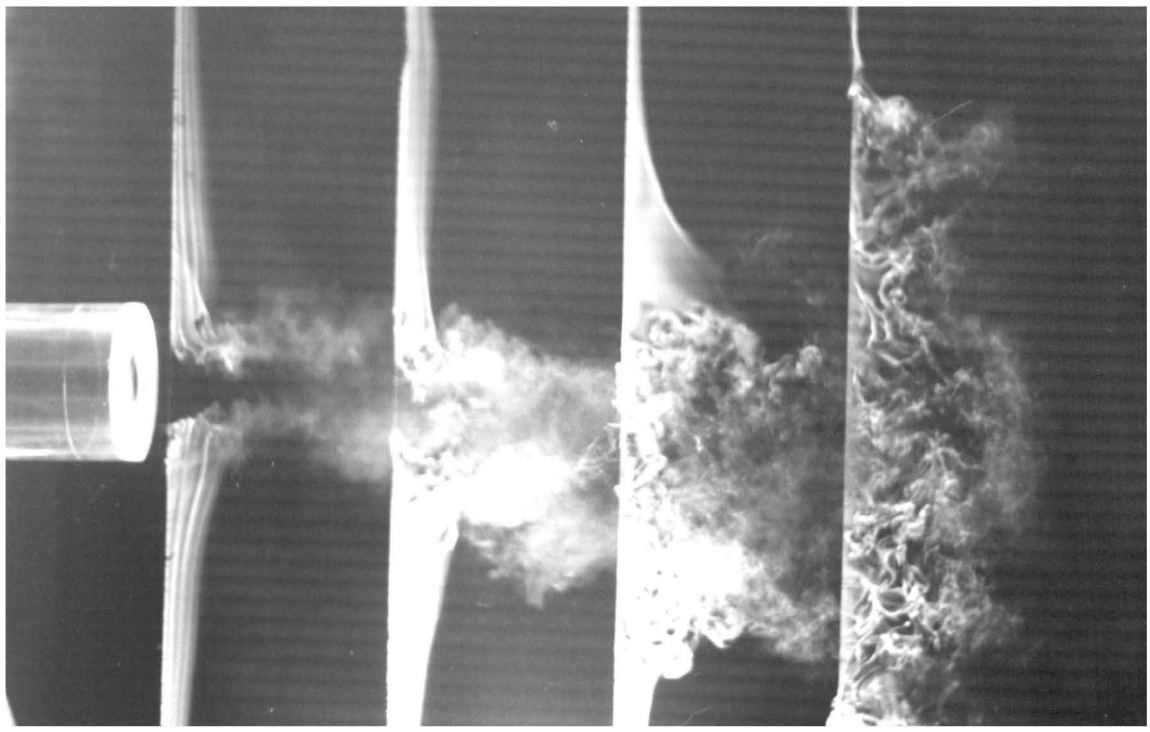

Figure 8.11: Smoke wire image of an instantaneous streakline pattern in the LC jet. – (b).

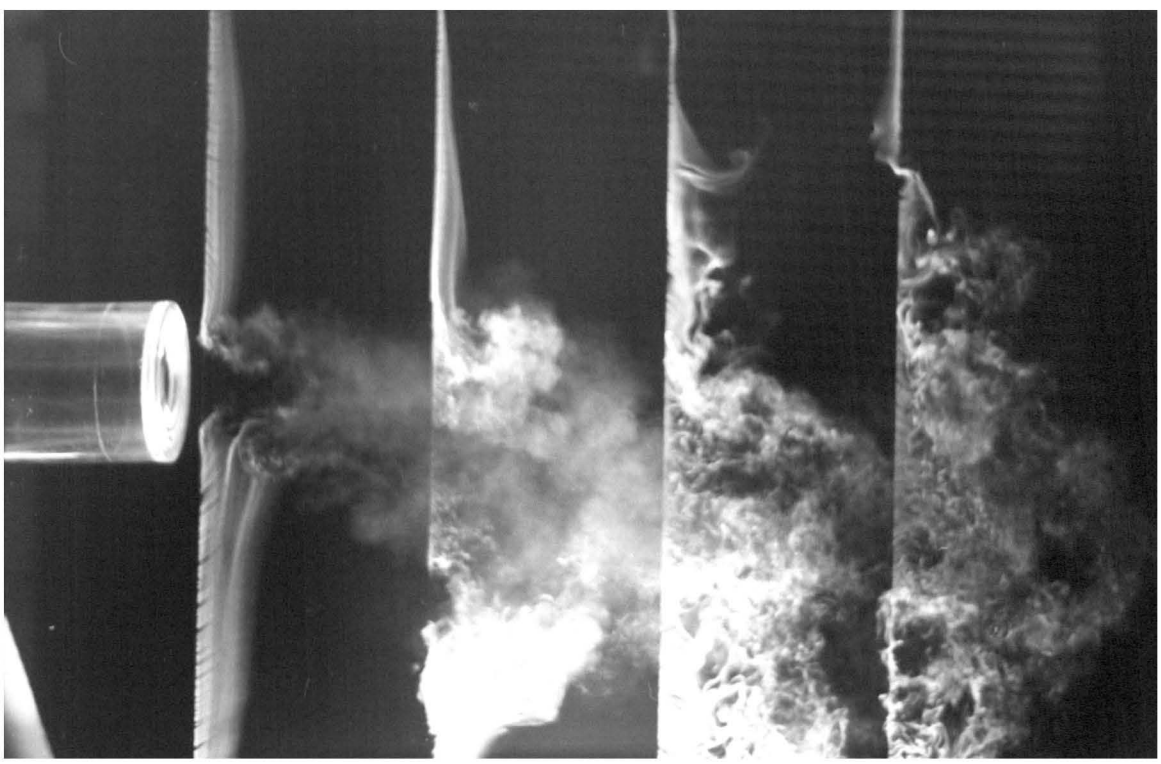

Figure 8.12: Smoke wire image of an instantaneous streakline pattern in the LC jet. – (c).

jet [93], then its diameter at the exit plane would approximately equal d_2. ie. l_{opt}/D increases with d_2/D. This implies that the jet which leaves the nozzle fills the exit plane.

- The MLC nozzle has a vena contracta just downstream of the exit plane (as shown in Figure 3.4). This is further evidence that the exiting jet fills the exit plane.
- The mean velocity profiles at the nozzle exit plane are symmetrical.
- It appears that the distance to the plane of (asymmetric?) reattachment is greater for the LC nozzle than for the MLC nozzle. (See Section 4.5.)
- The flow patterns of the jet downstream from the exit plane appear to be instantaneously asymmetric, in a manner analogous to, but but not as severe as, that of the MLC nozzle.
- The enhanced mixing is not caused by an acoustic resonance in the cavity.
- Dramatically increased rates of mixing relative to an unexcited jet are achieved, especially in the initial region of the jet.

From the above points, and from knowledge of the flow patterns in the MLC nozzle described in chapter 4, the following description of the flow within the nozzle seems likely.

The jet expands into the cavity from the throat in an asymmetric fashion, as in the MLC nozzle, because of the large expansion ratio. Because the length of the cavity is longer than that of the MLC nozzle, and/or the downstream orifice is smaller, the asymmetric jet expands sufficiently in its journey through the nozzle to fill the exit plane. As a consequence, it is not possible for ambient fluid to be entrained into the nozzle, and so the secondary flow patterns associated with the MLC nozzle cannot occur. Nevertheless, it seems highly unlikely that the flow within the LC nozzle are steady. Fluid from the reversed flow foot of the reattaching jet must return along the cavity wall and probably generates a motion similar to that in the MLC nozzle before being entrained into the jet. As the jet is almost certainly reattaching asymmetrically, it is inherently unstable and is likely to generate a precessing instability. It appears that the jet leaving the exit plane does precess in a manner similar to that of the MLC nozzle, but with a lot less asymmetry. Consequently, the mean jet retains a symmetric, bell-mouth shaped velocity profile throughout its length. Whilst the details of the motion are unknown, it is reasonable to suggest that this large scale motion is responsible for the observed increased rates of mixing.

8.5.2 Characteristics

- Spreading angles of a half jet of the order of 28 deg have been measured in cold flow.
- The blow off velocity (based on mean exit conditions) through the LC nozzle is not very different from that of a simple nozzle.
- The standoff distance (based on mean exit conditions) of the flame supported by an LC nozzle is a factor of about 2.5 times less than that of a simple nozzle.

Chapter 9

Conclusions

It has been found that the flow through an axi-symmetric, sudden expansion of sufficient magnitude will generate a precessing, highly asymmetric flow. If the length of the pipe into which the jet emanates is suitable, and if an appropriately sized lip is placed in the exit plane of the pipe, then the jet leaving this "nozzle" will instantaneously depart at an angle to the nozzle axis, and will precess. The resultant "Precessing Asymmetric Jet" has been found to generate very strong mixing over an extremely wide operating flow range. It has very high rates of entrainment, and consequently has potential application in many fields including combustion, ejectors, eductors and chemical processing plants.

Two broad flow types of flow patterns have been identified, seemingly dependent upon whether or not the instantaneous jet occupies all of the cross section of the exit plane. Because the instantaneous jet will expand in cross sectional area between the plane of the sudden expansion and the exit plane, this criteria will depend upon both the length of the cavity relative to its diameter, and the diameter of the exit plane relative to the cavity diameter. Consequently the nozzle which produces a jet which does not fill the exit plane has been dubbed the "Mid Length Cavity" (MLC) nozzle, and the nozzle whose jet does, the "Long Cavity" (LC) nozzle. (The term "Short Cavity" was avoided because jet excitation due to acoustic resonances within the cavity has been found to occur in "short" cavities.)

Because the jet in the exit plane of the MLC nozzle does not fully occupy the available exit area, the cavity is always vented to the atmosphere. Furthermore, the entrainment by the instantaneous jet within the nozzle cavity produces a sub-atmospheric pressure there. Thus it can be seen that there is an axial pressure gradient at the exit plane within the "vented area". The instantaneous jet reattaches asymmetrically to one circumferential part of the cavity, and

remains attached until it reaches the exit plane. Consequently, immediately downstream of the exit plane, one part of its circumference will be exposed to the vented area, and the other part to the atmosphere. This means that an asymmetric radial pressure gradient must exist across the jet, causing it to leave the nozzle at a large angle to the nozzle axis. The presence of the lip at the exit plane serves to increase the asymmetric radial pressure gradient.

By contrast, the instantaneous jet which leaves the LC nozzle is not exposed to an asymmetric radial pressure gradient in the exit plane. Nevertheless, there appears to be a precessing asymmetric pressure field within the cavity, causing the precessing jet to leave the nozzle at an angle to the nozzle axis. The forces imposed on the asymmetric jet in the exit plane by the LC nozzle are much weaker than those of the MLC nozzle. Consequently the spreading angles and entrainment appetite of the LC nozzle are also less than those of the MLC nozzle.

9.1 Evidence for the Postulated Flow Patterns

The flow patterns of the MLC nozzle have been investigated thoroughly, and a great deal of confidence can be placed in the postulated flow patterns. The flow patterns in the LC nozzle have been less thoroughly investigated, but the combination of the deductions relating to the MLC nozzle and the results of experiments conducted on the LC nozzle yield strong support for the postulate that it too involves jet precession.

Experimental evidence

The precessing motion of the MLC nozzle has been verified by the following experiments:

- High speed schlieren photography of the flow downstream of the exit plane.
- Visualisation of the flow patterns within the cavity using dye traces in water.
- Visualisation of a non-precessing, partially attached jet using smoke.
- Total and static pressure profiles downstream of the exit plane.
- Static pressure yaw meter measurements downstream of the exit plane.
- China clay surface flow visualisation.
- Hot wire anemometer measurements of the very low frequency precession motion, verified by dye visualisation experiments.

The following experiments indicate that the LC nozzle produces a jet with a precession motion:

- Smoke wire visualisation downstream of the exit plane.
- Total and static pressure profiles downstream of the exit plane.

Comparison with the literature

A comparison with the literature shows that:

- The expansion ratios in the MLC and LC nozzles are within the range where highly asymmetric flow would be expected, based on plane, two dimensional investigations. No investigation of the onset of azimuthal asymmetry behind axi-symmetric abrupt expansions has been found, although the simpler cases of flow over a backward facing step [33] and through a plane expansion [26,81] have been examined in some detail.
- The axial distance to the line of positive bifurcation (3-D reattachment), is much more comparable with a plane jet over a backward facing step which is open to the atmosphere on the other side of the jet [72], than a plane symmetric reattachment behind a sudden expansion.
- The Strouhal Number of the precession motion is remarkably similar to that of the well known low frequency "flapping" motion of a plane, 2-D jet.
- The mechanism is not acoustically excited.

9.1.1 Major experimental Results

Both the mechanism and the performance characteristics have been investigated for the MLC nozzle, whilst only the performance characteristics have been investigated for the LC nozzle.

Characteristics of the flow patterns

The major experimental findings for the MLC nozzle are:

- The Strouhal Number of the low frequency precession motion is constant when based of the following dimensions:
  - *precession frequency*, f_p
  - *mean velocity through the upstream orifice*, u_1

– *step height of the expansion*, h_1

- $St = f_p h_1 / u_1 \approx 0.005$
- The instantaneous jet typically leaves the nozzle at an angle of 60 deg.

Performance Characteristics of the MLC nozzle

Because the instantaneous jet which exits the MLC nozzle does not fill the exit plane of the nozzle, the physical dimensions of the nozzle are inappropriate for the scaling of characteristic parameters which can be compared with other nozzles. For this reason, an "equivalent exit diameter", d_{2eq} has been introduced. This is defined as the diameter, based on r_{half}, of the instantaneous jet in the exit plane of the nozzle. Whilst this diameter is the most appropriate scale for a comparison, it is less rigorous than a geometric dimension of the nozzle, and so comparisons are also made on the basis of the throat and exit diameters of the MLC nozzle. Combustion experiments have revealed the following characteristics:

- When compared with a simple, unswirled nozzle, a reduction in standoff distance by an order of magnitude based on both d_{2eq} and d_2 is achieved, whilst standoff distance is increased by a factor of two if the normalisation is based on d_1.
- In comparison with a simple, unswirled nozzle, increases in blow-off velocity based on d_{2eq} by a factor of four, and blow-off velocity based on d_1 by a factor of thirty are found. No significant change was found when v_{bo} was based on d_2.

Cold flow experiments have revealed:

- Spreading angles of the half jet of at least 70 deg.
- An increase in entrainment by a factor of five based on d_{2eq}, by an order of magnitude based on d_2 and by a factor of two based on d_1.

Performance Characteristics of the LC nozzle

Cold flow experiments have revealed the following characteristics:

- Spreading angles of the half jet of the order of 28 deg.

Combustion experiments have shown:

- A reduction in standoff distance based on mean exit conditions by a factor of about 2.5, when compared with a simple, unswirled nozzle.
- No significant change in the blow-off velocity compared with a simple nozzle when based on mean exit conditions.

9.1.2 Future Research

The present investigation has opened the door to a new means of generating large scale mixing using solely fluid mechanical means, and the means by which these scales are produced has been postulated. Nevertheless, the present investigation is of an introductory nature, and detailed flow measurements are yet to be made.

The low frequency precession motion of the jet generates very large scales of turbulent motion downstream from the exit plane. These large scales greatly enhance engulfment, the first stage of entrainment, but do not ensure that the mixing process is completed to the molecular level. It is the fine scales that must digest the engulfed fluid to complete the mixing process. This last phase is vital for complete combustion. Whilst fine scale motion is generated in the highly sheared motion of the instantaneous jet, the MLC nozzle in its present form does nothing to enhance those scales. Further work to measure the spectrum of scales which are produced and devise means which ensure that the engulfed fluid is properly digested would be profitable.

Detailed measurements of the flow within the cavity and the influence of a bluff body within the cavity would enable the phenomenon of intermittent enhancement to be more fully understood, thereby enabling a more effective solution to be implemented.

9.2 Potential Applications

An enhanced mixing jet has potential application in both combusting and non-combusting fields. However, the flow patterns produced by the "MLC nozzle", when used with a bell mouth contraction and expansion at the throat, also has application as a means of producing of a vectored jet.

9.2.1 Combustion Systems

Both of the enhanced mixing nozzles (LC and MLC) described in the present investigation have been demonstrated to provide improved flame stability when burning gas in an unconfined environment (free air). Further research is required to investigate their performance characteristics in a confined (furnace) space with the presence of surrounding air flows, and in the combustion of particulate (solid) or sprayed (liquid) fuels.

Applications where improved flame stability would be advantageous include:

- the combustion of low grade fuels such as gasified coal ("town gas"), bio-waste gas and low grade pulverised coal. The gasification of coal has the advantage of enabling pollutants such as sulphur and phosphorous to be removed prior to combustion within the furnace, thereby reducing environmental damage as well as eliminating the expensive exhaust clean up operations and furnace corrosion problems associated with the particulate combustion of many coals. The combustion of gasified coal is made more viable if there are not strict tolerances on the quality of the gas which may otherwise require it to be upgraded prior to combustion;

- the conversion of furnaces or boilers from oil firing to gas firing. Using current technology, is is frequently necessary to de-rate the plant after conversion because of combustion instabilities at high gas throughputs.

- high intensity combustion in gas turbines and ram jets.

The shape of the flame produced by the MLC nozzle is short and bulbous in comparison with that produced by a simple, unswirled nozzle, and it is established much closer to the nozzle tip. In many applications this is a desirable feature because the flame will fit in a smaller furnace and is less likely to excite the system instabilities often generated by an oscillating flame front.

In some furnace applications it is desirable to produce a flame with high axial momentum in order to drive large scale furnace-vortex structures, or to augment convective heat transfer coefficients downstream of the flame. In such applications the LC nozzle may prove to be more desirable than the MLC nozzle, although a suitably shaped "Vortex Burst Shroud", such as described in "PATENT PENDING; application number PI4068/87" [59], could be used to provide a high momentum in the flame produced by the MLC nozzle.

9.2.2 Ejectors and Eductors etc.

The capacity of a jet to entrain or mix with a surrounding fluid is utilized in various non-combusting applications such as ejectors, eductors, mixing in chemical processing plants and thrust augmenting nozzles. These mixing devices can either be reduced in size and weight or increased in efficiency if the entrainment appetite of the jet is increased. Consequently application is envisaged in:

- Eductors - which are used to produce a modest pressure rise in a large mass of fluid by injection of a small mass of high pressure fluid (eg. to raise LP steam to a useable state).
- Ejectors - which are used to induce a mass flow through the system (eg. a vacuum pump)
- Rocket assisted Ram-jets - which use a high temperature and pressure jet to entrain the surrounding air, thus producing a greater mass flow through the system than would occur simply through forward flight.

9.2.3 Vectored Jets

If the throat in the MLC nozzle is carefully shaped to a convergent-divergent profile, it is possible to cause the instantaneous jet to be *partially* attached to the inner surface of the nozzle along the entire length of the nozzle. In this case, the secondary flow patterns which occur within the enhanced mixing MLC nozzle cannot occur, and the jet does not precess. However, it still leaves the exit plane of the nozzle at a large angle to the nozzle axis, the exact value of which depends on the geometric configuration of the rest of the nozzle. If the throat is perfectly symmetrical in the azimuthal plane, there will be no preferred azimuthal position for the jet. However, the introduction of a small protuberance at a point on the surface of the throat will cause the jet to separate there and partially attach along the opposite side of the cavity. Hence it can be seen that a circumferential array of suitable protuberances can be inserted around the periphery of the nozzle throat can be used to control the direction with which the jet leaves the nozzle. Such a system could have application in providing rapid change in the direction of the thrust in rockets, missiles and V/STOL and high performance aircraft.

Bibliography

[1] Abbot,D.E. and Kline,S.J. (1962) "Experimental Investigation of Subsonic Turbulent Flow over Single and Double Backward Facing Steps", *Trans. ASME, J. Basic Engineering*, 84, Ser.D, 317–325.

[2] Abdel-Fattah A.M. (1984) "A Theoretical Study of Two Stage Thrust Augmenting Ejectors", *Aero-Propulsion Report 166* AR-003-973.

[3] Abell,C.J. (1977) "Acoustic Coupling in a Turbulent Flow", *Sixth Australasian Hydraulics and Fluid Mechanics Conference (Adelaide)*, pp 41–45.

[4] Abell,C.J. and Luxton,R.E. (1979) "Progress Report SENRAC Project P45 to June 1979", *Dept. of Mech. Eng. University of Adelaide.*

[5] Abell,C.J. and Luxton,R.E. (1980) 'NERDDP/SENRAC Grant 79/9174, "Mixing Enhancement in Combusting Flows, Progress Report June 1980" ', *Dept. of Mech. Eng. University of Adelaide.*

[6] Abell,C.J. and Luxton,R.E. (1981) 'NERDDP Projects 79/9174,80/0336,SENRAC Project P45., "Mixing Enhancement in Combusting Flows, Technical Progress Report June 1980–Dec 1981" ', *Dept. of Mech. Eng. University of Adelaide.*

[7] Agarwal,N.K. (1986) "Relationship between Internal Sound Generation and Characteristics of Flow in a Region of Flow Separation due to disturbance of Fully Develloped Turbulent Flow in a Pipe.", *PhD Thesis, University of Adelaide, Dept. of Mech. Eng.*

[8] Armaly,B.F.,Durst,F.,Perica,J.C.F. and Schonung,B. (1983) "Experimental and Theoretical Investigation of Backward Facing Step Flow", *J. Fluid Mech.*, **127**, 473–496.

[9] Badri Narayanan,M.A. (1987) "Excitation of Plane Jet by Twin Vane Oscillator: A Preliminary Investigation" *Report No. AE 87 FM 1, Interim Report, Fluid Dynamics Laboratory, Department of Aerospace Engineering, Indian Institute of Science, Bangalore.*

[10] Badri Narayanan,M.A. and Platzer,M,F. (1987) "The Mixing Mechanism by Organised Turbulence Structures in a Plane Jet Excitedegion", by a Novel Method", *Proceedings of the IUTAM Symposium on Turbulence Management and Relaminarisation, 19–23 Jan., 1987, Bangalore*, To be published in Springer-Verlag.

[11] Badri Narayanan,M.A. and Platzer,M,F. (1987) "Jet Excitation by a Bivane System and its application to an Ejector for Thrustegion", Augmentation", *Report No. NPS-67-87-004, Naval Postgraduate School, Monterey, California.*

[12] Badri Narayanan,M.A. and Raghu,S. (1982) "Two Dimensional Jet Subjected to Periodic Oscillations in the Potential Core Region", *Report No. 82FM2, Fluid Dynamics Lab., Dept. Aeronautical Engineering, Indian Institute of Science.*

[13] Bafuwa,G.C. and Maccallum,N.R.L. (1973) "Flame Stabilization in Swirling Jets", *Proc. Combustion Instute - European Symposium, Sheffield University*, pp 565–570.

[14] Beer,J.M. and Chigier,N.A. (1972) "Combustion Aerodynamics", Applied Science Publishers

[15] Binder,G. and Favre-Marinet,M. (1981) "Some Characteristics of Pulsating or Flapping Jets", *Michel,R.,Cousteix, J. and Houdeville (editors),"Unsteady Turbulent Shear Flows"*, Toulouse, France, pp.370–379, Springer-Verlag.

[16] Boersma,D. (1973) "Flame Stabilization and Heat Transfer in a Cylindrical Furnace", *Proc. Combustion Institute — European Symposium, Sheffield University*, pp 615–620.

[17] Bosio,M.,Linder,E.R.,Borio,R.W.,Hein,K.R.G. (1984) "Utilization of Fouling/Slagging/Corrosive Low Rank Coals — New Developments in South Australia", *Third Engineering Foundation Conference on Slagging/Fouling due to Impuriries in Combustion Gases*, July/August, Colorado.

[18] Bradbury,L.J.S. and Khadem,A.H. (1975) "The Distortion of a Jet by Tabs", *J. Fluid Mech.*, **170**, (4), 801–813.

[19] Bradshaw,P. (1970) "Experimental Fluid Mechanics", Second Edition, Pergamon Press.

[20] Bradshaw,P. and Pankhurst,R.C. (1961) "The Design of Low Speed Wind Tunnels". *NPL Aero. Rept. 1039, ARC 24041.*

[21] British Standard 1042: Part 1: (1964) "Methods for the Measurement of Fluid Flow in Pipes, Part 1. Orifice Plates, Nozzles and Venturi Tubes".

[22] Broadwell,J.E.,Dahm.W.J.A. and Mungal,M.G. (1984) "Blowout of Turbulent Diffusion Flames", *Twentieth Symposium (International) on Combustion, The Combustion Institute*, 303–310.

[23] Brown,G.L. and Lopez,J.M. (1988) "Axisymmetric Vortex Breakdown, Part 2: Physical Mechanisms" *Aero. Rept. 174, AR-004-573*, Aeronautical Research Laboratories, Melbourne.

[24] Brown,G.L. and Roshko,A. (1974) "On Density Effects and Large Structure in Turbulent Mixing Layers", *J. Fluid Mech.*, **64**, (4), 775–816.

[25] Cervantes de Gortari,J. and Goldschmidt,V.W. (1981) "The Apparent Flapping Motion of a Turbulent Plane Jet — Further Experimental Results", *A.S.M.E. Transactions, Journal of Fluids Engineering*, **103**, 119–126.

[26] Cherdron,W.,Durst,F. and Whitelaw,J.W. (1978) "Asymmetric Flows and Instabilities in Symmetric Ducts with Sudden Expansions", *J. Fluid Mech.*, **84**, 13–31.

[27] Chigier,N.A. (1981) "Energy, Combustion and Environment", McGraw-Hill.

[28] Cimbala,J., Nagib,H. and Roshko,A. (1981) "Wake Instability Leading to New Large Scale Structures Downstream of Bluff Bodies", *Bull. Am. Phys. Soc. SerII*, **26**, 1256.

[29] Claypole,T.C. and Syred,T.C. (1981) "The Effect of Swirl Burner Aerodynamics on NO_x Formation", *Eighteenth Symposium (International) on Combustion - The Combustion*

Institute,

pp 81–89

[30] Claypole,T.C. and Syred,N. (1982) "The Stabilization of Flames in Swirl Combustors", *Journal of the Instute of Energy*, vol **55**, pp14–19.

[31] Crow,S.C. and Champagne,F.H. (1971) "Orderly Structure in Jet Turbulence", *J. Fluid Mech.*, **48**, (3), 547–591.

[32] Driver,D.M., Seegmiller,H.L. and Marvin,J.G. (1987) "Time Dependent Behavior of a Reattaching Shear Layer", *AIAA Journal*, **25**, (7), 914–919.

[33] Eaton,J.K. and Johnston,J.P. (1981) "A Review of Research on Subsonic Turbulent Flow Reattachment", *AIAA Journal*, **19**, (9), 1093–1100.

[34] El-Mahallawy,F.M.,Farag,S.A. and Yowakim,F.M. (1978) "Effect of Some Parameters on the Radiant Heat Transfer in a Cylindrical Oil Fired Furnace", *Khalil K.H. (editor) Heat and Mass Transfer*, vol.2, *'Flow, Mixing and Heat Transfer in Furnaces'*, Pergamon Press.

[35] Engineering Science Data Unit (1972) Fluid Mechanics, Internal Flow. Volume 3: Ducts, Fittings and Equipment, No. 72009, "Pressure Drops in Ducts across Round-Wire Gauses normal to the flow".

[36] Engineering Science Data Unit (1972) Fluid Mechanics, Internal Flow. Volume 3: Ducts, Fittings and Equipment, No. 72010, "Pressure losses across perforated plates, orifice plates and cylindrical tube orifices in ducts".

[37] Engineering Science Data Unit (1972) Fluid Mechanics, Internal Flow. Volume 4: Ducts Expansions, Duct Contractions, No. 73024, "Performance of Connical Diffusers in Incompressible Flow".

[38] Favre-Marinet,M.,Binder,G. and Hac,Te.V. (1981) "Generation of Oscillating Jets", *A.S.M.E. trans. Journal of Fluids Engineering*, **103**, 609–614.

[39] Fricker,N. and Leuckel,W. (1976) "The Characteristics of Swirl Stabilized Natural Gas Flames. Part 3: The Effect of Swirl and Burner Mouth Geometry on Flame Stability", *J. Institute of Fuel*, Sept. 1976 pp 152.

[40] Galea,S.C. and Simmons,J.M. (1983) "Excitation of a Plane Jet by Periodic Perturbation of the Nozzle Area", *Eigth Australasian Fluid Mechanics Conference, University of Newcastle, NSW.*

[41] Gupta,A.K.,Beer,J.M. and Swithenbank,J. (1976) "Concentric Multi-Annular Swirl Burner — Stability Limits and Emission Characteristics", *Sixteenth Symposium (International) on Combustion, The Combustion Institute*, pp 79–91.

[42] Hill,W.G.Jr. and Greene,P.R. (1977) "Increased Turbulent Jet Mixing Rates Obtained by Self Excited Acoustic Oscillations", *J. Fluids Engineering.*, **99**, 520–525.

[43] Hornung,H. and Perry,A.E. (1984) "Some Aspects of Three Dimensional Separation, Part I: Streamsurface Bifurcations", *Z. Flugwiss. Weltraumforsch.*, 8, Heft 2, 77–87.

[44] Hunt,J.C.R.,Abell,C.J.,Peterka,J.A. and Woo,H. (1978) "Kinematical Studies of the Flows around Free or Surface-Mounted Obsticles; Applying Topology to Flow Visualisation", *J. Fluid Mech.*, **86**, (1), 179–200.

[45] Hussian,A.K.M.F. and Hasan,M.A.Z. (1983) "The 'Whistler Nozzle' Phenomenon", *J. Fluid Mech.*, **134**, 431–458.

[46] Ito,K. and Sasaki,M. (1984) "Stabilization of a Round Jet Flame with a Recirculation Zone in Parallel Air Flow", *Bulletin of J.S.M.E.*, **27**, (231), 1951–1956.

[47] Johnson,W.T. (1986) "Procedures for Noise Radiation Prediction from Pipes with Choked Valve Flow" *Postgraduate Progress Report, Dept. Mech. Eng., University of Adelaide.*

[48] Kawall,J.G. and Keffer,J.F. (1981) "The Role of Coherent Structures in the Develpment Region of a Uniformly Strained Turbulent Wake", *Turbulent Shear Flows 3, Ed. Bradbury,L.J.S., Durst,F., Launder,B.E., Schmidt,F.W. and Whitelaw,J.H.*, 132–145.

[49] Kremer,H.,Minx,E. and Rawe,R. (1973) "Stabiliztion of Parallel-Flow Turbulent Jet Diffusion Flames by Means of Flame Holders", *Proc. Combustion Institute, European Symposium, Sheffield University*, pp 536–541.

[50] Koochesfahani,M.M. and Dimotakis,P.E. (1986) "Mixing and Chemical Reactions in a Turbulent, Liquid Mixing Layer", *J. Fluid Mech.*, **170**, 83–112.

[51] Lai,J.C.S. and Simmons,J.M. (1980) "Instantaneous Velocity Measurements in a Pulsed, Plane Turbulent Jet", *AIAA Journal*, **18**, 1532–1534.

[52] Lai,J.C.S. and Simmons,J.M. (1985) "Instantaneous Velocity Measurements in a Vane-Excited Plane Jet", *AIAA Journal*, **23**, (8), 1157–1164.

[53] Lee,H.S. (1982) "Turbulent Jet Noise and Structure", *Ph.D. Thesis, Department of Mech. Eng., University of Adelaide.*

[54] Lepicovsky,J.,Ahuja,K.K. and Sulikuddin,M. (1986) "An Experimental Study of Tone Excited Heated Jets", *J. Propulsion* **2**, 149–154, March–April.

[55] Leuckel,W. and Fricker,N. (1976) "The Characteristics of Swirl Stabilized Natural Gas Flames. Part 1: Different Flame Types and their Relation to Flow and Mixing Patterns.", *Journal of the Institute of Fuel*, pp 103.

[56] Lopez,J.M. (1988) "Axisymmetric Vortex Breakdown, Part 1: Confined Swirling Flow" *Aero. Rept. 173, AR-004-572*, Aeronautical Research Laboratories, Melbourne.

[57] Ludweig,H. and Hornung,H. (1986) "The Instability of a Liquid Film on a Wall Exposed to an Air Flow", *D.F.V.L.R., Institute for Experimental Fluid Mechanics, D-3400, Gottingen, Bunsenstr. 10, FRG.*

[58] Luxton,R.E. (1985) "Mixing Enhancement in Combusting Flows – End of Grant Report", National Energy Research, Development and Demonstration Program. *Department of Resources and Energy, Australian Government, Canberra.*

[59] Luxton,R.E., Nathan,G.J. and Luminus Pty. Ltd. (1987) "Mixing of Fluids", *Patent Application Number PI4068/87, Australian Patent Office.*

[60] Manheimer-Timnat,Y.,Segal,A. and Wolfshtein,M. (1973) "Swirling Natural Gas Flames in Cylindrical Chambers", *Proc. Combustion Institute, European Synposium, Sheffield University*, pp. 571–576.

[61] Morse,P.M. and Ingard,K.U. (1968) "Theoretical Acoustics", *McGraw-Hill,Inc.*

[62] Mungal,M.G. and Dimotakis,P.E. (1984) "Mixing and Combustion with Low Heat Release in a Turbulent Mixing Layer", *J. Fluid Mech.*, **148**, 349–382.

[63] Mungal,M.G., Dimotakis,P.E. and Broadwell,J.E. (1984) "Turbulent Mixing in a Reacting Shear Layer", *AIAA Journal*,**22**,(6),797–800.

[64] Mungal,M.G. and O'Neil,J.M. (1988) "Visual Observations of a Turbulent Diffusion Flame", *submitted to Combustion and Flame*,

[65] Nathan,G.J. (1983) "Combustion Characteristics of Low Calorific Value Gases in an Enhanced Mixing Burner", *Final Year Research Project, University of Adelaide, Dept. Mech. Eng.*

[66] Nathan,G.J. and Luxton,R.E. (1984) "Discussion of 'Some Studies of Non-Simple Pipe Flows' – K.R.Sreenivasan", *Trans. I.E. Aust.*, Vol(**ME9**), 163–164.

[67] Nathan,G.J. and Luxton,R.E. (1988) "A Stable, Un-Premixed Gas Burner with Infinite Turn-Down Ratio", *First European Conference on Industrial Furnaces and Boilers*, March 1988, Lisbon, Portugal.

[68] Novick,A.S.,Miles,G.A. and Lilley,D.G. (1979) "Modeling Parameter Influences in Gas Turbine Combustor Design", *J. Energy*, **3**, (5), 257–262. (Article No.79-035R).

[69] Odgers,J.,White,I. and Kretschmer,D. (1980) "The Experimental Behavior of Premixed Flames in Tubes (The Effects of Dilutant Gases)", *Engineering for Power*, **102**, (2), 422–426.

[70] Ouwa,Y.,Watanabe,M. and Asawo,H. (1981) "Flow Visualisation of a Two Dimensional Water Jet in a Rectangular Channel", *Japanese Journal of Applied Physics*, **20**, (1), 243–247.

[71] Parekh,D.E., Reynolds,W.C. and Mungal,M.G.(1987) "Bifurcation of Round Air Jets by Dual-Mode Acoustic Excitation", *AIAA Paper 87-0164.*

[72] Pelfrey,J.R.R. and Liburdy,J.A. (1986) "Mean Flow Characteristics of a Turbulent Offset Jet"
J. Fluids Eng., Trans. A.S.M.E., **108**, 82–88.

[73] Pelfrey,J.R.R. and Liburdy,J.A. (1986) "Effect of Curvature on the Turbulence of a Two-Dimensional Jet" *Experiments in Fluids, Springer-Verlag*, **4**, 143–149.

[74] Perry,A.E. (1982) "Hot-Wire Anemometry", *Clarendon Press, Oxford.*

[75] Perry,A.E. and Chong,M.S. (1987) "A Description of Eddying Motions and Flow Patterns using Critical Point Concepts", *Ann. Rev. Fluid Mech.*, **19**, 125–155.

[76] Perry,A.E. and Hornung,H. (1984) "Some Aspects of Three Dimensional Separation, Part II: Vortex Skeleton", *Z. Flugwiss. Weltraumforsch.*, **8**, Heft 3, 155–160.

[77] Piatt,M. and Vietts,H. (1979) "Conditioned Sampling in an Unsteady Jet", *A.I.A.A. paper*
79-1857.

[78] Presser,C.,Greenberg,J.B.,Goldman,Y. and Timnat,Y.M. (1982) "A Numerical Study of Furnace Flame Root Stabilization using Conical Burner Tunnels", *Ninteenth Symposium (International) on Combustion, The Combustion Institute,* pp 519–527.

[79] Quinn,B.(Aug.1973) "Compact Ejector Thrust Augmentation", *J.Aircraft*, vol 10, No. 8,
pp 416–486.

[80] Rawe,R. and Kremer,H. (1981) "Stability Limits of Natural Gas Diffusion Flames with Swirl", *Eighteenth Symposium (International) on Combustion, The Combustion Institute.*

[81] Restivo,A. and Whitelaw,J.H. (1978) "Turbulence Characteristics of the Flow Downstream of a Symmetric, Plane Sudden Expansion", *ASME Trans., J. Fluids Eng.*, 100, 308–310.

[82] Ricou,P.F. and Spalding,D.B. (1961) "Measurement of Entrainment by Axisymmetrical Turbulent Jets", *J. Fluid Mech.*, *11*, 21–32.

[83] Rockwell,D. (1983) "Oscillations of Impinging Shear Layers", *A.I.A.A. Journal*, 21, (5), 645–664.

[84] Rockwell,D. and Naudascher,E. (1979) "Self-Sustaining Oscillations of Impinging Free Shear Layers", *Annual Review of Fluid Mechanics*, 11, 67–94.

[85] Simmons,J.M.,Lai,J.C.S. and Platzer,M.F. (1981) "Jet Excitation by an Oscillating Vane", *AIAA Journal*, 19, (6), 673–676.

[86] Simmons,J.M.,Plazer,M.F. and Smith,T.C. (1978) "Velocity Measurements in an Oscillating Plane Jet Issueing into a Moving Air Stream", *J. Fluid Mech.*, 84, (1), 33–53.

[87] Sreenivasan,K.R. (1983) "Some Studies of Non-Simple Pipe Flows", *Eighth Australasian Fluid Mechanics Conference, University of Newcastle, N.S.W.* ppK7.1–K7.8.

[88] South Australian Advisory Committee on Future Electricity Generating Options (1984)
vol1 "Main Report"
vol2 "Possible Contribution of Alternative Energy Sources"
vol3 "Long Term Development Options of South Australian Coals"
South Australian Department of Mines and Energy.

[89] Spalding,D.B. (1953) "Theoretical Aspects of Flame Stabilization", *Aircraft Engineering*, XXV (295), pp 264–268 & 276.

[90] Syred,N. and Beer,J.M. (1974) "Combustion in Swirling Flows: A Review", *Combustion and Flame* vol 23, 143–201.

[91] Syred,N.,Dahmen,K.R.,Styles,A.C. and Najim,S.A. (1977) "A Review of Combustion Problems Associated With Low Calorific Value Gases", *Journal of the Institute of Fuel*,

Dec.1977,

pp 195–207.

[92] Taylor,G.I. (1923), "Stability of a Viscous Liquid contained between Two Rotating Cylinders", *Roy. Soc. London, Phil. Trans.*, **A.**, **223**, 289.

[93] Tennekes,H. and Lumley,J.L. (1972) "A First Course in Turbulence", MIT Press.

[94] Tobak,M. and Peake,D.,J. (1982) "Topology of Three Dimensional Separated Flows", *Ann. Rev. Fluid Mech.*, **14**, 61–85.

[95] Viets,H. (1975) "Flip-Flop Jet Nozzle", *AIAA Journal*, **13**, (10), 1375–1379.

[96] Welsh,M.C. and Gibson,D.C. (1979) "Interaction of Induced Sound with Flow Past a Square Leading Edged Plate in a Duct", *J. Sound and Vibration*, **67**, (4), 501–511.

[97] Welsh,M.C., Stokes,A.N. and Parker,R. (1984) "Flow-Resonant Sound Interaction in a Duct Containing a Plate, Part I: Semi-Circular Leading Edge", *J. Sound and Vibration*, **95**, (3), 305–323.

[98] Wendt,J.O.L. (1980) "Fundamental Coal Combustion Mechanisms and Pollutant Formation in Furnaces", *Prog. Energy Combust. Sci.*, **6**, 201–222. Pergamon Press.

[99] Williams,R.G. and Manzoori,A.R. (1987) "Utilization of South Australian Low Rank Coals for Power Generation", *Coal Power '87, The AusIMM Annual Conference, Newcastle, NSW.*

Appendix A

Detail Drawings: $D = 13$mm

Enhanced Mixing Burner

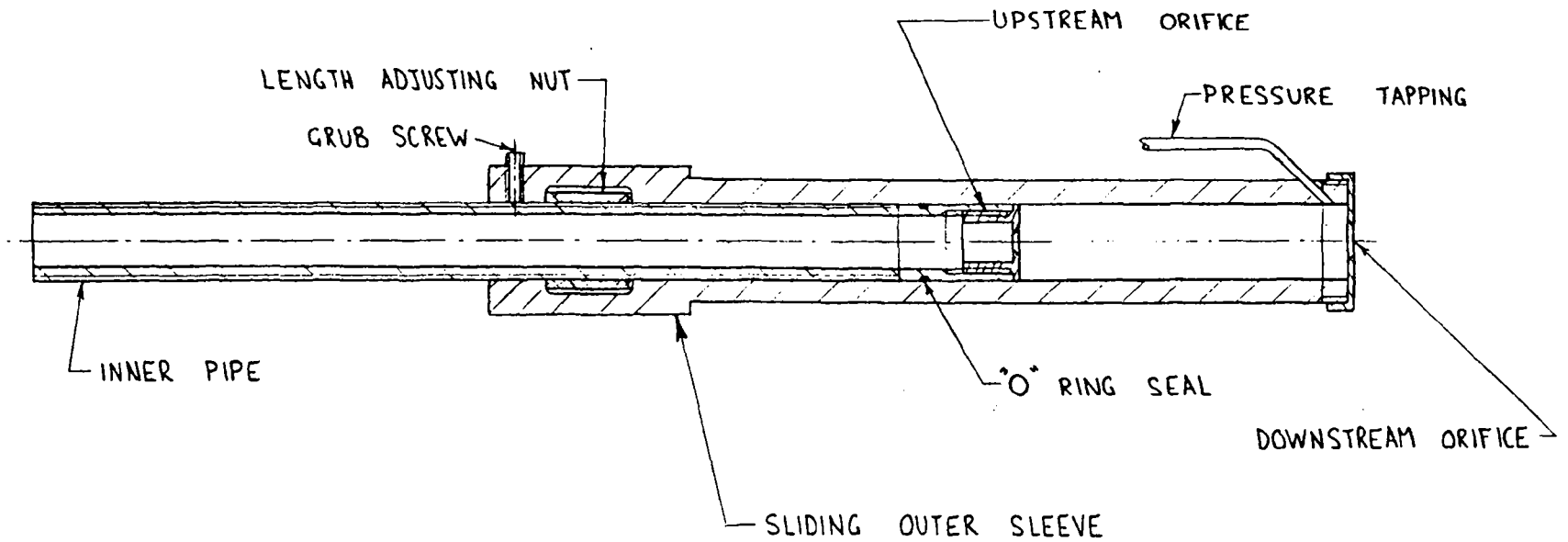

ALL MATERIAL - BRASS

ADELAIDE UNIVERSITY - MECH ENG DEPT.		
TITLE : ENHANCED MIXING BURNER (SMALL SCALE VERSION) - ASSY DWG.		
SCALE : 1:1	PROJ ANGLE : 3rd	DATE : 28.7.84
DRAWN : G NATHAN	APPROVED : R.E.L.	SHT : 1/6

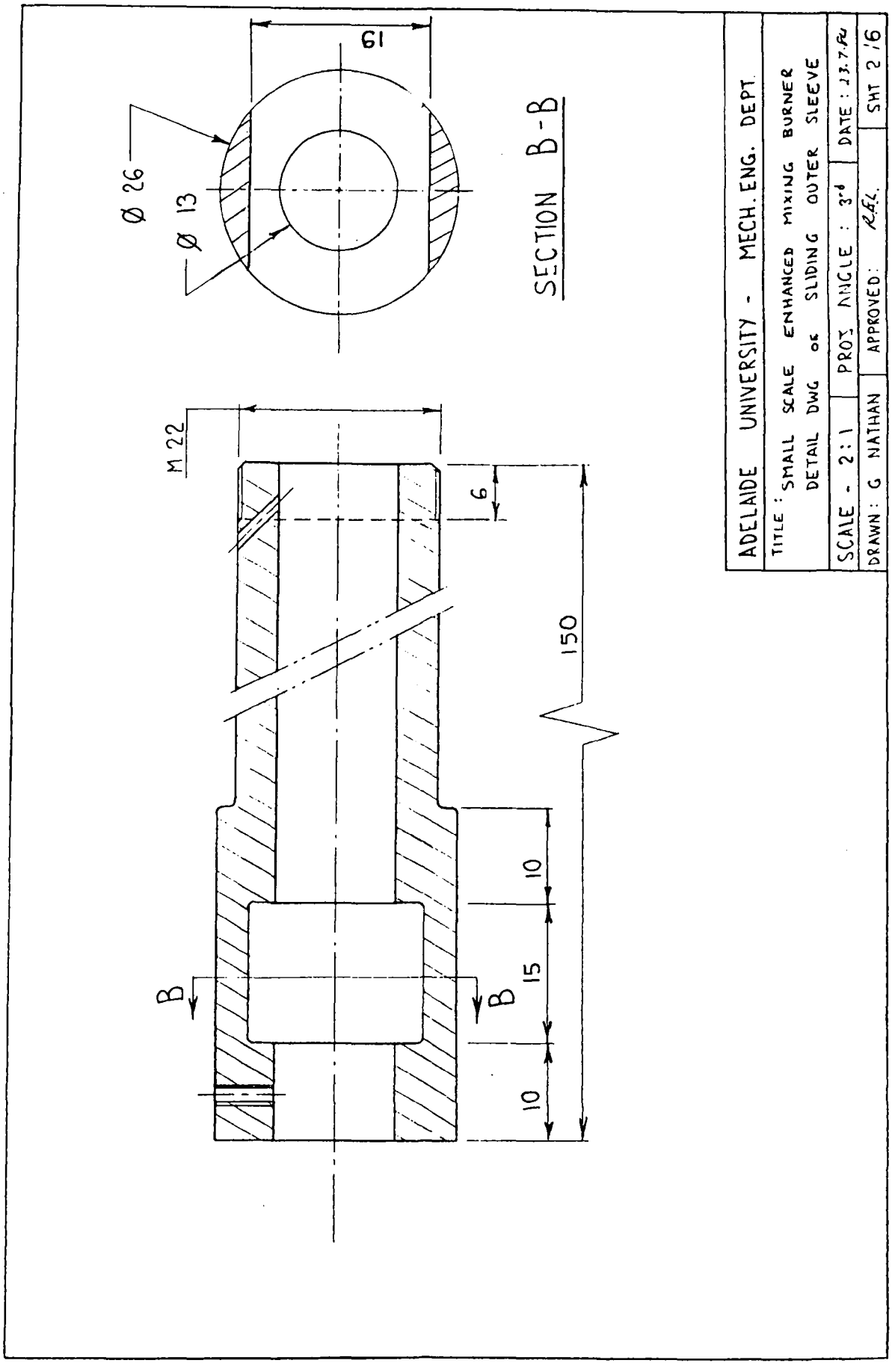
61
Ø 26
Ø 13
SECTION B-B
M 22
6
150
10
15
10
B
B
ADELAIDE UNIVERSITY - MECH. ENG. DEPT.
TITLE : SMALL SCALE ENHANCED MIXING BURNER
DETAIL DWG OF SLIDING OUTER SLEEVE
SCALE - 2:1
PROJ ANGLE : 3rd
DATE : 13.7.84
DRAWN : G NATHAN
APPROVED : R.E.L.
SHT 2 /6

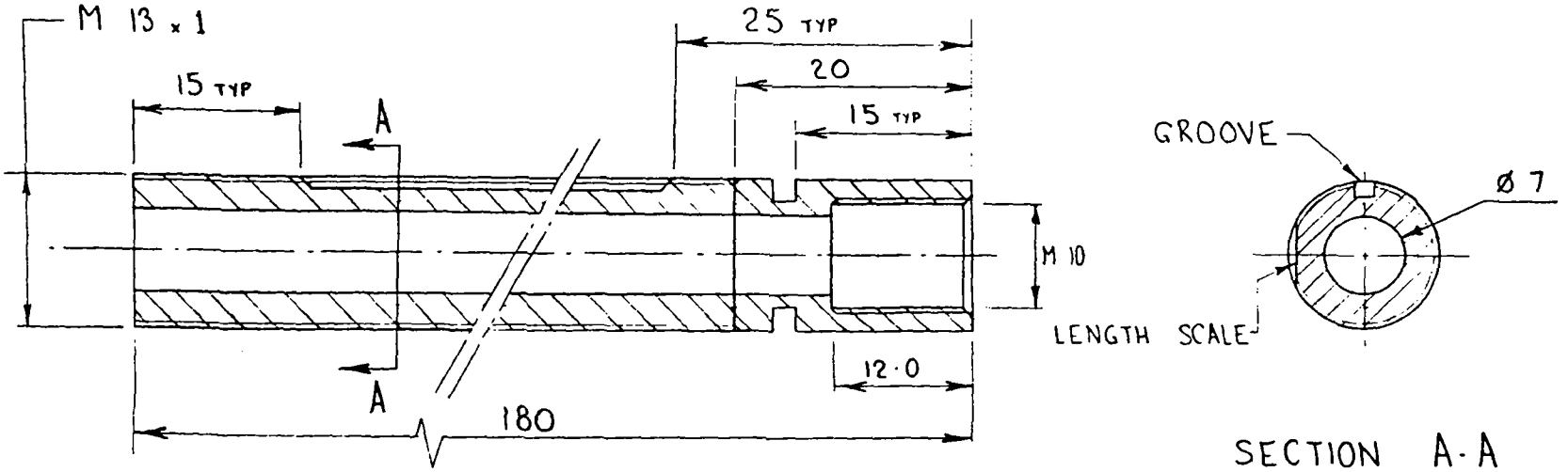

NOTE : 1) THE LENGTH SCALE SHOULD INDICATE THE DISTANCE BETWEEN THE ORIFICE PLATES, BY ALIGNING THE REAR OF THE OUTER SLEEVE WITH THE APPROPRIATE MARK.

2) THE GRUB SCREW (WHICH IS LOCATED IN THE OUTER SLEEVE) RUNS IN THE GROOVE TO PREVENT THE OUTER SLEEVE FROM ROTATING.

ADELAIDE UNIVERSITY - MECH ENG. DEPT.		
TITLE : SMALL SCALE ENHANCED MIXING BURNER DETAIL DWG OF INNER PIPE		
SCALE 2:1	PROT ANGLE : 3rd	DATE : 23-7-84
DRAWN : G NATHAN	APPROVED : R.E.C.	SHT 3/6

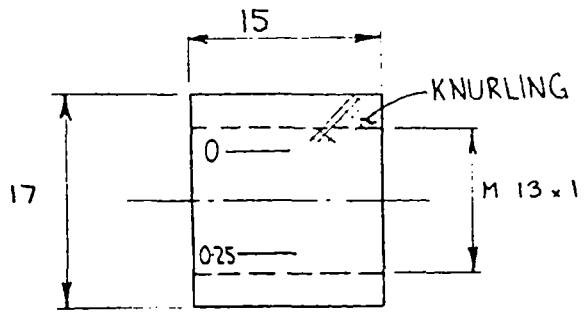

LENGTH ADJUSTING NUT

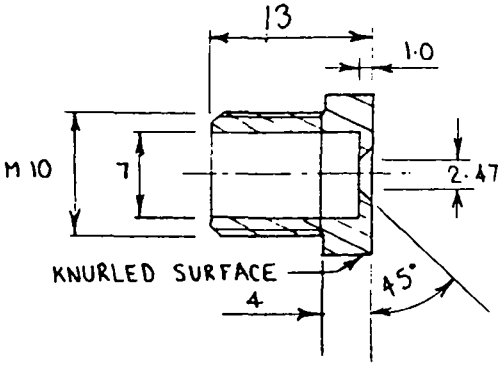

UPSTREAM ORIFICE

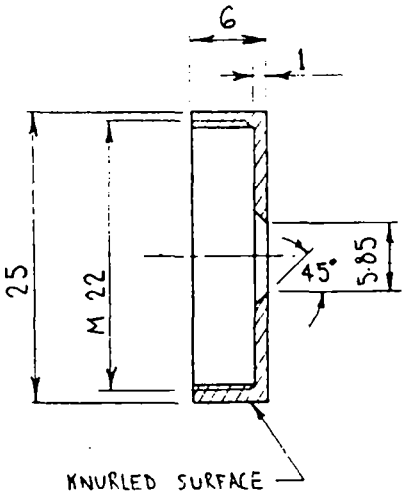

DOWNSTREAM ORIFICE

NOTE : THE LENGTH ADJUSTING NUT IS TO HAVE 4 MARKS TO ENABLE ACURATE ADJUSTMENT OF CAVITY LENGTH.

ADELAIDE UNIVERSITY - MECH. ENG. DEPT.		
TITLE : SMALL SCALE ENHANCED MIXING BURNER		
DETAIL DWGS : ORIFICE PLATES & LENGTH ADJUSTING NUT		
SCALE 2:1	PROJ. ANGLE : 3rd	DATE : 23.7.90
DRAWN : G NATHAN	APPROVED : R.E.L.	SHT 4 /6

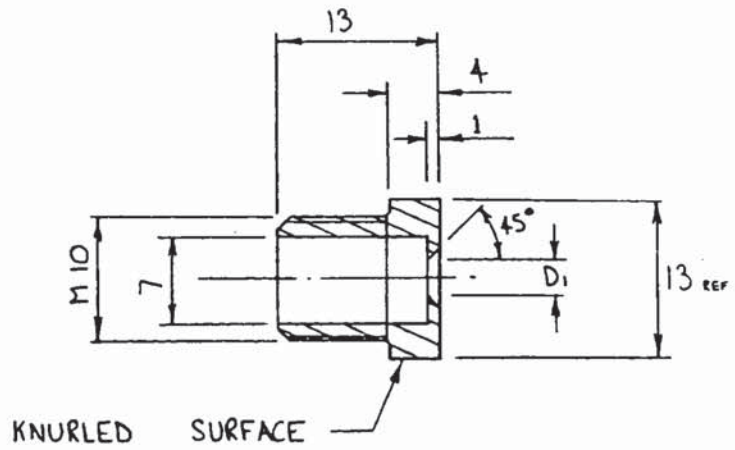

UPSTREAM ORIFICE

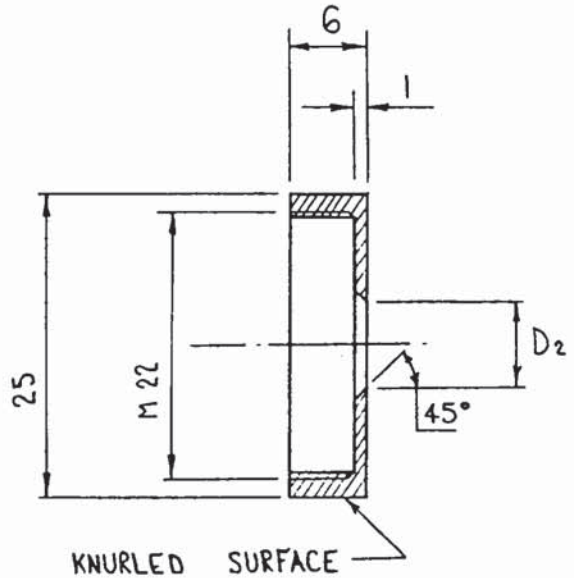

DOWNSTREAM ORIFICE

ONE (1) ORIFICE PLATE IS TO BE MADE FOR EACH OF THE VALUES OF D1 & D2 LISTED IN THE TABLES BELOW.

MATERIAL : BRASS

D1	D2
	11·4
	8·5
	9·75
1·30	7·16
3·02	6·46
2·02	5·03

UNIVERSITY OF ADELAIDE - MECH. ENG. DEPT.		
TITLE: SMALL SCALE ENHANCED MIXING BURNER		
DETAIL DWGS : ORIFICE PLATES		
SCALE 2:1	PROJ. ANGLE : 3rd	DATE : 4/2/85
DRAWN : G NATHAN	APPROVED :	SHT 5/6

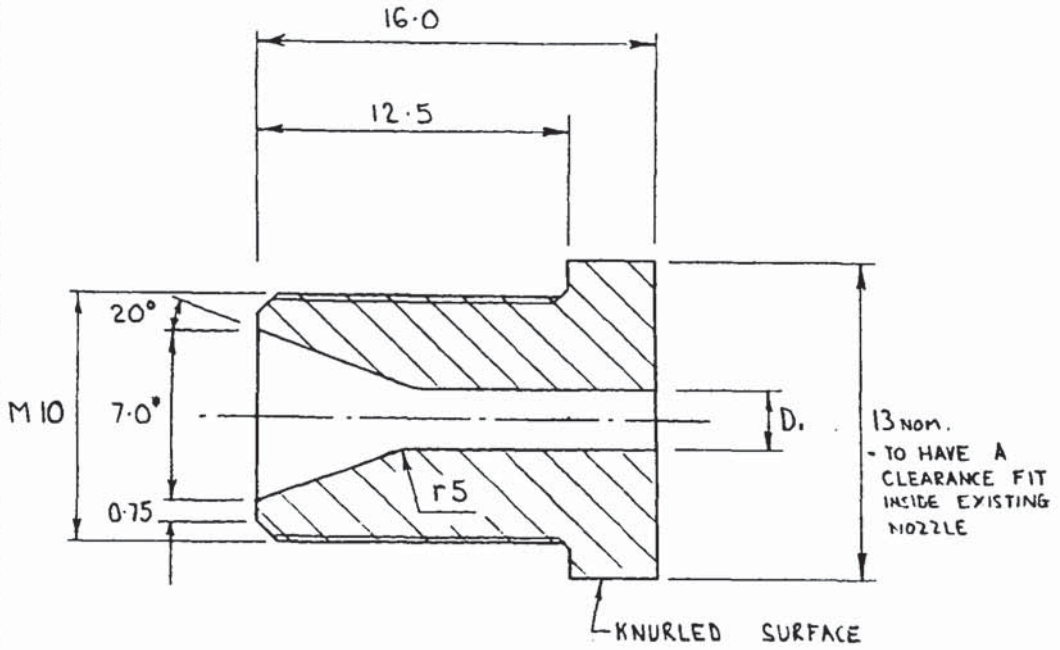

* TO HAVE A FLUSH FIT WITH BORE OF "INNER PIPE".

NOTE : ONE (1) "ABRUPT EXPANSION NOZZLE" IS TO BE MADE FOR EACH OF THE VALUES OF "D." LISTED.

DIM "D."
2·5
2·0
1·5

UNIVERSITY OF ADELAIDE - MECHANICAL ENGINEERING.		
TITLE : SMALL SCALE ENHANCED MIXING BURNER DETAIL DWG OF "ABRUPT EXPANSION NOZZLE"		
SCALE 4:1	PROJ. ANGLE 3rd	DATE : 3·10·95
DRAWN : G. NATHAN	APPROVED :	SHT 6/6

Appendix B

Detail Drawings: $D = 90\text{mm}$

Enhanced Mixing Nozzle

B.1 Cavity Pipe

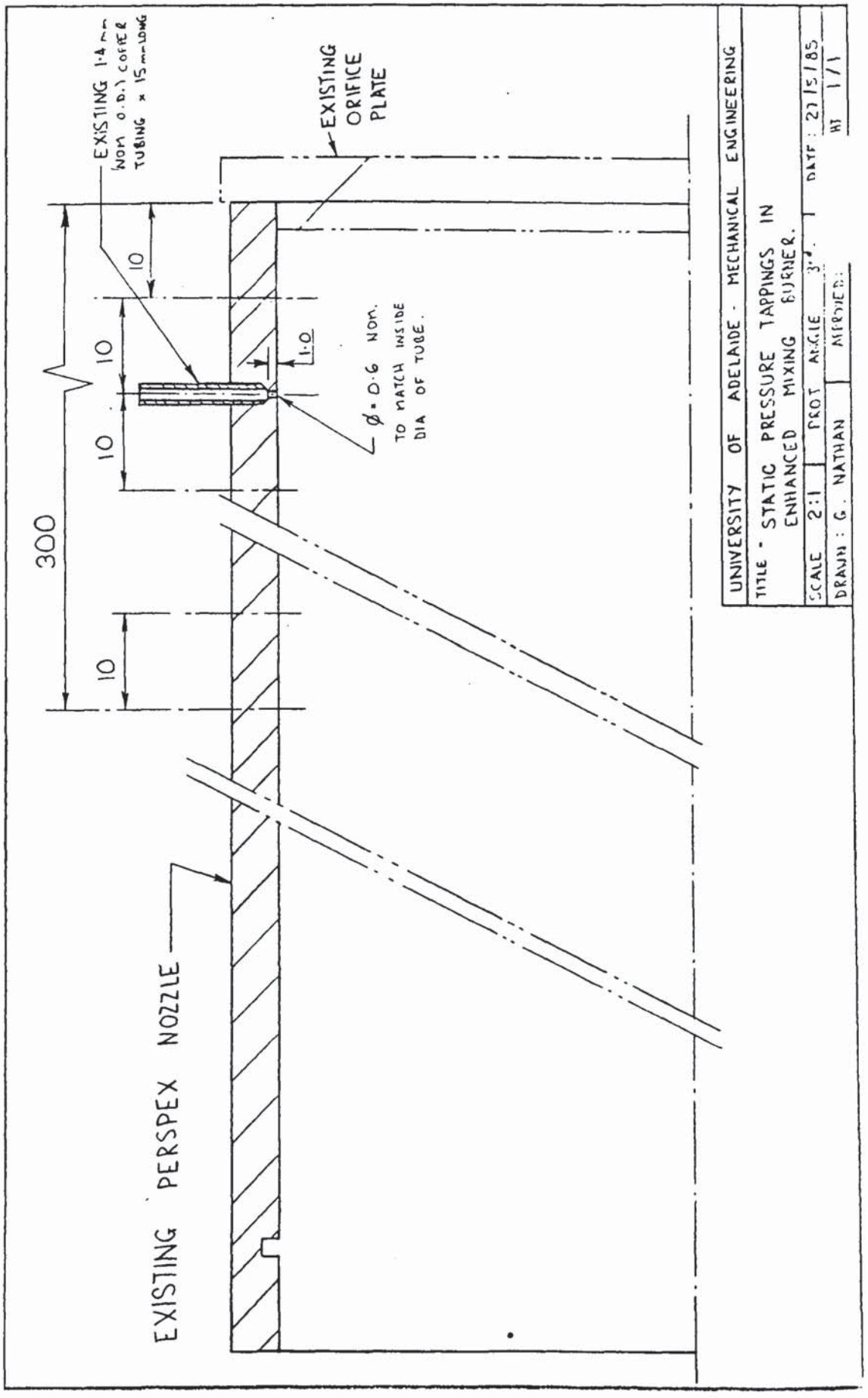

B.2 Pipes and Diffuser upstream of Cavity

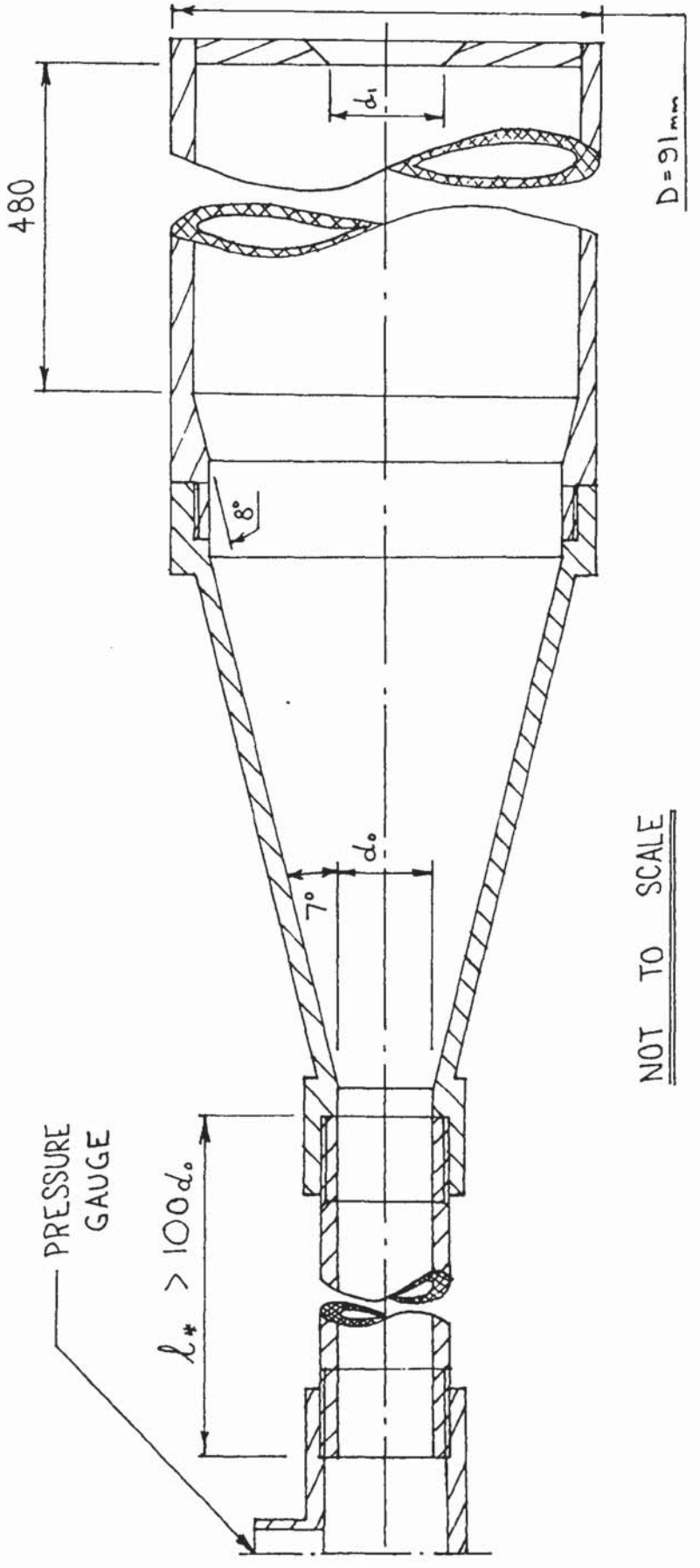

B.3 Upstream Swirl Vanes

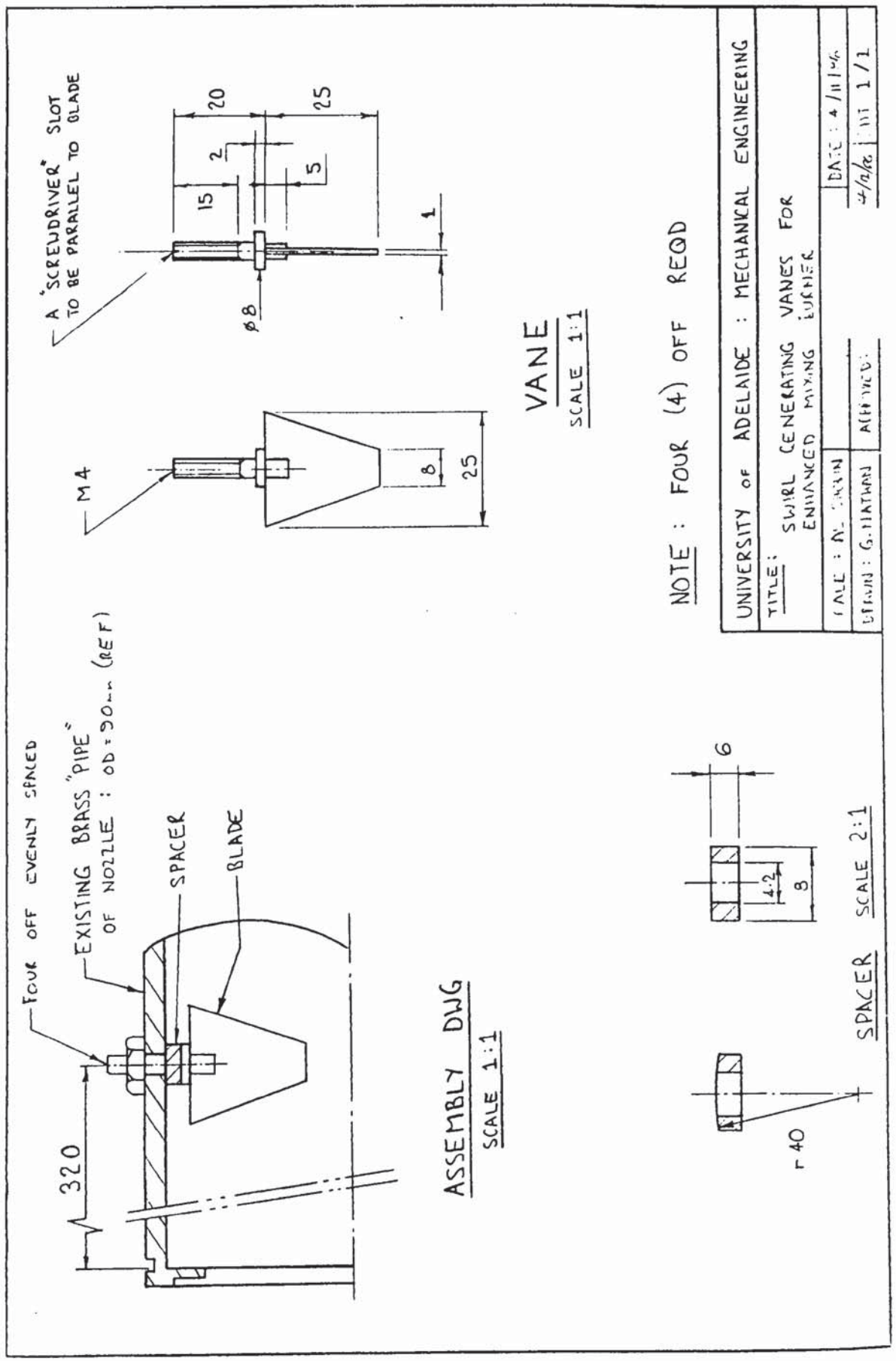

B.4 Orifice Plates

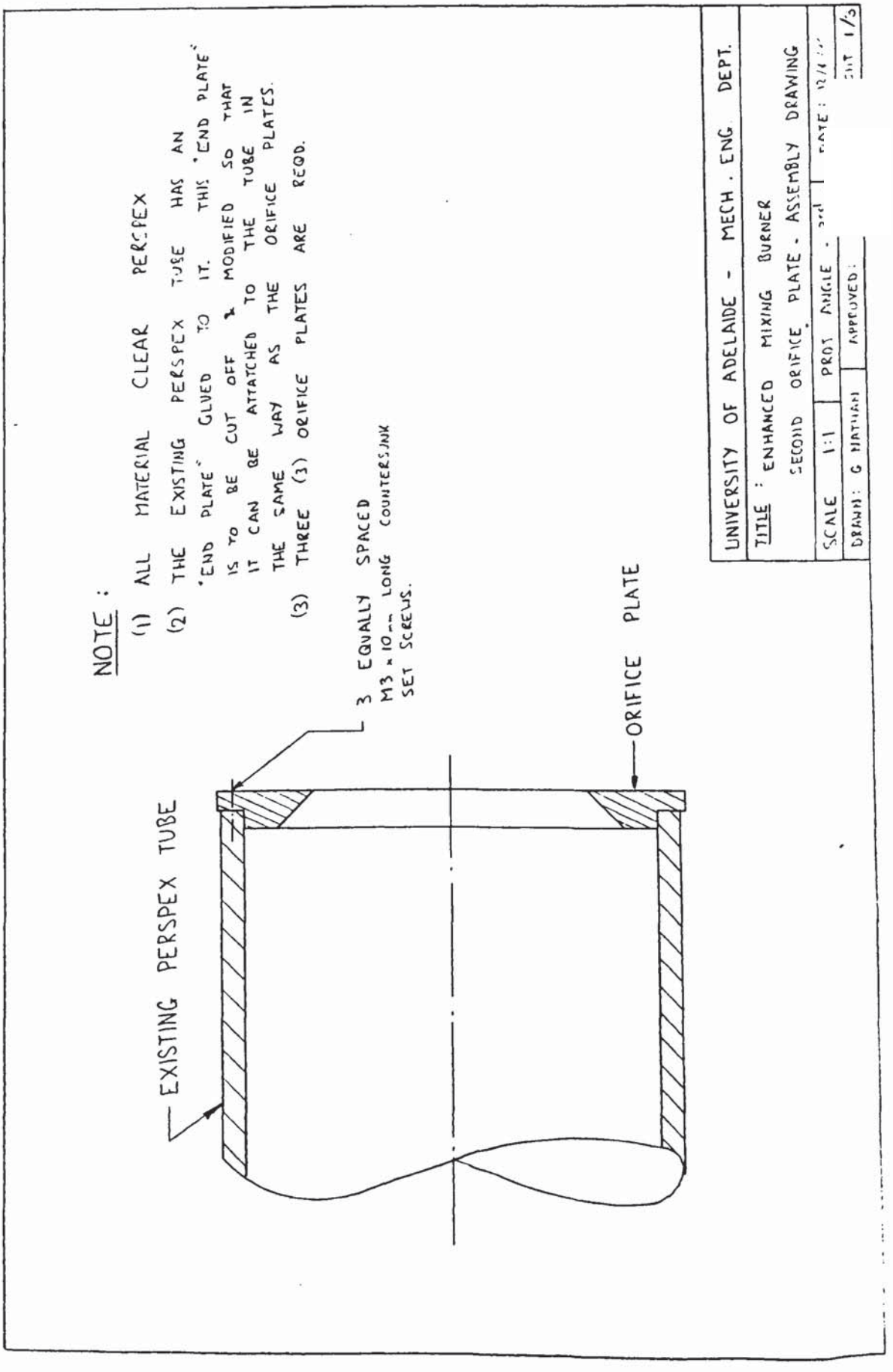

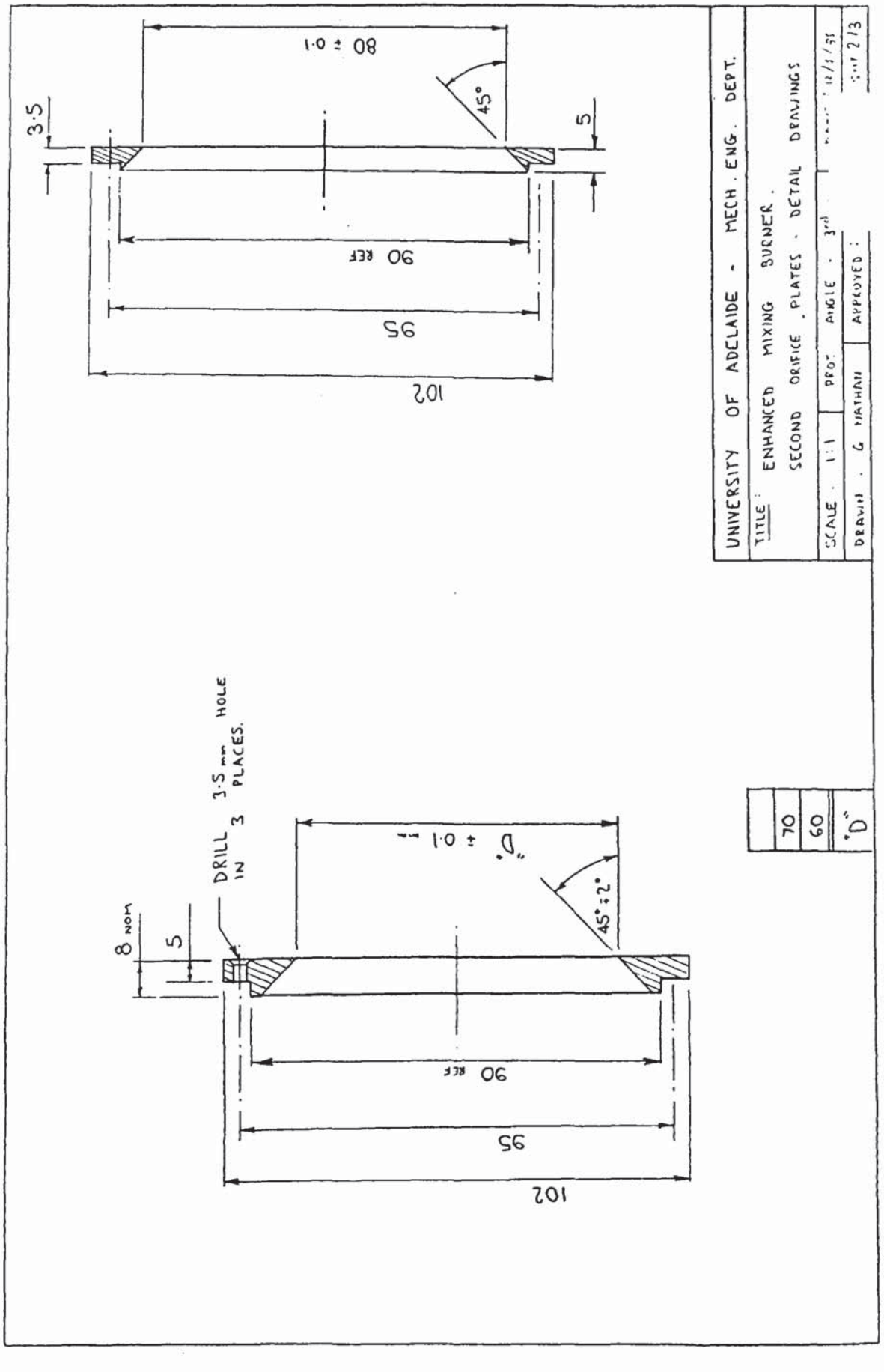
80 ± 0·1
45°
3·5
5
90 REF
95
102
UNIVERSITY OF ADELAIDE - MECH. ENG. DEPT.
TITLE: ENHANCED MIXING BURNER.
SECOND ORIFICE PLATES - DETAIL DRAWINGS
SCALE: 1:1
PROJ. ANGLE - 3rd
DRAWN: G NATHAN
APPROVED:
SHT 2/3
70
60
"D"
DRILL 3·5 mm HOLE IN 3 PLACES.
8 NOM
5
"D" ± 0·1
45° ± 2°
90 REF
95
102

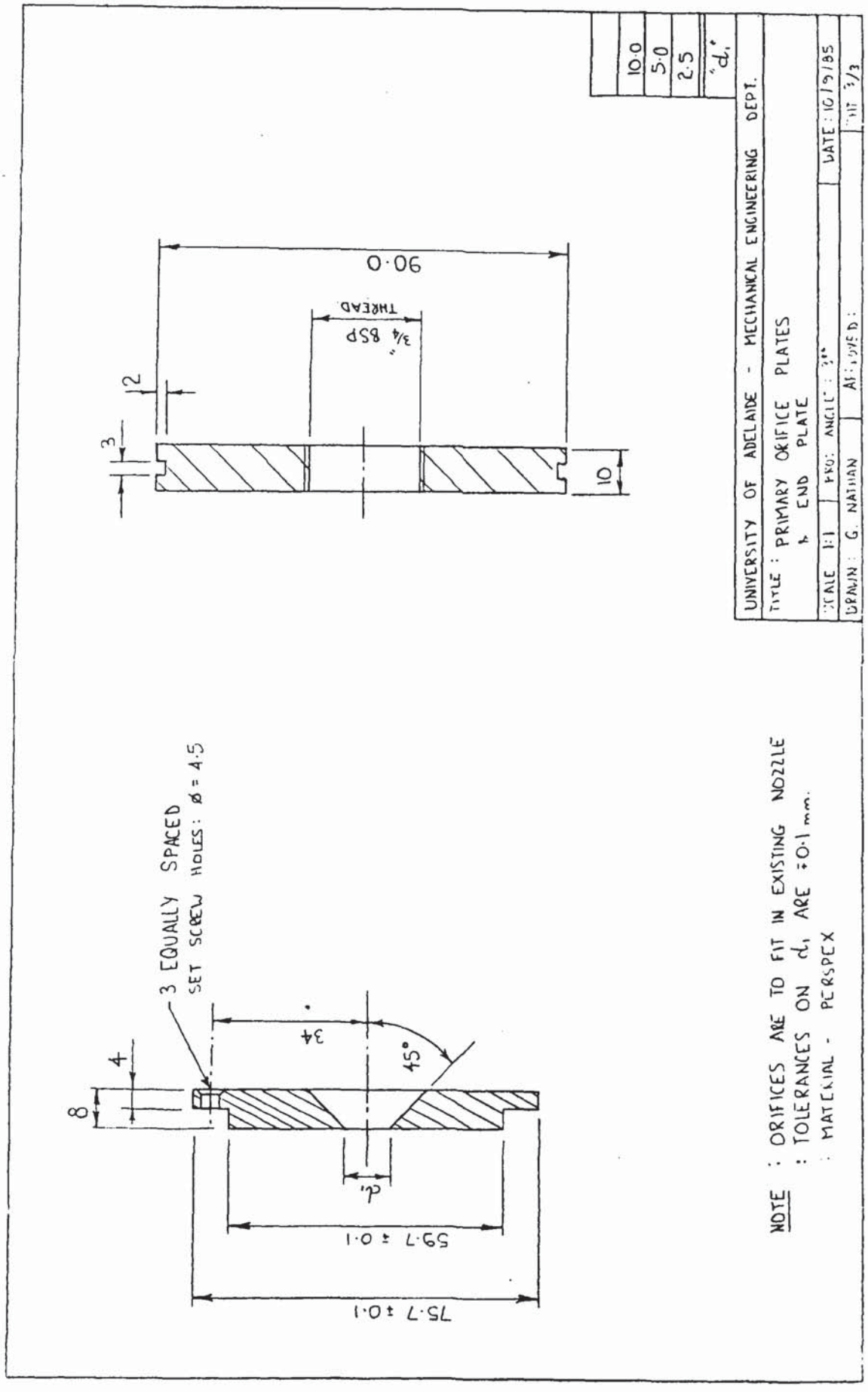
10·0
5·0
2·5
'd'
UNIVERSITY OF ADELAIDE - MECHANICAL ENGINEERING DEPT.
TITLE : PRIMARY ORIFICE PLATES
& END PLATE
SCALE 1:1
DRAWN : G. NATHAN
DATE : 10/9/85
SHT 3/3
90·0
THREAD
¾ BSP
12
3
10
3 EQUALLY SPACED
SET SCREW HOLES: ø = 4·5
4
8
34
45°
d
59·7 ± 0·1
75·7 ± 0·1
NOTE : ORIFICES ARE TO FIT IN EXISTING NOZZLE
: TOLERANCES ON d, ARE ±0·1 mm.
: MATERIAL - PERSPEX

B.5 Saw-Tooth Downstream Orifice Plate

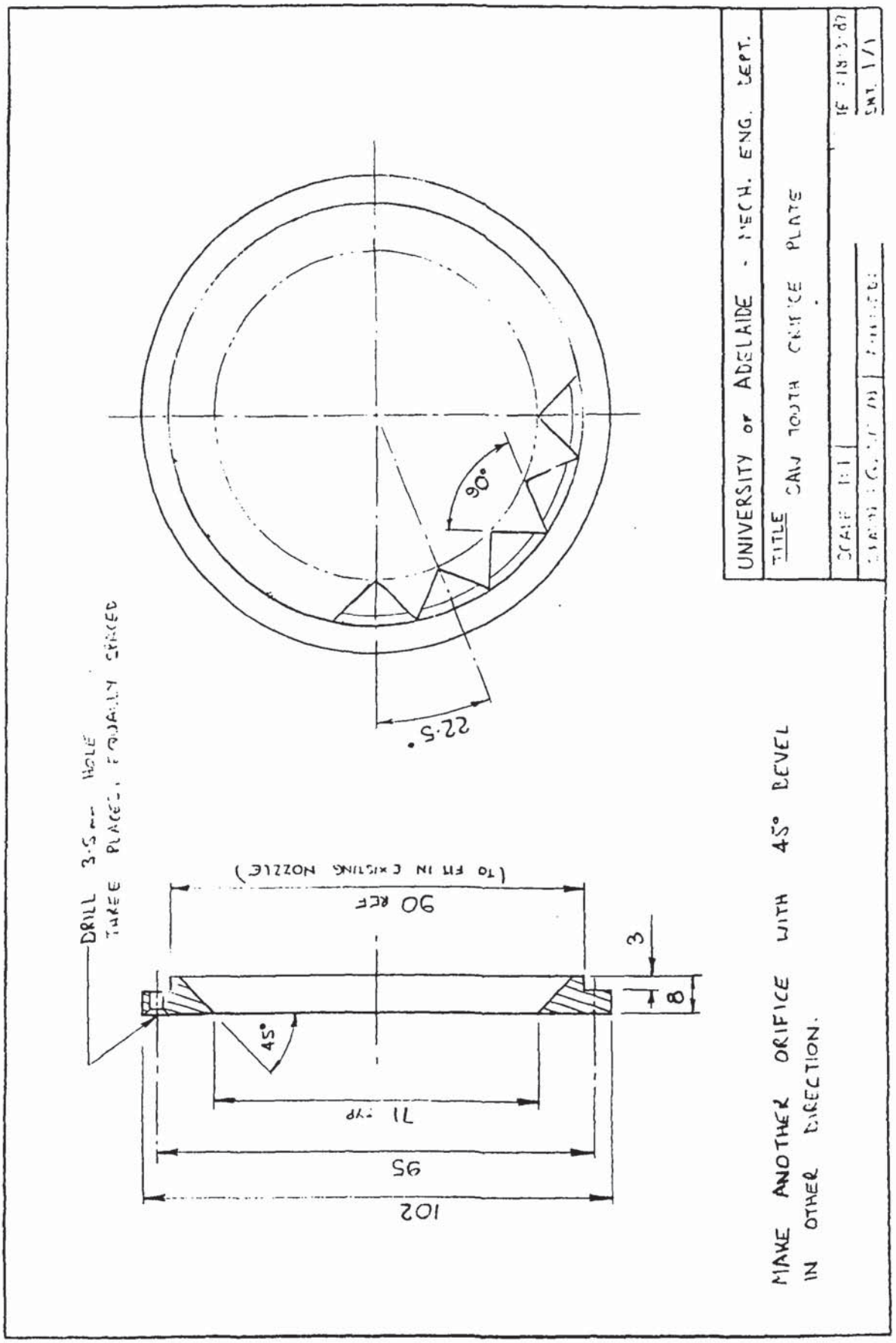

B.6 Bell-Mouth Throat

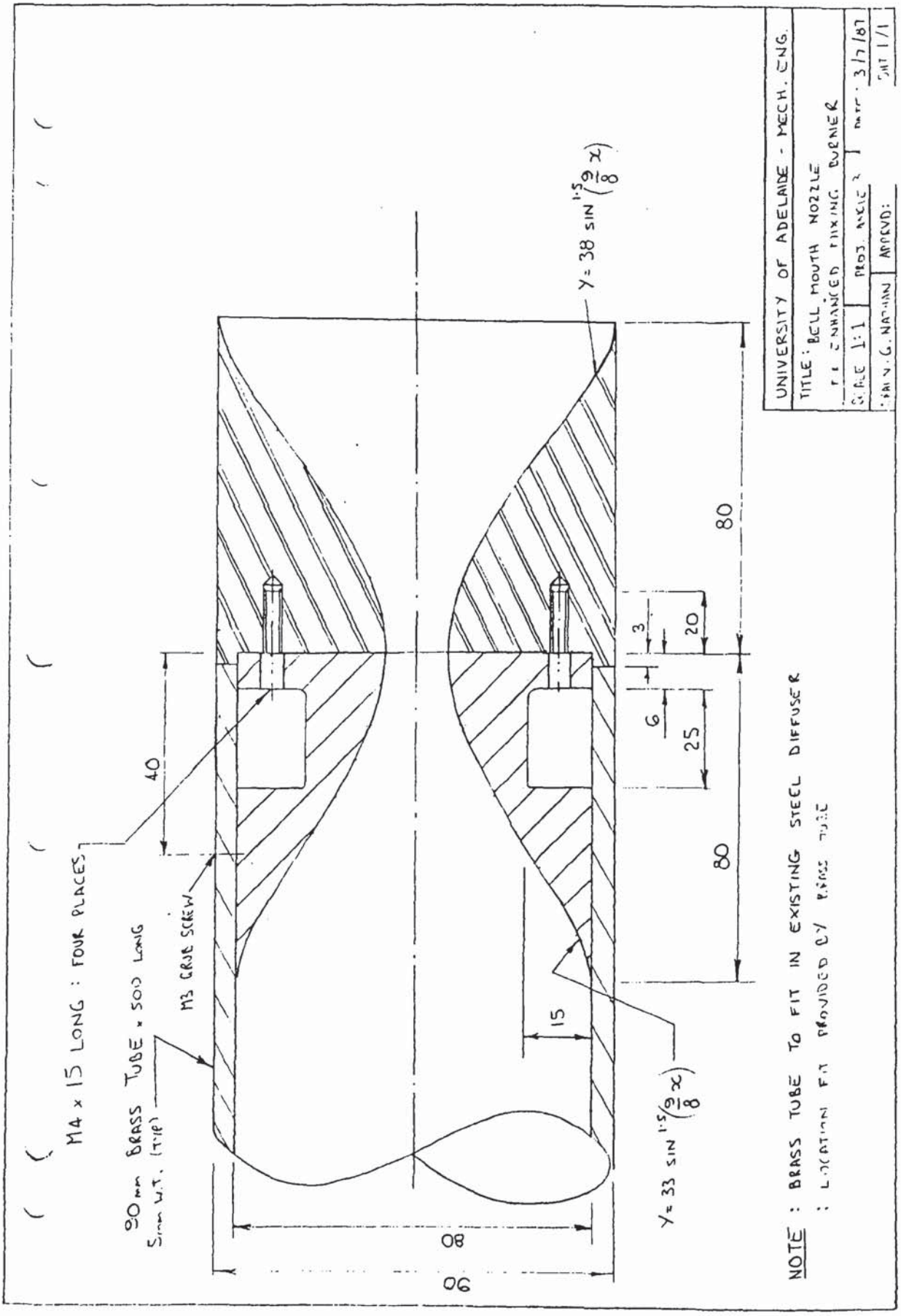

B.7 Flared Diffuser at Throat

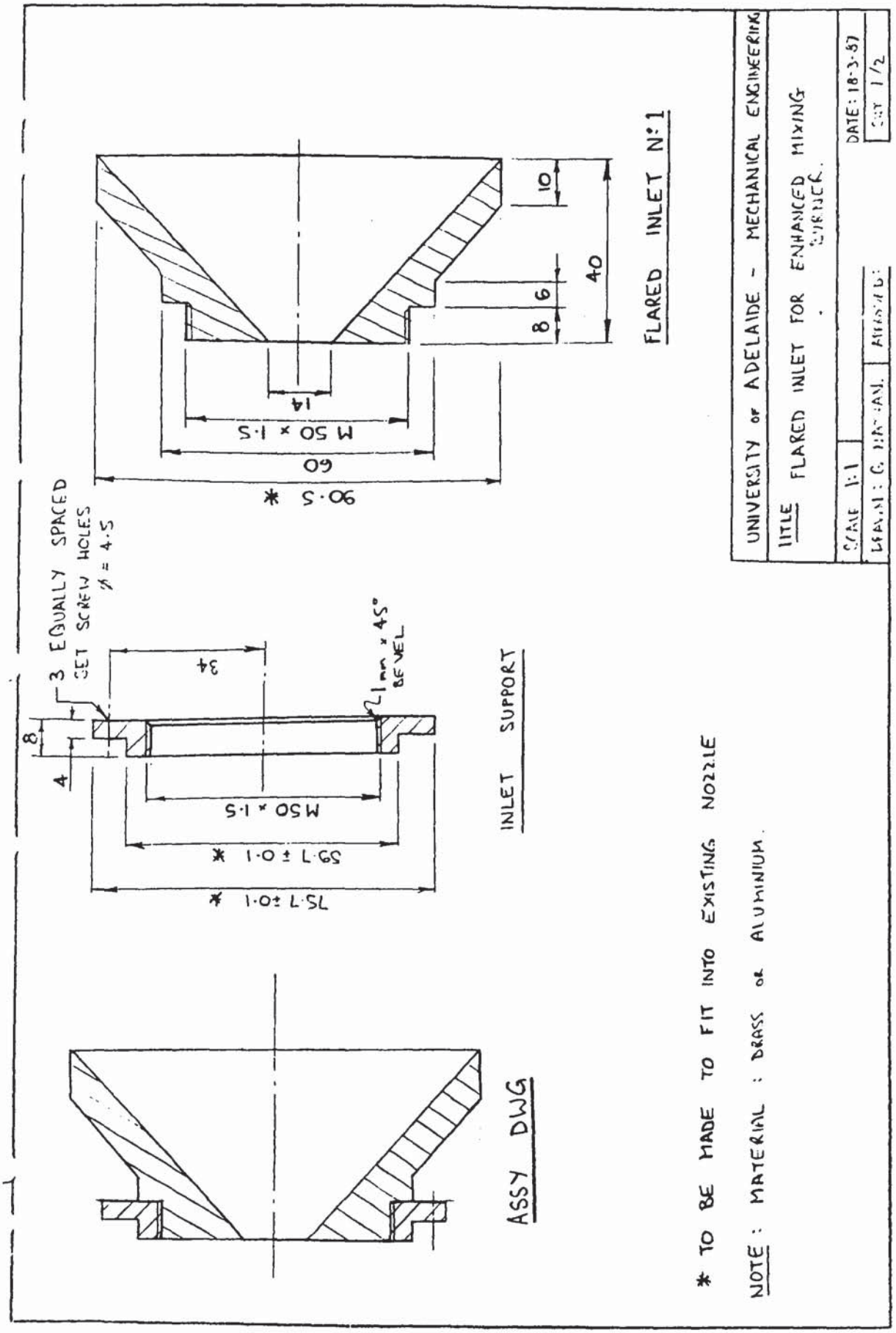

Appendix C

Detail Drawings: Ancillary Equipment

C.1 The Entrainment Shroud

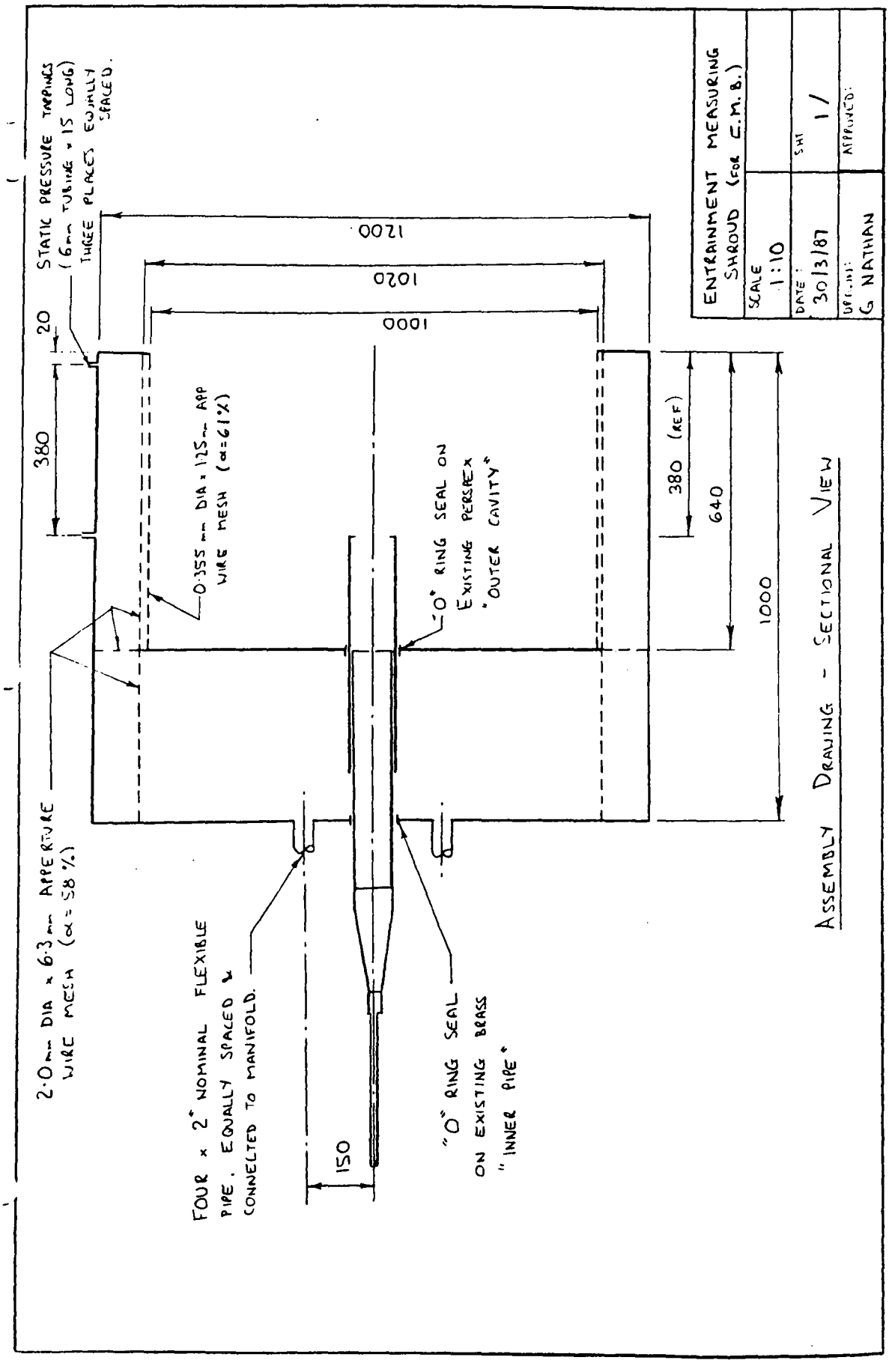

C.2 Schlieren Photography: Apparatus